

# ALT'18

Tarragona, Spain  
September 9-14 · 2018

BOOK OF ABSTRACTS

INTERNATIONAL CONFERENCE  
Advanced Laser Technologies

ALT\*



**BOOK OF ABSTRACTS**

# **ALT`18**

---

The 26th International Conference on Advanced Laser Technologies

---

September 09-14, 2018 / Tarragona, Spain

# PLENARIES

# High Repetition Rate Petawatt Lasers: technological challenges and solutions

**Luis Roso**<sup>1</sup>

*1- Spanish Center for Pulsed Lasers, CLPU, Villamayor, Salamanca, Spain.*

*\*Email address: roso@clpu.es*

Chirped Pulse Amplification allowed a very relevant increase of the laser peak power of sub-picosecond lasers. Now terawatt lasers are relatively common, petawatt (PW) lasers are operative in a number of laboratories around the world, and 10 PW lasers are under construction. The present world record of laser peak power is above 4 PW.

Arriving to the PW or to 10 PW is possible thanks to the solution of a number of bottlenecks during the last decade: Those include, high optical quality large crystal growing, pumping lasers, large diffraction gratings, pulse contrast enhancement, reduction of amplified spontaneous emission, and many others.

Most of the initial PW laser systems were able to fire at single shot, with minutes or hours to cool down the amplifiers and the pumps between shot and shot. Technology evolves increasing the peak power, and increasing the repetition rate. At present, there are only three PW lasers operative in the world able to fire at one shot per second: BELLA (at Berkeley, California), DRACO (at Dresden, Germany) and VEGA (at CLPU, Salamanca, Spain), and there are a few multi-PW lasers at this or higher repetition rates under construction (mainly in relation to the Extreme Light Infrastructure, ELI).

PW level experiments at high repetition rate (one shot per second or more) present a lot of challenges. Some of the challenges come from the laser operation, and some other challenges are related to the focusing systems and targeting.

PW lasers are considered as the future particle accelerators. A PW can accelerate electrons to GeV energies or protons to ten MeV, and acceleration occurs just in a few mm. While arriving to those limits on single shot regime is quite straightforward now, arriving at one shot per second is still quite demanding.

In the present talk, the state of the art of sub-picosecond PW and multi PW laser technology is going to be reviewed, as well as the possibilities to perform experiments at high repetition rate. This talk pretends to answer (briefly) two questions: what are the difficulties and limits of high repetition rate PW lasers; and how is it possible to design useful experiments (or useful accelerators) that use the full power and the full repetition rate.

# Ultrasensitive optical monitoring of interactions between biomolecules and nanoparticles: applications for advanced biosensors

**P.I. Nikitin**<sup>1,2</sup>

1- Prokhorov General Physics Institute, Russian Academy of Sciences, 38 Vavilov St., Moscow 119991, Russia

2- National Research Nuclear University MEPhI, 31 Kashirskoe shosse, 115409 Moscow, Russia

Email: [nikitin@kapella.gpi.ru](mailto:nikitin@kapella.gpi.ru)

Several original highly sensitive optical methods are introduced for advanced biosensing. These include the phase surface plasmon resonance (SPR) [1], the spectral-correlation interferometry (SCI) [2,3] and spectral-phase interferometry (SPI) [4], combined SPR and SERS chemical sensing on optoelectronic Au-Si grating microstructures, localized SPR on gold nanoparticles interacting with other type of particles [5], etc. We have shown that using phase peculiarities of light reflected under the SPR can improve sensitivity by 2 orders of magnitude compared to the traditional techniques that detect a shift of intensity minimum [1]. The sensitivity of label-free SCI and SPI based on functionalized glass slips employed as affordable single-use sensor chips is sufficient for many biomedical applications, food safety monitoring, e.g., detection of protein disease markers [3], mycotoxins [2], metabolite products of pyrethroids, for studies of smart polymers and mechanisms of drug action, etc. Besides, the sensitivities of these methods can be further increased by 3 orders of magnitude by nanoparticles to fit the clinical ranges of modern cardio and cancer diagnostics [6].

The designed optical sensing systems were also used as effective auxiliary tools for development of ultrasensitive electronic biosensors based on magnetic nanolabels, e.g., for optimization of dry-reagent immunomagnetic (DRIM) biosensing platform for rapid high-precision quantitative analyses of complex mediums [7]. The platform utilizes a highly sensitive method of magnetic particle quantification that provides record detection limit up to 39 pg of magnetic nanolabels [8] and extremely wide linear dynamic range of 7 orders [7]. The DRIM platform permits detection in human serum of as low as 25 pg/ml of total prostate specific antigen within 30 min. Besides, multiplex biosensing platforms were developed to measure very low concentrations of botulinum neurotoxins, staphylococcal enterotoxins, free thyroxine, thyroid-stimulating hormone, cardiac troponin and DNA.

In addition, the mentioned optical methods have demonstrated high efficiency in developments of intelligent biosensing nanoagents that can employ molecular interactions to perform any Boolean logic function [9], of smart materials based on self-assembly and disassembly of nanoparticles [5], for creation of new logic-gated nanosensors [4,5,9] capable of autonomous processing of multiple biochemical cues according to the Boolean logic rules and perform a biomedical action depending of the computation results. Such intelligent multifunctional nanoagents are promising for targeted drug delivery based on multiplex *in vivo* biosensing to be used in potential nanorobotic applications [10].

- [1] A.V. Kabashin, P.I. Nikitin, Surface plasmon resonance interferometer for bio and chemical sensors, *Opt. Comm.*, vol. 150, pp. 5-8 (1998).
- [2] A.V. Orlov, A.G. Burenin, N.G. Massarskaya, A.V. Betin, M.P. Nikitin, P.I. Nikitin, Highly reproducible and sensitive detection of mycotoxins by label-free biosensors, *Sensors Actuators, B: Chem.*, vol. 246, pp. 1080–1084 (2017).
- [3] A.G. Burenin, et al., Direct immunosensing by spectral correlation interferometry: assay characteristics versus antibody immobilization chemistry, *Anal. Bioanal. Chem.*, vol. 407, pp. 3955–3964 (2015).
- [4] A.V. Orlov, A.V. Pushkarev, E.N. Mochalova, P.I. Nikitin, M.P. Nikitin, Development and label-free investigation of logic-gating bilayers for smart biosensing, *Sensors Actuators, B: Chem.*, vol. 257, pp. 971–979 (2018).
- [5] K.G. Shevchenko, et al., Surface plasmon resonance as a tool for investigation of non-covalent nanoparticle interactions in heterogeneous self-assembly & disassembly systems, *Biosens. Bioelectron.*, vol. 88, pp. 3–8 (2017).
- [6] A.V. Orlov, et al., A new real-time method for investigation of affinity properties and binding kinetics of magnetic nanoparticles, *J. Magn. Magn. Mater.*, vol. 380, pp. 231–235 (2015).
- [7] A.V. Orlov, V.A. Bragina, M.P. Nikitin, P.I. Nikitin, Rapid dry-reagent immunomagnetic biosensing platform based on volumetric detection of nanoparticles on 3D structures, *Biosens. Bioelectron.*, vol. 79, pp. 423–429 (2016).
- [8] M.P. Nikitin, A.V. Orlov, I.L. Sokolov, A.A. Minakov, P.I. Nikitin, J. Ding, S.D. Bader, E.A. Rozhkova, V. Novosad, Ultrasensitive detection enabled by nonlinear magnetization of nanomagnetic labels, *Nanoscale*, vol.10, pp. 11642–11650 (2018).
- [9] M.P. Nikitin, V.O. Shipunova, S.M. Deyev, P.I. Nikitin, Biocomputing based on particle disassembly, *Nature Nanotechnology*, vol. 9, pp. 716–722 (2014).
- [10] I.L. Sokolov, et al., Smart materials on the way to theranostic nanorobots: nanomotors, advanced biosensors, and intelligent vehicles for drug delivery, *Biochim. Biophys. Acta – Gen. Subj.*, vol. 1861, pp.1530–1544 (2017).

# Optical clearing as a promising technology for *in vivo* laser diagnostics and treatment of hidden pathologies

V.V. Tuchin<sup>1-4</sup>

1 - Saratov State University, Astrakhanskaya str. 83, 410012 Saratov, Russia

2 - Tomsk State University, Lenin's av. 36, 634050 Tomsk, Russia

3 - ITMO University, Kronverkskiy pr., 49, 197101 St. Petersburg, Russia

4 - Institute of Precision Mechanics and Control RAS, Rabochaya str. 24, 410028 Saratov, Russia

tuchinvv@mail.ru

Many laser spectroscopic and imaging technologies applied in a wide wavelength range from UV to terahertz suffer from a low penetration depth of a probing beam and blurring of images caused by light scattering and absorption. One of the robust ways to overcome these problems is to use a so-called optical clearing (OC) technology based on tissue or cell impregnation by a biocompatible OC agent (OCA). In this lecture, OC methods aimed the enhancement of laser spectroscopy, imaging and treatment of living tissues and cells in a broad range of wavelengths from UV to terahertz will be presented. OC approach is based on controllable and reversible modification of optical properties of tissue or cell by their impregnation with an OCA.

The OC method explores three major concepts: refractive index matching of scatterers and surrounding medium, reversible dehydration caused by OCA osmolarity, and reduction of hydrodynamic radius of scattering particles at their interaction with OCA molecules [1-4]. As OCAs a variety of hyperosmotic, cryogenic and x-ray contrast liquids, such as glycerol, PEG, glucose, fructose, sucrose, mannitol, dextrans, propylene glycol, ethylene glycol, Omnipaque<sup>TM</sup> and some others, are considered and tested. Water transport and modification of tissue mechanical properties under OCA action such as reversible dehydration and shrinkage, balance of free and bound water are of great importance for successful application of such technology and thus will be analyzed in detail.

A significant probing depth and image contrast increase at application of OCAs to different human and animal tissues, such as skin, fat, eye sclera, muscle, cerebral membrane, digestive tract tissue, cartilage, bone, blood vessels, and blood, will be demonstrated using spectrophotometry, OCT, photoacoustic microscopy, linear and nonlinear fluorescence, SHG and Raman microscopies, polarization and speckle imaging. The technologies for effective OCA delivery due to hidden free diffusion, local heating, enforced tissue permeability (physical and chemical), OCA encapsulation, and blood and lymph vessel networking will be described. Impact of OCAs on tissue structure, free/bound water balance and blood microcirculation will be quantified. Experimental data on diffusivity and permeability of glucose, glycerol, PEG, Omnipaque<sup>TM</sup> and other OCAs for normal and pathological tissues will be presented.

[1] D. Zhu, K. V. Larin, Q. Luo, and V. V. Tuchin, "Recent progress in tissue optical clearing," *Laser Photonics Rev.* **7**(5), 732–757 (2013).

[2] E. A. Genina, A. N. Bashkatov, Yu. P. Sinichkin, I. Yu. Yanina, V.V. Tuchin, "Optical clearing of biological tissues: prospects of application in medical diagnostics and phototherapy [Review]," *J. Biomed. Photonics & Eng.* **1**(1), 22–58 (2015).

[3] V. V. Tuchin, "Polarized light interaction with tissues," *J. Biomed. Opt.* **21**(7), 071114-1-37 (2016).

[4] A. Yu. Sdobnov, M. E. Darvin, E. A. Genina, A. N. Bashkatov, J. Lademann, V. V. Tuchin, "Recent progress in tissue optical clearing for spectroscopic application," *Spectrochim. Acta Part A: Molec. Biomolec. Spectrosc.* **197**, 216-229 (2018).

# Non-equilibrium structural dynamics in laser-driven materials

**Klaus Sokolowski-Tinten**

*Faculty of Physics and Center for Nanointegration (CENIDE), University of Duisburg-Essen, Lotharstr. 1, 47057  
Duisburg, Germany*

*Klaus.Sokolowski-Tinten@uni-due.de*

Ultrafast laser excitation of solids creates highly non-equilibrium states of materials which subsequently may lead to very rapid structural changes. Time-resolved diffraction using modern high brightness femtosecond X-ray or electron sources allows to directly follow these processes with atomic scale spatial and temporal resolution even under excitation conditions where the irradiated sample is irreversibly modified. In this contribution I will discuss some examples of our work in this field carried out at X-ray free electron laser as well as using ultrashort electron pulses:

(1) We have carried out time-resolved transmission electron diffraction experiments at the MeV Ultrafast Electron Diffraction (UED) at SLAC National Accelerator Laboratory [1] to study non-equilibrium energy relaxation and transport in nanoscale materials after fs laser excitation. Precise measurements of the transient Debye-Waller-effect in different metal-insulator and metal-metal-heterostructures highlight the importance of interface effects [2,3] and reveal the competition between local relaxation and transport. At stronger excitation levels phase transitions may occur. Experiments on Au give direct evidence for a transition from heterogeneous melting at lower fluences to a homogeneous process at higher fluences [4].

(2) Chalkogenide-based phase change materials (PCMs) exhibit rapid and reversible phase transitions between an amorphous and a crystalline state, which can be triggered by short light or electrical pulses. Since the structural changes are associated with large differences in the electronic of the two phases, PCMs are used for non-volatile electronic memory applications. Single pulse time-resolved X-ray scattering at the LCLS free electron laser has been used to study the phase transition dynamics in different laser-excited PCMs, providing a complete picture of the structural changes during switching at an atomic level and on the relevant time-scales. The response was found to be similar for all investigated materials involving fast melting on sub-ps to ps time-scales, resolidification into an intermediate amorphous-like state within a few ns, eventually followed by the formation of the final amorphous or crystalline state on a tens of ns to  $\mu$ s-scale. These time-scales imply purely thermal mechanisms despite the high degree of electronic excitation initially created by fs laser irradiation. Our data suggest that a liquid-liquid structural phase transition in the deeply undercooled state enables fast and long-term data storage in PCMs.

[1] S. P. Weathersby et al., Rev. Sci. Instrum. **86**, 073702 (2015).

[2] K. Sokolowski-Tinten et al., New J. Phys. **17**, 113047 (2015).

[3] K. Sokolowski-Tinten et al., Struct. Dyn. **4**, 054501 (2017).

[4] M. Mo et al., Science **360**, 1451 (2018).

[5] P. Zalden et al., in preparation

# Coherent scatter-controlled phase change grating structures in silicon: Femtosecond-resolved imaging during laser structuring

Y. Fuentes-Edfuf<sup>1</sup>, M. Garcia-Lechuga<sup>1</sup>, D. Puerto<sup>1</sup>, C. Florian<sup>1</sup>, A. Garcia-Leis<sup>2</sup>, S. Sánchez-Cortés<sup>2</sup>, J. Siegel<sup>1</sup> and J. Solis<sup>1</sup>

<sup>1</sup>- Laser Processing Group, Instituto de Óptica, IO-CSIC, Serrano 121, 28006, Madrid, Spain

<sup>2</sup>- Instituto de Estructura de la Materia, CSIC, Serrano 121, 28006, Madrid, Spain

[j.solis@io.cfmac.csic.es](mailto:j.solis@io.cfmac.csic.es), [j.siegel@io.cfmac.csic.es](mailto:j.siegel@io.cfmac.csic.es)

Laser-induced periodic surface structures (LIPSS) are a universal phenomenon observed in dielectrics semiconductors and metals irradiated with short laser pulses. They appear in the form of a variety of sub-wavelength periodic surface structures with features that depend on the processing parameters [1]. Their formation typically involves material ablation, often leading to an unwanted increase of surface roughness. In this presentation we describe a different type of LIPSS in silicon, based on melting and rapid solidification, combined with self-organization, and leading to the formation of nanograting structures in the form of alternating amorphous and crystalline lines. By controlling the processing parameters, the size of a single fringe can be tuned over the three spatial dimensions over a wide range of values. The fabrication strategy can also be extended into one and two dimensions by scanning the laser beam over the sample surface (c.f. Fig. 1 (a-f)) [2].

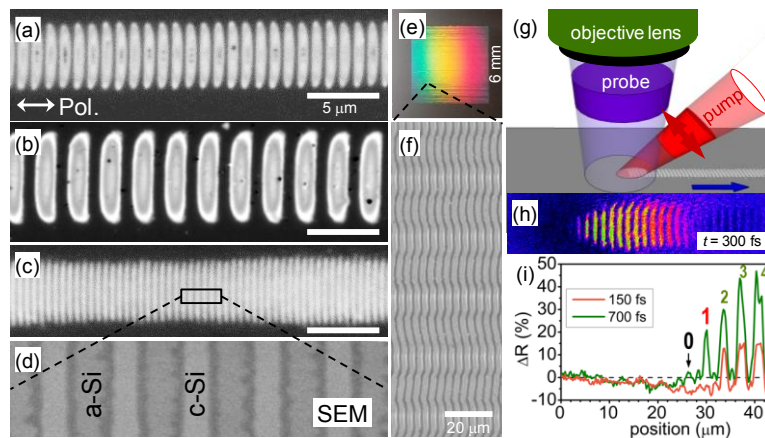


Figure 1 : (a-c) Optical micrographs of self-organized amorphous fringes with different periods written on the surface of crystalline silicon. (d) SEM image of the region marked in (c). (e) Colour photograph of a fabricated area grating ( $6 \times 6$  mm) upon illumination with white light, illustrating wavelength-dependent diffraction. (f) Optical micrograph in reflection of region marked in (e). (g) Experimental configuration employed for moving-spot femtosecond microscopy, yielding (h) time-resolved images of the transient surface reflectivity at certain delays  $t$  after arrival of the pump pulse, which are analyzed (i) in order to clarify the formation dynamics of amorphous-crystalline LIPSS.

We will additionally present a time-resolved experimental technique, namely moving-spot femtosecond microscopy [3], which is capable to spatially and temporally resolve the birth and growth of individual fringes, as illustrated in Fig. 1 (g-i). By means of the analysis of the images recorded upon laser excitation and comparison to a single pulse reference experiment, the different phase changes locally taking place in the sample can be monitored. We will show that the formation process is initiated by free electron generation, leading to thermal and non-thermal melting, liquid phase overheating and rapid solidification into the amorphous phase [3].

[1] J. Bonse, S. Hohm, S. Kimer, A. Rosenfeld, Laser-Induced Periodic Surface Structures – a Scientific Evergreen, *IIEEE J. Sel. Top. Quantum Electron.* 23, 9000615 (2016).

[2] Y. Fuentes-Edfuf, M. Garcia-Lechuga, D. Puerto, C. Florian, A. Garcia-Leis, S. Sanchez-Cortés, J. Solis and J. Siegel, Coherent scatter-controlled phase change grating structures in silicon using femtosecond laser pulses, *Scientific Reports* 7, 4594 (2017).

[3] M. Garcia-Lechuga, D. Puerto, Y. Fuentes-Edfuf, J. Solis and J. Siegel, Ultrafast Moving-Spot Microscopy: Birth and Growth of Laser-Induced Periodic Surface Structures, *ACS Photonics* 3, 1961–1967 (2016).

# Progress in the generation of ultrashort light pulses in the 2-micron spectral range by passive mode-locking of Tm and Ho bulk solid-state lasers

**Valentin Petrov<sup>1</sup>**

*1-Max Born Institute for Nonlinear Optics and Short Pulse Spectroscopy, D-12489 Berlin, Germany*

*\*Email address: [petrov@mbi-berlin.de](mailto:petrov@mbi-berlin.de)*

Mode-locked lasers emitting ultrashort pulses in the 2- $\mu\text{m}$  spectral range at high ( $\sim 100$  MHz) repetition rates are important for time-resolved molecular spectroscopy in this molecular fingerprint region but are also of particular interest as pump sources for synchronously-pumped optical parametric oscillators operating in the mid-IR above 5  $\mu\text{m}$ , including frequency comb generators, as seeders of near-degenerate chirped-pulse optical parametric amplifiers pumped at  $\sim 1$   $\mu\text{m}$  for high-order harmonic and soft-X-ray generation, for seeding of regenerative amplifiers to boost the pulse energy at lower repetition rates, as well as for IR supercontinuum and THz generation [1].

Passively mode-locked lasers based on  $\text{Tm}^{3+}$ - and  $\text{Ho}^{3+}$ -doped bulk solid-state materials that can be diode-pumped have been under development at the Max Born Institute in Berlin for about a decade. In 2009 we demonstrated for the first time steady-state operation of such a  $\text{Tm}:\text{KLu}(\text{WO}_4)_2$  laser using a single-walled carbon nanotube (SWCNT) saturable absorber (SA) which generated  $\sim 10$ -ps pulses at 1.95  $\mu\text{m}$  [2]. In 2012 it produced for the first time femtosecond ( $\sim 140$  fs) pulses at 2.037  $\mu\text{m}$  through shifting of the wavelength by a selective outcoupler [3]. In the last year, the study of numerous active media with different SAs resulted in the first generation of sub-100-fs pulses ( $< 10$  optical cycles) (Fig. 1). Materials with broad and smooth spectral gain profile were selected, naturally emitting above 2  $\mu\text{m}$  to avoid the water vapor absorption/dispersion effect. Few approaches were employed, including anisotropic materials, strong crystal-field distortion in hosts that do not contain rare-earths to be substituted, crystals with structural or compositional (i.e. mixed compounds) disorder that exhibit inhomogeneous line broadening, mixed laser ceramics, and Tm,Ho-codoped crystals.

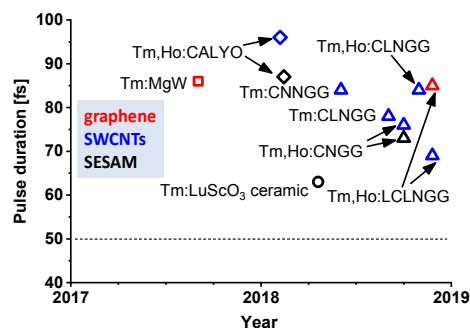


Fig. 1. Sub-100-fs mode-locked bulk solid-state lasers near 2  $\mu\text{m}$  based on  $\text{Tm}^{3+}$  and  $\text{Ho}^{3+}$  emission. CALYO:  $\text{CaYAlO}_4$ , MgW:  $\text{MgWO}_4$ ,  $\text{LuScO}_3$ :  $(\text{Lu}_{2/3}\text{Sc}_{1/3})_2\text{O}_3$ , CNGG:  $\text{Ca}_3\text{Nb}_{1.5}\text{Ga}_{3.5}\text{O}_{12}$ , CLNGG and CNNGG:  $\text{Li}^+$  and  $\text{Na}^+$  doped CNGG, LCLNGG:  $\text{La}^{3+}$ -doped CLNGG.

Desirable properties of SAs include broadband absorption, fast recovery, optimum saturable and low non-saturable losses. A broad absorption band in semiconducting SWCNTs spans from 1.6 to 2.1  $\mu\text{m}$  whereas the absorption of graphene extends into the mid-IR and scales for multilayers, increasing the modulation depth. In both cases the saturation mechanism is related to the filling of states. Apart from the high optical damage threshold and much broader spectral range, the main advantages of the carbon nanostructures over GaSb-based semiconductor SA mirrors (SESAMs) are related to the simple and inexpensive fabrication methods. Chirped mirrors were implemented for group-velocity dispersion compensation, to generate the shortest pulses, see Fig. 1 (down to 63 fs).

[1] V. Petrov, "Frequency down-conversion of solid-state laser sources to the mid-infrared spectral range using non-oxide nonlinear crystals," *Progress Quantum Electron.* **42**, 1 (2015).

[2] W. B. Cho, A. Schmidt, J. H. Yim, S. Y. Choi, S. Lee, F. Rotermund, U. Griebner, G. Steinmeyer, V. Petrov, X. Mateos, M. C. Pujol, J. Carvajal, M. Aguilo, F. Diaz, "Passive mode-locking of a Tm-doped bulk laser near 2  $\mu\text{m}$  using a carbon nanotube saturable absorber," *Opt. Express* **17**, 11007 (2009).

[3] A. Schmidt, S. Y. Choi, D.-I. Yeom, F. Rotermund, X. Mateos, M. Segura, F. Diaz, V. Petrov, U. Griebner, "Femtosecond pulses near 2  $\mu\text{m}$  from a Tm:KLuW laser mode-locked by a single-walled carbon nanotube saturable absorber," *Appl. Phys. Express* **5**, 092704 (2012).

# LASER-MATTER INTERACTION

# Laser matter interaction in the relativistic regime to produce a high photon flux $K_{\alpha}$ Mo x-ray source.

Y. Azamoum, R. Clady, A. Ferré, O. Utéza and M. Sentis

*Aix –Marseille Univ, CNRS, LP3, Marseille, France.*

[Sentis@LP3.univ-mrs.fr](mailto:Sentis@LP3.univ-mrs.fr)

The interest towards developing intense and compact ultrashort x-ray sources is motivated by scientific applications like time-resolved x-ray diffraction or x-ray absorption spectroscopy [1], and societal applications such as phase contrast imaging for biology and medicine [2].

We will present an extended study of the absolute yield of  $K_{\alpha}$  x-ray source (17.48 keV) produced by interaction of an ultrahigh intensity femtosecond laser with a solid Mo target for laser temporal contrast ratios in the range of  $\sim 10^7$  -  $10^9$  and on three decades of intensity  $10^{16}$  -  $10^{19}$  W/cm<sup>2</sup>.

We demonstrate that for intensity  $I \geq 2 \times 10^{18}$  W/cm<sup>2</sup> the  $K_{\alpha}$  yield is independent of the value of the contrast ratio. Furthermore, at  $I = 10^{19}$  W/cm<sup>2</sup> the  $K_{\alpha}$  energy conversion efficiency reaches the same high plateau equal to  $\sim 2 \times 10^{-4}$  (in  $2\pi$  sr) for all the studied contrast ratios [3].

This original result suggests that the relativistic  $\mathbf{J} \times \mathbf{B}$  heating becomes the dominant absorption mechanism in these operating conditions where it is supposed to be insensitive to the electron density gradient scale length  $L/\lambda$ . An additional experimental study performed by changing the angle of incidence of the laser beam onto the solid target highlights a clear signature of the interplay between collisionless absorption mechanisms depending on the contrast ratio and intensity. Furthermore, a yield of  $\sim 2 \times 10^{10}$  photons/sr/s is obtained at 10 Hz and  $I \sim 10^{19}$  W/cm<sup>2</sup> [3]. Increasing the repetition rate of the driving laser source up to 100 Hz [4], we measure the highest molybdenum  $K_{\alpha}$  photon production reported to date corresponding to a  $K_{\alpha}$  photon flux of  $1 \times 10^{11}$  ph/(sr.s).

- [1] T. Elsaesser and M. Woerner, " Perspective: Structural dynamics in condensed matter mapped by femtosecond x-ray diffraction ", THE JOURNAL OF CHEMICAL PHYSICS, 140, 020901 (2014). <http://dx.doi.org/10.1063/1.4855115>.
- [2] R. Toth, J.C. Kieffer, S. Fourmaux, T. Ozaki, and A. Krol, "In-line phase-contrast imaging with a laser-based hard x-ray source", Review of Scientific Instruments 76, 083701 (2005). DOI: 10.1063/1.1989407.
- [3] Y. Azamoum, V. Tcheremiskine, R. Clady, A. Ferré, L. Charmasson, O. Utéza, and M. Sentis, "Impact of the pulse contrast ratio on molybdenum  $K_{\alpha}$  generation by ultrahigh intensity femtosecond laser solid interaction" Scientific Reports, 8, 4119 (2018). doi:10.1038/s41598-018-22487-3.
- [4] R. Clady, Y. Azamoum, L. Charmasson, A. Ferré, O. Utéza, and M. Sentis, " 22 W average power multiterawatt femtosecond laser chain enabling  $10^{19}$  W/cm<sup>2</sup> at 100 Hz" Applied Physics B, Lasers and Optics, 124, 89 (2018). <https://doi.org/10.1007/s00340-018-6958-1>.

# Optoelectronic Applications of Vanadium Dioxide

**N. Charipar, R.J. Suess, H. Kim, K. Charipar, S. Mathews, R.C.Y Auyeung, A. Piqué**

*Naval Research Laboratory, 4555 Overlook Ave. SW, Washington, DC, USA 20375*

*nicholas.charipar@nrl.navy.mil*

While the metal-insulator transition (MIT) of vanadium dioxide ( $\text{VO}_2$ ) has been known for decades[1], there has been a resurgence in interest due to advances in material synthesis that have produced materials with tailored properties such as a reduced MIT temperature. The large change in physical properties near the phase transition has made  $\text{VO}_2$  an attractive material for active devices such as optical switches, photoconductive emitters, and modulators. Devices that rely on electrically controlled Joule heating to generate an optical or electrical response are inherently slow (nanoseconds) due to the thermal mass and diffusion times in the  $\text{VO}_2$  films. This talk will focus on tuning the properties of vanadium dioxide for ultrafast optoelectronics. We demonstrate  $\text{VO}_2$ -based photoconductive terahertz emitters that illustrate the ultrafast optoelectronic switching properties of  $\text{VO}_2$  as well as the shortfalls of using canonical  $\text{VO}_2$  films grown on c-cut  $\text{Al}_2\text{O}_3$  [2]. The influence of strain and the use of near lattice matched substrates and buffer layers to modify the intrinsic film properties will also be discussed [3]. To this end, the phase transition dynamics of strained and relaxed  $\text{VO}_2$  films will be compared using an optoelectronic autocorrelation method that directly probes the electrical conductivity in response to an optical excitation with a temporal resolution on the order of 100 fs[4]. It will be shown that it is possible to modulate the electrical conductivity of  $\text{VO}_2$  by a factor of one hundred in less than 500 fs using strained films, opening new possibilities for optoelectronic devices based on this material.

- [1] F. J. Morin, "Oxides which show a metal-to-insulator transition at the Neel temperature," *Phys. Rev. Lett.* 3, 34-36, 1959.
- [2] N.A. Charipar, H. Kim, S.A. Mathews, and A. Piqué, "Broadband terahertz generation using the semiconductor-metal transition in  $\text{VO}_2$ ," *AIP Advances*, 6 (1), p. 015113, Jan. 2016.
- [3] E. Breckenfeld, H. Kim, K. Burgess, N.A. Charipar, S.-F. Cheng, R. Stroud, and A. Piqué, "Strain effects in epitaxial  $\text{VO}_2$  thin films on columnar buffer-layer  $\text{TiO}_2/\text{Al}_2\text{O}_3$  virtual substrates," *ACS Appl. Mat. & Interfaces* 9 (2), 1577-1584, Dec. 2016.
- [4] R.J. Suess, N.S. Bingham, K.M. Charipar, H. Kim, S.A. Mathews, A. Piqué, and N.A. Charipar, "Ultrafast Phase Transition Dynamics in Strained Vanadium Dioxide Films," *Advanced Materials Interfaces*, 4 (22), p. 1700810, Sep. 2017.

# Evidence of non collisional femtosecond laser electron heating in dielectric materials

**G. Duchateau<sup>1</sup>, B. Chimier<sup>1</sup>, S. Coudert<sup>1</sup>, E. Smetanina, L. Barilleau<sup>1</sup>, N. Fedorov<sup>1</sup>,  
P. Martin<sup>1</sup>, G. Geoffroy<sup>1</sup>, and V.T. Tikhonchuk<sup>1,2</sup>**

*1- Université de Bordeaux-CNRS-CEA, Centre Lasers Intenses et Applications, UMR 5107, 351 Cours de la Libération, 33405 Talence, France*

*2- ELI-Beamlines, Institute of Physics, Czech Academy of Sciences, 25241 Dolni Brezany, Czech Republic*

*Email address: guillaume.duchateau@u-bordeaux.fr*

The understanding and a theoretical/numerical description of the electron dynamics induced by femtosecond laser pulses in dielectric materials is crucial for various applications as material nano-structuration, writing of optical functionalities, non linear optics, damage, spectroscopy, etc. Indeed the material modifications are primarily due to the laser induced excitation and relaxation of electrons: when in the conduction band, the electrons undergo various collisional processes leading to a complex dynamics. This whole dynamics coupled to the pulse propagation lead to the laser energy deposition into the lattice, possibly inducing the previous material modifications.

The full electron dynamics including excitation and relaxation processes will be first described. It is addressed by solving the state-of-the-art Boltzmann kinetic equation which allows one to evaluate the energy distribution of conduction electrons. In addition to the standard collisional processes for energy transfer such as electron–phonon–photon and electron–electron interactions [1], a non-collisional process for photon absorption in the conduction band is included [2]. It relies on direct transitions between sub-bands of the conduction band through multiphoton absorption. This mechanism is theoretically shown to significantly contribute to the laser heating of conduction electrons for large enough laser intensities. It also increases the time required for the electron distribution to reach the equilibrium as described by the Fermi–Dirac statistics. Quantitative results will be provided for quartz irradiated by a femtosecond laser pulse with a wavelength of 800 nm and for intensities in the range of tens of TW/cm<sup>2</sup>, lower than the ablation threshold.

Actually, by using the previous laser parameters, electrons with unexpected energies in excess of 40 eV have been observed by using the photoemission spectroscopy (see [3] for first observations). The previous theoretical approach based on the Boltzmann kinetic equation is used to interpret these experimental observations. A direct comparison of experimental and numerical energy distributions shows that both electron heating in the bulk and a further laser field acceleration after ejection from the material contribute equivalently to the final electron energy gain. The electron heating in the bulk is further shown to be significantly driven by the non-collisional process, i.e. the direct multiphoton transitions between sub-bands of the conduction band. This work also sheds light on the contribution of the standard electron excitation/relaxation collisional processes, providing a new baseline to study the electron dynamics in dielectric materials and associated applications as laser material structuring.

[1] A. Kaiser, B. Rethfeld, M. Vicanek, and G. Simon, Microscopic processes in dielectrics under irradiation by subpicosecond laser pulses, *Phys. Rev. B* **61**, 11437 (2000).

[2] L. Barilleau, G. Duchateau, B. Chimier, G. Geoffroy and V. Tikhonchuk, Influence of non-collisional laser heating on the electron dynamics in dielectric materials, *J. Phys. D: Appl. Phys.* **49**, 485103 (2016).

[3] A. Belsky, P. Martin, H. Bachau, A. N. Vasil'ev, B. N. Yatsenko, S. Guizard, G. Geoffroy, and G. Petite, Heating of conduction band electrons by intense femtosecond laser pulses, *Europhys. Lett.* **67**, 301 (2004).

# Femtosecond ablation of optical crystals featured by long electron lifetime: experimental methods and contributing phenomena

**Sergey Klimentov<sup>1,2</sup>, Stéphane Guizard<sup>3</sup>, Nikita Fedorov<sup>4</sup>, Allan Bildé<sup>3</sup>,  
Alexandros Mouskeftraras<sup>2</sup>**

*1 National Research Nuclear University "MEPhI", Moscow, Russia*

*2 General Physics Institute of the Russian Academy of Sciences, Moscow, Russia*

*3 Laboratoire des Solides Irradiés, Ecole Polytechnique, Palaiseau, France,*

*3 Centre Lasers Intenses et Applications, Université Bordeaux I, Talence, France*

*smklimentov@mephi.ru*

Today laser technologies and high power optical engineering call for detailed knowledge of laser-matter interaction mechanisms resulting in breakdown and ablation of materials exposed to ultrashort laser pulses. These mechanisms are strongly dependent on variety of factors like parameters of laser pulses, environment and nature of the irradiated material. That explains why no universal laser damage mechanism is discovered up to now. In our study, we focus in interaction of femtosecond IR, visible and UV pulses with the oxide optical materials featured by relatively long, picosecond or subnanosecond, lifetime of free electrons generated in their conduction band by intense pulsed radiation in the vicinity of the breakdown threshold.

Multistage ultrafast photo-electron kinetics plays the clue role in deposition of energy into the lattice of a transparent dielectric resulting, in the long run, in breakdown or surface ablation. Crystalline sapphire and magnesium oxide are mostly in the scope of the research. These crystals can be considered as model materials due to their high initial transparency and lack of fast trapping in the conduction band which enables two-pulse experimental configurations where the first pulse in the couple is tailored to generate free electrons via simultaneous absorption of several quanta across the band gap, while the second aims to probe characteristics and mechanisms of intraband absorption. According to the goal of a particular experiment, pulsewidth, wavelength and delay between the two pulses were optimized or varied. Two-pulse ultrafast interferometry was used in the experiments for *in situ* monitoring of electron concentrations. Simultaneously, optical absorption induced by the first pulse in the excited domain on the surface was measured by means of the transmission imaging technique. Taking account of the fact that the main portion of energy acquired by the material and resulting finally in optical breakdown is deposited via transient absorption associated with the free electrons, variety of ablation thresholds was measured, in the same experimental conditions, for the second laser pulse at variation of electron concentration controlled by the first one in the couple. Energy of the electrons inside the conduction band, before and after the second "heating" laser pulse, was estimated in two-pulse photo-electron spectroscopy experiments. This way, the complete set of direct measurements was performed for quantitative characterization of all stages ending up at optical breakdown in these materials.

The obtained experimental data, estimations and the results of modeling, indicate the intraband absorption and the following electron-phonon relaxation to play the clue role in laser ablation of optical crystals known for long free electron lifetime. Cascade intraband transitions followed by relaxation of energy via electron-phonon coupling bring the lattice to thermal instability. In spite of popular opinion, no trace of ionization via impact was observed in the experiments.

This research received funding from LASERLAB-EUROPE (grant agreements 654148) and was partially supported by the Russian State Programs for Universities (projects 16.2969.2017/4.6 and 16.7917.2017/8.9)

# Experimental investigations of fundamental mechanisms involved in femtosecond laser modification of dielectric materials.

Stéphane Guizard<sup>1</sup>, Allan Bildé<sup>1</sup>, Sergei Klimentov<sup>2</sup>, Andrius Melninkaitis<sup>3</sup>,  
Julius Vaicenavicius<sup>3</sup>, Balys Momgaudis<sup>3</sup>, Nikita Fedorov<sup>4</sup>

1. *Laboratoire des Solides Irradiés, CEA/CNRS, Université Paris-Saclay, Ecole Polytechnique, 91128 Palaiseau, France,*
2. *General Physics Institute of the Russian Academy of Sciences, Vavilova St 38, 11991 Moscow, Russia.*
3. *Institute of Applied Research, Vilnius University, Sauletekio 10, 10223 Vilnius, Lithuania.*
4. *Laboratoire CELIA, Université Bordeaux-CEA/CNRS, Cours de la Libération, Talence, France.*

*stephane.guizard@cea.fr*

**Abstract:** The interaction of intense light pulses with transparent materials is a domain of research with a long history which is however more active than ever, and this revival concerns both applied science and fundamental research. It has been shown in the last decade that femtosecond lasers can be used to drill, ablate, cut, or more importantly, to permanently modify – in 3 dimensions - the optical properties of glasses, opening a broad field of applications. Very recently, other attractive domains have emerged, linked to the possibility to modulate, by using extremely short - few cycles- laser pulses, the optical or insulating properties of dielectric materials and to generate high order harmonics.

The shared issue of all this domain is a better knowledge of electronic excitation and relaxation processes in the solid during and immediately after the exciting pulse. It is a challenging task, due to the competition between many different elementary physical mechanism, all occurring at sub-picosecond or femtosecond time scale: electron phonon interaction, elastic and inelastic electron-electron scattering - including impact ionization, formation of transient or permanent defect states, exciton self-trapping, exciton-exciton interaction, etc. The direct observation of these processes is beyond the capacity of traditional time resolved femtosecond experiment due to a lack of temporal resolution. To go beyond this difficulty, we used a double pump scheme which allows to modulate independently the density and temperature of excited carriers. Then, using time resolved interferometry, we demonstrate directly for the first time the mechanism of carrier multiplication which leads to electronic avalanche in SiO<sub>2</sub>. The avalanche process is in competition with formation of self trapped exciton, which we could also observe with temporal and spatial resolution using time resolved digital holography. Finally, we show that avalanche is not observed in Al<sub>2</sub>O<sub>3</sub>. In this material we measured the time resolved in a wide dynamical range. We demonstrate that the decay of carriers is complex, depends on the initial carrier excitation density, and we show that it can be explained using a two steps relaxation model. Finally, in SiO<sub>2</sub>, using time resolved absorption with different polarization sensitivity, we demonstrate for the first time the influence of excited carriers on the damping time of coherently excited optical phonon, which is an indirect observation of electron-phonon collisions.

# Laser-ablative synthesis of nanophotonic materials for biomedical applications

**Irina N. Zavestovskaya**

*NRNU "MEPhI", Institute of Engineering Physics for Biomedicine (PhysBio), 115409 Moscow, Russia  
Quantum Radiophysics Department of P.N. Lebedev Physical Institute, Moscow, Russia  
E-mail address: [INZavestovskaya@mephi.ru](mailto:INZavestovskaya@mephi.ru)*

**Abstract:** This presentation will overview on-going activities of MEPHI's PhysBio institute on theoretical modeling of laser-matter processes leading to material nanostructuring and experimental implementation of different approaches to synthesize ultrapure photonic nanomaterials for variety of applications. We will also demonstrate applications of laser-synthesized nanomaterials in biomedicine.

Laser micro- and nanostructuring of materials is important in many scientific, technological and medical applications, as nanostructures formed by laser material processing have unique properties and often cannot be reproduced by other techniques. Our project is aimed at the improvement of our understanding of processes during laser-matter interaction, which lead to the formation of nanomaterials exhibiting unique photonic and other properties, as well as the use of these nanomaterials in biomedical tasks.

Here, by developing a series of analytical and numerical theoretical approaches we significantly advanced in clarifying physics of processes related to surface micro- and nanostructuring of metals and other materials by short and ultrashort laser pulses. Particular attention was paid to direct laser irradiation involving melting of the material (with or without ablation), followed by ultrafast surface solidification after the laser pulse. A physical model of metal nanoparticles fragmentation in liquids under the action of femtosecond laser pulses at the example of gold particles in water was introduced. The obtained data are used to optimize laser-ablative synthesis routes in order to achieve desirable characteristics of nanophotonic structures.

As experimental implementations, we use a plethora of laser synthesis methods to produce photonic nanomaterials with a particular emphasis on highly biocompatible nanoparticles (Si, Au, Ge), as well as tested these nanomaterials in biological models. As an example, we elaborated synthesis routes based on pulsed laser deposition (PLD) in residual gases (e.g. He) to form Si nanocrystal-based films exhibiting bright, long-decaying PL (QY > 5%) in the window of biological tissues transparency (750–900 nm). We further managed to mill Si nanocrystals by ultrasound to produce water-dispersible biodegradable Si-based QDs, and successfully used them as markers for bioimaging in cellular models. It is implied that laser-synthesized Si nanoparticles will be properly functionalized and applied in tasks of cancer imaging. We also actively use the technique of ultrashort (femtosecond, fs) laser ablation in liquids to produce Au, Si and composite nanostructures exhibiting promising photonic properties. This regime of fs laser ablation enables one to tune the mean size of produced NPs between 2-5 and hundreds of nm under fairly low size dispersion. We also demonstrated successful applications of nanostructures prepared by pulsed laser ablation in liquids in bioimaging (linear and non-linear) and therapy of cancer.

A physical model of gold nanoparticles (NPs) fragmentation in water under the action of femtosecond laser pulses is presented. When the colloids of relatively large gold NPs (several tens of nm) are irradiated by femtosecond laser pulses, one can observe their fragmentation into smaller NPs (up to several nm). The model of fragmentation is based on the electrolyzation of metal NPs heated by a laser pulse, and their division under the development of instability of a charged drop of liquid metal. The problem of gold NPs heating at femtosecond laser pulse absorption has been solved. The particle fragmentation parameter has been defined.

We examine absorption of electromagnetic radio-frequency (RF) radiation in aqueous suspensions of silicon and gold NPs and theoretically investigate the heat release in these systems. The absorption of RF radiation is considered in both bulk electrolyte and the region around the NPs. Simulations show a strong dependence of the heating rate on electrical conductivity of the electrolyte rather than on that of NPs properties.

The obtained results demonstrate that non-toxic, biodegradable Si-based nanomaterials are promising for applications in both medical diagnostics and therapy.

The work was partially supported by the Russian State Programs for Universities (projects 16.2969.2017/ПЧ and 16.7917.2017/БЧ).

# Effects of spatiotemporal coupling in ultrashort laser pulses upon volumetric modification of transparent dielectrics

Nadezhda M. Bulgakova<sup>1</sup>, Vladimir P. Zhukov<sup>1,2</sup>, Selçuk Aktürk<sup>3</sup>

<sup>1</sup>HiLASE Centre, Institute of Physics of the Czech Academy of Sciences, Za Radnicí 828, 25241 Dolní Břežany, Czech Republic

<sup>2</sup>Institute of Computational Technologies SB RAS, 6 Lavrentyev Ave., 630090 Novosibirsk, Russia

<sup>3</sup>Eğercili Mah., Gokler Sok. 9-2, Çarşamba, Samsun, Turkey

bulgakova@fzu.cz

A remarkable phenomena of 3D direct laser writing inside transparent materials is writing anisotropy that is a dependence of modification structure on laser scanning direction [1,2]. This effect is usually attributed to the beam pulse front tilt (PFT) [3]. It is believed that the key parameters, which lead to the observed anisotropies, are the angle between the PFT and scanning direction as well as between the PFT and light polarization [1,2]. However, mechanisms of this phenomenon, which can strongly affect processing quality, are still hidden. Ultrashort laser pulses are usually described, assuming that the spatial and time dependences of the electric field are separable. But generally, spatial and temporal coordinates of ultrashort beams are coupled, resulting in the beam distortions [3].

In this work, we have studied the dynamics of propagation of ultrashort focused laser pulses with spatiotemporal coupling through transparent medium (fused silica), based on Maxwell's equations supplemented by the equations for hydrodynamics of free electron plasma [4]. To account for the PFT, which implies cylindrical asymmetry of the beam, the model was reduced to the 2D ("laser knife") geometry, thus enabling to get qualitative insights to the PFT effects while overcoming the requirements of extremely large computational resources [5]. The "laser knife" model allows simulations of multi-pulse irradiation regimes with scanning the solid sample across the laser beam.

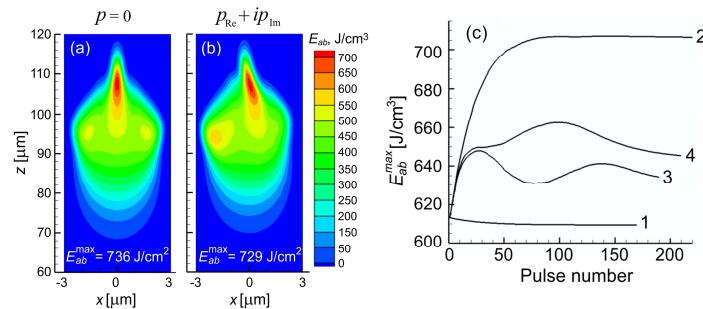


Fig. 1. (a),(b) Distributions of the absorbed laser energy density after single laser beam propagation through the focal region located at 120  $\mu\text{m}$  inside fused silica glass. The laser pulses propagated from the bottom. The parameters of the Gaussian laser beams: pulse energy of 2.4  $\mu\text{J}$ , pulse duration 73 fs, beam waist is 1  $\mu\text{m}$ . (a) Pulse front tilt  $p = 0$ ; (b)  $p = p_{\text{Re}} + i p_{\text{Im}} = -1 + i 0.8$  fs/ $\mu\text{m}$  at  $z = 0$  (sample surface) [3]; (c) Dependences of  $E_{\text{ab}}^{\text{max}}$  on number of the pulses with the laser parameters as in (b). Lines 1 and 2 correspond to a stationary target without and with accounting refractive index change due to defect accumulation. Lines 3 and 4 were obtained with shifting the sample between successive pulses perpendicular to the pulse propagation by 50 nm to the right and to the left respectively.

A series of simulations performed for fused silica as an example at different irradiation conditions (laser pulse energy and duration, PFT parameters, spatial chirp, single and multiple pulse action, scanning speed and direction for laser writing regime) have confirmed an important role of the PFT in the volumetric laser processing of transparent materials and enabled to reveal the roles of different factors in localized absorption and energy coupling strength (Fig. 1). Numerical results reproduce such experimental peculiarities as violation of axial symmetry of laser energy absorption and the effect of directional asymmetry in direct laser writing.

- [1] P. G. Kazansky, W. Yang, E. Bricchi, "Quill" writing with ultrashort light pulses in transparent materials," *Appl. Phys. Lett.* **90**, 151120 (2007).
- [2] D. N. Vitek, E. Block, Y. Bellouard, D. E. Adams, S. Backus, D. Kleinfeld, C. G. Durfee, J. A. Squier, "Spatio-temporally focused femtosecond laser pulses for nonreciprocal writing in optically transparent materials," *Opt. Express* **18**, 24673-24678 (2010).
- [3] S. Aktürk, X. Gu, P. Bownan, R. Trebino, "Spatio-temporal couplings in ultrashort laser pulses," *J. Opt.* **12**, 093001 (2010).
- [4] N. M. Bulgakova, V. P. Zhukov, Y. P. Meshcheryakov, "Theoretical treatments of ultrashort pulse laser processing of transparent materials: Towards understanding the volume nanograting formation and 'quill' writing effect," *Appl. Phys. B* **113**, 437-449 (2013).
- [5] V. P. Zhukov, N. M. Bulgakova, "Asymmetry of light absorption upon propagation of focused femtosecond laser pulses with spatiotemporal coupling through glass materials," *Proc. SPIE* **10228**, 102280D (2017).

# Nanoscale processing using ultrafast laser engineered beams.

**R. Stoian**

1- Laboratoire Hubert Curien, CNRS UMR 5516, Université Jean Monnet, 42000 St Etienne, France

razvan.stoian@univ-st-etienne.fr

Nowadays micro/nano- technologies are dependent on the development of processing tools able to structure materials in two- and three-dimensions with utmost precision. Ultrafast lasers can take up ambitious processing challenges where energy localization is critical. An interesting perspective is related to the field of photonics, notably the development of optical devices based on laser-induced 3D refractive index engineering. Ultrafast laser photoinscription can confine energy in micro-domains of arbitrary geometries, modifying the material refractive index and laying down the concept of 3D design for efficient optical functions. Here nanoscale precision can deliver high levels of performance. Therefore bypassing the diffraction limit is key for a new range of applications in optics and mechanics requiring optical access to the nanoscale. Exploiting the nonlinearity of excitation, ultrashort laser pulses show remarkable capacity to localize light on subwavelength scales, building up on collective carrier effects on surfaces and in the bulk. Control of laser interaction by beam design can drive selected physical paths and geometries and we focus here on structural evolutions and dimensional scales enabled by spatio-temporal beam shaping [2]. Sculpting beams in space and time can bring advantages for controlling the interaction between light and matter and for ensuring correct energy delivery to the impact point. Beam engineering controls propagation by acting on various self-induced nonlinear phenomena (self-focusing, defocusing) or by correcting wavefront distortions and the geometry of excitation. We will discuss physical mechanisms of photoinscription, outlining the possibility of refractive index engineering. We will follow the dynamics of electronic excitation in confinement conditions and point out characteristic times of energy deposition, serving as guidelines for control. We will equally explore the influence of pulse temporal and spatial design in achieving index structures on scales approaching 100 nm, either in direct focusing or in self-organization schemes in model fused silica. Non-diffractive beam excitation can take advantage of this localization and achieve unprecedented high aspect ratio structuring with aspect ratios in excess of 1000 [3-5]. Subsequently we will present different photoinscription schemes and pinpoint their potential to generate photonic systems where hybrid micro/nanoscale features can develop advanced optical functionalities. Finally we indicate a range of applications, from telecom to astrophotonics. We will discuss specifically applications designed for the mid-IR spectral range, which have a strong potential in sensing and imaging [6,7]. Light transport can be efficiently achieved with large area modes and field distributions can be non-perturbatively accessed.

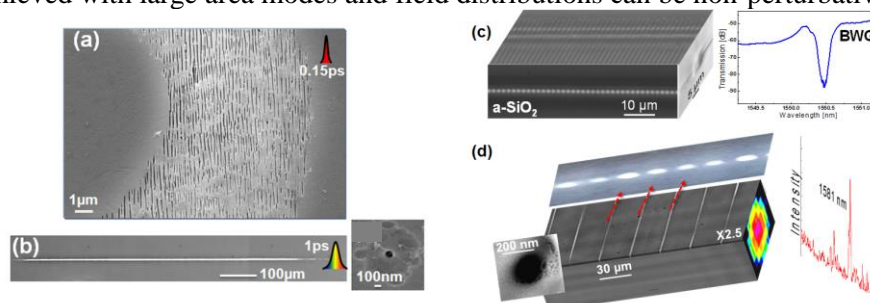


Fig 1. (a,b) Laser-induced bulk nanostructures. (a) Periodic nanostructures. (b) Volume nanostructuring using non-diffractive beams. (c,d) Photonic systems with hybrid 3D micro/nanostructures. (c) Bragg sensor. (d) Embedded spectrometer with evanescent field read-out.

1. K. Sugioka and Y. Cheng, Ultrafast lasers-reliable tools for advanced materials processing, *Light: Sci. Appl.* 1, e149 (2014).
2. R. Stoian, M. Wollenhaupt, T. Baumert, and I.V. Hertel, Temporal pulse tailoring in ultrafast laser manufacturing technologies, *Laser Precision Microfabrication*, Eds: K. Sugioka, M. Meunier, A. Piqué. (Springer Verlag, Heidelberg) 135, 121-144 (2010).
3. M. Bhuyan, P.K. Velpula, J.P. Colombier, T. Olivier, N. Faure, and R. Stoian, Single-shot high aspect ratio bulk nanostructuring of fused silica using chirp-controlled ultrafast laser Bessel beams, *Appl. Phys. Lett.* 104, 021107 (2013).
4. P.K. Velpula, M.K. Bhuyan, F. Courvoisier, H. Zhang, J.P. Colombier, and R. Stoian, Spatio-temporal dynamics in nondiffractive Bessel ultrafast laser nanoscale volume structuring *Laser Photon. Rev.* 10, 230-244 (2016).
5. M. K. Bhuyan, M. Somayaji, A. Mermillod-Blondin, F. Bourquard, J.P. Colombier, and R. Stoian, Ultrafast laser nanostructuring in bulk silica, a slow microexplosion, *Optica* 4, 951-958 (2017)
6. G. Martin, M.K. Bhuyan, J. Troles, C. D'Amico, R. Stoian, and E. Le Coarer, Near infrared spectro-interferometer using femtosecond laser written GLS embedded waveguides and nano-scatterers *Opt. Express* 25, 8386 (2017).

# Laser microstructuring of titanium surface to improve implants biocompatibility

**V. P. Veiko<sup>1</sup>, Y. Y. Karlagina<sup>1</sup>, G. V. Odintsova<sup>1</sup>, V. V. Romanov<sup>1</sup>,  
R. M. Yatsuk<sup>1</sup>, D. S. Kuznetsova<sup>2</sup>**

<sup>1</sup>*ITMO University, 49 Kronverksky Pr., St. Petersburg, 197101, Russia*

<sup>2</sup>*Institute of Biomedical Technologies Privolzhsky Research Medical University*

*Main author email address: vadim.veiko@mail.ru*

Implant survival rate is among of the essential problems of modern dentistry. It was established that the key factors affecting the biocompatibility and osseointegration of the implant in the recipient organism are the morphology and chemical composition of the surface [1]. Structured implants with a porous surface have stronger bonding at the bone-implant site due to contact area increase, and porosity promotes the adhering of bone tissue into the implant. The surface structure of the implant should keep both a microrelief for cells engagement and a nanorelief for smaller biological objects, for example, proteins [2]. To enhance implant surface fouling with cellular elements and wetting with biological fluids it has to be hydrophilic. Existing methods of surface structuring (abrasive jet, hydrothermal, alkaline treatment and anodic micro arc oxidation) are not able to provide a sufficiently considerable and multiscale surface relief, as well as the necessary cleanliness factor of the surface. Laser processing offers new opportunities for the control of surface morphology and structural-phase composition.

The work objective is to determine correlations between the relief and the structural and chemical composition of the surface of titanium dental implants after laser treatment and their biocompatibility with various biological objects (Fig. 1). The impact of surface relief and chemical composition after exposure by nanosecond laser pulses on the bio-integration of stem mesenchymal stromal cells of the human bone marrow was studied. It is demonstrated that structures with sizes comparable to biological objects size provide better viability and adhesion of cultured cells. An increase of laser intensity within the range of 30-250 MW/cm<sup>2</sup> and spatial overlapping of laser pulses results in a decrease of wetting angle and the formation of a 6Al-4V titanium super-hydrophilic surface.

The reported study was financially supported by the Ministry of Education and Science of Russia, research agreement №14.587.21.0197 (RFMEFI57816X0197).

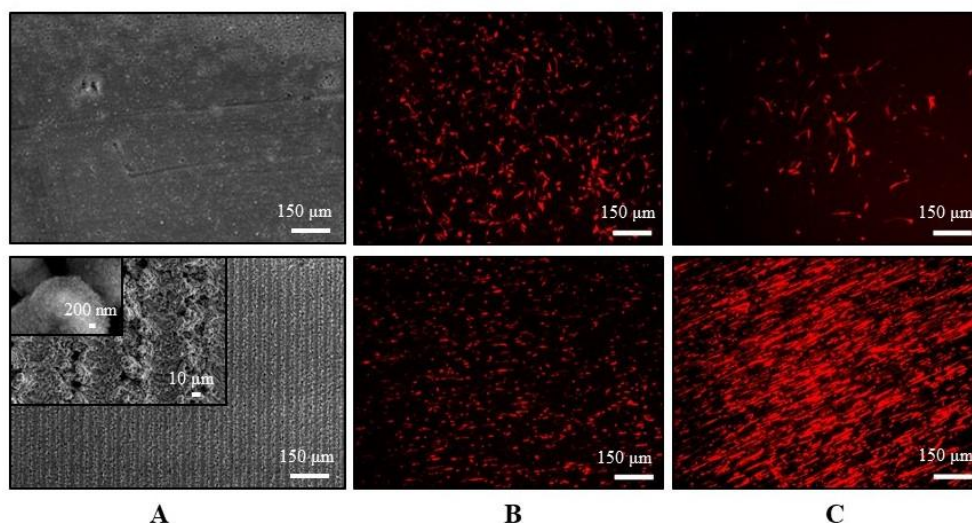


Fig. 1. SEM images of a 6Al-4V titanium surface before and after laser exposure (A). Stem MSC of the bone marrow after one day (B) and seven days (C) of aging on the obtained structure

[1] D.J. Cohen, A. Cheng, K. Sahingur, R.M. Clohessy, L.B. Hopkins, B.D. Boyan, & Z. Schwartz, Performance of laser sintered Ti-6Al-4V implants with bone-inspired porosity and micro/nanoscale surface roughness in the rabbit femur, *Biomedical Materials*, vol. 12, № 2, pp. 025021, (2017).

[2] R. A. Gittens, L. Scheideler, F. Rupp, S. L. Hyzy, J. Geis-Gerstorfer, Z. Schwartz, B. D. Boyan, A review on the wettability of dental implant surfaces II: biological and clinical aspects, *Acta biomaterialia*, vol. 10, № 7, pp. 2907-2918, (2014).

# Nanostructured plasmonic metamaterials for ultrasensitive optical biosensing

**A. V. Kabashin**

*Aix Marseille Univ, CNRS, LP3, 13288, Marseille, France*

*MEPhI, Institute of Engineering Physics for Biomedicine (PhysBio), 115409 Moscow, Russia*

Within last 15 years, plasmonic biosensing has become a leading label-free technology for studies of biological binding events between a target analyte and its corresponding selective receptor immobilized on the gold surface with a variety of applications in biomedicine, food and environmental safety, security. Using excitations of surface plasmons over a thin gold film in ATR geometry, Surface Plasmon resonance (SPR) is known as a conventional implementation of plasmonic biosensing technology [1]. An extension of SPR called localized plasmon resonance (LPR) employs metallic nanostructures and thus makes possible an excellent compatibility of the sensor transducer with modern bio-molecular nano-architectures [2]. The detection limit of SPR and LPR in terms of resolvable surface coverage of biomaterial is of the order of 1 pg/mm<sup>2</sup> and 1 ng/mm<sup>2</sup>, respectively, which makes possible label-free studies of many interactions, but still inferior to labeling methods by more than 2 orders of magnitude.

Our project is aimed at the improvement of sensitivity of plasmonic biosensors. To reach this objective, we recently introduced the concept of “plasmonic metamaterial for biosensing”, which was defined as “artificial material, composed of nanoscale gold blocks (metaatoms) with nanoscale distance between them, which can provide a much improved response compared to natural plasmonic materials (Au, Au) and/or enable new functionalities” [3]. One of geometries of such metamaterial uses a “forest” of long gold nanorods, oriented perpendicularly to the glass substrate. Such plasmonic nanorod metamaterial is capable of supporting a new guided mode, which propagates over discontinuous “forest” structure and in terms of sensitivity (> 30000 nm/RI units) outperforms both localized plasmon resonance (LPR) [2] and surface plasmon resonance (SPR) [1] biosensors. Another promising metamaterial is based on a periodic array of gold nanodots (~100 nm in size), which makes possible the excitation of diffraction-coupled localized plasmons, leading to a drastic narrowing of resonance width and nearly zero light intensity in it (“light darkness”) [4,5]. As a consequence of this darkness, phase of light starts to experience singularities [6,7], which can be used to improve an areal mass sensitivity down to the record 1 fg/mm<sup>2</sup> level corresponding to singular molecule label-free detection [4]. We also for the first time explored the excitation of plasmons in 3D plasmon crystal metamaterials and reported the observation of a guiding plasmon mode, providing extremely high spectral sensitivity to refractive index variations [8]. We finally proposed novel graphene-gold metasurface architectures, which render possible the improvement of sensor response in conventional SPR due to the concentration of local electric field on the graphene sheet and specific graphene-related chemistry [9]. Depending on a concrete biosensing task, the metamaterials can be designed either to record several binding events (a way toward ultimate label-free single molecular detection) or to enable large surface coverage in order to improve integral sensitivity. Combined with tuneable spectral response and strong local field enhancement, the designed biosensors outperform conventional plasmonics-based counterparts and open up new opportunities for the advancement of label-free biosensing technology.

- [1] B. Liedberg, C. Nylander and I. Lundstrom, *Biosens. Bioelectron.* Vol. 10, pp. i-ix (1995).
- [2] J. N. Anker, W. P. Hall, O. Lyandres, N. C. Shah, J. Zhao, R. P. Van Duyne, *Nature Mater.* Vol. 7, pp. 442-453 (2008).
- [3] A. V. Kabashin, P. Evans, S. Patskovsky, G. Wurtz, W. Hendren, W. Dickson, R. J. Pollard, V. Podolsky and A. V. Zayats, *Nature Mater.*, Vol. 8, pp. 867-871 (2009).
- [4] V. G. Kravets, F. Schedin, R. Jalil, L. Britnell, R. V. Gorbachev, D. Ansell, B. Thackray, K. S. Novoselov, A. K. Geim, A. V. Kabashin, and A. N. Grigorenko, *Nature Mater.*, Vol. 12, pp. 304-309 (2013).
- [5] A. Danilov, G. Tselikov, F. Wu, V. G. Kravets, I. Ozerov, F. Bedu, A. Grigorenko, A. Kabashin, *Biosens. Bioelectron.* Vol. 104, pp. 102-112 (2018).
- [6] A. V. Kabashin, S. Patskovsky, A. N. Grigorenko, *Opt. Express*, Vol. 17, pp. 21191-21204 (2009).
- [7] Y. H. Huang, H.-P. Ho, K. S. Kong and A. V. Kabashin, *Annal. der Physik*, Vol. 524, pp. 637-662 (2012).
- [8] A. I. Aristov, M. Manousidaki, A. Danilov, K. Terzaki, C. Fotakis, M. Farsari and A. V. Kabashin, *Sci. Reports*, Vol. 6, pp. 25380 (2016)
- [9] S. Zeng, K. V. Srekanth, J. Shang, T. Yu, C.-K. Chen, F. Yin, D. Baillargeat, P. Coquet, H.-P. Ho, A. V. Kabashin and K.-T. Yong *Adv. Mater.*, 27, 6163 (2015).

# 3D Microfluidic SERS Chips Fabricated by All-Femtosecond-Laser-Processing

**K. Sugioka<sup>1</sup>, S. Bai<sup>1,2</sup>, and A. Hu<sup>2,3</sup>**

*1- RIKEN Center for Advanced Photonics, RIKEN, Wako, Saitama 351-0198, Japan*

*2- Institute of Laser Engineering, Beijing University of Technology,  
100 Pingle Yuan, Beijing 100124, People's Republic of China*

*3- Department of Mechanical Aerospace and Biomedical Engineering,  
University of Tennessee Knoxville, 1512 Middle Drive, Knoxville, TN 37996, USA*

*Main author email address: ksugioka@riken.jp*

We propose a novel all-femtosecond-laser-processing technique fabricating three-dimensional (3D) microfluidic surface-enhanced Raman scattering (SERS) chips for highly sensitive real-time sensing of toxic substances [1]. Figure 1 shows the fabrication procedure of the SERS chips; (a), (b) 3D glass microfluidic channels are fabricated by femtosecond-laser-assisted wet etching (FLAE: femtosecond laser direct writing followed by thermal treatment and successive wet chemical etching in a hydrofluoric solution). (c), (d) FLAE is then followed by the space-selective formation of Cu-Ag layered thin films inside the microfluidic structure via femtosecond laser direct writing ablation and electroless metal plating. (e) The deposited Cu-Ag films are subsequently nanostructured by irradiation with linearly polarized beams to form periodic surface nanostructures. This work demonstrated that a double exposure to laser beams having orthogonal polarization directions can generate 2D arrays of layered Cu-Ag nanodots with dimensions as small as 25% of the laser wavelength (1045 nm) and a gap of  $\sim 50$  nm between each nanodot. The resulting SERS microchip was able to detect Rhodamine 6G, exhibiting an enhancement factor of  $7.3 \times 10^8$  in conjunction with a relative standard deviation of 8.88%. This 3D microfluidic chip was also found to be capable of the real-time SERS detection of  $\text{Cd}^{2+}$  ions at concentrations as low as 10 ppb in the presence of crystal violet. This technique shows significant promise for the fabrication of high performance microfluidic SERS platforms for the real-time sensing of toxic substances with ultrahigh sensitivity.

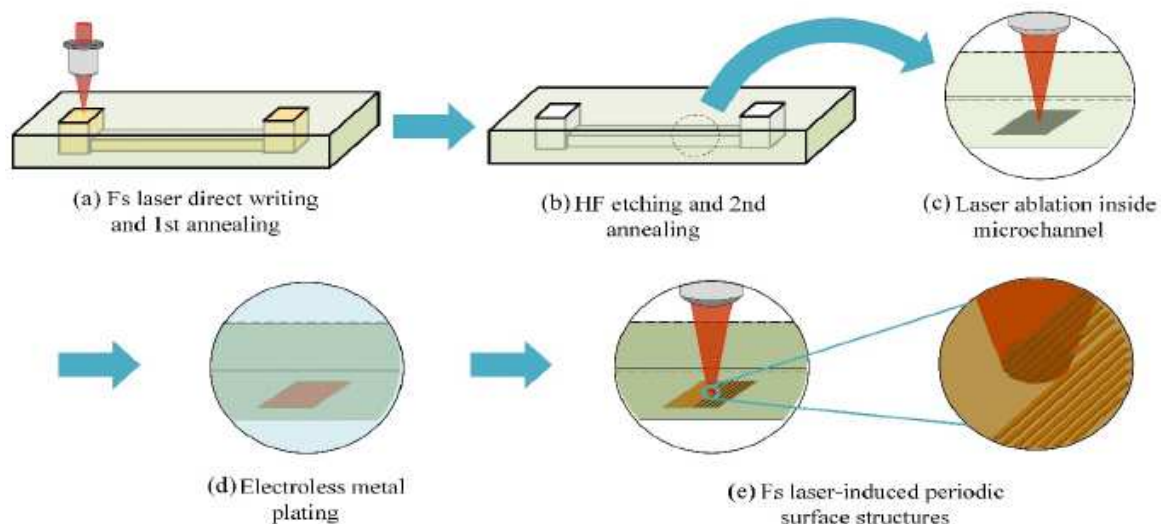


Fig. 1. Procedure used to fabricate a 3D microfluidic SERS chip by all-femtosecond-laser-processing.

[1] S. Bai, D. Serien, A. Hu, and K. Sugioka, "Three-dimensional microfluidic SERS chips fabricated by all-femtosecond-laser-processing for real-time sensing of toxic substances", *Adv. Func. Mater.* **28**, 1706262 (2018).

# High-Throughput Microfabrication by Ultrashort Laser Pulses

**A. Ionin<sup>1</sup>, S. Kudryashov<sup>1,2</sup>, P. Danilov<sup>1</sup>, N. Smirnov<sup>1</sup>, E. Ageev<sup>2</sup>,  
A. Samokhvalov<sup>2</sup>, T. Itina<sup>2</sup>, V. Veiko<sup>2</sup>, A. Porfirev<sup>3</sup>, S. Khonina<sup>3</sup>**

*1- Lebedev Physical Institute, Moscow, Russia*

*2- ITMO University, St. Petersburg, Russia*

*3- IPSI RAS – Branch of the FSRC “Crystallography and Photonics” RAS, 443001 Samara, Russia*

*aion@sci.lebedev.ru*

High-throughput laser micromachining by ultrashort (femto-picosecond) laser pulses was explored in terms of optimal pulsewidth and fluence, efficient pulse energy utilization via beam multiplexing by means of diffractive optical elements (spatial splitting) and ultrafast laser scanning speeds in order to employ the available multi-MHz repetition rates [1] (Fig.1). The underlying physical processes and ablation mechanisms were overviewed [2].

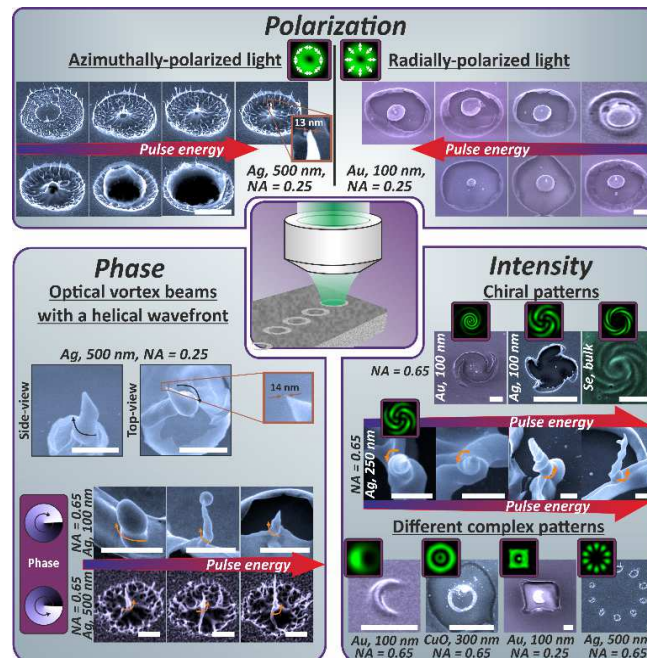


Fig.1. Ultrafast laser printing of intricate plasmonic nanoelements

Optimal pulse separation in their trains and bursts (MHz-THz) was explored by means of our pump/probe and double-pump-laser ablation studies [3], indicating the most efficient operation window for various ablation mechanisms, emerging on different – from sub-ps till sub-ns – temporal scales.

Large-scale advanced anti-fouling nanopatterns were printed by MHz-rate fs-laser pulses using the previous technical advances.

This research was supported by the Russian Science Foundation (Project № 18-15-00220).

[1] A. Kuchmizhak, A. Porfirev, S. Syubaev, P. Danilov, A. Ionin, O. Vitrik, Yu. Kulchin, S. Khonina, S. Kudryashov, Multi-beam pulsed-laser patterning of plasmonic films using broadband diffractive optical elements, *Optics Letters*, vol. 42, pp. 2838-2831 (2017).

[2] A. Ionin, S. Kudryashov, A. Samokhin, Material surface ablation produced by ultrashort laser pulses, *Physics-Uspekhi*, vol. 60, pp. 149-160 (2017).

[3] S. Kudryashov and A. Ionin, Multi-scale dynamics of front-side femtosecond laser heating, melting and ablation of thin supported aluminum film, *International Journal of Heat & Mass Transfer*, vol. 99, pp. 383-390 (2016).

# Laser-pumping-based control of dielectric properties of dispersive nanosystems in the optical range

Dmitry A. Zimnyakov<sup>1,2</sup>, Sergey A. Yuvchenko<sup>1</sup>, Sergey S. Volchkov<sup>1</sup>

<sup>1</sup> Yury Gagarin State Technical University of Saratov, 77 Polytechnicheskaya st., 410054, Saratov, Russia

<sup>2</sup> Precision Mechanics and Control Institute of the Russian Academy of Sciences, 24 Rabochaya st. 410024, Saratov, Russia

Interaction of the high-power laser radiation with semiconductor and semi-metallic nanoparticles in the absorption bands of particle materials causes significant changes in the density of electronic states due to photoinduced interband transitions. This leads to changes in the real and imaginary parts of the effective dielectric function of nanoparticle material and manifests itself in the dependencies of the scattering and absorption efficiencies on the pumping light intensity. Pumping-induced variations of the effective dielectric function are governed not only by the rate of interband transitions but also other factors affecting the density of states (the electron trapping by surface and bulk defects, ground state depletion, etc). A variety of physical mechanisms that control charge transfer in laser-pumped nanoparticles makes the effective dielectric functions of particles dependent not only on the pumping light intensity but also on the pumping duration and the detuning of the light frequency from the frequency of maximal absorption. Analysis of these dependences using appropriately chosen kinetic models can provide the comprehensive information about the structure of electron states of the probed nanoparticles. Besides, this opens up the possibility of sufficiently flexible control of optical properties of dispersive nanosystems with the use of laser pumping.

We present the results of application of this approach to various dispersive nanosystems prepared on the base of semiconductor and semi-metallic nanoparticles (titanium dioxide, molybdenum dicilicide, hybrid Si/SiO<sub>x</sub> nanoparticles, etc.). A multi-wave z-scan technique combined with simultaneous measurements of the scattered light intensity [1,2] was applied to recover dependencies of the effective dielectric functions of the probed nanosystems on the parameters of laser pumping (the intensity of a single laser pulse, the pumping duration, and the frequency detuning). The recovery procedure [1] is based on solution of the system of equations establishing the relationships between the real and imaginary part of the dielectric function and measured values of the intensities of scattered and transmitted light. It is resulted in the parametric presentation of the effective dielectric functions (the modified Cole-Cole diagrammatic technique). A kinetic model describing the influence of various charge transfer channels on the real and imaginary parts of the effective dielectric function is presented.

This work was supported by grant # 16-19-10455 from the Russian Science Foundation.

[1] D.A. Zimnyakov and S.A. Yuvchenko, Effective dielectric function of TiO<sub>2</sub> nanoparticles under laser pumping in the fundamental absorption band, *Quantum Electronics*, 47, pp. 547-552 (2017).

[2] D.A. Zimnyakov, S.A. Yuvchenko, and N.S. Markova, Dielectric function of TiO<sub>2</sub> nanoparticles under laser pumping, *Proc. SPIE*, 10336, pp. 1033619-1 -1033619-6 (2017).

# Improved laser glass cutting by spatio-temporal control of energy deposition using bursts of femtosecond pulses

**K. Mishchik<sup>1</sup>, B. Beuton<sup>2</sup>, O. Dematteo-Caulier<sup>2</sup>, S. Skupin<sup>2,3</sup>, B. Chimier<sup>2</sup>,  
G. Duchateau<sup>2</sup>, B. Chassagne<sup>4</sup>, R. Kling<sup>4</sup>, C. Hönninger<sup>1</sup>, E. Mottay<sup>1</sup>, J. Lopez<sup>2</sup>**

*1- Amplitude Systèmes, 11 avenue de Canteranne, 33600 Pessac, France*

*2- Université Bordeaux CNRS CEA, CELIA UMR 5107, 33405 Talence, France*

*3- Institut Lumière Matière, UMR 5306 Université Lyon CNRS, Université de Lyon, 69622 Villeurbanne, France*

*4- ALPhANOV, rue François Mitterrand, 33400 Talence, France*

*Main author email address: kmishchik@amplitude-systemes.com*

Glass cutting is a subject of high interest for flat panel display and consumer electronics industries. In comparison to diamond tool-based or laser-based existing solutions, ultrafast lasers appear as a promising technology allowing to produce various complex cutting 2D and 3D shapes without direct contact of a cutting tool with glass material. Better quality and higher precision of cuts can be achieved since this laser technology has the unique capacity to produce highly localized bulk modification due to non-linear absorption [1, 2]. However, several key issues dealing with spatio-temporal energy deposition must be considered for glass cutting. Indeed, we need an elongated bulk modification along the glass thickness in order to induce a cleaving phenomenon that can propagate along the laser beam trajectory. We need also a fine control of micro cracking orientation. Finally, scalability of the cutting process on brittle and heat-sensitive transparent materials must be possible using high repetition rate and high average power.

In this communication we report on experimental results and corresponding theoretical analysis dealing with elongated bulk modification into glass material using femtosecond laser operating in burst mode [3]. The intense and elongated bulk modification is obtained combining a customized non-diffractive Gaussian-Bessel beam shaping [4, 5, 6] with bursts of femtosecond pulses [3, 7]. These experimental observations are supported by multi-scale modelling the key physical mechanisms leading to permanent modifications into the glass through local heating [3, 8]. To start with, non-linear beam propagation based on non-linear optical Schrödinger equation, including Kerr effect and light defocusing, have been considered. Thereafter, energy deposition via nonlinear photoionization mechanisms was calculated. The resulting energy density map is then used as a source term in a heat equation to compute the evolution of the thermal distribution [3, 8] and to estimate the stress leading to crack generation.

- [1] R. Gatass and E. Mazur, Femtosecond laser micromachining in transparent materials, *Nature Photonics*, Vol. 2, 219-225 (2008)
- [2] P.K. Velpula, M.K. Bhuyan, C. Mauclair, J.P. Colombier and R. Stoian, Role of free carriers excited by ultrafast Bessel beams for submicron structuring applications, *Opt. Eng.*, Vol. 53, Issue 7, 0761081-0761086 (2014)
- [3] K. Mishchik, R. Beuton, O. Dematteo Caulier, S. Skupin, B. Chimier, G. Duchateau, B. Chassagne, R. Kling, C. Hönninger, E. Mottay and J. Lopez, Improved laser glass cutting by spatio-temporal control of energy deposition using bursts of femtosecond pulses, *Opt. Expr.*, Vol. 25, No. 26, 33271-33282 (2017)
- [4] M. K. Bhuyan, O. Jedrkiewicz, V. Sabonis, M. Mikutis, S. Recchia, A. Aprea, M. Bollani, and P. Di Trapani, "High-speed laser-assisted cutting of strong transparent materials using picosecond Bessel beams, *Appl. Phys. A*, Vol. 120, 443 - 446 (2015)
- [5] F. Courvoisier, R. Stoian and A. Couairon, Ultrafast laser micro and nano processing with non-diffracting and curved beams, *Opt. Laser & Techn.*, Vol. 80, 125-137 (2016)
- [6] K. Mishchik, B. Chassagne, C. Javaux-Léger, C. Hönninger, E. Mottay, R. Kling, and J. Lopez, Dash line glass-and sapphire-cutting with high power USP laser, in *Proceedings of SPIE*, Vol. 9740, 97400 (2016)
- [7] K. Bergner, L. Müller, R. Klas, J. Limpert, S. Nolte and A. Tünnermann, Scaling ultrafast laser pulse induced glass modifications for cleaving applications, *Appl. Opt.*, accepted in June 2018
- [8] O. Dematteo-Caulier, K. Mishchik, B. Chimier, S. Skupin, A. Bourgeade C. Javaux-Léger, R. Kling, C. Hönninger, J. Lopez, V. Tikhonchuk, and G. Duchateau, Femtosecond laser pulse train interaction with dielectric materials, Vol. 107, 181110 (2015)

# Laser synthesis of 2D structures with variable band gap for thermo-photo sensors with high sensitivity received in the reaction of chromium atoms with methane molecules

**S.A. Mulenko<sup>1</sup>, N.A. Skoryk<sup>1</sup>, N. Stefan<sup>2</sup>, I.N. Mihailescu<sup>2</sup>, V. M. Popov<sup>3</sup>, N.T. Gorbachuk<sup>4</sup>**

*1-G.V. Kurdyumov Institute for Metal Physics NAS of Ukraine, 36, Academician Vernadsky Blvd., UA-03142, Kiev-142, Ukraine*

*2-National Institute for Laser, Plasma and Radiation Physics, PO Box MG-54, RO-77125, Magurele, Romania*

*3-Institute for Microdevices NAS of Ukraine, 3, Severo-Syretskaya, UA-04136, Kiev-136, Ukraine*

*4-Kiev State University of Technology and Design, UA-03011, Kiev-11, Ukraine*

*Main author email address: mulenko@ukr.net*

The reactive pulsed laser deposition (RPLD) based on a KrF-laser ( $\lambda = 248$  nm) and laser (light) chemical vapour deposition (LCVD) based on InGaN photodiode ( $\lambda = 360$  nm) were used before for photon synthesis of iron oxide and chromium oxide 2D structures, 2D heterostructures and their applications for thermo-photo-chemical sensors [1-6].

Here, RPLD based on a KrF laser was used for the synthesis of 2D structures with variable band gap received in the reaction of chromium (Cr) atoms with methane (CH<sub>4</sub>) molecules. Synthesized 2D structures were deposited on 293 or 800 K <100> Si substrate at CH<sub>4</sub> pressure changing in the range 1.0-3.0 Pa. The thickness of these structures was 30-90 nm depending on substrate temperature and CH<sub>4</sub> pressure in the reactor. XRD analysis confirmed amorphous or polycrystalline structure of these deposits. Element analysis was carried out by an energy dispersive X-ray spectroscopy (EDXS). All synthesized 2D structures demonstrated semiconductor temperature trend with variable energy band gap ( $E_g$ ) in the range 0.45-2.1 eV depending on substrate temperature and CH<sub>4</sub> pressure in the reactor. Optimum experimental parameters were found out to receive the highest thermo-photosensitivity of 2D structures. The highest obtained photosensitivity was about 700 V<sub>C</sub>/W at white light power density  $\sim 6 \times 10^{-3}$  W/cm<sup>2</sup>. V<sub>C</sub> is “chemical” photo electromotive force induced in the deposited 2D structure while it irradiating with white light, W is white light power. The highest thermo sensitivity (Seebeck coefficient) to have been obtained was about 2.6 mV/K. Photosensitivity and thermosensitivity nature of 2D structures synthesized at these conditions was explained. Therefore, such 2D structures exhibiting high photosensitivity and high thermosensitivity are exceptionally strong candidates for effective photo-thermo sensors operating at moderate temperature.

[1] S.A. Mulenko, N.T. Gorbachuk, Synthesis of nanometric iron oxide films by RPLD and LCVD for thermo-photo sensors, Appl. Phys., B Laser and Optics, vol. 105, pp. 517-523, (2011).

[2] S.A. Mulenko, Yu. N. Petrov, N.T. Gorbachuk, Photon synthesis of iron oxide thin films for thermo-photo-chemical sensors, Appl. Surf. Science, vol. 258, pp. 9186-9191, (2012).

[3] S.A. Mulenko., N.T. Gorbachuk and N. Stefan, Laser Synthesis of Nanometric Iron Oxide Films with High Seebeck Coefficient and High Thermoelectric Figure of Merit, Lasers Manufact. Materials Process., vol. 1, pp.21-35, (2014).

[4] S.A. Mulenko, N.T. Gorbachuk, and N. Stefan, Laser synthesis of nanometric chromium oxide films with high Seebeck coefficient and high thermoelectric figure of merit, Intern. Res. Journ. Nanoscience and Nanotechn., vol. 1 (2), pp. 008-016, (2014).

[5] S.A. Mulenko, N. T. Gorbachuk, N. Stefan, F. Miroiu, Laser Synthesis of Transitional Metal Oxides in 2D Structure and Heterostructure for Thermo Sensors with High Seebeck Coefficient, Frontiers in Sensors, vol. 4, pp. 16-26, (2016).

[6] S.A. Mulenko, N. Stefan, F. Miroiu, I.N. Mihailescu, N.T. Gorbachuk, V.A. Nikirin, Laser synthesis of 2D heterostructures of transitional metal oxides for photo sensors with high sensitivity, J. Laser Appl., vol. 28, pp. 042006-1-042006-8, (2016).

# Improved laser microprocessing of diamond covered by thin absorbing films

**T.V. Kononenko, P.A. Pivovarov, V.I. Konov<sup>1</sup>**

*1- A.M. Prokhorov General Physics Institute, Russian Academy of Sciences, Vavilov str 38, 119991 Moscow, Russia*

*Main author email address: taras.kononenko@nsc.gpi.ru*

Many potential applications of synthesised diamonds, including the fabrication of diamond elements for optics and photonics, microelectromechanical systems, biochemical reactors, sensors, field emitters, etc., require precise microstructuring of its surface and laser ablation provides promising base for development of such technology. Diamond is a wide-band-gap (5.45 eV) dielectric, but it can be effectively ablated by visible and IR laser pulses of femto-, pico- and nanosecond pulsewidths due to surface graphitization inevitably accompanying the ablation process. There is a wide variety of modern laser sources generating such pulses at high repetition rate (up to MHz range) and providing high laser beam quality that are important preconditions for precise and highly productive microprocessing of different materials. However, usage of IR and visible laser pulses for microprocessing of diamond surface meets with significant problems, namely, with occurrence of graphitic microinclusions inside diamond bulk and/or uncontrolled explosive crater formation (see, for instance, [1]) being the result of numerous optical breakdowns. Preliminary covering of the diamond surface by a thin absorbing layer (metal or graphite) was proposed to solve this problem. The experimental verification of the given approach for picosecond (1 ps) and nanosecond (10 ns) laser pulses at the wavelength of 1030 nm is presented here.

It has been established that presence of the absorbing layer results in two significant changes in the diamond ablation process. The first is that the self-maintaining graphitized layer at the diamond surface forms before the initial absorbing film becomes totally removed. This means considerable weakening of the laser radiation penetrating inside diamond bulk comparing with the uncoated diamond during the whole irradiation process. The second change is reduction of the ablation threshold for the diamond surface covered by the absorbing layer that is negligible for the picoseconds pulses, but exceeds order of magnitude for the nanosecond pulses [2].

Occurrence of the self-maintaining graphitized layer at the diamond surface doesn't guarantee absence of optical breakdowns inside diamond as transmittance of the graphitized layer strongly fluctuates from point to point reaching about 30% as a maximum (for picosecond pulses). In the case of the nanosecond pulses, multifold reduction of the ablation threshold for the coated diamond compensates relatively low opacity of the graphitized layer and allows ablation of the diamond surface in the wide range of the fluence values, which are far below the threshold of optical breakdown in the diamond bulk. On the contrary, for the picosecond pulses the damage-free surface microstructuring is possible only under usage of low fluence being just above the thresholds of surface ablation and optical breakdown in diamond bulk. These conclusions are confirmed by transmittance measurements performed after ablation of the polycrystalline diamond using the different pulsewidths and the absorbing coatings.

[1] J. Smedley, J. Bohon, Q. Wu, T. Rao, J. Appl. Phys., 105, 123107 (1-5) (2009).

[2] T.V. Kononenko, P.A. Pivovarov, A.A. Khomich, R.A. Khmel'nitskii, V.I. Konov, Quantum Electronics, 48, 244–250 (2018).

# Optical monitoring of Si nanoparticle evolution in aqueous media for biomedical applications

Viktor Yu. Timoshenko

*Lomonosov Moscow State University, Physics Department, 119991 Moscow, Russia*  
*National Research Nuclear University "MEPhI", 115409 Moscow, Russia*  
*Lebedev Physical Institute of RAS, 119333 Moscow, Russia*  
*E-mail: vtimoshe@gmail.com*

Optical methods of the Raman scattering (RS), photoluminescence (PL) spectroscopy, second harmonic generation (SHG), and two-photon excited luminescence (TPEL) were used to monitor dissolution of silicon nanoparticles (SiNPs) as well as uptake and dissolution of SiNPs in cancer cells *in vitro*. SiNPs were formed by laser ablation of crystalline Si (c-Si) targets at low pressure helium atmosphere or in de-ionized water as well as by electrochemical etching of c-Si wafers followed by mechanical grinding of the prepared porous Si layers in a ball mill. SiNPs were found to be non-toxic, biodegradable and possess a lot of promising physical properties, which can be useful for biophotonic applications, e.g. bioimaging and phototherapy. The prepared aqueous suspensions of SiNPs were studied by means of the linear and non-linear optical spectroscopy and were analyzed as active agents for both therapy and diagnosis, i.e. theranostics, of cancer. The PL properties of microporous and laser-ablated SiNPs were explored for the bioimaging of cancer and normal cells. SiNPs suspended in aqueous media have been tested as sensitizers for hyperthermia induced by irradiation with near-infrared lasers.

According to the one-phonon RS spectroscopy SiNPs stored in water for 1 day and more revealed a strong decrease of the RS intensity and a low energy shift of the Raman spectrum, which were explained by size reduction of SNPs below 10 nm.

Crystalline SiNPs with initial mean size above 10 nm, which is essentially beyond the quantum confinement regime, were served as efficient non-linear optical contrast agents via combined (TPEL) and SHG information channels under femtosecond near-infrared laser excitation. To illustrate the feasibility of these large Si crystals in bioimaging, we demonstrate their efficient tracking and accumulation in different compartments of living cells by following combined TPEL and SHG signals. Here, TPEL channel enables us to track the distribution of SiNPs, while SHG channel serves to determine the localization of nanoparticle agglomerations. The obtained results can be used to choose an optimal size and dissolution stage of SiNPs for biomedical applications.

The work was partially supported by the Russian State Programs for Universities (projects 16.2969.2017/4.6 and 16.7917.2017/8.9).

## ***Sub-ns Laser Surface Structuring of Metals***

**L. A. Angurel<sup>1</sup>, G. F. de la Fuente<sup>1</sup>, A. I. Borrás<sup>2</sup>, A. R. González-Elipe<sup>2</sup>, A. Agüero<sup>3</sup>,  
J. Mora<sup>3</sup>, P. García<sup>3</sup>, J. A. Rojo<sup>1</sup>, R. Navarro<sup>1</sup>**

1- ICMA (CSIC-Universidad de Zaragoza) c/María de Luna, 3 50018 Zaragoza

2- ICMS (CSIC-Universidad de Sevilla), c/Américo Vespucio 49, 41092 Sevilla

3- Área de Materiales Metálicos, INTA, Carretera de Torrejón a Ajalvir, Km. 4, 28850 Madrid

*xerman@unizar.es*

Periodic surface structuring of metal surfaces has become a topic of great interest for a number of biomedical and industrial applications; structural color, wetting, tribology, cell growth, etc. [1]. Among them, icephobicity appears to be evermore important, because of safety considerations in Aircraft and also due to a large number of problems identified in civil structures present in cold climate regions.

Until recently, a large number of scientific publications have addressed the formation of Laser-induced characteristic surface morphologies as ripples (HSFL and LSFL) [1], grooves and spikes [2], which have also been demonstrated on scaleable size [3]. These surface nanostructures may pave the way to important advancements towards design of surface functionality related to ice formation and accretion, besides the frequently studied hydrophobicity character of treated surfaces [4].

The use of pulsed ps lasers to control surface structuring will be described in this talk, along with the properties associated with a diversity of nanostructures attained by working in laser beam and line scan modes, in the attempt to understand the relationship between laser irradiation parameters, surface nanostructure generation and functionalization of the irradiated surface.

[1] J. Bonse, S. Höhm, S. V. Kimer, A. Rosenfeld, J. Krüger, Laser-Induced Periodic Surface Structures- A Scientific Evergreen, IEEE J. Selected Topics in Quantum Electronics, vol. 23, 9000615- pp 1-15, (2017).

[2] U. Hermens, S.V. Kirner, C. Emonts, P. Comanns, E. Skoulas, A. Mimidis, H. Meschedera, K. Winandsa, J. Krügerb, E. Stratakis J. Bonse, Mimicking lizard-like surface structures upon ultrashort laser pulse irradiation of inorganic materials, Applied Surface Science vol 418, 499–507 (2017).

[3] A. Ruiz de la Cruz, R. Lahoz, J. Siegel, G. F. de la Fuente, J. Solís, High speed inscription of uniform, large-area laser induced periodic surface structures in Cr films using a high repetition rate fs-laser, Optics Letters Vol. 39 (8), 2491–2494 (2014).

[4] D. F. Carpen, M. Dickinson, C. Seal, and M. Hyland, Induced hydrophobicity in micro and nanostructured nickel thin films obtained by ultraviolet pulsed laser treatment, Phys. Status Solidi A 213, No. 10, 2709–2713 (2016).

# Laser control of metal surfaces optical properties due to structural colors formation

**G. V. Odintsova, Ya. M. Andreeva, E. I. Ageev, V.C. Luong,  
M. K. Moskvin and V. P. Veiko**

*ITMO University, 49 Kronverksky Pr., St. Petersburg, 197101, Russia*

*Main author email address: gvodintsova@corp.ifmo.ru*

Natural colors (of some insects, birds, fishes, plants, etc.) are mainly formed because of light interaction with ordered structures of micro and nanoscale sizes without the use of dyes. When light interacts with micro- and nanoobjects (gratings, nanoparticles, transparent films, etc.) various phenomena take place such as diffraction and interference or surface plasmon resonance. It results in the surface coloration. Simultaneously with the coloring it is possible to provide desired functional properties: hydrophilic, hydrophobic, optical, anticorrosive, etc due to the formation of periodic surface structures. Using laser exposure, looks quite promisingly to control the abovementioned properties locally, by altering the chemical composition (due to thin oxide films appearance [1]), and by adjusting the surface morphology (due to formation of periodic structures [2]), and as well as by generating of nanoparticles [3].

The work objective is the laser control of metals surface optical properties due to the structural colors formation. The possibility to control local spectral and colorimetric characteristics of the metal surface is shown based on four different mechanisms:

- light interference in thin films formed by laser oxidation of metals (Fig. 1B);
- light diffraction on surface periodical structures induced by interference between laser radiation and surface electromagnetic waves (Fig. 1C);
- plasmonic resonance in precious metals nanoparticles fabricated at pulsed laser action (Fig. 1D);
- light scattering due to multiple reflections on laser-induced periodical structures of metals.

To obtain these effects, it has been proposed to use a commercially available fiber laser source with a nanosecond duration of pulses (Fig. 1A). Results allow the local formation of fixed chemical composition and morphology on the metals surface and providing specified spectral and colorimetric characteristics. A combination of the abovementioned phenomena makes it possible to get biomimetic structures and to develop new functional properties of treated materials.

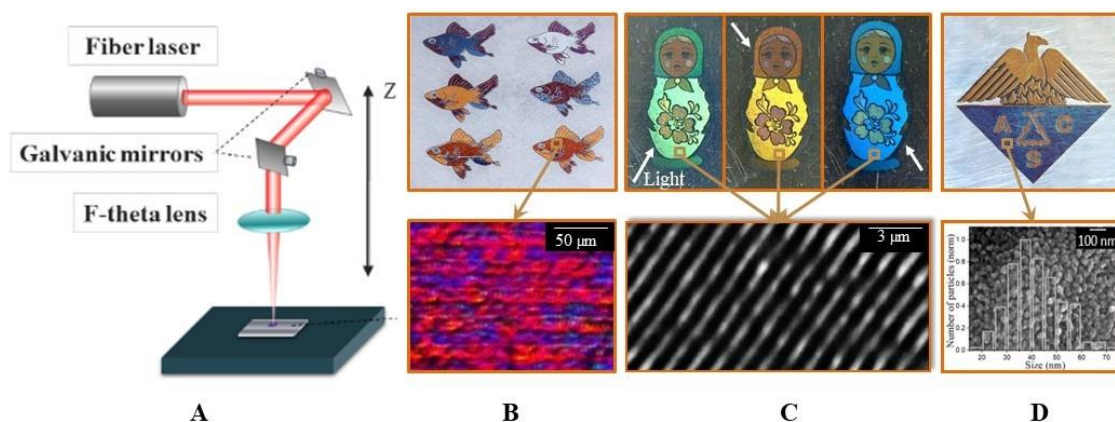


Fig. 1. Laser experimental setup (A); laser-induced structural colors on titanium (B), steel (C) and silver (D) surfaces based on different coloration mechanisms

[1] V. Veiko, G. Odintsova, E. Gorbunova, E. Ageev, A. Shimko, Y. Karlagina, Y. Andreeva, Development of complete color palette based on spectrophotometric measurements of steel oxidation results for enhancement of color laser marking technology, *Material and Design*, vol. 89, pp. 684-688, (2016).

[2] E. Ageev, V. Veiko, E. Vlasova, Y. Karlagina, A. Krivososov, M. Moskvin, G. Odintsova, V. Pshenichnov, V. Romanov, and R. Yatsuk, Controlled nanostructures formation on stainless steel by short laser pulses for products protection against falsification, *Optics Express*, vol. 26, N. 2, pp. 2117-2122, (2018).

[3] J-M. Guay, A. Calà Lesina, G. Côté, M. Charron, D. Poitras, L. Ramunno, P. Berini, A. Weck, Laser-induced plasmonic colours on metals, *Nature communications*, vol. 8, p. 16095, (2017).

# Ultrafast Laser Texturing on Si with Burst-mode Picosecond Laser Pulses

Iaroslav Gnilitskiy<sup>1,2</sup>, Leonardo Orazi<sup>2</sup>, Tommi White<sup>3</sup> and Vitaly Gruzdev<sup>4</sup>

1 - NoviNano Inc., Lviv, Ukraine and 2 - UNIMORE, Modena, Italy

3 - Electron Microscopy Core Facility, University of Missouri, Columbia, USA

4 - Department of Mechanical & Aerospace Engineering, University of Missouri, Columbia, USA

Author e-mail address: iaroslav.gnilitskiy@unimore.it

In this paper, picosecond LIPSS were imprinted on Si surface in regime of strong ablation partially using method HR-LIPSS [1,2]. Moreover, regimes of uniform and burst-mode were investigated and discussed in terms of chemical, morphological and mechanical properties. First, there is a fundamental interest to compare the HR-LIPSS produced by femto- and picosecond laser pulses since those pulses generate the LIPSS under fundamentally different regimes, i. e., non-thermal and mild thermal. Second, study of the LIPSS formation by the picosecond pulses is highly reasonable in view of the advantages of the picosecond lasers for industrial applications. Those lasers are more probable candidates for mass-production laser lines. Third, the burst mode of laser operation delivers several pulses separated by a time gap that is not enough for total dissipation of heat from laser radiation absorbed within a laser spot. Therefore, the burst mode is favourable for enhancing the thermal effects and production of specific heat-affected HR-LIPSS. The thermal effects are expected to substantially change both morphology and properties of the LIPSS. The point is to identify and characterize those changes.

Figure 1 confirms the expected influence of the thermal effects on LIPSS generation by the picosecond burst mode.

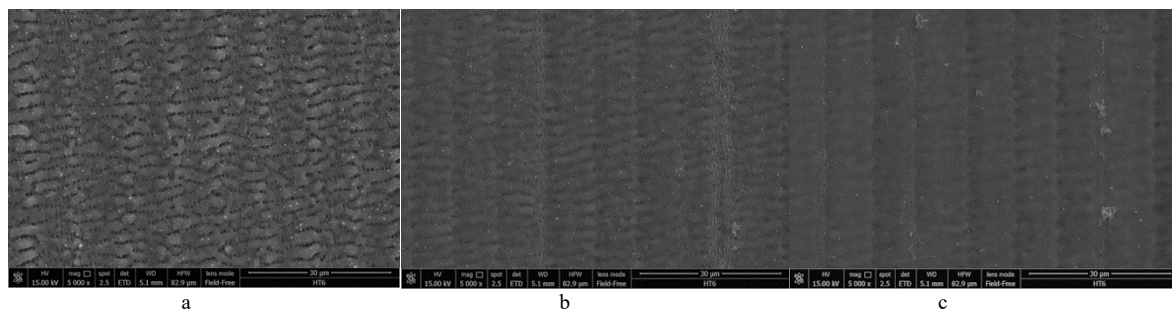


Fig. 1. Picosecond LIPSS on Si in uniform mode (a), 3 burst pulses (b) and 5 burst pulses (c).

Therefore, the morphology of the slightly melted LIPSS departs from that of the femtosecond-laser-induced LIPSS [2] and approaches that of the melting-driven LIPSS produced by long pulses [3]. This change of the LIPSS morphology suggests consideration of the traditional thermal mechanisms of the LIPSS generation [4]. Also, it must substantially affect properties and responses of the LIPSS. In particular, the usage of few-pulse bursts can deliver the LIPSS with specific response that is intermediate between that of the thermal LIPSS and that of the non-thermal LIPSS.

[1] I. Gnilitskiy, V. Gruzdev, N. M. Bulgakova, T. Mocek, and L. Orazi, Mechanisms of high-regularity periodic structuring of silicon surface by sub-MHz repetition rate ultrashort laser pulse, *Appl. Phys. Lett.*, **109**, 143101 (2016)

[2] I. Gnilitskiy, T. J.-Y. Derrien, Y. Levy, N. M. Bugakova, T. Mocek and L. Orazi, "High-speed, highly regular femtosecond laser printing of laser-induced periodic surface structures on metals: physical origin of the regularity", *Scientific Reports*, **7**, 8485 (2017).

[3] J. F. Young, J. S. Preston, H. M. van Driel, J. E. Sipe, "Laser-induced periodic surface structure. II. Experiments on Ge, Si, Al, and brass," *Phys. Rev. B* **27** (2), 1155-1171 (1983).

[4] J. E. Sipe, J. F. Young, J. S. Preston, H. M. van Driel, "Laser-induced periodic surface structure. I. Theory," *Phys. Rev. B* **27** (2), 1141-1154 (1983).

# Ion Chamber Array Detector for Laser Accelerated Charged Particle Characterization: Prototype, Measurements and FLUKA Simulation Results

**C.E. Matei<sup>1</sup>, R. Vasilache<sup>2</sup>, M.A. Popovici<sup>3</sup>, M. Straticiuc<sup>4</sup>, L. Craciun<sup>4</sup>, D. Stroe<sup>5</sup>,  
D. Dumitras<sup>1</sup>**

*1 - National Institute for Laser, Plasma and Radiation Physics - INFLPR, 409 Atomistilor Str., 077125 Magurele, Romania*

*2 - CANBERRA PACKARD S.R.L., 18 Clejani Str., 051036 Bucuresti, Romania*

*3 - Politehnica University of Bucharest, Faculty of Applied Sciences, 313 Splaiul Independentei, 060042 Bucharest, Romania*

*4 - Horia Hulubei National Institute of Physics and Nuclear Engineering - IFIN HH, 30 Reactorului Str., 077125 Magurele Romania*

*5 - Clinical Hospital "COLTEA", Department of Radiation Oncology, 1 I.C. Bratianu Blvd. 030171 Bucharest, Romania*

*consuela.matei@inflpr.ro*

The production of laser accelerated particles by high power laser interaction with different targets has already several years of experimental practice and is sustained by numerous theoretical and numerical approaches. Despite all the acquired experience, the characterization of the charged particles obtained by laser acceleration remains a challenge in terms of precise in-beam dose measurements. Though the ion chambers represent the gold standard in dose measurement, they are limited by the large number of corrections to be applied in order to calculate a correct dose from the measured charge.

We tried to address this problem, in the frame of the ELIDOSE project, by proposing an array detector that would allow the simultaneous measurement of the recombination and polarity corrections, as well as of the dose. We built a prototype detector consisting of 4 identical Advanced Markus ion chambers mounted together in a PMMA frame, obtaining a detector array that allows the simultaneous measurement of the recombination and polarity corrections, as well as of the dose. In order to calibrate the array detector we performed measurements in controlled beams to obtain the correction factors needed to calculate the correct dose from the measured charge and also to assess the reciprocal influences of the chambers on each other. All the measurements were correlated with FLUKA simulations.

The paper presents the prototype of our detector, together with initial measurements in the 3 MeV and 18 MeV proton beams at the Tandetron and TR19 Cyclotron accelerators of the IFIN-HH and the comparison between the experimental results and the FLUKA based simulations, as well as the results obtained in the 6 to 19 MeV electron beams generated by a Siemens radiotherapy LINAC (Clinical Hospital "COLTEA"). These results will be used to further improve the design of the array detector and to perform measurements on laser accelerated particles at the 1PW laser beam of CETAL, in order to develop a reliable equipment for the experiments to follow in ELI-NP facility.

## **Acknowledgements**

This work has been supported by the national projects PNCDI III 5/5.1/20-ELI/2016 ("ELIDOSE") under the financial support of Institute for Atomic Physics – IFA and "LAPLAS V" – Nucleu under the financial support of Ministry of Research and Innovation.

# Deep investigation of picosecond laser micromachining of silicon for electron microscopy sample preparation.

A. Sikora, D. Grojo, G. Coustillier, T. Sarnet M. Sentis

*Aix Marseille Université, CNRS, LP3 UMR 7341, 13288, Marseille, France*

In order to qualify the manufacturing quality of integrated circuits, scanning or transmission electron microscopy is usually performed. To get access to the deep layers of a component, a large quantity of matter has to be removed and the surface smoothed using Focused Ion Beam (FIB). Currently, the highest rates achieved by FIB methods reach hardly  $10^4 \mu\text{m}^3/\text{s}$ , which corresponds typically to several hours of processing to reach the targeted zone. Thus alternative strategies such as femtosecond or nanosecond laser ablation (LA) [1-3] are investigated to reduce the processing time. LA removal rates are high but the process induces damages around the ablated area. Thus, the micromachining has to be optimized in order to limit the size of the heat affected and induced dislocation zones. Moreover, the side wall cavities must be as much as possible vertical and smooth to minimize the final FIB polishing time. In the present work, we perform an extensive study (ablation rate, HAZ, roughness,...) using picosecond lasers at three wavelengths (343, 515 and 1030 nm).

In a first part, we show that single shot laser ablation thresholds of silicon ( $F_{\text{th}}$ ) vary from 0.01 to  $0.57 \text{ J}/\text{cm}^2$ , confirming a strong dependence on the wavelength. Using the experimental data, a simplified modelling approach allows to identify the main absorption modes and the free carrier generation mechanisms. Theoretical and experimental thresholds are consistent when the main absorption mechanisms and the variations of the physical properties of silicon with temperature are taken into account. The highest removal rate and efficiency is found at 1030 nm. The optimal normalized fluence for which the efficiency is maximal is  $\sim 8F_{\text{th}}$  for each wavelength [4]. Removal rates are typically hundred times higher than those achieved by ion milling.

In a second part the roughness evolution of sidewalls engraved in silicon is studied as a function of the pulse overlap and the applied fluence. We demonstrate that a fine tuning of the pulse overlap drastically enhances the smoothness of the flanks. Moreover, it is found that the repetitive laser scanning of the surface induces a structuring of the sidewall with a periodicity matching the inter pulse distance. The lateral roughness  $R_a$  (measured along the laser scanning direction) increases with this distance in accordance with a simple geometrical model. However, the minimum measured roughness was found near 30 nm for an overlap of about 80%. Beyond this limit, the surface quality deteriorates.

Finally, clear cross sections of bumps and cavity openings, exposing multilayer interfaces obtained by optimized ps laser micromachining are demonstrated as well as the achievement of very thin lamellas ( $< 7 \mu\text{m}$ ) with a very high aspect ratio for TEM observation [5].

- [1] M. Halbwax; T. Sarnet; J. Hermann; P. Delaporte; M. Sentis; L. Fares; G. Haller, *Applied Surface Science* 2007, 254 (4), 911-915. DOI <http://dx.doi.org/10.1016/j.apsusc.2007.07.202>.
- [2] L. Kwakman; M. Straw; G. Coustillier; M. Sentis; J. Beyersdorfer; J. Schischka; F. Naumann; F. Altmann In *Sample Preparation Strategies for Fast and Effective Failure Analysis of 3D Devices*, International Symposium for Testing and Failure Analysis, ASM International: 2013; pp 17-26.
- [3] M. Petzold; F. Altmann; M. Krause; R. Salzer; C. Schmidt; S. Martens; W. Mack; H. Dömer; A. Nowodzinski In *Micro structure analysis for system in package components ; Novel tools for fault isolation, target preparation, and high-resolution material diagnostics*, Electronic Components and Technology Conference (ECTC), 2010 Proceedings 60th, 1-4 June 2010; 2010; pp 1296-1302.
- [4] A. Sikora, D. Grojo, M. Sentis, "Wavelength scaling of silicon laser ablation in picosecond regime", *Journal of Applied Physics* 122, 045702 (2017); doi: 10.1063/1.4994307.
- [5] A. Sikora, L. Fares, J. Adrian, V. Goubier, A. Delobbe, A. Corbin, M. Sentis, T. Sarnet (2017) Picosecond laser micromachining prior to FIB milling for electronic microscopy sample preparation, *Applied Surface Science*, 418, 607-615.

# Modeling of optical response of metals to ultrafast laser irradiation: Comparison with experiment

Sergei A. Lizunov,<sup>1,2</sup> Nadezhda M. Bulgakova,<sup>1,2</sup> Vladimir P. Zhukov,<sup>1,3</sup> Ranran Fang,<sup>4,5</sup> Anatoliy Y. Vorobyev,<sup>4,5</sup> Chunlei Guo<sup>4,6</sup>

<sup>1</sup>*HiLASE Centre, Institute of Physics of the Czech Academy of Sciences, Za Radnicí 828, 25241 Dolní Břežany, Czech Republic*

<sup>2</sup>*Institute of Thermophysics SB RAS, 1 Lavrentyev ave., 630090 Novosibirsk, Russia*

<sup>3</sup>*Institute of Computational Technologies SB RAS, 6 Lavrentyev Ave., 630090 Novosibirsk, Russia*

<sup>4</sup>*The Institute of Optics, University of Rochester, Rochester, NY, USA*

<sup>5</sup>*School of Science, Chongqing University of Posts and Telecommunications, Chongqing, China*

<sup>6</sup>*The Guo China-US Joint Laboratory, Changchun, China*

[lizunov@fzu.cz](mailto:lizunov@fzu.cz)

Ultrashort-pulse lasers are an excellent tool for processing of any kind of materials. By proper choosing the irradiation conditions, it is possible to create highly-localized surface modifications with minimal heat-affected zone due to minimized heat diffusion effects. The interaction of ultrashort laser pulses with surfaces involves a wealth of the physical processes, depending on the material kind and laser light properties. Even within the same material family, considerably different modifications can be achieved when applying similar laser pulses. Improvement in understanding of the physical mechanisms of laser-induced material modification/ablation and contributions of individual processes is of vital need for further advance of ultrafast laser processing of materials.

The optical response of metal surfaces to high-power laser excitation (HPLE) is one of important topics of laser-matter interaction which is still not completely understood. It is known that certain metals, which are highly reflective at normal conditions, become considerably absorbing radiation during the HPLE stage. The amount of the absorbed energy is a key parameter which determines the post-irradiation evolution of the material. Numerous optical models have been proposed to describe this effect and to link the actually absorbed laser energy with the incident laser energy for direct comparison of the simulated material dynamics and the experimental irradiation conditions. This includes variations of the Drude and Drude-Lorentz models, contribution of plasma-like response of free electrons in metal, as well as attempts of ab initio simulations of the optical response. However, all these models give satisfactory agreement with measurements only at limited range of applied laser fluences that calls for further studies.

In this work, the results of numerical simulations of ultrashort laser action (800 nm wavelength, 66 fs pulse duration) on two metals, gold and chromium, are reported for a wide range of laser fluences. The existing models of the optical response of metals were juxtaposed in the simulations in respect of their applicability to the conditions of HPLE, based on direct comparison with the experimental data obtained with hemiellipsoidal metallic reflector technique [1]. The core of the model employs the two-temperature approach [2] which is supplemented by the optical response models and the integration of the reflected part of the laser beam over the irradiation spot. In the modeling, the swift change of the physical properties of the laser-excited free electrons (heat capacity, thermal conductivity, electron-phonon coupling factor, collision frequency [3]) is analyzed from the viewpoint of optical response of laser-excited metals. It has been found that an optical model itself cannot describe the experimentally measured data on reflectivity without an accurate knowledge about dynamic behavior of thermophysical properties of metal upon laser excitation. Some implications on mutual impact of dynamically varying properties of free electrons in metals and their optical response will be discussed.

[1] A. Y. Vorobyev, Chunlei Guo, "Reflection of femtosecond laser light in multipulse ablation of metals," *J. Appl. Phys.* **110**, 043102 (2011).

[2] S. I. Anisimov, B. L. Kapeliovich, and T. L. Perel'man, "Electron emission from metal surfaces exposed to ultrashort laser pulses," *Sov. Phys. - JETP* **39**, 375 (1974).

[3] Z. Lin, L. V. Zhigilei, V. Celli, "Electron-phonon coupling and electron heat capacity of metals under conditions of strong electron-phonon nonequilibrium," *Phys. Rev. B* **77**, 075133 (2008).

# Nonlinear stage of ionization-field instability in transparent dielectric

V.B. Gildenburg<sup>1,2</sup>, I.A. Pavlichenko<sup>1,2</sup>

<sup>1</sup> *University of Nizhny Novgorod, 23 Gagarin Avenue, Nizhny Novgorod 603950, Russia*

<sup>2</sup> *Institute of Applied Physics RAS, 46 Ulyanov Street, Nizhny Novgorod 603950, Russia*

*gil@appl.sci-nnov.ru*

The grating structures arising in the volume of transparent media (e.g. fused silica) under the action of the series of femtosecond laser pulses is considered now as a promising technique of the material optical properties modification. This technique is nowadays widely demanded and already finds numerous applications in various functional devices based on three-dimensional photonic structures in the bulk of optical materials. The dynamics of plasma-field structures underlying the nanograting formation was studied in numerous papers [1-8]. Nevertheless the physical mechanisms predetermining these structure appearance are not revealed completely and remain the subject of discussion. One of the possible mechanisms is associated with the development of ionization-field (plasma-resonance) instability in laser-pulse-induced optical breakdown. This instability is due to the mutually amplifying action of one-dimensional perturbations of the optical field and electron concentration in plasma of subcritical density. At the very beginning of its development (in the linear stage) this instability, in principle, can lead to the formation of the periodic plane-layered structure with the orientation and spatial period appropriate to the observed gratings [5]. In the present work, based on a simple 1D electro-dynamical model [7], the nonlinear stage of plasma-resonance instability in the laser-silica interaction is analyzed with the main processes governing the plasma density evolution taken into account (multiphoton and avalanche ionization, recombination and diffusion). The distributions of the field amplitude, plasma density, and energy transferred to the media during single pulse are calculated and different scenarios of spatio-temporal evolution of the field and plasma are found. It was shown that the character of the structure formed on the nonlinear stage crucially depends on whether the plasma resonance conditions in the discharge were achieved. In the definite laser intensity range, the field enhancement in the plasma resonance regions results in the formation of a contrast periodic plasma structure consisting of the thin overcritical plasma layers oriented perpendicular to the laser polarization. These layers are found to be also the regions of high energy deposition that allow us to consider the plasma resonance instability as a physical mechanism underlying the nanograting formation by repeated pulses. The calculated intensity range of nanograting existence is in a qualitative agreement with the experimental results [2].

[1] Y. Shimotsuma, P. Kazansky, J. Qiu, and K. Hirao, Self-Organized Nanogratings in Glass Irradiated by Ultrashort Light Pulses, *Phys. Rev. Lett.*, vol. 91, 247405 (2003).

[2] C. Hnatovsky, R. S. Taylor, P. P. Rajeev, E. Simova, V. R. Bhardwaj, D. M. Rayner, and P. B. Corkum, Pulse duration dependence of femtosecond-laser-fabricated nanogratings in fused silica, *Appl. Phys. Lett.*, vol. 87, 014104 (2005).

[3] N. Bulgakova, V. Zhukov, Y. Meshcheryakov. Modification of transparent materials with ultrashort laser pulses: What is energetically and mechanically meaningful?, *Appl. Phys. B*, vol. 113, p.437 (2013).

[4] R. Buschlinger, S. Nolte, and U. Peschel, Self-organized pattern formation in laser-induced multiphoton ionization, *Phys. Rev. B*, vol. 89, 184306 (2014).

[5] V.B. Gildenburg and I.A. Pavlichenko, Volume nanograting formation in laser-silica interaction as a result of the 1D plasma-resonance ionization instability, *Phys. Plas.*, vol. 23, 084502 (2016).

[6] A. Rudenko, J. P. Colombier, and T. E. Itina, From random inhomogeneities to periodic nanostructures induced in bulk silica by ultrashort laser, *Phys. Rev. B* 93, 075427 (2016).

[7] V.B. Gildenburg and I.A. Pavlichenko, High contrast periodic plasma pattern formation during the laser-induced breakdown in transparent dielectric, *Phys. Plas.*, vol. 24, 122306 (2017).

[8] A. Rudenko, J.-P. Colombier and T. E. Itina, Nanopore-mediated ultrashort laser-induced formation and erasure of volume nanogratings in glass, *Phys. Chem. Chem. Phys.*, vol. 20, 5887-5899, (2018).

# Femtosecond laser interactions with silicon surface: the coupling of surface ripples and the sub-surface modifications

**Iaroslav Gnilitzkiy<sup>1,2</sup>, Vitaly Gruzdev<sup>3</sup>, Xiaoqing He<sup>4</sup>, Olga Sergaeva<sup>3</sup>, Pengfei Ji<sup>5</sup>, Tommi White<sup>4</sup>, and Yuwen Zhang<sup>3</sup>**

*1 - DISMI, University of Modena and Reggio Emilia (UNIMORE), Reggio Emilia, 41122, Italy*

*2 - NoviNano Inc., Lviv, 79021 Ukraine*

*3 - Department of Mechanical & Aerospace Engineering, College of Engineering, University of Missouri, Columbia, MO, 65211, USA*

*4 - Electron Microscopy Core Facility, University of Missouri, Columbia, MO, 65211, USA*

*5 - Department of Mechanical and Energy Engineering, Southern University of Science and Technology, Shenzhen, Guangdong, China 518055*

*Main author email address: iaroslav.gnilitzkiy@unimore.it*

We report experimental studies of the relation between structure of surface modifications and that of sub-surface layer of a single-crystal silicon surface irradiated by near-infrared femtosecond laser pulses. Number of pulses per single site and laser fluence were varied to mimic the most typical regimes: a) large number of laser pulses per single site at near-threshold fluence; and b) a few high-fluence pulse per site. Polished (100) surface of a single-crystal n-type silicon sample was irradiated by laser pulses at normal incidence at wavelength 772 nm and fixed pulse width 150 fs. Focal length of a focusing system is 5 cm. Number of laser pulses delivered to a single spot at 1 kHz repetition rate varied from 1 to 10. Laser fluence varied from threshold of single-pulse surface modification to approximately 4-fold the threshold. Structure of the laser-modified surface was characterized by scanning electron microscope (SEM). Structure of the sub-surface layers was characterized by FEI Scios ultra-high-resolution analytical Dual-Beam system that reached the sub-surface layer using focused ion beam (FIB) technique.

The surface modification by multiple pulses at fluence close to the surface-modification threshold (Fig. 1) showed low-frequency laser-induced periodic surface structures (LIPSS) in the center of a laser spot and high-frequency LIPSS in the peripheral area. Sub-surface layers under the high-frequency LIPSS contained high-aspect-ratio (1:10) voids parallel to the LIPSS ripples. They were attributed to strong-ablation effects like phase explosion. The LIPSS generated by few pulses at high fluence did not show any sub-surface nano-voids or fractures. They contained a 30-40-nm thick layer of modified silicon on top of the crystalline silicon. Therefore, the LIPSS generated by a few laser pulses are not produced by the strong-ablation processes. The amorphous layer may result from destruction of the initial crystalline structure by point defects produced by photoionization, relaxation of laser-induced electron-hole plasma, or atom repulsion induced by the laser-driven electron emission. Ultrafast generation of the defects is a very likely mechanism to imprint the interference pattern of electromagnetic waves into a semiconductor.

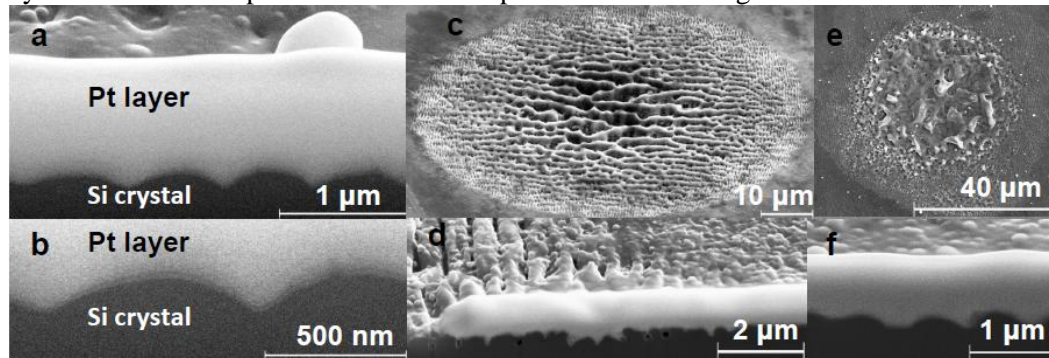


**Fig. 1.** (a, b) –A cross section of the LIPSS formed by two subsequent pulses at fluence 2.5-fold threshold of a single-pulse surface-modification. (b) is an enlarged image of panel (a) to show the modified sub-surface layer. SEM images of the modifications produced by (c, d) –10 pulses at the modification threshold; (e, f) - by 3 pulses at fluence 4-fold the threshold. Panels (d) and (f) are SEM images of the cross sections produced by FIB on the laser-modified surface areas depicted in the corresponding upper parts (c and e) of the figure.

# Numerical simulations of the electromagnetic field shielding in petawatt regime using Finite-Difference Time-Domain method

L. Ionel, A. Marcu

National Institute for Laser, Plasma and Radiation Physics, Atomistilor 409, P. O. Box MG-36, 077125  
Magurele-Bucharest, Romania

*laura.ionel@inflpr.ro*

**Abstract.** The recent progresses made in the development of high intensity lasers open new perspectives of fundamental physics and also impacts applications from laboratory astrophysics and inertial confinement fusion to laser matter interaction in ultra-intense regimes. The interaction of high power laser pulses with a solid target generates intense broadband electromagnetic pulses in a wide frequency regime, from radio frequency to x-rays. In the petawatt regime, these intense laser pulses are expected to be emitted in the Giga to Tera-Hertz domain, being also called Giant Electro-Magnetic Pulses (GEMP) [1].

Starting from the cells response on particular wavelengths and respectively during petawatt irradiation experiments and considering the GEMP spectra generated during real experiments, we had performed 3D numerical simulations to investigate the behavior of different shielding materials by using a scaled configuration setup. The main objective is to compare the performances of these materials at some different frequencies, considered as relevant both for the generated frequencies and for the cell's absorbed wavelengths under the conditions imposed by high energy experiments planned to be performed at CETAL PW facility. The 3D numerical simulations of the electromagnetic field shielding have been made using Finite-Difference Time-Domain (FDTD) method using FullWave, a package of the commercial software RSoft (by Synopsys Optical Solution Group) which solves Maxwell equations. Lately, a plenty of FDTD studies had been elaborated in order to determine the optimum conditions for extreme electric field generation [2-4]. A detailed study concerning the electromagnetic field shielding under petawatt irradiation conditions has been elaborated using different structures both as metallic foil or mesh in order to measure its efficiency in a wide frequency regime (100-4000 MHz). The results obtained by this method will be presented and discussed.

This work has been financed by the national project: PN III 5/5.1/ELI-RO, Project 17-ELI/2016 ("BIOSAFE"), under the financial support of Institute for Atomic Physics – IFA.

- [1] M. J. Mead, D. Neely, J. Gauoin, R. Heathcote, P. Patel, "Electromagnetic pulse generation within a petawatt laser target chamber", *Rev. Sci. Instrum.* 75, 4225 (2004)
- [2] L. Ionel, D. Ursescu, "Non-collinear spectral coherent combination of ultrashort laser pulses", *Opt. Express* 24(7) 7046–7054 (2016)
- [3] L. Ionel, D. Ursescu, "Spatial extension of the electromagnetic field from tightly focused ultra-short laser pulses", *Laser Part. Beams* 32(1), 89-97 (2014)
- [4] Z. Lin, X. Chen, P. Ding, W. Qiu, J. Pu, "Modeling the ponderomotive interaction of high-power laser beams with collisional plasma: the FDTD-based approach", *Opt. Express*, 25(7) 8440-8449 (2017)

# Theoretical and experimental study of laser crystallization of thin amorphous layers of silicon under continuous and pulsed irradiation.

**Jiří Beránek<sup>1</sup>, Ozan Aktas<sup>2</sup>, Stuart MacFarquhar<sup>2</sup>, Yohann Franz<sup>2</sup>, Sakellaris Mailis<sup>2</sup>,  
Nadezhda M. Bulgakova<sup>1</sup>, Anna C. Peacock<sup>2</sup>**

<sup>1</sup>*HiLASE Centre, Institute of Physics of the Czech Academy of Sciences, Za Radnicí 828, 25241 Dolní Břežany, Czech Republic*

<sup>2</sup>*ORC, University of Southampton, University Road, Southampton, SO17 1BJ, United Kingdom*

*beranekj@fzu.cz*

The unique electrical and optical properties of crystalline silicon and silicon-based materials are of fundamental importance for applications in electronics, photovoltaics and communications. Thus these materials have shaped our technical progress in many fields in recent decades. One area in particular that is experiencing rapid growth is silicon photonics, where nanoscale waveguides are finding use in components that range from passive interconnects to active modulators and emitters. Such structures can be fabricated on various kinds of substrates and integrated with other electronic and optical components. However, the current methods used for producing high-quality crystalline silicon typically require high temperatures, which places important restrictions on device integration and miniaturization. On the other hand, amorphous silicon (a-Si) is relatively easy to deposit on various substrates at relatively low temperatures, but with inferior optical and electronic properties.

A solution to this problem is to fabricate high quality crystalline silicon waveguides and components by laser crystallizing deposited a-Si structures. Here we report our experimental and numerical investigations of laser processing silicon waveguides using a continuous wave (cw) argon ion laser. The aim of this work is to crystallize amorphous waveguides with dimensions of 1–2  $\mu\text{m}$  that have been selectively etched from a uniform layer of a-Si, with a 400 nm thickness, deposited on thick layer of  $\text{SiO}_2$ . The focused cw laser of 488 nm wavelength heats the silicon to a temperature sufficient to melt the material, but below its evaporation point. The molten silicon then solidifies to a polycrystalline form. The crystallinity has been verified by Raman spectroscopy and X-ray diffraction. Typically, the grain sizes range from several to tens of micrometers. Thus these results show that we are able to obtain high optical quality poly-silicon waveguides at low temperatures [1], consistent with our modelling and interpretation of the physical process [2].

However, further work remains to fully understand the process of silicon crystallization in different regimes that can help to overcome drawbacks in production of high-quality silicon structures. Since the process of cw laser irradiation is well-established, we employ a theoretical model to understand thermodynamic processes when pulsed lasers are used, with parameters that correspond to the parameters of sources available at HiLASE.

Physical modelling of laser-matter interaction provides an important insight for laser microfabrication as the processes of laser energy absorption and heat transfer during ultrafast irradiation are far from equilibrium [3]. To model thermodynamic changes in such cases, it is necessary to utilize a numerical code operating with high temporal and spatial resolution, which is tailored to specific 2D and 3D geometries. We apply the finite-difference implicit scheme with splitting by the coordinates that provides high stability at reasonable simulation times and good energy conservation. In addition, we will carry out an experimental study of crystallization under the effect of pulsed lasers supported by numerical simulation of the interaction. As pulsed laser processing typically induces growth of smaller grains than cw irradiation [3], we will use beam shaping and select an optimum laser wavelength to maximally increase solidification time for achieving large crystal growth. The first simulation results will be presented and discussed in comparison with experimental findings.

[1] Yohann Franz et al. Laser “Annealing of Low Temperature Deposited Silicon Waveguides”, Conference on Lasers and Electro-Optics (CLEO), OSA Technical Digest (online) (Optical Society of America, 2017), paper SM3K.4.

[2] N. Healy et al., “Extreme electronic bandgap modification in laser-crystallized silicon optical fibres”, *Nat. Mater.* **13**, 1122-1127 (2014).

[3] N. H. Nickel, “Laser Crystallization of Silicon – Fundamentals to Devices”, Chapter 1 (Academic Press, 2003).

# Femtosecond laser modification of amorphous silicon films: control of structural anisotropy.

D.V. Shuleiko<sup>1</sup>, S.V. Zobotnov<sup>1</sup>, D.E. Presnov<sup>2,1</sup>, F.V. Potemkin<sup>1</sup>, I.A. Romanov<sup>3</sup>,  
I.N. Parhomenko<sup>3</sup>, P.K. Kashkarov<sup>4,1</sup>, L.A. Golovan<sup>1</sup>

1- Faculty of Physics, Lomonosov Moscow State University, Moscow 119991, Russia

2- Skobeltsyn Institute of Nuclear Physics, Lomonosov Moscow State University, Moscow, 119991, Russia

3- Belarusian State University, Minsk, 220030, Republic of Belarus

4- National Research Center "Kurchatov Institute", Moscow, 123182, Russia

shuleyko.dmitriy@physics.msu.ru

Amorphous hydrogenated silicon films (a-Si:H) modified by femtosecond laser radiation are of great interest for thin-film photovoltaics. Using ultrashort laser pulses allows to obtain silicon nanocrystals that are uniformly distributed over the entire volume of a-Si:H film [1]. Such treatment can be used to reduce photodegradation of the a-Si:H film electric properties under long-term light irradiation (Staebler-Wronski effect) and also enhance light absorption. In addition, femtosecond laser modification leads to anisotropy of the structural, optical and electrical properties of irradiated surfaces. In particular, periodic structures can be formed on the a-Si:H surface by femtosecond laser pulses due to plasmon-polariton excitation [2].

In this paper, a-Si:H films were irradiated by femtosecond laser pulses (1250 nm, 125 fs) in the raster mode. Scanning electron microscopy revealed presence of various laser-induced periodic surface structures (LIPSS) on the treated surface of a-Si:H (Figure 1, a–c), including one-dimensional gratings with a period of  $1.20 \pm 0.02 \mu\text{m}$  (Figure 1 a, c). The shape and orientation of the observed LIPSS is determined by incident beam polarization and changes depending on the number of femtosecond laser-irradiated spots  $N_s$  that were overlapping during rastering of the a-Si:H film. The observed LIPSS evolution with increasing  $N_s$  is due to the emerging of a feedback between the formed surface relief and the electronic processes in the film.

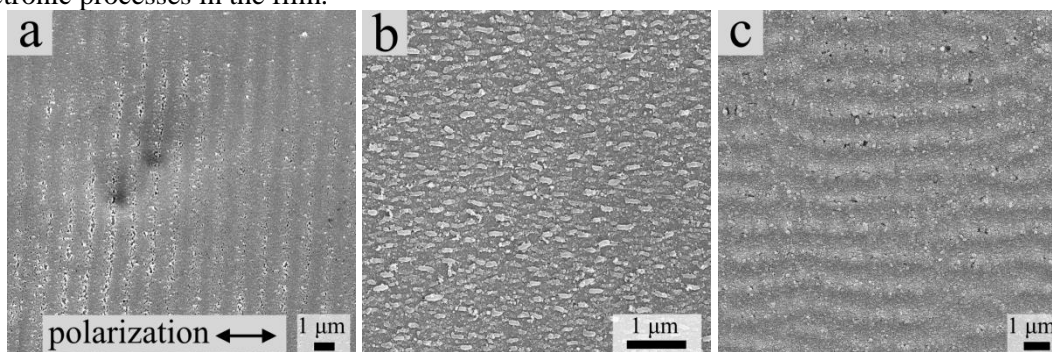


Figure 1. The images of a-Si:H film surface, processed with  $N_s = 50$  (a), 200 (b) and 1000 (c), obtained by scanning electron microscopy.

Raman spectroscopy revealed the formation of silicon nanocrystals in the a-Si:H films caused by ultrashort laser pulses of high power. The calculated nanocrystalline silicon phase volume fraction ranges from 15 to 67% depending on processing conditions of the a-Si:H film.

In addition, the presence of silicon polymorphs Si-III and Si-XII was detected in the a-Si:H films processed with  $N_s \geq 500$ . The proposed explanation of the observed Raman signal anisotropy is related to the ordered crystallographic axes orientation of silicon polymorphous nanocrystals formed in the film as a result of pulsed laser modification.

Thus the considered anisotropic structures based on a-Si:H can be used to create polarization-sensitive elements of optics and photovoltaics.

This work was supported by the Russian Foundation for Basic Research (project 17-52-04062) and Belarussian Republican Foundation for Fundamental Research (project F17RM-079)

[1] P.D. Rybalko, M.V. Khenkin, P.A. Forsh, et al., Femtosecond Laser Crystallization of Boron-doped Amorphous Hydrogenated Silicon Films, *J. Nano- Electron. Phys.* 2016. vol. 8, art. 03038 (2016).

[2] D.V. Shuleiko, F.V. Potemkin, I.A. Romanov, et al., Femtosecond laser pulse modification of amorphous silicon films: control of surface anisotropy, *Laser Phys. Lett.*, vol. 15, art. 056001 (2018).

# Enhancement of luminescence intensity and absorptivity in silicon via its structuring by ns pulses of Yb fiber laser

**D.S. Polyakov<sup>1</sup>, V.P. Veiko<sup>1</sup>, A.E. Kalyadin<sup>2</sup>, N.A. Sobolev<sup>2</sup>, S.V. Ponomar<sup>1</sup>, N.M. Salnikov<sup>1</sup>**

*1- ITMO University, Kronverksky 49, Saint-Petersburg, Russia  
2- Ioffe Institute, Polytekhnicheskaya 26, Saint-Petersburg, Russia  
polyakovdmitry1988@gmail.com*

It is well known that laser processing of silicon has many potential applications in semiconductor technology. For example, laser radiation can be used for damage annealing of ion implanted silicon [1], for creation of antireflective relief [2], which allows to improve the efficiency of solar cells, and so on. At the same time the influence of laser treatment of silicon on luminescent properties in near IR range is not studied practically. Such investigations is very important for development of novel methods of improvement of luminescent properties of silicon for creation of effective silicon light emitting diodes. So the aim of this work was to study the impact of laser pulsed irradiation on luminescent properties of silicon in near IR range.

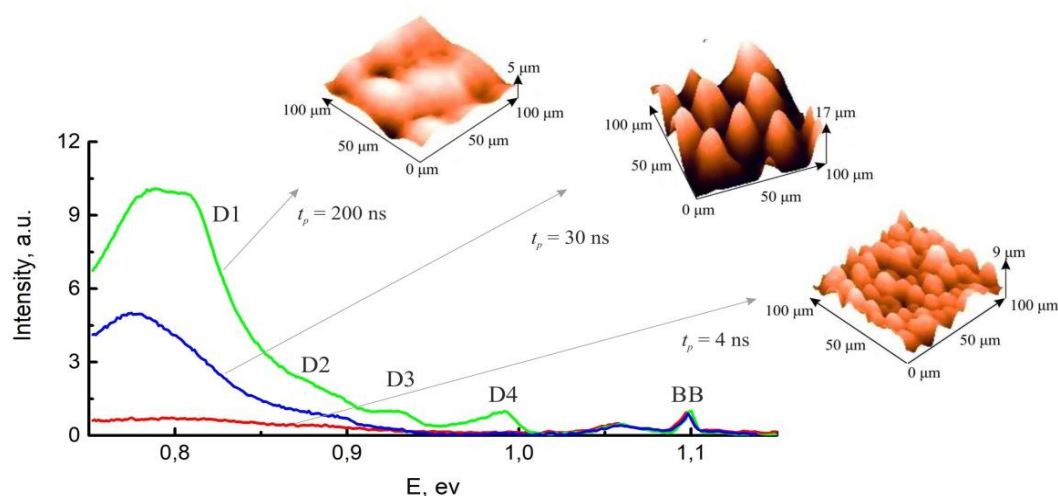


Fig. 1. Luminescent spectra (at 10 K) and AFM images of the surfaces taken at various irradiation conditions.

Wafers of n-Cz-Si (100) were irradiated by nanosecond pulsed periodic Yb fiber laser with a wavelength of 1.07  $\mu\text{m}$ . We used a laser intensity higher than the melting threshold, different numbers of surface scan cycles and pulse durations from a nanosecond range (4, 30 and 200 ns). Surface relief was studied by the techniques of optical and atomic force microscopy (AFM). Luminescent properties were measured in the range of 1000 – 1650 nm at temperatures 10 - 180 K. A reflection coefficient was studied in a visible range.

We observed the formation of microrelief consisting of microconical tips (for pulse durations 4 and 30 ns), which decrease reflection coefficient below 10% in visible range of spectrum, and relief consisting of grooves intersecting at an angle of 90° (for pulse duration 200 ns). Such modification was followed by the appearance of so called D1 – D4 dislocation-related luminescence lines (see Fig.1). The influence of a laser treatment mode on an intensity of the D1 line and an absorptivity of the laser-treated silicon was examined. The dependences of the D1 line intensity and its spectral position on the measurement temperature were also studied.

This work was supported by RSF grant # 18-79-10171

[1] W. Yang, J. Mathews, J.S. Williams. Hyperdoping of Si by ion implantation and pulsed laser melting, *Materials Science in Semiconductor Processing*. vol. 62, pp. 103-114, (2017)

[2] X. Liu et al, Black silicon: fabrication methods, properties and solar energy applications, *Energy Environ. Sci*, vol.7, pp. 3223-3263, (2014).

## Laser synthesis of the WO<sub>3</sub> thin films

O. Novodvorsky<sup>1</sup>, L. Parshina<sup>1</sup>, O. Khramova<sup>1</sup>, A. Lotin<sup>1</sup>, V. Mikhalevsky<sup>1</sup>, P. Shchur<sup>2</sup>

<sup>1</sup>ILIT RAS, Branch of the Federal Scientific Research Center «Crystallography and Photonics» of Russian Academy of Sciences, 140700 Shatura, Russia

<sup>2</sup> Federal State Unitary Enterprise «All-russian scientific research institute of aviation materials» State Research Center of the Russian Federation, 105005 Moscow, Russia

[ParshinaLiubov@mail.ru](mailto:ParshinaLiubov@mail.ru)

Interest in the WO<sub>3</sub> films is caused by their electrochromic properties which are found out in the wavelength range from UV to long-wave IR of the spectral region [1], that allows to create photodetectors in a wide interval of the wavelengths. The electrochromic properties of the WO<sub>3</sub> films allow to control their optical characteristics depending on the size and the sign of the applied voltage.

The WO<sub>3</sub> thin films on the *c* - sapphire substrates has been received by the pulse laser deposition method at a different oxygen pressure in the vacuum chamber. Ablation of the metal targets was performed by the excimer KrF-laser radiation with the wavelength of 248 nm. The oxygen pressure in the vacuum chamber in the course of the film growth was changed from 20 to 60 mTorr. The film thickness was varied from 42 to 275 nm. Synthesis of all layers was carried out at the room temperature of the substrate in the droplet-free mode of the pulse laser deposition method [2]. The oxygen pressure influence on the optical transmission and morphology of the WO<sub>3</sub> films was investigated. The dependence of the films transmission in the range from 250 to 2000 nm from the oxygen pressure in the vacuum chamber in the course of the film growth was established (Fig.1).

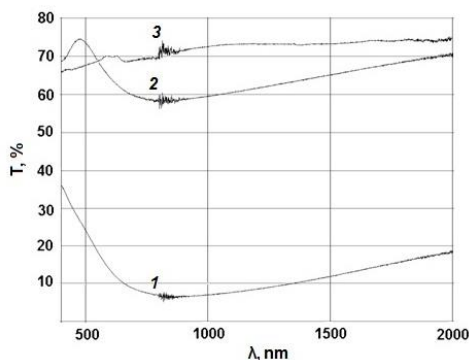


Fig. 1. Transmission spectra of the WO<sub>3</sub> films in the range from 400 to 2000 nm produced at a different oxygen pressure in the course of the film growth: 1 - 20 mTorr, 2 - 40 mTorr, 3 - 60 mTorr.

It was established that the transmission of the films exceeds 70% in visible and IR of the spectral region at the oxygen pressure of 60 mTorr. The surface roughness of the films poorly depends on the oxygen pressure at the film growth. The surface roughness was 4-5 nm.

This work was supported by the Federal Agency of Scientific Organizations (Agreement № 007-Г3/У3363/26) in part of produce of the films and by the Russian Science Foundation (Project № 16-29-05385, 16-07-00842, 17-07-00615) in part of investigation of the films.

[1] K. Sauvet, L. Sauques, A. Rougier, Electrochromic properties of WO<sub>3</sub> as a single layer and in a full device: From the visible to the infrared, *J. Phys. Chem. Solid.*, vol. 71, pp. 696–699, (2010).

[2] L.S. Parshina, O.D. Khramova, O.A. Novodvorsky, A.A. Lotin, I.A. Petukhov, F.N. Putilin, K.D. Shcherbachev, Effect of energy density on the target on SnO<sub>2</sub>:Sb film properties when using a high-speed particle separator, *Semiconductors*, vol. 51, № 3, pp. 407–411, (2017).

# Modeling of the dynamics of processes in a laser-plasma plume during the ablation of a metal target in a gas

**V.I.Mazhukin<sup>1,2</sup>, A.V.Shapranov<sup>1,2</sup>, M.M.Demin<sup>1</sup>**

1- Keldysh Institute of Applied Mathematics of RAS, Miusskaya sq., 4, Moscow, 125047, Russia

2- National Research Nuclear University "MEPhI", Kashirskoe shosse, 31, Moscow, 115409, Russia

e-mail: vim@modhef.ru

Irradiation of metal targets placed in the atmosphere of the surrounding gas by laser pulses of nanosecond duration initiates a sequence of complex processes that occur during and after exposure.

Modeling of pulse ablation processes includes laser and radiation (plasma radiation flux) heating of the target, heterogeneous phase transitions of the first kind (melting, evaporation), space-time transport of mass, momentum and energy, ionization of the vaporized matter and the surrounding gas in the laser field and plasma radiation.

The mathematical description of the processes in the target is realized in the 1-D approximation of the nonstationary multi-front hydrodynamic Stefan problem. In a gaseous medium, the processes are described in the framework of the 1-D radiation gas dynamic model.

The results of the simulation testify about the key role of the interaction of the laser plasma with the target. The high pressure in the plasma contributes to the change in the mechanism of laser evaporation by the mechanism of surface condensation of a previously evaporated substance, Fig. 1,2. In the plasma, shock waves appear that interact with the target surface and a shock wave traveling along the cold gas. The use of the dynamic adaptation method in modeling made it possible to explicitly identify and track the dynamics of phase, contact boundaries and fronts of shock waves, establish the role of phase transitions, laser plasma, and the thermal and contact interaction of a plasma plume with the evaporating target surface.

The work was supported by Russian Science Foundation, grant No. 18 - 11-00318

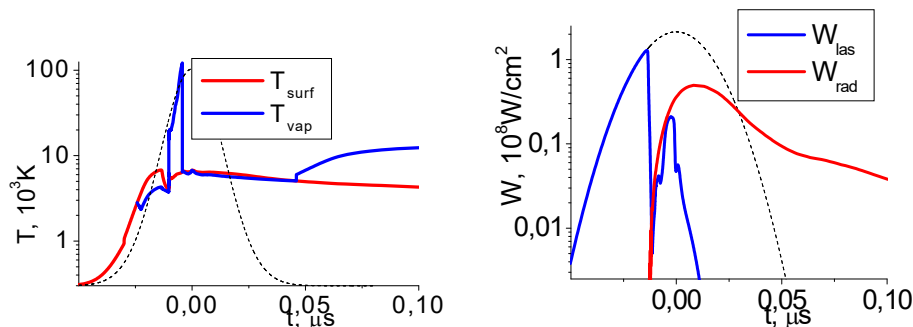


Fig. 1. Surface and vapor temperature versus time. Fig. 2. Laser and plasma radiation flux versus time.

[1] V.I. Mazhukin, A.V. Mazhukin, M. G. Lobok, Comparison of Nano- and Femtosecond Laser Ablation of Aluminium, *Laser Physics*, vol. 19(5), pp. 1169 – 1178, (2009).

[2] V.I. Mazhukin, A.V. Shapranov, A.V. Mazhukin, O.N. Koroleva, Mathematical formulation of a kinetic version of Stefan problem for heterogeneous melting/crystallization of metals, *Mathematica Montisnigri*, vol. 36, pp. 58-77, (2016).

[3] A.V. Mazhukin, V.I. Mazhukin, Dynamic Adaptation for Parabolic Equations, *Computational Mathematics and Mathematical Physics*, vol. 47(11), pp. 1833 – 1855, (2007).

[4] P.V. Breslavskii, V.I. Mazhukin, Dynamically adapted grids for interacting discontinuous solutions, *Computational Mathematics and Mathematical Physics*, vol. 47(4), pp. 687-706, (2007).

# Recoil pressure behavior in nanosecond laser ablation: theory and experiment

A.A. Samokhin<sup>1</sup>, E.V. Shashkov<sup>1</sup>, N.S. Vorob'ev<sup>1</sup>, A.E. Zubko<sup>1</sup>

*1- Prokhorov General Physics Institute of the Russian Academy of Science, Moscow, Russia*

*aleksey.zubko11@gmail.com*

In [1] recoil pressure behavior in absorbing liquids (water, ethanol) irradiated with erbium laser pulses ( $\lambda = 2.94 \mu\text{m}$ , 200 ns duration and the harmonic modulation period 7 ns due to mode beating) was investigated with the help of pressure transducer. It was found that at sufficiently low intensity modulated part of acoustic signal is similar to the modulated part of laser intensity while at higher intensity the acoustical modulation amplitude behavior is strongly non-monotonous. This behavior was attributed to the interference effect between thermoacoustic and vaporization mechanisms of recoil pressure generation.

Here it is shown that surface vaporization contribution is insufficient to describe recoil pressure behavior in [1] so that bulk vaporization processes should be taken into account. It is worthwhile to note that the surface-bulk evaporation problem in comparison of thermoacoustic and vaporization pressure contributions to observed recoil pressure was not discussed in [1-3].

Using nanosecond laser pulses with modulated intensities and comparison of acoustical and laser modulation signals provides realization of ablation front displacement during irradiation as it was shown in [3] in conditions similar to [1]. The acoustical monitoring method is based on the difference between acoustical and laser modulation signals due to acoustical Doppler effect from moving subsurface irradiated zone where light energy is absorbed.

In absorbing dielectrics [1, 3] radiation penetration length  $l \gtrsim 1 \mu\text{m}$  is not small and this fact leads to severe restriction on the surface evaporation model applicability. For metals and optical radiation  $l$  is rather small so that the difference between surface temperature and subsurface maximum temperature values is also small so that the surface evaporation model can be used approximately up to the surface temperature superheating limit [4].

However, for metals another problem arises which is connected with interplay between thermoacoustic and surface evaporation mechanisms of recoil pressure generation. This interplay results in additional deformation of recoil pressure and leads to complication in evaluation of irradiated surface displacement from comparing modulated parts of laser intensity and acoustic signals.

To avoid this complication it is possible to use for laser intensity modulation mode-locking process instead of mode-beating which was applied in earlier papers [1, 3]. This modification gives rise to relative increasing of thermoacoustic pressure signals compared with surface vaporization contribution and diminishes unwanted here interference effect between thermoacoustic and vaporization mechanisms of recoil pressure generation. Experimental realization of such laser-metal ablation acoustical monitoring is described which includes two different laser generating simultaneously a train of about 80 short mode-locked pulses (each 60 ps duration with period 8 ns) and a heating pulse of about 50 ns duration. Preliminary results of the experiment are also reported.

[1] A.A. Samokhin, V.I. Vovchenko, N.N. Il'ichev, Photoacoustic and evaporation pressure signals in water irradiated with erbium laser pulses, *Physics of Wave Phenomena*, Vol. 16, No. 4, pp. 275–282, (2008).

[2] A.A. Samokhin and N.N. Il'ichev, On photoacoustic monitoring of laser evaporation front movement, *Quantum Electron.* Vol. 40, No. 8, pp. 659–660 (2010).

[3] A.A. Samokhin. First-order phase transitions induced by laser radiation in absorbing condensed matter, in *Effect of laser radiation on absorbing condensed matter*, Nova Science Publishers, ed. by V.B. Fedorov, (1990).

[7] M.W. Sigrist and F.K. Kneubuhl. Laser-generated stress waves in liquids, *J. Acoust. Soc. Am.*, Vol. 64, pp. 1652-1663 (1978).

# On critical parameters manifestations during nanosecond laser ablation of metals

**A.A. Samokhin<sup>1</sup>, V.I. Mazhukin<sup>2,3</sup>, M.M. Demin<sup>2</sup>, A.V. Shapranov<sup>2,3</sup>, A.E. Zubko<sup>1</sup>**

1- Prokhorov General Physics Institute of the Russian Academy of Science, Moscow, Russia

2- Keldysh Institute of Applied Mathematics, RAS, Moscow, Russia

3- National Research Nuclear University "MEPhI", Moscow, Russia

asam40@mail.ru

Despite several decades of nanosecond laser ablation investigations some important fundamental aspects remain unclarified yet which concern, among others, to the problem of non-equilibrium behavior of irradiated matter. Such studies are necessary *e.g.* for obtaining information on metal critical parameters most of which can not be determined in quasi-equilibrium experiments.

In our previous papers (see *e.g.* ref. [1] and references therein) non-equilibrium pressure  $P$ , temperature  $T$  and density  $\rho$  behavior during ablation of thin (450 nm) liquid Al film under the action of nanosecond laser pulses was considered in the framework of molecular dynamic modeling for different constant intensities  $I = 33, 44, 55, 66$  and  $110 \text{ MW/cm}^2$ . It was found that the recoil pressure demonstrates several pulsations due to repeating explosive boiling processes which are clearly visible at  $I = 33$  and  $44 \text{ MW/cm}^2$  and vanishes at higher intensities (fig. 1a) when mean recoil pressure exceeds the value 0.6 compared with critical pressure  $P_C = 1400 \text{ bar}$  in the model used.

In the present report density fluctuations behavior are presented for the same irradiation intensities the highest of which provides realization of transcritical ablation regime. Fig 1b-d shows 2D density distribution as well as curves of pressure, temperature, density and density fluctuations  $\Delta\rho = (\langle\rho^2\rangle - \langle\rho\rangle^2)^{1/2}$  distributions at  $I = 110 \text{ MW/cm}^2$  and  $t = 300, 650$  and  $900 \text{ ps}$  after the irradiation is switched on. The brackets  $\langle \dots \rangle$  denote averaging over the volume  $\Delta Z \times \Delta X \times \Delta Y$  where  $\Delta Z = 20 \text{ nm}$  and  $\Delta X = \Delta Y = 37.3 \text{ nm}$  are space dimensions in periodical boundary condition of the calculation procedure while  $\rho$  corresponds to average particle number in the volume  $\Delta Z_1 \times \Delta X \times \Delta Y$  with  $\Delta Z_1 = 1 \text{ nm}$ . Large fluctuations values at the left film side are due to presence of sharp density jump at liquid-vapor boundary.

It is evident from the curve 2 behavior in fig. 1b-d that the density fluctuations distributions have a maximum value which located at the same point as critical density value  $\rho_C = 0.5 \text{ g/cm}^3$  in the model used. In subcritical and critical region this maximum value exceeds the fluctuation level outside the region by factor about 9 (fig. 1b,c) which diminishes in supercritical region (fig. 1d).

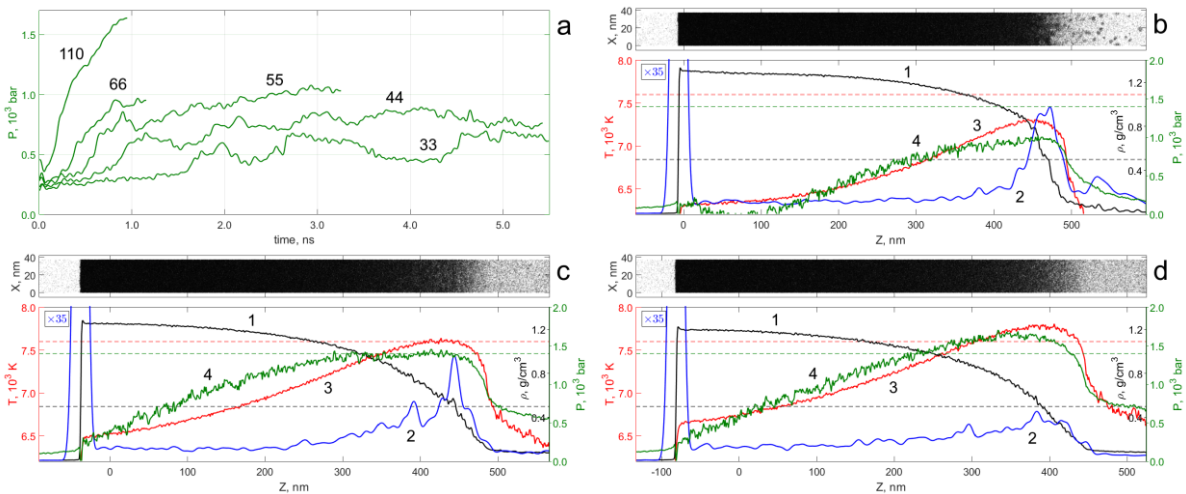


Fig. 1. Pressure recoil time evolution (a) at different intensity values shown in  $\text{MW/cm}^2$  above the corresponding pressure curve. Parts (b-d) shows 2D density distribution as well as 1D density (1), density fluctuations (increased by factor 35 with respect to the  $\rho$  scale) (2), temperature (3), pressure (4) distributions at  $I = 110 \text{ MW/cm}^2$  and  $t = 300, 650$  and  $900 \text{ ps}$ . Dashed lines is the model critical parameters values  $T_C = 7600 \text{ K}$ ,  $P_C = 1400 \text{ bar}$ ,  $\rho_C = 0.5 \text{ g/cm}^3$ .

[1] A.A. Samokhin, V.I. Mazhukin, M.M. Demin, A.V. Shapranov, A.E. Zubko, Molecular dynamics simulation of Al explosive boiling and transcritical regimes in nanosecond laser ablation, *Mathematica Montisnigri*, vol. 41, pp. 55-72, (2018).

# High intensity pulsed coils for the investigation of laser-plasma interaction with ambient magnetic field

A. Luchinin, V. Malyshev, M. Morozkin, M. Starodubtsev, M. Proyavin, A. Fokin,  
**T. Krapivnitskaia** and M. Glyavin

*Institute of Applied Physics, 46 Ulyanov Street, 603950 Nizhny Novgorod, Russia  
 kto465@yandex.ru*

The studies on the formation of different plasma structures in an ambient magnetic field are of great interest for astrophysics and inertial fusion. Different astrophysical objects could be modeled in such laboratory experiments. Such astrophysical objects characterizes by the perturbation of the magnetic field structure and development of different magneto-hydrodynamic instabilities, which could not be studied analytically and should be studied through laboratory modeling [1]. The needed conditions for investigation of plasma dynamics in magnetic field are provided by the specially designed magnetic coil. The design scheme of the coil is presented in Fig. 1. To satisfy the requirements for the plasma formation and diagnostics the coil must have three mutually perpendicular apertures of free space inside the coil, that provide the possibility of positioning the target, irradiating the target with powerful nanosecond laser beam and observing the dynamics of plasma expansion perpendicular to the main axis of the direction of propagation of the plasma stream.

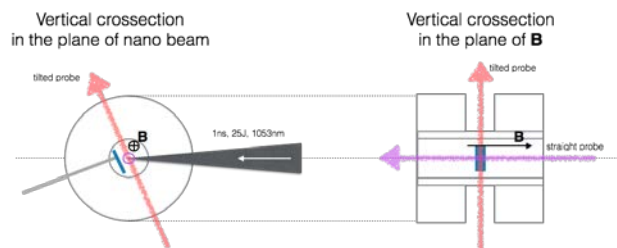


Fig. 1. Magnetic coil

The report presents the Helmholtz magnetic coil, developed and manufactured by the IAP RAS, based on the existing technology successfully applied for high intensity (up to 50T) pulsed magnets [2]. The coil current is controlled by a capacitor discharge unit with maximum current up to 8 kA. The discharge of the coil occurred over times of the order of several milliseconds. The field was considered stationary at time scales of the order of several microseconds, much larger than the times of the investigated plasma dynamics of the order of 100 ns. The magnetic field was practically uniform in the axial and radial directions at scales of the order of 20 mm, which exceeded the characteristic scales of the investigating plasma ( $\sim 10$  mm). The repetition of the magnetic field amplitude and profile was ensured by cryogenic cooling of the system with liquid nitrogen. Typically, the coil can operate 1 short per 10 minute. The obtained profiles of magnetic field for co- and counter-directional coil setup are presented on Fig. 2.



Fig. 2. Magnetic field profile

The operating magnetic field used in experiment was 15 T for the co-directional setup, which was good enough for successful experiments, made on PEARL facility.

The work supported in part by the Russian Scientific Foundation under the project 14-12-00887.

[1] M. Starodubtsev et al. Laboratory investigation of magnetized laser plasmas expansion into the vacuum, ICONO/LAT 2016, Minsk, Belarus.

[2] M. Glyavin et al. A pulse magnetic field generator for terahertz gyrodevices, Instruments and Experimental Techniques 54(1):77-80, 2011

# Influence of carrier degeneracy and the band gap on the melting of silicon and its thermophysical properties

O.N. Koroleva, A.V. Mazhukin

1- Keldysh Institute of Applied Mathematics of RAS, 125047, Russia, Moscow, Miusskaya sq., 4

2- National Research Nuclear University MEPhI, 115409, Russia, Moscow, Kashirskoe shosse, 31

e-mail: koroleva.on@mail.ru

With the help of mathematical modeling, the melting characteristics and thermophysical characteristics of silicon in the region of semiconductor-metal phase transformation are studied. The influence of degenerate carriers and the band gap on the melting of silicon and its properties is considered in the temperature range 300-2000 K. Various mechanisms that cause the narrowing of the band gap in strongly heated silicon are analyzed. Since in the high-temperature region at high carrier concentrations, the degeneracy of the electron gas occurs earlier than the melting of silicon, it becomes necessary to use Fermi-Dirac quantum statistics [1, 2]. It is shown that under conditions of sufficiently strong heating of the intrinsic semiconductor, when the quasineutrality is satisfied, the effects of carrier degeneracy cause a strong narrowing of the band gap. The obtained temperature dependences of the band gap and thermal characteristics are compared with the experimental results (Fig. 1.2).

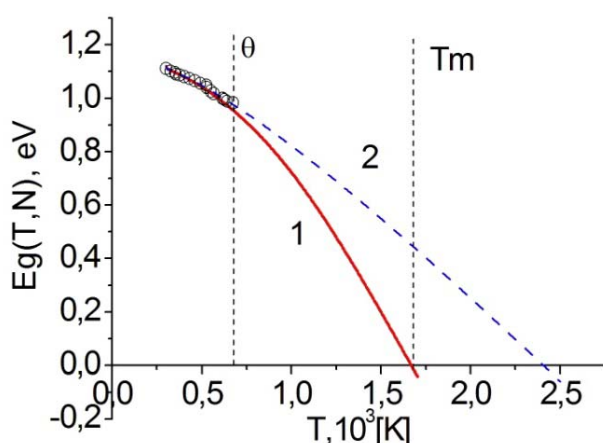


Figure 1. Temperature dependence of the band gap of silicon, calculated using: 1 - quantum and 2 - classical statistics. Markers - experimental data [3].

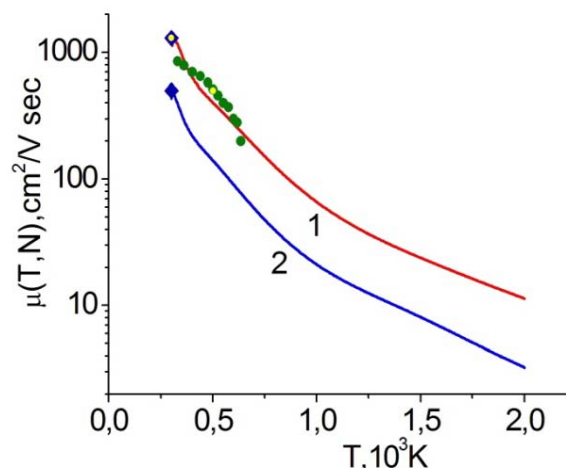


Figure 2. Temperature dependences of mobilities (1) of electrons, (2) holes. Markers - reference [4] and experimental data [5-6].

**Acknowledgements:** This study was supported by the Russian Science Foundation (project no. 18-11-00318)

- [1] O.N. Koroleva, V.I. Mazhukin and A.V. Mazhukin. "Calculation of silicon band gap by means of Fermi-Dirac integrals", *Mathematica Montisnigri*, 38, 49-63, 2017
- [2] O.N. Koroleva, A.V. Mazhukin, V.I. Mazhukin, and P.V. Breslavskiy, "Analytical Approximation of the Fermi-Dirac Integrals of Half-Integer and Integer Orders", *Mathematical Models and Computer Simulations*, 9(3), 383-389 (2017).
- [3] Y. P. Varshni, "Temperature dependence of the energy gap in semiconductors", *Physica*, 34 (1), 149-154 (1967).
- [4] "Fizicheskie velichiny", *Spravochnik pod red. I.S. Grigoreva, E.Z. Meilihova*. M.: Energoatomizdat (1991).
- [5] Iu.P. Kardona, "Osnovy fiziki poluprovodnikov", FIZMATLIT, (2002)
- [6] J. Batista, A. Mandelis, and D. Shaughnessy, "Temperature dependence of carrier mobility in Si wafers measured by infrared photocarrier radiometry", *Appl. Phys. Lett.*, 82 (23), 4077-4079 (2003).

# Percolation thresholds in the composites with the cermet topology in the Bruggeman approximation

L. Apresyan<sup>1</sup>, S. Rasmagin<sup>1</sup>, V. Krasovskii<sup>1</sup>, V. Krysh Tob<sup>1</sup>, V. Pustovoy<sup>1</sup>

*1- Prokhorov General Physics Institute of Russian Academy of Sciences  
38, Vavilov st, Moscow, 119991, Russia*

*krasovskii@nsc.gpi.ru*

In the description of optical phenomena in a wide variety of randomly inhomogeneous media, the well-known Bruggeman approximation [1] is widely used, which makes it possible to qualitatively describe the occurrence of the flow threshold and the sharp change in the observed characteristics of the medium associated with its passage. Randomly inhomogeneous composites consisting of several macroscopic components are usually divided into aggregates (statistically symmetric, such as mixtures of powders) and cermets (asymmetric, in which the statistics of the spatial distribution of the matrix is different from the statistics of fillers, as in the case of media with random inclusions) [2]. The symmetric approximation of the effective field of Bruggeman formally refers to composites of the first type, although the applications are widely used and for the case of cermet [3, 4]. The work considers variants of generalizations of this approximation for multicomponent randomly inhomogeneous media containing discrete inclusions with different morphology [5, 6], carbon nanotubes and graphene, for example. The expressions for the thresholds of flow was obtained. It shows that the considered approximations imply the "formula of inverse threshold addition" derived earlier in the literature based on the exclusive volume estimation [7]. This formula does not allow taking into account the synergetic effects that lead to a decrease in the flow threshold of a multi-component composite compared to the threshold when using only one of the components. The description of synergism lies beyond the approximation of the effective environment and requires taking into account correlation effects, for example, with the involvement of a generalization of the theory of the exclusive volume [8], implicitly taking into account interparticle correlations.

This work was supported by the Presidium of RAS (Program I.7 "Modern problems of photonics, the probing of inhomogeneous media and materials")

[1] D.Bruggeman, Berechnung verschiedener physikalischer Konstanten von heterogenen Substanzen. I. Dielektrizitätskonstanten und Leitfähigkeiten der Mischkörper aus isotropen Substanzen, Ann.Phys., vol.23. pp. 636-664 (1935).

[2] W. Lamb, D. M. Wood, N. W. Ashcroft, Long-wavelength electromagnetic propagation in heterogeneous media Phys.Rev.B 21(6) pp.2248-2266 (1980).

[3] Quinten M. Optical properties of nanoparticle systems: Mie and beyond. Weinheim: Wiley-VCH (2011).

[4] F. Qin and C. Brosseau. A review and analysis of microwave absorption in polymer composites filled with carbonaceous particles, J. Appl. Phys. 111, 061301 (2012).

[5] Y. Wang and G. J. Weng. Electrical Conductivity of Carbon Nanotube and Graphene-Based Nanocomposites, In: S.A. Meguid, G.J. Weng (eds.), Micromechanics and Nanomechanics of Composite Solids, Springer International Publishing AG Ch. 4 (2018).

[6] L. Apresyan, D. Vlasov, D. Zadorin, V. Krasovskii, On the Effective Medium Model for Particles with a Complex Structure, Technical Physics, , Vol. 62(1), pp.6–13 (2017).

[7] Y. Sun, H.-D. Bao, Z.-X. Guo, J. Yu., Modeling of the Electrical Percolation of Mixed Carbon Fillers in Polymer-Based Composites, Macromolecules, 42, pp.459-463 (2009).

[8] Y. Chen, F. Pan, S. Wang, B. Liu, J. Zhang. Theoretical estimation on the percolation threshold for polymer matrix composites with hybrid fillers, Composite Structures 124 pp.292–299 (2015).

# Application of Effective Medium Approximations for Multicomponent Composites Description

L.Apresyan<sup>1</sup>, S.Rasmagin<sup>1</sup>, V.Krasovskii<sup>1</sup>, V.Krysh Tob<sup>1</sup>, V. Pustovoy<sup>1</sup>

1- Prokhorov General Physics Institute of Russian Academy of Sciences  
38, Vavilov st, Moscow, 119991, Russia

*krasovskii@nsc.gpi.ru*

In describing of the most experiments connected with the passage of laser radiation through nanocomposite media, the concept of effective parameters is widely used, which makes it possible to estimate the observed optical characteristics in a quasistatic approximation without solving the rigorous equations of electrodynamics (the so-called homogenization theory [1]). There is a set of heuristic approaches to the determination of these parameters, one of which is the well-known Bruggeman effective medium approximation [2]. In this paper we compare several variants of its generalizations using elliptic cells ("uniaxial" approximation, the approximation with averaging over chaotic particle orientations [3], the modified Bruggeman approximation [4]) for the description of statistically isotropic composite media containing multicomponent fillers with strongly different structures. Expressions for the corresponding percolation thresholds are given. It is shown that all these approximations lead to the same "rule of addition of inverse percolation thresholds" obtained earlier in the literature with the use of the exclusive volume estimates [5]. On the example of a model problem with parameters corresponding to a polymer matrix with carbon nanotubes and graphene used as a filler shows that all the models considered lead to an effective conductivity lying within the Hashin-Shtrikman boundaries [6, 7]. Note that this "rule of addition" does not describe the synergistic effect often observed for the percolation thresholds (in contrast to the statements found in the literature [8]).

This work was supported by the Presidium of RAS (Program I.7 "Modern problems of photonics, the probing of inhomogeneous media and materials")

[1] A. Sihvola, H. Wallén, Homogenization of amorphous media. In *Amorphous Nanophotonics*, Series: Nano-Optics and Nanophotonics, Springer, Berlin, Chapter 3, 67-87 (2013).

[2] D. Bruggeman, Berechnung verschiedener physikalischer Konstanten von heterogenen Substanzen. I. Dielektrizitätskonstanten und Leitfähigkeiten der Mischkörper aus isotropen Substanzen, *Ann. Phys.* Vol.23, pp.636-664 (1935).

[3] Y. Wang, G. Weng, Electrical Conductivity of Carbon Nanotube and Graphene-Based Nanocomposites, S.A. Meguid, G.J. Weng (eds.), *Micromechanics and Nanomechanics of Composite Solids*, Springer International Publishing, Ch. 4 (2018).

[4] L. Apresyan, D. Vlasov, D. Zadorin, and V. Krasovskii, On the Effective Medium Model for Particles with a Complex Structure, *Technical Physics*, Vol. 62 (1), pp.6-13 (2017).

[5] Y. Sun, H.-D. Bao, Z.-X. Guo, and J. Yu., Modeling of the Electrical Percolation of Mixed Carbon Fillers in Polymer-Based Composites, *Macromolecules*, 42, pp.459-463 (2009).

[6] Z. Hashin, S. Shtrikman, A Variational Approach to the Theory of the Elastic Behaviour of Multiphase Materials, *J. Mech Phys. Solids*, vol. 11, pp. 127-140 (1963).

[7] G.W. Milton. *The Theory of Composites*, Cambridge University Press (2004).

[8] H. Liu, J. Gao, W. Huang, K. Dai et al., Electrically Conductive Strain Sensing Polyurethane Nanocomposites with Synergistic Carbon Nanotubes and Graphene Bifillers, *Nanoscale*, Vol. 8, pp.12977-12989 (2016).

# **LASER SYSTEMS AND MATERIALS**

# Photonic Engineered Crystals: Laser Crystals with Embedded Sub-Wavelength Nanophotonics

**A. Ródenas and R. Osellame**

*Istituto di Fotonica e Nanotecnologie (IFN), Consiglio Nazionale delle Ricerche (CNR), Milano, Italy*

*Main author email address: [arodenas@gmail.com](mailto:arodenas@gmail.com)*

We present a technique for the direct volume nanostructuring of brittle crystalline optical media at large scale. The work paves the way to the merging of diverse fields of photonic crystal fibers and solid state lasers, opening a road towards novel monolithic 3D nanophotonic crystalline devices for both coherent light generation and control.

We will show how the creation of air pore lattices with feature sizes at the 100 nm level and lengths on the cm scale is feasible inside a laser crystal in absence of crack formation and damage, this allowing to directly engineer seamless sub-wavelength photonic structures inside high quality optical crystals for the first time to our knowledge. First results on the fabrication of inside-the-crystal photonic elements with optical responses driven by sub-wavelength confined light modes will be presented, such as high-efficiency sub-wavelength diffraction gratings, photonic crystal waveguides and nanopore lattices with spacing down to 250 nm level.

The achievement of true 3D nanolithography in optical crystals could give birth to a new field of "photonic engineered crystals", where standard homogeneous crystals are engineered at sub-wavelength scale, effectively achieving metamaterial bespoke properties.

# Nonlinear optical properties of Langasite crystals

Haohai Yu

*State Key Laboratory of Crystal Materials and Institute of crystal Materials, Shandong University, 27 Shanda Nanlu, Jinan 250100, China*

*haohaiyu@sdu.edu.cn*

Mid-infrared lasers using nonlinear optical (NLO) crystals have essential applications in science as well as daily life, such as infrared remote sensing, biological tissue imaging, environmental monitoring, and minimally invasive medical surgery. For generating mid-infrared lasers in the spectral range of 3–20  $\mu\text{m}$ , NLO materials are indispensable by optical parametric oscillation (OPO) or difference frequency generation (DFG) [1]. It is common that the available wavelength range is limited by the multi-phonon absorption in the oxide crystal and the damage threshold of the semiconductor is relatively low, the development of useful mid-IR NLO materials is thus limited by the requirements of a wide mid-IR transparent window, high laser damaged threshold (LDT), and strong NLO effect. Therefore, the rapid development of current mid-IR lasers urgently requires the discovery of new mid-IR NLO materials with good performance.

In this work, we focused on langasite family compounds, with the general formula of  $A_3BC_3D_2O_{14}$ , proper effective nonlinear coefficient, high LDT, good growth habits, and excellent thermo-mechanical properties. Based on the theoretical analysis of the coupling between optical activity and the electro-optic properties of  $\text{La}_3\text{Ga}_5\text{SiO}_{14}$  (LGS) during the Q-switching process, we constructed a LGS Q-switched laser with a  $\text{Nd}:\text{LuVO}_4$  as the laser crystal. Second-order nonlinear properties of  $\text{La}_3\text{Ga}_{5.5}\text{Nb}_{0.5}\text{O}_{14}$  (LGN) crystal have been evaluated, including the Sellmeier equations, nonlinear coefficients, and optical damage threshold. The results show that LGN is a very promising nonlinear optical crystal that can be used for OPO in the atmospheric transmission band II (3–5  $\mu\text{m}$ ), and so on. We also built structure-composition-property maps that describe the NLO properties in these materials by combining computational property prediction and experimental characterization. Accordingly, rational molecular design was performed, a new member of the langasite family,  $\text{La}_3\text{SnGa}_5\text{O}_{14}$  (LGSn), was synthesized, and single crystals were grown. The produced material exhibits the widest transparent region among available oxides, the largest LDT among materials that are transparent to 10  $\mu\text{m}$ , and the strongest SHG effect among langasite. They are potential mid-infrared nonlinear optical crystals.

[1] V. Petrov, "Frequency down-conversion of solid-state laser sources to the mid-infrared spectral range using non-oxide nonlinear crystals," *Progress in Quantum Electronics*, vol. 42, pp. 1–106, 2015.

## Monoclinic Monotungstates – Novel Efficient Laser Materials

**P. Loiko<sup>1,2,\*</sup>, L. Zhang<sup>3</sup>, H. Lin<sup>3</sup>, G. Zhang<sup>3</sup>, J.M. Serres<sup>1</sup>, E. Kifle<sup>1</sup>, Y. Wang<sup>4</sup>,  
J. R. Vázquez de Aldana<sup>5</sup>, Carolina Romero<sup>5</sup>, M. Aguiló<sup>1</sup>, F. Díaz<sup>1</sup>, V. Petrov<sup>4</sup>,  
U. Griebner<sup>4</sup>, Z. Lin<sup>3</sup>, W. Chen<sup>3,4</sup>, and X. Mateos<sup>1</sup>**

*1-Universitat Rovira i Virgili, Departament Química Física i Inorgànica, Física i Cristal·lografia de Materials i Nanomaterials (FiCMA-FiCNA)-EMaS, Campus Sescelades, 43007 Tarragona, Spain*

*2-ITMO University, 49 Kronverkskiy pr., 197101 St. Petersburg, Russia*

*3-Key Laboratory of Optoelectronic Materials Chemistry and Physics, Fujian Institute of Research on the Structure of Matter, Chinese Academy of Sciences, Fuzhou, 350002 Fujian, China*

*4-Max-Born-Institute for Nonlinear Optics and Short Pulse Spectroscopy, Max-Born-Str. 2a, 12489 Berlin, Germany*

*5- Aplicaciones del Láser y Fotónica, University of Salamanca, 37008 Salamanca, Spain*

\*Email address: [kinetic@tut.by](mailto:kinetic@tut.by)

Monoclinic divalent-metal monotungstates with a wolframite-type structure,  $M^{2+}WO_4$  where  $M = Mg, Cu, Ni, Co, Fe, Zn, Mn$  or  $Cd$ , are novel host materials for laser-active rare-earth ions ( $RE^{3+}$ ). Magnesium tungstate,  $MgWO_4$ , a representative of this crystal family, possesses high thermal conductivity [1], and intense, broad and strongly polarized spectral bands for the  $RE^{3+}$  ions [2]. The spectral broadening originates mostly from the doping mechanism, namely the replacement of small  $Mg^{2+}$  ions in  $C_2$  symmetry sites by the large  $RE^{3+}$  ones with univalent  $Na^+$  serving as charge compensator. In the present work, we review our recent achievements on the growth, structural, spectroscopic and laser characterization of monoclinic  $MgWO_4$  crystals doped with  $Yb^{3+}$ ,  $Tm^{3+}$  and  $Ho^{3+}$  ions. These materials are found to be exceptionally suitable for sub-100 fs mode-locked lasers at  $\sim 1$  and  $\sim 2$   $\mu m$ .

Room- and low-temperature spectroscopy of  $Yb^{3+}:MgWO_4$  has been studied. The optical indicatrix axes have been assigned. A compact microchip  $Yb^{3+}:MgWO_4$  laser has generated an output power of 5.12 W at  $\sim 1.06$   $\mu m$  with a slope efficiency  $\eta$  of 77%.

$Tm^{3+}:MgWO_4$  has been characterized in terms of structure, Raman spectroscopy, Judd-Ofelt analysis and crystal-field modeling yielding the Stark splitting. A unique feature of this crystal to generate linearly polarized laser output at  $> 2$   $\mu m$  has been established. A microchip  $Tm^{3+}:MgWO_4$  laser has generated an output power of 3.06 W at 2.03  $\mu m$  with  $\eta = 50\%$  [3]. Passive Q-switching of this laser has been realized using graphene, carbon nanotubes and  $Cr^{2+}:ZnS$  as saturable absorbers [3]. A  $Tm^{3+}:MgWO_4$  laser was continuously tuned from 1.897 to 2.062  $\mu m$  and “vibronic” laser operation (relying on electron-phonon coupling) at wavelengths as long as 2.093  $\mu m$  was achieved. A  $Tm^{3+}:MgWO_4$  laser mode-locked by graphene saturable absorber generated sub-100 fs (86 fs) pulses at 2.017  $\mu m$  with a repetition rate of 76 MHz [4].

The first channel waveguide  $Tm^{3+}:MgWO_4$  laser fabricated by femtosecond direct laser writing (fs-DLW) generated a record output power (0.32 W at 2.02  $\mu m$ ) for this type of lasers, featuring a slope efficiency as high as 71% and passive losses as low as  $\sim 0.1$  dB/cm. The first “vibronic” Tm waveguide laser emitting at 2.08  $\mu m$  has also been demonstrated.

For  $Ho^{3+}:MgWO_4$ , the spectroscopic properties were studied and the first in-band-pumped laser operation was realized at 2.104  $\mu m$  reaching a slope efficiency of 72%.

[1] L. Zhang, Y. Huang, S. Sun, F. Yuan, Z. Lin, and G. Wang, "Thermal and spectral characterization of  $Cr^{3+}:MgWO_4$  – a promising tunable laser material," *J. Lumin.*, vol. 169, part A, pp. 161-164 (2016).

[2] L. Zhang, W. Chen, J. Lu, H. Lin, L. Li, G. Wang, G. Zhang, and Z. Lin, "Characterization of growth, optical properties, and laser performance of monoclinic  $Yb:MgWO_4$  crystal," *Opt. Mater. Express*, vol. 6, pp. 1627-1634 (2016).

[3] P. Loiko, J. M. Serres, X. Mateos, M. Aguiló, F. Díaz, L. Z. Zhang, Z. B. Lin, H. F. Lin, G. Zhang, K. Yumashev, V. Petrov, U. Griebner, Y. C. Wang, S. Y. Choi, F. Rotermund, and W. D. Chen, "Monoclinic  $Tm^{3+}:MgWO_4$ : Novel crystal for continuous-wave and passively Q-switched lasers at  $\sim 2$   $\mu m$ ," *Opt. Lett.*, vol. 42, pp. 1177-1180 (2017).

[4] Y. Wang, W. Chen, M. Mero, L. Zhang, H. Lin, Z. Lin, G. Zhang, F. Rotermund, Y. J. Cho, P. Loiko, X. Mateos, U. Griebner, and V. Petrov, "Sub-100 fs Tm:MgWO<sub>4</sub> laser at 2017 nm mode-locked by a graphene saturable absorber," *Opt. Lett.*, vol. 42, pp. 3076-3079 (2017).

## High-power, narrow-linewidth DUV laser source for advanced semiconductor inspection

**Kentaro Miyata<sup>1</sup>, Mizuki Mohara<sup>2</sup>, Kei Shimura<sup>2</sup>, Akihiro Tanabashi<sup>1</sup>, Louis Desbiens<sup>3</sup>, Vincent Roy<sup>3</sup>, Taillon Yves<sup>3</sup>, Shinichi Nakayama<sup>4</sup>, and Satoshi Wada<sup>1</sup>**

*1- RIKEN Center for Advanced Photonics, 2-1 Hirosawa, Wako Saitama 351-0198, Japan*

*2- Hitachi High-Technologies Corporation, Ichige, Hitachinaka, 312-8504 Japan*

*3- INO, 2740 rue Einstein, Quebec City, QC, G1P 4S4*

*4. Megaopto Co., Ltd., 2-3-13 Minami, Wako, Saitama 351-0104, Japan*

*Main author email address: nlocystal@gmail.com*

Advanced semiconductor inspection systems based on deep UV (DUV) laser light source support the present accelerating miniaturization of digital devices in the industry. To attain high sensitivity and high throughput inspections, the system requires high-average-power outputs with either continuous-wave (CW) or quasi-CW (QCW) operation in the short-wavelength range, together with narrow spectrum. Several attempts have been made to obtain high-power CW DUV light source by using extra-cavity frequency conversion systems [1,2]. In these configurations, as the power level increases, technical difficulties tend to arise, to stabilize the performance against perturbations, which are caused by conditional changes such as environmental temperature variations, optical-path change by the material degradation under DUV light irradiations, and instabilities of high-power fundamental source. As an alternative to the CW laser systems, a QCW 199 nm laser source using a single-pass frequency conversion scheme has been previously reported [3], resulting the successful long-term operation with the average power of 100mW at the repetition rate of 2.4 MHz [4]. The output power scalability is however, somewhat limited, owing to the sharply increased optical absorption of nonlinear materials below 200 nm. To fully utilize the benefits given by high-power laser technologies developed for laser processing markets, we have redesigned the DUV laser source by using cascaded fifth-harmonic generation outputs of a state-of-the-art, fiber master oscillator and power amplifier (MOPA) system. Here, we demonstrate highly stable 213 nm-output operation with the average power of 500 mW at the repetition rate of 120 MHz. A discussion will be given to compare the performance with those given by other DUV laser systems reported in the literature.

[1] J. Sakuma, Y. Asakawa, and M. Obara, "Generation of 5-W deep-UV continuous-wave radiation at 266 nm by an external cavity with a CsLiB<sub>6</sub>O<sub>10</sub> crystal," *Opt. Lett.* **29**, 92-94 (2004).

[2] J. Sakuma, Y. Asakawa, T. Imahoko, and M. Obara, "Generation of all-solid-state, high-power continuous-wave 213-nm light based on sum-frequency mixing in CsLiB<sub>6</sub>O<sub>10</sub>," *Opt. Lett.* **29**, 1096-1098 (2004).

[3] Y. Urata, T. Shinozaki, Y. Wada, Y. Kaneda, S. Wada, and S. Imai, "Deep UV light generation by a fiber/bulk hybrid amplifier at 199 nm," *Appl. Opt.* **48**, 1668-1674 (2009).

[4] S. Imai, K. Matsuki, N. Kikuri, K. Takayama, O. Iwase, Y. Urata, T. Shinozaki, Y. Wada, and S. Wada, "Highly reliable 198-nm light source for semiconductor inspection based on dual fiber lasers," *Proc. SPIE 7580, Fiber Lasers VII: Technology, Systems, and Applications*, 75800H (17 February 2010).

# Spectroscopy and laser operation of Yb doped materials at cryogenic temperatures

**V. Jambunathan, P. Navratil, S.P. David, F. Yue, A. Lucianetti, T. Mocek**

*HiLASE Centre, Institute of Physics of the Czech Academy of Sciences, Za Radnicí 828, 25241 Dolní Brežany, Czech Republic*

*Main author email address: jambunath@fzu.cz*

Diode pumped compact all-solid-state lasers have received considerable interest within the scientific community due to their vast scientific and technological applications. In particular, ytterbium ( $\text{Yb}^{3+}$ ) ion based laser sources have been developed with a great number of hosts.  $\text{Yb}^{3+}$  ion exhibits several advantages such as simple energy level structure, absence of higher energy levels, low quantum defect and ease of pumping using commercially available InGaAs laser diodes. Nevertheless, at room temperature  $\text{Yb}^{3+}$ -doped materials behave as quasi three-level lasers due to a finite population of the lower laser level leading to reabsorption at laser wavelength and limiting the power scaling capabilities. The same materials when cooled down to cryogenic temperatures behave as four-level laser which can significantly enhance the output parameters and efficiency. Furthermore, cryogenic cooling improves the thermo-optic and spectroscopic properties of the material which has direct implication on the overall improvement in laser performance [1].

Based on the importance, we systematically analyzed the spectroscopic characteristics such as absorption and emission cross section values along with band width of absorption bands of various  $\text{Yb}^{3+}$  doped laser materials such as Yb:YAG, Yb:LuAG, Yb:CaF<sub>2</sub>, Yb:FP15-glass, Yb:YGAG [2,3] at cryogenic temperatures. Such measurement of spectroscopic properties at cryogenic temperatures is important because these values help in determining the crucial laser design parameters such as maximum extracted energy, small signal gain, exact pump wavelength and operating temperature for developing high-energy class lasers [4]. In addition, we also studied the cryogenic temperature dependent laser performance of these materials both in continuous wave and pulsed laser regime [5-8].

In the case of Yb:YAG, cryogenic laser operation was performed by two pump strategies: one with conventional 940 nm pumping and the other with VBG stabilized 969 nm pumping under identical experimental conditions. We found that zero phonon line (ZPL) pumping at 969 nm gives better output and slope efficiency compared to conventional 940 nm pumping. Concerning the Yb:YGAG, we observed that the emission band-width at cryogenic temperatures is three times broader than Yb:YAG, which makes this Yb:YGAG material a promising candidate for the generation of ultra-short pulses. A detailed summary of our extensive study on the fore-mentioned materials will be presented.

- [1] T. Y. Fan, D. J. Ripin, R. L. Aggarwal, J. R. Ochoa, B. Chann, M. Tilleman, and J. Spitzberg, "Cryogenic  $\text{Yb}^{3+}$ -doped solid-state lasers," *IEEE J. Sel. Top. Quantum Electron.* **13**, 448-459 (2007)
- [2] J. Körner, V. Jambunathan, J. Hein, R. Seifert, M. Loeser, M. Siebold, U. Schramm, P. Sikocinski, A. Lucianetti, T. Mocek, Malte C. Kaluza, "Spectroscopic characterization on  $\text{Yb}^{3+}$ -doped laser materials at cryogenic temperatures", *Appl. Phys. B* **116**(1), 75-81 (2014).
- [3] V. Jambunathan, L. Horackova, T. Miura, J. Sulc, H. Jelínková, A. Endo, A. Lucianetti and T. Mocek, "Spectroscopic and lasing characteristics of Yb:YGAG ceramic at cryogenic temperatures", *Opt. Mater. Exp.* **5**(6), 1289-1295 (2015).
- [4] J.-C. Chanteloup and D. Albach, "Current status on high average power and energy diode pumped solid state lasers," *IEEE Photon. J.* **3**(2), 245-248 (2011).
- [5] V. Jambunathan, T. Miura, L. Těsnohlídková, A. Lucianetti and T. Mocek, "Efficient laser performance of cryogenic Yb:YAG laser pumped by fiber coupled 940 nm and 969 nm laser diodes", *Laser Phys. Lett.* **12**(1), 015002/1-6 (2015).
- [6] V. Jambunathan, L. Horackova, P. Navratil, A. Lucianetti and T. Mocek, "Cryogenic Yb:YAG laser pumped by VBG-stabilized narrowband laser diode at 969 nm *IEEE Photon. Technol. Lett.* **28**(12), 1328-1331 (2016).
- [7] V. Jambunathan, P. Navratil, L. Horackova, A. Lucianetti and T. Mocek, "Zero-phonon-line pumped cryogenic Yb:YAG passively Q-switched by Cr:YAG", *Proc. SPIE* **9893**, 98930C (2016).
- [8] V. Jambunathan, P. Navratil, T. Miura, F. Yue, A. Endo, A. Lucianetti, and T. Mocek, "Cryogenic Yb:YGAG ceramic laser pumped at 940 nm and zero-phonon-line: a comparative study", *Opt. Mater. Exp.* **7**(2), 477-483 (2017).

# Few-cycle, Millijoule, 5 $\mu\text{m}$ Optical Parametric Chirped-Pulse Amplifier at a 1 kHz Repetition Rate

**U. Griebner, L. von Grafenstein, M. Bock, D. Ueberschär and T. Elsaesser**

*Max Born Institute for Nonlinear Optics and Short Pulse Spectroscopy, Max-Born-Str. 2a, Berlin 12489, Germany*

*Main author email address: [griebner@mbi-berlin.de](mailto:griebner@mbi-berlin.de)*

High intensity, power-scalable laser sources in the mid-wave infrared (MWIR) are a key element for applications in strong-field physics. Optical parametric chirped-pulse amplification (OPCPA) has emerged as a powerful technique for the generation of high-energy broadband MWIR pulses. For efficient parametric down-conversion to the MWIR selected non-oxide crystals, in particular ZnGeP<sub>2</sub> (ZGP) and CdSiP<sub>2</sub> (CSP), have proven their suitability. Applying these crystals in an OPCPA system, high-performance 2- $\mu\text{m}$  pump sources are required. Using few-millijoule 2- $\mu\text{m}$  pump pulses, pulses around 5  $\mu\text{m}$  have been generated at 1 kHz with energies of 33  $\mu\text{J}$  [1] and 40  $\mu\text{J}$  [2] and durations of 13 fs [1] and 100 fs [2], respectively. The described systems [1,2] are rather complex because each contains several optical parametric amplification (OPA) stages for the 2- $\mu\text{m}$  seed pulse generation. Recently, an OPCPA system delivering 180 fs pulses at 7  $\mu\text{m}$  with energy of 200  $\mu\text{J}$  pumped by a comparably compact 2  $\mu\text{m}$  source were demonstrated, however, at a rather low repetition rate of 0.1 kHz [3]. Here we present a millijoule-level few-cycle pulse source operating at 1 kHz repetition rate in the MWIR.

For our MWIR OPCPA system we developed a 2- $\mu\text{m}$  Ho:YLF chirped pulse amplifier (CPA) pump source delivering more than 50 mJ pulse energy per pulse with a duration <10 ps at a 1 kHz repetition rate. This 2- $\mu\text{m}$  CPA system is distinguished by an excellent pulse-to-pulse stability with an rms <0.3% and described in [4]. A 3-color front-end based on a fs Er: fiber master oscillator operating at 40 MHz serves as seed for the 2- $\mu\text{m}$  pump channel and the signal pulse for the OPA which is generated at 3.5  $\mu\text{m}$  via difference-frequency generation between the 1.0 and 1.5  $\mu\text{m}$  pulses of the front-end. The spectrum of the signal pulses covers >700 nm bandwidth (FWHM) and the pulses are stretched to ~3 ps duration. The OPA chain is composed of three stages containing AR-coated ZGP crystals and is designed for different gain levels. The first and the second stage are built in a non-collinear geometry. Applying 14 mJ of the 2  $\mu\text{m}$  pulse energy in the third stage in a collinear geometry, 1.2 mJ per pulse is generated in the idler around 5  $\mu\text{m}$ . Given the 1 kHz repetition rate of the OPCPA system a noticeable average power of 1.2 W is achieved. The emitted broadband idler spectrum extends from 4350 to 5400 nm at  $1/e^2$  and supports a Fourier-transform limited pulse duration of 60 fs. Successful recompression of the positively chirped idler pulses was achieved using CaF<sub>2</sub> crystals in combination with a MWIR spatial light modulator. The latter compensated the residual group delay dispersion and the third- and fourth-order dispersion of the pulses. The retrieved pulse shape from a SHG-FROG characterization delivered a pulse duration to 80 fs with an estimated energy content of 88% in the main peak, translating into a high peak power of 11 GW. The emitted pulses are nearly diffraction-limited with a sizeable stability of the recompressed pulses with an rms of 1.3% [5].

In conclusion, we have demonstrated a high-power OPCPA at 5  $\mu\text{m}$  wavelength delivering up to 1.2 mJ pulse energy at a 1 kHz repetition rate. Compression of the pulses resulted in a duration of 80 fs which is shorter than five optical cycles. The corresponding pulse peak power is 11 GW and, if focused to a 15  $\mu\text{m}$  spot diameter, the pulses would reach a peak intensity of  $\sim 1 \times 10^{16}$  W/cm<sup>2</sup>. These results represent record values for high-energy MWIR OPCPAs beyond 4  $\mu\text{m}$  so far. Future efforts will focus on increasing the mid-IR pulse energy by profiting from higher 2- $\mu\text{m}$  pump pulse energy [4].

[1] H. Liang et al., "High-energy mid-infrared sub-cycle pulse synthesis from a parametric amplifier," Nat. Commun. **8**, 141 (2017).

[2] T. Kanai et al., "Parametric amplification of 100 fs mid-infrared pulses in ZnGeP<sub>2</sub> driven by a Ho:YAG chirped pulse amplifier," Opt. Lett. **42**, 683 (2017).

[3] D. Sanchez et al., "7  $\mu\text{m}$ , ultrafast, sub-millijoule-level mid-infrared optical parametric chirped pulse amplifier pumped at 2  $\mu\text{m}$ ," Optica **3**, 147 (2016).

[4] L. von Grafenstein et al., "Ho:YLF chirped pulse amplification at kilohertz repetition rates - 4.3 ps pulses at 2  $\mu\text{m}$  with GW peak power," Opt. Lett. **41**, 4668 (2016).

[5] L. von Grafenstein et al., "5  $\mu\text{m}$ , few-cycle pulses with multi-GW peak power at a 1 kHz repetition rate," Opt. Lett. **42**, 3796 (2017).

# New Nonlinear Crystals for Advanced Mid-IR Laser Sources

**Peter G. Schunemann**

*BAE Systems, Inc., MER15-1813, P.O. Box 868, Nashua, NH 03061-0868*

*peter.g.schunemann@baesystems.com*

The emergence of new laser applications ranging from frequency-comb-based spectroscopy to high harmonic generation has led to a growing demand for improved nonlinear optical (NLO) materials for mid-infrared frequency conversion. NLO semiconductors such as ZnGeP<sub>2</sub> (ZGP) and orientation-patterned GaAs (OP-GaAs) offer transparency deep into the mid-infrared and THz with d-coefficients 5-10 times higher than those of oxides. ZGP and OP-GaAs must be pumped at wavelengths  $\geq 1.9 \mu\text{m}$ , but new analogs for these materials – cadmium silicon phosphide (CdSiP<sub>2</sub>, or CSP) and orientation-patterned GaP (OP-GaP) – can be pumped with widely-available 1- $\mu\text{m}$  and 1.5- $\mu\text{m}$  lasers.

ZnGeP<sub>2</sub> remains the NLO material of choice for frequency conversion between 2 and 8 microns. Continued efforts to improve ZGP crystal quality and aperture size for high-energy laser applications are ongoing, enabling record-level peak- and average-output powers in the mid-IR. ZGP, however, still has two main limitations: 1) its transparency and phase-matching range make it incompatible with 1- and 1.5-micron laser pumping; and 2) its usefulness for generating output in the 8-12 micron atmospheric window is limited by severe multi-phonon absorption.

CdSiP<sub>2</sub> (CSP) is a new bulk birefringent chalcopyrite analog of ZGP grown by horizontal gradient freeze (HGF) growth in a transparent furnace. Its larger band gap (512 nm) and birefringence (-0.05) allows for 1- and 1.5- $\mu\text{m}$  pumping, and its nonlinear coefficient ( $d_{14}=85 \text{ pm/V}$ ) and thermal conductivity (13 W/mK) are dramatically higher than existing materials (AgGaS<sub>2</sub>, AgGaSe<sub>2</sub>, and PPLN) that can be pumped at these wavelengths.

OP-GaAs and OP-GaP are quasi-phases-matched (QPM) NLO semiconductors grown by all-epitaxial processing: first, polar-on-nonpolar MBE produces GaAs (GaP) with an inverted orientation inverted with respect to the substrate which is photo-lithographically patterned, etched with the desired grating structure, and re-grown by hydride vapor phase epitaxy (HVPE) at rates up to 200 $\mu\text{m/hr}$  to produce thick ( $> 1 \text{ mm}$ ), low-loss ( $< 0.01 \text{ cm}^{-1}$ ) QPM layers for in-plane laser pumping. OP-GaAs has the highest gain among all QPM materials ( $d_{14}=94 \text{ pm/V}$ ), and can be pumped at 2- $\mu\text{m}$  to generate 8-12  $\mu\text{m}$  output and beyond, whereas OP-GaP is a low-loss QPM ZGP analog than can be pumped with 1- $\mu\text{m}$  lasers. Numerous OP-GaP device demonstrations have been achieved based on 1-, 1.5- and 2- $\mu\text{m}$  laser pumping, and highly parallel grating propagation during growth promises to extend aperture sizes well beyond 1 mm.

Finally, BAE Systems is developing new QPM and bulk birefringent crystals for long wavelength infrared generation. Orientation-patterned zinc selenide (OP-ZnSe) is an exciting new QPM semiconductor at the very early stages of development which offers an extremely broad transparency range (0.5-22  $\mu\text{m}$ ) and a high-nonlinear Figure-of-Merit. Preliminary results based on physical vapor transport growth of ZnSe on lattice-matched OP-GaAs templates looks extremely promising. In addition, Two new compounds, BaGa<sub>4</sub>S<sub>7</sub> and BaGa<sub>4</sub>Se<sub>7</sub>, are actively being grown which exhibit low vapor pressures and highly favorable crystallization behavior enabling scaling to large diameters. These materials, recently been reported by Badikov and Petrov, combine wide band gaps ( $>2.6 \text{ eV}$ ) for near-infrared pumping with deep-infrared transparency out to 13 and 20 microns respectively. BaGa<sub>4</sub>Se<sub>7</sub> has a respectable d-coefficient of 20 pm/V, and single crystals measuring 27 mm in diameter and 150 mm in length have been grown by the horizontal gradient freeze technique in transparent furnaces. In addition, we are investigating a new chalcopyrite crystal with ZGP-like properties but with high transparency beyond 12 microns.

# Advances in backward-wave optical parametric oscillators

**V. Pasiskevicius, A. Zukauskas, A.-L. Viotti, R. S. Coetzee, C. Canalias**

*Department of Applied Physics, Royal Institute of Technology (KTH), Roslagstullsbacken 21, Stockholm, Sweden  
vp@laserphysics.kth.se*

In the spectral region of millimeter and submillimeter waves, electronic backward-wave oscillators (BWO) are devices widely used since 1950's to generate tunable, narrowband and high power radiation, which are still being exploited in THz spectroscopy applications [1]. In BWO, the oscillation is conditioned by positive feedback provided by the interacting counter-propagating electromagnetic wave and electron beam. In 1966 S. Harris theoretically proposed an all optical BWO, based on three-wave mixing, i.e. backward-wave optical parametric oscillator (BWOPO) [2]. However, his conclusion was that realizing such oscillation would be practically impossible owing to insufficient birefringence in all known second-order nonlinear optical materials. Practical realization of such device, has recently become possible due to advances in quasi-phase matched (QPM) materials, primarily KTP and Rb:KTP [3]. These ferroelectric crystals can be structured through the bulk with sub- $\mu\text{m}$  periodicity QPM gratings as required for BWOPO operating in the near- and mid-infrared spectral regions. Positive feedback for oscillation in BWOPO is provided by the counter-propagating signal and idler waves, therefore the device does not require external cavity mirrors or coatings, making it a very simple and robust device.

More importantly, BWOPO offers spectral properties rather unusual for optical parametric oscillators. Specifically, the bandwidth of the wave generated in the direction opposite to the pump is two orders of magnitude narrower than that of the pump. In turn, the wave generated in the direction of the pump retains the frequency and phase information of the pump [4]. This property arises due to the fact, that the wavelength of the backward generated wave is mostly determined by the wave-vector of the QPM grating, making BWOPO the device suitable for frequency translation applications, i.e. situations, where the spectral and temporal phase properties of the pump need to be transferred onto a different carrier frequency.

Recent advances in high-yield fabrication of the sub- $\mu\text{m}$ -periodicity structures resulted in substantial decrease in the oscillation thresholds compared to initial demonstration. The thresholds, in fact are now comparable to those typically obtained in conventional optical parametric oscillators employing standard co-propagating interactions in Rb:KTP. This allowed demonstrations of BWOPOs pumped by Q-switched nanosecond lasers and generation of milli-Joule-level BWOPO output in near- and mid-infrared [5] as well as operation of cascade of BWOPO in the same nonlinear crystal [6]. Owing to the above-mentioned spectral quality, transform-limited milli-Joule nanosecond pulses can be directly produced in BWOPO with efficiency exceeding 50% and could be used directly for seeding high-energy optical parametric amplifiers, for applications in remote sensing and LIDARs. While in conventional optical parametric oscillators, back-conversion process and associated  $\chi^{(2)}$ :  $\chi^{(2)}$  cascading impose temporal and spatial intensity-dependent phase modulation and result in a decrease in temporal and spatial coherence of the output beams, this process is drastically reduced in BWOPO due to spatial separation of the signal and idler intensity maxima in the crystal. Therefore the spectra, even at such high efficiencies remains narrow and spatial beam distributions remain unaffected.

[1] R. Kompfner, "Backward-wave tubes," Proc.IRE, vol. 41, pp. 1602-1611, (1953).

[2] S. E. Harris, "Proposed backward wave oscillation in the infrared," Appl. Phys. Lett., vol. 9, pp. 114-116 (1966).

[3] C. Canalias, V. Pasiskevicius, "Mirrorless optical parametric oscillator," Nature Phot. vol.1, pp. 459-462 (2007).

[4] G. Strömqvist, V. Pasiskevicius, C. Canalias, C. Montes, "Coherent phase-modulation transfer in counterpropagating parametric down-conversion," vol. 84, pp. 0823825 (2011).

[5] C. Liljestränd, A. Zukauskas, V. Pasiskevicius, C. Canalias, "Highly efficient mirrorless optical parametric oscillator pumped by nanosecond pulses," Opt. Lett., vol. 42, pp. 2435-2438 (2017).

[6] A. Zukauskas, A.-L. Viotti, Ch. Liljestränd, V. Pasiskevicius, C. Canalias, "Cascaded counter-propagating nonlinear interactions in highly-efficient sub- $\mu\text{m}$  periodically poled crystals," Scientific Reports, vol. 7, pp. 8037 (2017).

# Robust optical vortex beam generation from diode-side-pumped solid-state lasers

**Weidong Chen<sup>\*</sup>, Wenbin Fang, Ruxue Bai, Haifeng Lin and Ge Zhang**

*Key Laboratory of Optoelectronic Materials Chemistry and Physics, Fujian Institute of Research on the Structure of Matter, Chinese Academy of Sciences, 350002 Fuzhou, China*

*\*Email address: [chenweidong@fjirsm.ac.cn](mailto:chenweidong@fjirsm.ac.cn)*

The simplest optical vortex field carrying well-defined OAM associated with spiral phase-front structure is the paraxial Laguerre-Gaussian ( $LG_{p,l}$ ) beam [1]. Here index  $p$  is the number of radial nodes; and index  $l$  characterizes the topological charge of the optical vortex field with an azimuthal phase dependence of  $\exp(il\varphi)$  carrying orbital angular momentum of  $l\hbar$  per photon ( $\varphi$  is the azimuthal angle). The index  $l$  can take any real integer value, positive or negative, which corresponds to the opposite chirality gyration of the spiral phase-front. The distinct features of the  $LG_{01}$  beam open up diverse promising applications [2].

So far, most of the reported in the literature for direct emission of a  $LG_{01}$  beam from solid-state laser would mainly relate to use of the spatially-matched gain distribution or spatially-inversed loss controlling from end-pumped configuration [3, 4]. Alternatively, diode-side-pumped lasers are very competitive technology due to its reliability, power scalability, simplicity, availability and low cost of components [5]. Reports on direct vortex beam generation from diode-side-pumped lasers are mostly related to the bounce configuration [6-8]. Although the performance of Nd:YAG diode-side-pumped rod lasers have been intensively investigated, they have been no reports on employing them for generation of multi-watt vortex laser beam with high mode purity and good beam quality.

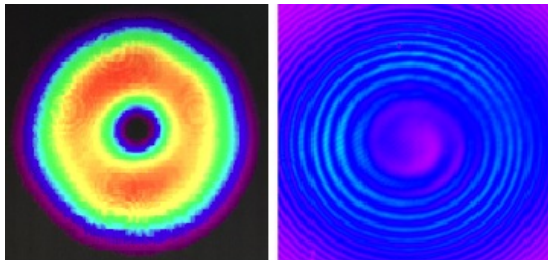


Fig.1. Far-field beam profile of  $LG_{01}$  mode and image of the spiral interferogram of Nd:YAG side-pumped rod laser.

Diode-pumped-side rod lasers are typically limited by its beam quality due to the large pump volume compared to the laser mode size. Here we present an efficient approach based on the manipulation of the astigmatism induced thermal lens for direct generation of robust optical vortex beam with multi-watt output power and high mode purity as well as good beam quality. Figure 1 shows the far-field beam profile of  $LG_{01}$  mode and its image of the spiral interferogram.

- [1]. 1. M. Padgett, and L. Allen, "Light with a twist in its tail," *Contemp Phys* 41, 275-285 (2000).
- [2]. 2. A. M. Yao, and M. J. Padgett, "Orbital angular momentum: origins, behavior and applications," *Adv Opt Photonics* 3, 161-204 (2011).
- [3]. 3. D. J. Kim, J. W. Kim, and W. A. Clarkson, "Q-switched Nd:YAG optical vortex lasers," *Opt Express* 21, 29449-29454 (2013).
- [4]. 4. A. Ito, Y. Kozawa, and S. Sato, "Generation of hollow scalar and vector beams using a spot-defect mirror," *J. Opt. Soc. Am. A* 27, 2072-2077 (2010).
- [5]. 5. A. Berezcki, and N. U. Wetter, "100 W continuous linearly polarized, high beam quality output from standard side-pumped Nd:YAG laser modules," *Opt Laser Technol* 96, 271-275 (2017).
- [6]. 6. G. M. Thomas, A. Minassian, and M. J. Damzen, "Optical vortex generation from a diode-pumped alexandrite laser," *Laser Physics Letters* 15, 045804 (2018).
- [7]. 7. S. P. Chard, P. C. Shardlow, and M. J. Damzen, "High-power non-astigmatic TEM00 and vortex mode generation in a compact bounce laser design," *Appl Phys B-Lasers O* 97, 275-280 (2009).
- [8]. 8. M. Okida, and T. Omatsu, "Direct generation of high power Laguerre-Gaussian output from a diode-pumped Nd : YVO4 1.3- $\mu$ m bounce laser," *Opt Express* 15, 7616-7622 (2007).

# Plasmon-induced narrowband emission and multiline operation from a solid-state nanolaser

D. Hernández-Pinilla<sup>1</sup>, J. Cuerda<sup>1</sup>, P. Molina<sup>1</sup>, M. O. Ramírez<sup>1</sup>, and L. E. Bausá<sup>1</sup>

1- Dept. Física de Materiales, Instituto de Materiales Nicolás Cabrera and Condensed Matter Physics Center (IFIMAC), Universidad Autónoma de Madrid, 28049-Madrid, Spain

javier.cuerda@uam.es

The association of optical gain media with plasmonic nanostructures has opened up new pathways for room-temperature nanoscale coherent light sources [1, 2]. Recently, the first report of a solid-state based nanolaser has allowed bringing the inherent thermal and chemical stability of solid-state gain materials to nanoscale architectures, and generate subwavelength-confined laser emission at  $\sim 1 \mu\text{m}$  [3].

Here, we present our results on lasing action in a  $\text{Nd}^{3+}:\text{LiNbO}_3$  crystal, on which long chains of closely spaced silver (Ag) nanoparticles are deposited. The excitation of a radiative plasmonic mode along the nanoparticle chains allows lasing at the nanoscale at around  $1 \mu\text{m}$  ( ${}^4\text{F}_{3/2} \rightarrow {}^4\text{I}_{13/2}$  transition) and enables sub-wavelength confined multiline operation at the blue and green spectral region by means of different frequency-conversion processes that take place in the vicinities of the plasmonic chain [4].

In addition, taking advantage of the variety of emission bands featured by  $\text{Nd}^{3+}$  ions, lasing at the nanoscale can be achieved in a different spectral region. In particular, plasmon assisted lasing is demonstrated at  $1.3 \mu\text{m}$  ( ${}^4\text{F}_{3/2} \rightarrow {}^4\text{I}_{13/2}$   $\text{Nd}^{3+}$  transition), which is of special interest to develop nanoscopic bright probes at the second biological window. By means of spatially-resolved gain measurements, we found a systematic narrowing of the laser linewidth of around 30% in the vicinities of the plasmonic Ag chains, as compared with the standard bulk operation. We accounted for this behavior in terms of a laser rate-equation analysis to conclude that the excitation of plasmonic modes at the absorption wavelength ( $\lambda_a=808 \text{ nm}$ ) leads to the enhancement of the optical gain generated in the active medium, thus further improving the temporal confinement properties of the solid-state laser.

This work paves the way towards functional subwavelength laser devices based on solid-state gain materials, suitable for integration within photonic circuits, and anticipates applications such as *in vivo* imaging of nanoscale biological systems.

[1] M. Noginov, G. Zhu, A. M. Belgrave, R. Bakker, V. M. Shalaev, E. E. Narimanov, S. Stout, E. Herz, T. Suteewong, and U. Wiesner, Demonstration of a spaser-based nanolaser. *Nature (London)* 460, pp.1110-1112 (2009).

[2] R. F. Oulton, V. J. Sorger, T. Zentgraf, R.-M. Ma, C. Gladden, L. Dai, G. Bartal, and X. Zhang, Plasmon lasers at deep subwavelength scale. *Nature (London)* 461, pp. 629-632 (2009).

[3] P. Molina, E. Yraola, M. O. Ramírez, C. Tserkezis, J. L. Plaza, J. Aizpurua, J. Bravo-Abad, and L. E. Bausá, Plasmon-assisted  $\text{Nd}^{3+}$ -based solid-state nanolaser. *Nano Letters* 16 (2), pp 895-899 (2016).

[4] D. Hernández-Pinilla, P. Molina, C. de las Heras, J. Bravo-Abad, L. E. Bausá, and M. O. Ramírez, Multiline operation from a single plasmon-assisted laser. *ACS Photonics* 5 (2), pp 406-412 (2018).

## Ridge waveguide laser of Nd doped KGd(WO<sub>4</sub>)<sub>2</sub> on SiO<sub>2</sub> platform using saw dicing

Marc Medina<sup>1</sup>, Airán Rodenas<sup>3</sup>, Ginés Lifante<sup>4</sup>, Eugenio Cantelar<sup>4</sup>, Christian E. Rüter<sup>2</sup>,  
Jaume Masons<sup>1</sup>, Detlef Kip<sup>2</sup>, Maria Cinta Pujol<sup>1</sup>, Magdalena Aguiló<sup>1</sup> and Francisco Díaz<sup>1</sup>

<sup>1</sup> Física i Cristal·lografia de Materials i Nanomaterials (FiCMA-FiCNA-EMaS), Universitat Rovira i Virgili (URV), Campus Sescelades, C/Marcel·lí Domingo 1, E-43007, Tarragona, Spain

<sup>2</sup> Faculty of Electrical Engineering, Helmut Schmidt University, 22043 Hamburg, Germany

<sup>3</sup> Istituto di Fotonica e Nanotecnologie (IFN)- Consiglio Nazionale delle Ricerche (CNR), Milano, Italy

<sup>4</sup> Departamento de Física de Materiales, Facultad de Ciencias. Universidad Autónoma de Madrid, 28049-Madrid (Spain)

Email address: gines.lifante@uam.es

Channel optical waveguides provide ideal structures for lasing action. In particular, optically pumped waveguide lasers have an inherent advantage over conventional bulk lasers in that both the pump light and the laser radiation are constrained to propagate together in the small cross section of the waveguide, and thus the overlap between both beams is necessarily quite high for unlimited propagation distances [1]. The small spot sizes lead to high intensities for relative low power. This is already true for planar waveguide lasers, but particularly in channel waveguides, which provide two-dimensional light confinement. If the propagation loss of the waveguide can be maintained low, a high gain per unit pump power and a low laser threshold can be achieved. As the device length can be very long, low RE concentrations are required, allowing to avoid up-conversion, cross-relaxation and other mechanisms that would otherwise reduce laser performance. Channel waveguides lasers can be integrated with other elements to achieve a full compact and functional integrated optic device, that is, easy on-chip integration with other optical components.

Along this line, new materials and novel fabrication techniques are always welcome to fulfil new requirements. In this work we have investigated the possibility of fabrication ridge waveguides using ultra-precise cutting with a Disco DAD322 dicing saw [2]. Following this approach, a set of ridge waveguides on a Nd:KGd(WO<sub>4</sub>)<sub>2</sub>/SiO<sub>2</sub> platform was fabricated, using Nd<sup>3+</sup> as an active ion for laser generation. ESEM images of the fabricated structures shows ridge geometry of the waveguide's cross section. The waveguides show low surface roughness and hardly any chipping coming from the dicing process. The shape of the ridge waveguide is trapezoidal, with width dimensions in the range 8-20 μm and height ranging from 10 to 30 μm, with a remaining planar waveguide from 1 to 5 μm. Under Ti:Sapphire laser excitation, and using a double-pass cavity with attached multilayer dielectric mirrors at the waveguide's end faces, laser emission is observed in these structures with a halfwidth less than 0.25 nm, being linearly polarized with a polarization ratio better than 1/150. The characteristic curve of the laser emission at 1067.7 nm shows a threshold of 11 mW, and a slope efficiency of 15%. The demonstration of laser oscillation in this platform proves the potential of the configuration and the fabrication technique here used to deliver on other requirements where integrated photonics are needed.

### References

[1] E.Cantelar, *et al.*: Waveguide lasers based on dielectric materials, *Opt. Mat.*, vol. 34. pp 555-571, 2012.

[2] F. Martin, *et al.*: Low loss ridge waveguides in lithium niobate thin film by optical grade diamond blade dicing, *Opt. Express*, vol. 2. pp 1386-1391, 2016.

# All-optical associative memory

**Byoung S. Ham**

*EECS, Gwangju Institute of Science and Technology,  
123 Chumdangwagi-ro, Buk-gu, Gwangju 61005, S. Korea*

*bham@gist.ac.kr*

For all-optical information processing, both all-optical logic gates [1] and dynamic optical random access memory (DORAM) are essential hardwares. In addition to DORAM, an all-optical associative memory (OAM) is also a key component for all-optical pattern recognition [2-4]. Although DORAM and OAM have been intensively investigated over the last few decades, no such optical hardwares exist yet mainly due to the limitations of fundamental nonlinear optics. Here, I present for the first time both DORAM and OAM using a backward controlled echo [5], where the backward controlled echo is new and shows near perfect conversion efficiency even without amplifications owing to the quantum coherence control of coherent transients and phase conjugation [6]. The DORAM offers a new functionality of ultralong storage time and spatial multiplexing, where DORAM can now be applied for OAM-based real-time pattern recognition and laser target tracking in both air and underwater applications. Moreover, such functionality can also be applicable to real-time medical diagnostics and all-automatic therapy [7].

## References

- [1] B. S. Ham, J. Hahn, Observations of ultraslow light-based photon logic gates : NAND/OR. *Appl. Phys. Lett.* **94**, 101110 (2009).
- [2] Y. Owechko et al., Holographic associative memory with nonlinearities in the correlation domain. *Appl. Opt.* **26**, 1900-1910 (1987).
- [3] M. N. Belov and E. A. Manykin, Optical associative memory based on an echo correlator. *Opt. Lett.* **16**, 327-329 (1991).
- [4] M. Papaioannou, E. Plum, N. I. Zheludev, All-optical pattern recognition and image processing on a metamaterial beam splitter. *ACS Photonics* **4**, 217-222 (2017).
- [5] B. S. Ham, Wavelength convertible quantum memory satisfying ultralong photon storage and near perfect retrieval efficiency. *Sci. Rep.* (to be published); *ibid.*, arXiv :1802.06996 (2018).
- [6] J. Hahn, B. S. Ham, Rephasing halted photon echoes using controlled optical deshelling. *New J. Phys.* **13**, 093011 (2011).
- [7] B. S. Ham, Ultraslow Light and Nondegenerate Phase Conjugation-Based Real-Time, Non-Invasive, In-Vivo Deep-Tissue Optical Imaging Apparatus, Photodynamic Therapy Apparatus, Optical Imaging Method and Photodynamic Therapy Method. (US Patent: 15/247919) (2016).

# High resolution and sensitivity broadband vibrational sum-frequency generation spectrometer at 100 kHz and its bioapplications

F. Yesudas<sup>1,2</sup>, M. Mero<sup>3</sup>, J. Kneipp<sup>1,2</sup>, Z. Heiner<sup>1,2</sup>

1- School of Analytical Sciences Adlershof, Albert-Einstein-Str.5-11, 12489 Berlin, Germany

2- Department of Chemistry, Humboldt Universität zu Berlin, 12489 Berlin, Germany

3- Max Born Institute for Nonlinear Optics and Short Pulse Spectroscopy, 12489 Berlin, Germany

heinerzs@hu-berlin.de

Broadband vibrational sum-frequency generation spectroscopy (BB-VSFG) is a promising label-free and interface specific analytical tool which serves rich vibrational information on molecules even at (sub)monolayer surface coverage. During BB-VSFG measurements, typically few-picosecond visible (ps-vis) laser pulses are spatially and temporally overlapping with broadband, few-cycle mid-infrared (MIR) laser pulses at the surface. The MIR pulses produce an infrared vibrational fingerprint which is up-converted with the help of the ps-vis pulses from the MIR to the visible spectral range through the sum-frequency generation process. From the resulting VSFG spectra, the amplitudes and resonance frequencies of vibrational transitions can be extracted indicating the composition and conformation of molecules at the surface.

Recently, we constructed the first 100 kHz BB-VSFG spectrometer [1,2] which has two orders of magnitude higher repetition rate compared to typical BB-VSFG setups. The home-built laser system consists of a continuum-seeded two-stage, dual-beam optical parametric amplifier delivering 32 fs signal pulses at 1.5  $\mu\text{m}$  and 63 fs idler pulses at 3.2  $\mu\text{m}$ , and a chirped sum-frequency generation unit producing transform-limited narrowband, 515 nm, picosecond pulses. The BB-VSFG spectrometer including the light sources is currently unique because (i) it is the first spectrometer operating at a variable repetition rate up to 100 kHz, (ii) it allows fast, single-shot, broadband ( $800\text{ cm}^{-1}$ ) spectral acquisition with high spectral resolution ( $3\text{ cm}^{-1}$ ), and (iii) it is a user-friendly, small, and cost-effective spectrometer compared to traditional, Ti:sapphire-based systems.

To demonstrate the applicability of our BB-VSFG spectrometer, various vibrational spectra at air/solid, air/liquid, and solid/liquid interfaces will be discussed at different laser repetition rates of 5, 10, 50, and 100 kHz at constant pulse energy. First, the laser-driven, thermally-induced orientational changes and disorder in organic molecular layers was monitored by looking for changes in the vibrational spectra at an air/solid interface where the solid was transparent. As a second step, we also performed a systematic study of heat-induced distortions at a water surface, as an absorbing and natural bio-environment.

Our results provide implications for future high repetition rate BB-VSFG studies on thin films and real biological samples, and guidelines for simultaneously achieving high spectral resolution, high sensitivity, and fast acquisition time.

Funding by the Deutsche Forschungsgemeinschaft (DFG GSC 1013 SALSA) to F.Y. and Z.H., and by Leibniz- Gemeinschaft Grant No. SAW-2012-MBI-2 to M.M. are gratefully acknowledged.

[1] Z. Heiner, V. Petrov, M. Mero, Compact, high-repetition-rate source for broadband sum-frequency generation spectroscopy, *APL Photonics*, vol. 2, 066102 (2017).

[2] F. Yesudas, M. Mero, J. Kneipp, Z. Heiner, Vibrational sum-frequency generation spectroscopy of lipid bilayers at repetition rates up to 100 kHz, *J. Chem. Phys.*, vol. 148, 104702 (2018).

## High-power slab laser systems with diode pumping

**I.A. Shcherbakov, V.B. Tsvetkov**

*A.M. Prokhorov General Physics Institute RAS, 119991, Vavilov str., 38, Moscow, Russia.*

*e-mail: [tsvetkov@lsg.gpi.ru](mailto:tsvetkov@lsg.gpi.ru)*

High power laser-diode-pumped lasers are required for many applications. Zig-zag slab lasers and amplifiers have long been used to provide high-power laser output with high spatial-mode quality. As heat is extracted through the largest faces the slab has a non-uniform temperature profile in the heat removal direction introducing a thermal lens. The laser beam propagates down the length of the sample, performing total-internal-reflection (TIR) bounces off of the cooling faces. This propagation path is to cancel out, to first-order, the thermal lens.

During the past years we attacked a number of technical issues which were important in the quest for improved performance and efficiency of the slab geometry Nd:YAG laser source and amplifier. Results of experimental studies and computer modelling of distribution of phase distortions, gain coefficient and CW lasing are summarized at use of three configurations of an optical pumping: end pumping (along the optical axis), edge pumping and face pumping. Most part of experiments was done with the slabs while using zigzag beam propagation that allow minimizing the effects introduced by optical quality of active medium. Based on measurements of focusing, birefringence, fracture stress, pumping efficiency, gain oscillator performance and laser beam quality, we have verified our model of slab geometry lasers.

The obtained data allows to find advantages and disadvantages of each of optical pumping schemes and to define optimum for a specific task.

## Prospective mid-IR solid-state laser sources for technical and medical applications

**M.K. Tarabrin<sup>1,2</sup>, S.M. Tomilov<sup>1,2</sup>, A.A. Bushunov<sup>1,2</sup>, D. V. Ustinov<sup>1</sup>, V.A. Lazarev<sup>1</sup>,  
Yu.V. Korostelin<sup>2</sup>, M. P. Frolov<sup>2</sup>, Ya.K. Skasyrsky<sup>2</sup>, V.I. Kozlovsky<sup>2,3</sup>**

*1 – Bauman Moscow State Technical University, Moscow 105005, Russia;*

*2 – P.N. Lebedev Physical Institute of RAS, Moscow 119991, Russia;*

*3 – National Research Nuclear University MEPhI, Moscow 115409, Russia;*

[vladmir.al.lazarev@gmail.com](mailto:vladmir.al.lazarev@gmail.com).

Nowadays tunable mid-infrared laser sources have drawn great scientific and technical interest. Solid-state broadly-tunable lasers emitting in the 1.8-3.0  $\mu\text{m}$  range are already used for spectroscopy, optical frequency standards and medical applications [1-3]. Efficient lasing has been demonstrated with  $\text{Cr}^{2+}$  ions doped into CdSe types of mid-IR lasers [4–6]. Recently we have demonstrated cw Cr: CdSe laser with output power more than 1.8 W at 2.65  $\mu\text{m}$  and the absorbed power slope efficiency of 49 %. We are planning to tune it up to 2.9  $\mu\text{m}$  to use this laser in medicine due to strong water and collagen absorption [7, 8].

An important potential application of mid-infrared lasers is in master oscillators with a high short-term frequency stability, which are based on lasers stabilized by saturated dispersion resonances in low-pressure methane cell. We have demonstrated a setup based on a Cr:ZnSe laser for Doppler-free spectroscopy of methane with the maximum achievable relative frequency instability of  $2.5 \times 10^{-15}$  at 1 s [9].

Mode-locked mid-IR lasers are important for remote sensing and spectroscopy across the ‘fingerprint region’ [10]. We have demonstrated SESAM mode-locked Cr:ZnSe laser emitting at 2.45  $\mu\text{m}$  with maximum output power of 520 mW, and pulse duration of 350 fs. We are planning to implement the same schematic based on Cr: CdSe single crystal with lasing near 3  $\mu\text{m}$ .

For mid-IR lasers, surface AR techniques are indispensable for improving the performance of optical windows and gain media [11]. Replacement the conventional coatings by AR microstructures deposited directly on the polished crystal surfaces is highly urgent task. We demonstrated a facile approach of AR microstructures fabrication on the CdSSe single crystal substrate by femtosecond laser direct ablation [12].

The authors acknowledge the Russian Science Foundation support, project No. 17-79-20431.

- [1] S. Mirov et al., *IEEE J. Sel. Top. Quantum Electron.* in press (2018).
- [2] I. Sorokina, *Opt. Mater.* **26**, 395–412 (2004).
- [3] S. Mirov et al., *J. Lumin.* **133**(01) (2013).
- [4] T. Fernandez et al., *Opt. Mater. Express* **7**, 3815-3825 (2017).
- [5] V. Lazarev et al., *Las. Phys. Lett.* **12**(12), 125003 (2015).
- [6] V. Lazarev et al., *J. Phys.: Conf. Ser.* **673**(1), 012015 (2016).
- [7] T. Lin et al., *Lasers in Surgery and Medicine* **48**(10), 965-977 (2016).
- [8] M. Tarabrin et al., *Proceedings SPIE Saratov Fall Meeting* **10717**, 1071707 (2017).
- [9] M. Tarabrin et al., *J. Quant. Spectrosc. Radiat. Transfer* **177**, 241-247 (2016).
- [10] C. Petersen et al, *Nat. Photonics* **8**(830) (2014)
- [11] S. Mirov et al., *IEEE J. Sel. Top. Quantum Electron.* **21**, 292–310 (2015).
- [12] M. Tarabrin et al., *Frontiers in Optics 2017*, paper JTU2A.20 (2017).

# RECENT STUDIES ON NEW NONLINEAR CRYSTALS GENERATING MID-INFRARED PARAMETRIC LIGHT

Patricia Segonds<sup>1</sup> and Benoit Boulanger<sup>1</sup>

<sup>1</sup> Université Grenoble Alpes / CNRS, Institut Néel, 38402 Grenoble Cedex 09, France

[patricia.segonds@neel.cnrs.fr](mailto:patricia.segonds@neel.cnrs.fr)

Nowadays, there is a real need in all solid-state sources able to emit a high energy and tunable coherent light in the mid-infrared range, for various applications. It is the case of spectroscopy and detection of molecules from the atmosphere, for example. The best alternative is the generation of parametric light from a second order frequency down-conversion process in a nonlinear crystal. In such a process, signal and idler beams, at the corresponding wavelengths  $\lambda_s$  and  $\lambda_i$ , are generated using as a pump beam with a monochromatic wavelength  $\lambda_p$  emitted by a commercial laser [1, 2].

The requested performances of nonlinear crystals are the widest transparency range, a high damage threshold, phase-matching conditions and large associated nonlinear coefficients, over the mid-infrared [2]. However, the choice of crystals with such performances is rather limited. For an emission of mid-infrared parametric light covering Band II of transparency of the atmosphere (2  $\mu\text{m}$  - 5  $\mu\text{m}$ ), KTiOPO<sub>4</sub> (KTP) and a periodically poled LiNbO<sub>3</sub> (PPLN) are the two crystals mainly used. It is ZnGeP<sub>2</sub> (ZGP) or CdSiP<sub>2</sub> (CSP) crystals when the emission covers Band III (5  $\mu\text{m}$  - 8  $\mu\text{m}$ ) [1].

Then, the selection of new nonlinear crystals remains of prime importance but it relies on their full characterization especially of the optical properties mentioned above. By using the sphere and slab methods we developed many years ago, we provide direct measurements of conversion efficiencies under phase-matching conditions [3, 4]. Recently they were also recorded out-of phase-matching conditions by using our newly implemented tunable fringes method.

All these data can be used *per se*. But they also lead to the determination of the main parameters of the studied crystal with the best accuracy *i.e.* the value of the principal refractive indices as a function of wavelength [4], and the magnitudes [3] and relative signs of all the non-zero elements of the second-order electric susceptibility. Using the main parameters, we calculate tuning curves associated with maximal conversion efficiency for the generation of mid-infrared parametric light in a device using the crystal.

With our unique methods, we recently fully characterized the nonlinear optical properties of the new BaGa<sub>4</sub>Se<sub>7</sub> (BGSe) nonlinear crystal that is transparent between 0.47 and 18  $\mu\text{m}$  [3, 4]. The goal of this talk is to give an overview of this work, and to show our calculations for the generation of mid-infrared parametric light using the main parameters of BGSe we determined.

## References

- [1] A. Godard, "Optical parametric sources for the infrared (2–12  $\mu\text{m}$ ) solid-state laser sources: a review" C.R. Phys. 8, 1100–1128 (2007).
- [2] B. Boulanger and J. Zyss, in International Tables for Crystallography, A. Authier, ed., Vol. D of Physical Properties of Crystals (Kluwer Academic, 2004), pp. 178–219.
- [3] E. Boursier, P. Segonds, J. Debray, P. L. Inácio, V. Panyutin, V. Badikov, D. Badikov, V. Petrov, and B. Boulanger, "Angle noncritical phase-matched second-harmonic generation in the monoclinic crystal BaGa<sub>4</sub>Se<sub>7</sub>," Opt. Lett. 40, 4591–4594 (2015).
- [4] Boursier E., Segonds P., Ménaert B. J., Inácio P. L., Panyutin V., Badikov V., Badikov D., Petrov V., Boulanger B. "Phase-matching directions and refined Sellmeier equations of the monoclinic acentric crystal BaGa<sub>4</sub>Se<sub>7</sub>" Optics Letters, 41(12), 2731-2734 (2016).

# Nanocarbon Q-switched and mode-locked compact solid-state lasers near 1 $\mu\text{m}$

F. Rotermund

Department of Physics, Korea Advanced Institute of Science and Technology (KAIST), Daejeon 34141, Korea  
email address: [rotermund@kaist.ac.kr](mailto:rotermund@kaist.ac.kr)

Carbon-based nanomaterials such as carbon nanotubes (CNTs) and graphene have been widely used for a variety of applications in electronics and photonics. One of the most successful applications in photonics is their use as saturable absorbers (SAs). Q-switching and mode-locking by using suitable SAs is the widespread well-known technique for the pulsed operation of lasers. Since CNTs and graphene possess broadband absorption with large and ultrafast third-order nonlinearities providing an efficient nonlinear optical switching mechanism with ultrafast responses and the fabrication of such nanocarbon-based SA devices needs relatively simple manufacturing processes, they can be used for developing diverse Q-switched and mode-locked lasers. The applicable wavelength and the spectral bandwidth of CNT-based SAs are controllable by chirality and diameter of carbon nanotubes distributed in the absorber layer [1], while graphene intrinsically provides ultra-broadband absorption even beyond 2  $\mu\text{m}$  without bandgap engineering due to unique point-bandgap structure and linear dispersion of Dirac electrons [2,3]. In the present talk, nanocarbon Q-switched and mode-locked compact bulk and waveguide lasers operating near 1  $\mu\text{m}$  will be mainly discussed with their characteristics [4-6].

- [1] W. B. Cho, J. H. Yim, S. Y. Choi, S. Lee, A. Schmidt, G. Steinmeyer, U. Griebner, V. Petrov, D.-I. Yeom, K. Kim, F. Rotermund, "Boosting the nonlinear optical response of carbon nanotube saturable absorbers for broadband mode-locking of bulk lasers," *Adv. Funct. Mater.* **20**, 1937 (2010).
- [2] W. B. Cho, J. W. Kim, H. W. Lee, S. Bae, B. H. Hong, S. Y. Choi, I. H. Baek, K. Kim, D.-I. Yeom, F. Rotermund, "High-quality, large-area monolayer graphene for efficient bulk laser mode-locking near 1.25  $\mu\text{m}$ ," *Opt. Lett.* **36**, 4089 (2011).
- [3] W. B. Cho, S. Y. Choi, C. Zhu, M. H. Kim, J. W. Kim, J. S. Kim, H. J. Park, D. H. Shin, M. Y. Jung, F. Wang, F. Rotermund, "Graphene mode-locked femtosecond  $\text{Cr}^{2+}:\text{ZnS}$  laser with  $\sim 300$  nm tuning range," *Opt. Express* **24**, 20774 (2016)
- [4] S. Y. Choi, J. W. Kim, M. H. Kim, D.-I. Yeom, B. H. Hong, X. Mateos, M. Aguiló, F. Díaz, V. Petrov, U. Griebner, F. Rotermund, "Carbon nanostructure-based saturable absorber mirror for a diode-pumped 500-MHz femtosecond  $\text{Yb:KLu}(\text{WO}_4)_2$  laser," *Opt. Express* **22**, 15626 (2014).
- [5] M. H. Kim, T. Calmano, S. Y. Choi, B. J. Lee, I. H. Baek, K. J. Ahn, D.-I. Yeom, C. Kränkel, F. Rotermund, "Monolayer graphene coated  $\text{Yb:YAG}$  channel waveguides for Q-switched laser operation," *Opt. Mater. Express* **6**, 2468 (2016).
- [6] S. Y. Choi, T. Calmano, F. Rotermund, C. Kränkel, "2-GHz carbon nanotube mode-locked  $\text{Yb:YAG}$  channel waveguide laser," *Opt. Express* **26**, 5140 (2018).

## 2.3 $\mu\text{m}$ laser emission in Tm-doped crystals

R. Soulard<sup>1</sup>, P. Loiko<sup>1</sup>, J. L. Doualan<sup>1</sup>, A. Braud<sup>1</sup>, A. Tyazhev<sup>2</sup>, A. Hideur<sup>2</sup>, F. Druon<sup>3</sup>, L. Guillemot<sup>3</sup> and P. Camy<sup>1</sup>

<sup>1</sup>Centre de recherche sur les Ions, les Matériaux et la Photonique (CIMAP), UMR 6252 CEA-CNRS-ENSICAEN, Normandie Université, 6 Blvd Maréchal Juin, 14050 Caen, France

<sup>2</sup>CORIA UMR6614, CNRS-INSA-Université de Rouen, Normandie Université, Avenue de l'université, BP. 12, 76801 Saint Etienne du Rouvray, France

<sup>3</sup>Laboratoire Charles Fabry, 2 avenue Augustin Fresnel 91127 Palaiseau, France

patrice.camy@ensicaen.fr

One approach to produce laser emission above 2  $\mu\text{m}$  wavelength consists to investigate Tm-doped crystals. Indeed, in addition to the well-known 1.9  $\mu\text{m}$  transition ( $^3\text{F}_4 \rightarrow ^3\text{H}_6$ ), Tm<sup>3+</sup> ions also exhibits an optical emission around 2.3  $\mu\text{m}$  ( $^3\text{H}_4 \rightarrow ^3\text{H}_5$  transition, see Fig. 1) being far from than the water absorption band near 1.9  $\mu\text{m}$  and therefore interesting to have a stable mode-locked laser. This laser transition can be pumped around 780 nm, a wavelength at which high power laser diodes are commercially available, and operated according to a 4 levels laser scheme. The laser operation has been already demonstrated in the 90's in some Tm- and (Yb,Tm)-doped fluoride hosts [1,2]. The use of fluorides with low doping concentrations (<1.5%) were mostly investigated because the cross-relaxation process, which was proved to be very efficient to populate the  $^3\text{F}_4$  laser emitting level at 1.9  $\mu\text{m}$ , so not favorable to achieve an efficient population inversion between  $^3\text{H}_4$  and  $^3\text{H}_5$  levels. As a matter of fact, the laser efficiencies reported so far around 2.3  $\mu\text{m}$  have been relatively modest and limited anyway by the Stokes factor  $\eta = \lambda_p / \lambda_l$  with a maximum value of 34%.

However, higher Tm<sup>3+</sup> ions concentrations were recently investigated in YLF crystals and it was shown that higher laser efficiencies than expected can be reached thanks to energy transfer mechanisms (Fig. 2) [3-4].

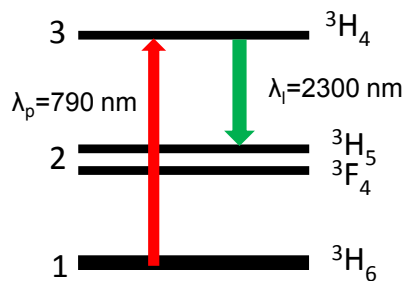


Figure 1 : Energy level diagram of Tm<sup>3+</sup>:YLF

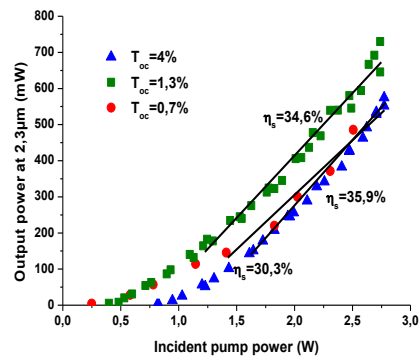


Figure 2 : Output power delivered at 2.3  $\mu\text{m}$  versus incident pump power for Ti:Sa pumping for different output couplers

The present communication will give an overview of the results and perspectives concerning 2.3  $\mu\text{m}$  Tm transition including recent laser results obtained with waveguide devices.

[1] J.F. Pinto, L. Esterowitz, G. Rosenblatt, "Tm<sup>3+</sup>:YLF laser continuously tunable between 2.20 and 2.46  $\mu\text{m}$  » Opt. Lett. 19(12) 883-890 (1994)

[2] A. Diening, B.-M. Dicks, T. Jensen, F. Heine, E. Heumann, G. Huber, "Diode-pumped cw and quasi-cw lasing in Yb, Tm -doped fluorides at 1.5  $\mu\text{m}$  and 2.3  $\mu\text{m}$ " Conf. Lasers & Electro-Optics, vol. 11, OSA Tech. Dig. Series paper CTuE3 (1997)

[3] F. Canbaz, I. Yorulmaz, and A. Sennaroglu, "2.3  $\mu\text{m}$  Tm<sup>3+</sup>:YLF laser passively Q-switched with a Cr<sup>2+</sup>:ZnSe saturable absorber," Opt. Lett. 42, 1656-1659 (2017)

[4] R. Soulard, A. Tyazhev, J. L. Doualan, A. Braud, A. Hideur, M. Laroche, B. Xu, P. Camy, 2.3- $\mu\text{m}$  Tm<sup>3+</sup>:YLF Mode-locked laser, Opt. Lett. 42, 3534-3536 (2017)

# Transverse optical pumping of e-beam excited high-pressure He/Ar mixture with a laser diode array

A.A. Ionin, A.E. Drakin, I.V. Kholin, A.Yu. L'dov, N.N. Ustinovskii and D.A. Zayarnyi

*P.N. Lebedev Physical Institute of the Russian Academy of Sciences,*

*53 Leninsky prospect, 119991, Moscow, Russia*

*aion@sci.lebedev.ru*

Transition from an electric discharge to e-beam pumping in the development of a high-pressure gas laser on low-lying electronic ArI transitions previously launched with combined pumping by an electric discharge and laser diode emission [1-2] allows one not only to scale such a laser system, but also to increase energy deposition from a high-power laser diode due to the best matching spectral widths of the laser diode spectral line and absorption line of the 1s5-2p9 ArI electronic transition with an enhancement of gas mixture He/Ar pressure up to several atmospheres. Previously, by the procedure of absorption probing, we demonstrated the optimal conditions for quasi-cw lasing of this type of a laser to be obtained with an increase of He/Ar mixture pressure up to 4 atm [3]. It was also shown in that paper that at high pressure of this mixture with a low Ar content excited by a relativistic e-beam, anomalously wide absorption lines with  $\sim 5$  nm FWHM were observed for the transitions 1s5-2p10 and 1s5-2p9 ArI. This may be due to the rapid formation processes from ArI into the metastable 1s5 state and backward decay into this state of the HeAr\* excimer complex in the reaction  $\text{Ar}^* + 2\text{He} \leftrightarrow \text{ArHe} + \text{He}$  (1) with very low binding energy of the atoms in this molecule and leading, respectively, to this level broadening, many times exceeding the classical interatomic collisional one. In this case, the total speed of process (1), which leads to depopulation of the 1s5 ArI level, is only  $(4.4 \pm 0.9)10^{-36}\text{cm}^6/\text{s}$ , according to our measurements.

A laser with combined e-beam and optical pumping was simulated in a chamber with an internal volume of  $15 \times 15 \times 10$  mm<sup>3</sup>, which allowed one to observe an increase in the photoluminescence signal upon application of transverse optical pumping with a laser diode array at the wavelength of 811.5 nm with the cross-section of  $\sim 3 \times 1$  mm<sup>2</sup> at the center of the active volume filled with He/Ar gas mixture (argon content was from 2 to 4%) of a total gas pressure up to 4 atm excited by a 2.5 microsecond 400 keV e-beam. It was shown that the most optimal conditions for quasi-cw lasing at the 2p10-1s5 transition with the wavelength of 912.3 nm were formed in the afterglow of the e-beam (Fig. 1a). An application of a semitransparent cavity resulted in a significant increase of the photoluminescence signal in the afterglow (Fig. 1b) at least indicating to amplified spontaneous emission forming.

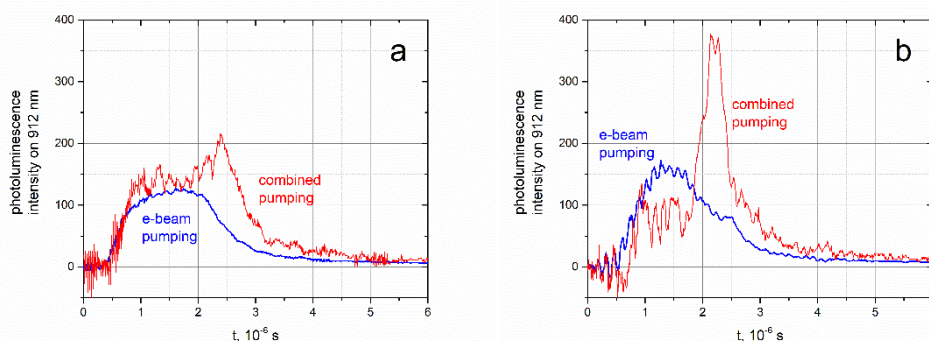


Fig.1 Photoluminescence signal on the 2p10-1s5 transition of ArI (912.3 nm) without (a) and with (b) a 50% flat resonator.

Further optimization of optical pumping due to an increase in the length of the active region makes it possible to get lasing at this wavelength in a He/Ar laser with optical pumping of metastable levels formed by an e-beam. Acknowledgements to Dr. G. Mikaelyan. This research was supported by the Russian Foundation for Basic Research (Project 17-02-00241).

[1] J. Han and M. Heaven. Gain and lasing of optically pumped metastable rare gas atoms. *Opt. Lett.*, **37**, 2157–2159 (2012).

[2] J. Han, L. Glebov, G. Venus, and M. Heaven. Demonstration of a diode-pumped metastable Ar laser. *Opt. Lett.*, **38**, 5458–5461 (2013).

[3] A.A. Ionin, I.V. Kholin, A.Yu. L'dov, L.V. Seleznev, N.N. Ustinovskii and D.A. Zayarnyi. On the possibility of developing quasi-CW high-power high-pressure laser on 4p–4s transition of ArI with electron beam—optical pumping: quenching of 4s (<sup>3</sup>P<sub>2</sub>) lower laser level. *Laser Phys.*, **27**, 125803 (2017).

# Laser Technologies for Manufacturing and Reworking of Marine Engineering Parts

Valeriy M. Levshakov<sup>1</sup>, Natalia A. Steshenkova<sup>1</sup>, Nikolay A. Nosyrev<sup>1</sup>, Artem G. Zhmurenkov<sup>1</sup>

*1- JSC «Shipbuilding & Shiprepair Technology Center» (JSC «SSTC»),  
7, Promyshlennaya Street, St. Petersburg 198095 Russia*

*info@sstc.spb.ru*

The level of technological development is a key factor that determines the competitiveness of industrial enterprise. In this connection, an important task is the modernization of the existing and the creation of new technological processes to provide high performance items production with least costs. JSC “Shipbuilding & Shiprepair Technology Center” is a leading design and technology shipbuilding center in Russia. For 75 years upon establishment (since 1939) it has been developing and implementing high-efficient technologies for domestic shipbuilding related to marine equipment construction, operation and repair. In particular, JSC SSTC actively develops and applies plasma and laser technologies for shipbuilding industry.

Analysis of marine diesel engines shows, that high-loaded parts (pistons, valves, valve lands), uses in their constructions, can break before the planning engine overhaul. For this purpose, it is necessary to withdrawal the engine for repairing these high-loaded parts. The report describes experience of many years of using equipment and technologies for cladding (hardfacing) the critical engineering maritime machinery parts, transition to high automation level and application of robotized equipment. The report presents results of researches and development technologies for laser cladding of marine engine valves and valve lands. Different types of Fe-, Ni- and Co-based cladding materials were investigated and the evaluation of metallurgical process features were carried out in this work.

**Keywords:** laser cladding, hardfacing, marine engine valves, marine engine valve lands

# High-precision Measurement Using the Frequency Modulated Continuous Wave Ladar At Long Distance

Hao Pan, Xinghua Qu, Fumin Zhang\*

State Key Laboratory of Precision Measurement Technology and Instrument, Tianjin University, Tianjin 300072, China

Main author email address: zhangfumin@tju.edu.cn, zeratul\_ph@tju.edu.cn

Nowadays, the requirements of high-speed, multi-target, high dynamic range, and high-precision seem to be a shared vision in various fields, such as manufacturing, aerospace etc. Frequency modulated continuous wave (FMCW) ladar has proved to be competent in the above high-precision fields [1,2]. As everyone knows, every promising measurement technology will have its technical obstacles, and FMCW ladar is no exception. In early work, the peer workers spent lots of time making research on the influence of non-linearity of laser frequency sweeps, which deteriorates the spectrum and makes it unable to obtain the absolute distance precisely. Usually, this can be solved by the active linearization technique [3] and post-processing schemes [4]. In the large-bandwidth and long-distance measurements, a long fiber used in these methods causes dispersion mismatch problems, which result in spectral broadening and distance shifting. In addition, the sampling errors caused by jitter and hardware delay could also lead to spectral distortion.

To eliminate the dispersion mismatch, a chirp decomposition [5] method and interpolation technique [2] can be used to solve this problem. However, these methods were not suitable for low signal-to-noise ratio measurement situations. In this study, we proposed a more erasable compensation method as follows: First, we used Hilbert transform to remove the envelope of the resampled signal. Then, we performed Hilbert transform again on the new signal to obtain the instantaneous phase. The compensation was determined by a least-squares fit to the phase curve. The distance spectra without dispersion compensation (red), and with compensation (black), at a distance up to 60 m, as shown in left panel of Fig. 1.

To reduce the sampling errors, we used the  $H^{13}C^{14}N$  gas cells absorption line certified by NIST [6] to track the actual sweep rate curve, which was used as an aligning tool to measure the sampling error caused by jitter. Then, the adjacent points replacement and spline interpolation were used for resolution-enhancement and sampling error correction. The uncorrected sampling errors and corrected by adjacent points and spline interpolation were shown in right panel of Fig. 1.

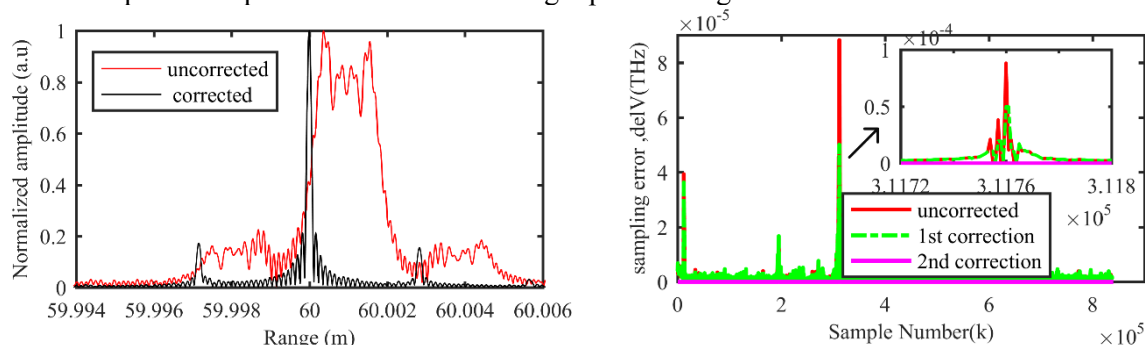


Fig. 1 (left panel) The distance spectrum without dispersion compensation (red) and with dispersion compensation; (right panel) the sampling error uncorrected (red) and corrected with adjacent points (green) and correction with interpolation (purple).

This work was supported by the National Natural Science Foundation of China (NSFC) (51675380)

- [1] P. A. Coe et al., Frequency scanning interferometry in ATLAS: remote, multiple, simultaneous and precise distance measurements in a hostile environment, *Meas. Sci. Technol.* 15(11), 2175-2187 (2004).
- [2] T. DiLazaro et al., Large-volume, low-cost, high-precision FMCW tomography using stitched DFBs, *Opt. Express* 26(3), 2891-2904 (2018).
- [3] P. A. Roos et al., Ultrabroadband optical chirp linearization for precision metrology applications, *Opt. Lett.* 34(23), 3692-3694 (2009).
- [4] H. Pan et al., High-precision frequency estimation for frequency modulated continuous wave laser ranging using the multiple signal classification method, *Appl. Opt.* 56(24), 6956-6961 (2017).
- [5] C. Lu et al., Method based on chirp decomposition for dispersion mismatch compensation in precision absolute distance measurement using swept-wavelength interferometry, *Opt. Express* 23(25), 31662-31671 (2015)
- [6] W. C. Swann and S. L. Gilbert, Line centers, pressure shift, and pressure broadening of 1530-1560 nm hydrogen cyanide wavelength calibration lines, *J. Opt. Soc. Am. B* 22(8), 1749-1756 (2005).

# Intracavity optical parametric oscillator pumped by a semiconductor disk laser: A numerical modeling of a time-delay system

**Yu. A. Morozov<sup>1</sup>, M. I. Balakin<sup>2</sup>, L. A. Kochkurov<sup>2</sup>, A. I. Konukhov<sup>3</sup>**

*1 – Kotelnikov Institute of RadioEngineering & Electronics (Saratov Branch), Russian Ac. Sci.  
38 Zeleynaya Str. 410019, Saratov, Russia*

*2 – Yuri Gagarin State Technical University of Saratov, 77 Politechnicheskaya Str., 410054, Saratov, Russia*

*3 – Saratov State University, 83 Astrakhanskaya Str., 410012, Saratov, Russia*

*yuri.mor@rambler.ru*

High-resolution spectroscopy needs for continuous-wave (CW) sources of coherent radiation in mid- and far-infrared bands. Difference-frequency generators (DFGs) and optical parametric oscillators (OPOs) are believed to be almost ideally suitable for such an application. Some realizations of the devices can be made simple, compact and easy to use [2]. The compactness of the oscillators may be achieved through using an intracavity setup, i.e. with a nonlinear crystal for parametric interaction located in a short-length cavity.

The preliminary analysis of dynamic behaviour of both the intracavity difference-frequency generator (ICDFG) and intracavity singly resonant optical parametric oscillator (ICSRO) [3] confirm suitability of such devices for spectroscopic applications. Like the most of known papers, the mathematical model [3] is based on the mean-field approach which implies averaging of all optical fields along the laser cavity. Such an approach results in slow variations of the field amplitudes on the photon lifetime scale. To study the possibility of more fast amplitude oscillations, we adopted the model [4] with time-delayed feedback of large value. This model is in sharp contrast to the well-known Lang-Kobayashi model [5] adopting only small reflections from a distant mirror. We have developed the model of [4] by taking into account the impact of three-wave nonlinear interaction in an intracavity nonlinear crystal on the ICSRO dynamics.

Fig.1 shows emission of the ICSRO in transient regime after turning on a primary pump. The time-delay approach implying a dynamic system with an infinite number degree of freedom, demonstrates more complex dynamics in comparison with the mean-field approximation: long-lived oscillations of emission intensity can be observed in the framework of the first model. With specific values of parameters, the laser radiation was found to lose stability via such oscillations.

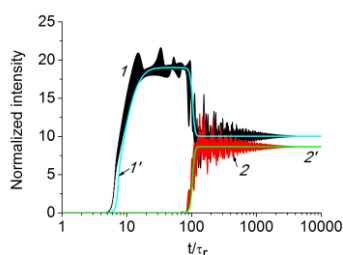


Fig.1. Transient dynamics of the pump (1,1') and signal (2,2') emission in the ICSRO. The mean-field approximation (1',2') and the time-delayed feedback system approximation (1,2) are shown. The time axes is normalized to the carrier lifetime.

This study was supported by RFBR grant No.18-08-00599-a.

- [1] Solid-state mid-infrared laser sources, T. Sorokina, K. L. Vodopyanov, Eds. (Springer-Verlag Berlin Heidelberg), Chapter 11, (2003).
- [2] Yu. A. Morozov, M. Yu. Morozov, V. I. Kozlovsky, O. G. Okhotnikov. Compact intracavity singly-resonant optical parametric oscillator pumped by GaSb-based vertical external cavity surface-emitting laser: Concept and the main operational characteristics. IEEE Journ. of Sel. Top. in Quantum Electronics, vol.21, p.1603105-1—1603105-5, (2015).
- [3] Yu. A. Morozov. Multi-mode dynamics of optical oscillators based on intracavity nonlinear frequency down-conversion. Applied Physics B, vol.124, p12-1—12-7, (2018).
- [4] Yu. A. Morozov, T. Leinonen, A. Härkönen, M. Pessa. Simultaneous dual-wavelength emission from vertical external-cavity surface-emitting laser: A numerical modeling. IEEE Journ. of Quantum. Electronics, vol.42, p.1055-1061, (2006).
- [5] R. Lang, K. Kobayashi. External optical feedback effects on semiconductor injection laser properties. IEEE Journ. of Quantum. Electronics, vol.16, p.347-355, (1980).

## Effect of IR, visible, UV and gamma irradiation on optical properties of bismuth doped fibers

**A. V. Kharakhordin<sup>1</sup>, S. V. Alyshev<sup>1</sup>, K. E. Riumkin<sup>1</sup>, S. V. Firstov<sup>1,3</sup>, V. F. Khopin<sup>2</sup>, M. A. Melkumov<sup>1</sup>, A. N. Guryanov<sup>2</sup>, E. M. Dianov<sup>1</sup>**

*1 - Fiber Optics Research Center, Russian Academy of Sciences, Moscow, Russia*

*2 - Institute of Chemistry of High-Purity Substances, Russian Academy of Sciences, Nizhny Novgorod, Russia*

*3 - Institute of Physics and Chemistry, Ogarev Mordovian State University, Saransk, Russia*

*e-mail: kharakhordin@fo.gpi.ru*

By now, it was shown that bismuth-doped high-GeO<sub>2</sub> silica-based fibers are promising materials for achieving of optical amplification and laser generation in the wavelength range 1600-1800 nm. The photobleaching phenomenon of absorption and luminescence bands belonging to bismuth-related active centers (BAC) was discovered in [1].

In this report, we present the results of investigation of optical properties of Bi-doped fibers exposed to laser radiation with various wavelengths (IR, visible, UV and gamma-ray irradiation). The effect of the irradiation was investigated by monitoring the intensity of BAC luminescence during the irradiation process. For that purpose, at pre-selected points in time the bleaching irradiation was turned off, the fiber was excited at 1550 nm, and the luminescence signal was recorded. The characteristic times of bleaching process were estimated. Typical dependence of characteristic bleaching time of IR luminescence on the irradiation photon energy is presented in Fig. 1. It is seen that the characteristic time of the bleaching became greater with the increase of photon energy.

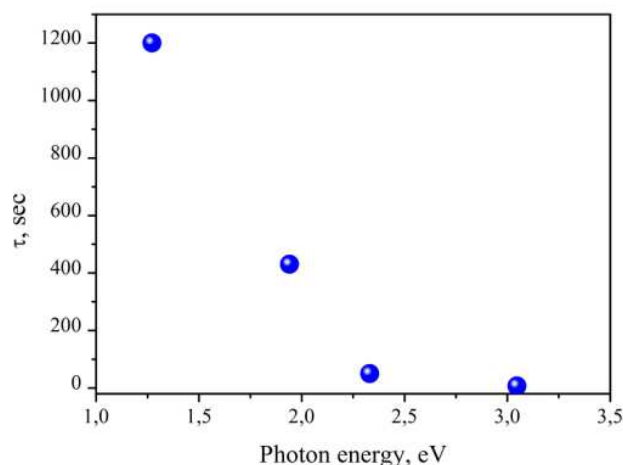


Fig. 1. Bleaching time as a function of photon energy [2].

Also, the effect of gamma irradiation on optical properties was studied. As a result, except of growth of background loss appearance of absorption band peaked near 1200 nm was observed in bismuth-doped fibers after irradiation. A similar phenomenon occurs when the active fiber is exposed to visible radiation [3].

This research was supported by Russian Science Foundation (Grant 16-12-10230).

[1] S.V. Firstov *et al.*, Bismuth-doped optical fibers and fiber lasers for a spectral region of 1600–1800 nm, *Optics Letters*, vol. 39, pp. 6927-6930, (2014)

[2] S.V. Firstov *et al.*, Dependence of the photobleaching on laser radiation wavelength in bismuth-doped germanosilicate fibers, *Journal of Luminescence*, vol. 182, pp. 87-90, (2017)

[3] S. V. Firstov *et al.*, Laser-Active Fibers Doped With Bismuth for a Wavelength Region of 1.6–1.8 μm, *IEEE Journal of Selected Topics in Quantum Electronics*, vol. 24, no. 5, pp. 1-15, (2018).

# Chromium Doped Forsterite Cr:Mg<sub>2</sub>SiO<sub>4</sub> Laser Crystals Grown from Non-Stoichiometric Melts and Annealed at High-Temperature

V.V.Sanina<sup>1,2</sup>, K.A.Subbotin<sup>1,2</sup>, D.A.Lis<sup>1</sup>, V.V.Voronov<sup>1</sup>, E.V.Zharikov<sup>1</sup>

1- Prokhorov General Physics Institute of Russian Academy of Sciences, Vavilova str. 38, Moscow, Russia

2- Mendeleev University of Chemical Technology of Russia, Miusskaya sq. 9, Moscow, Russia

vika29@lsk.gpi.ru, VictoriaSlavkina29@gmail.com

Tetravalent chromium doped forsterite Cr<sup>4+</sup>:Mg<sub>2</sub>SiO<sub>4</sub> (Cr-Fo) single crystals are used as the active media of tunable and femtosecond solid-state lasers, which have great potential of wide application in various fields, including telecommunications, medicine, LIDARs, spectroscopy, photochemistry, etc. The working particles of Cr-Fo lasers are tetrahedrally coordinated Cr<sup>4+</sup> ions. Besides that, chromium in some parasitic oxidation states (e.g., octahedrally coordinated Cr<sup>2+</sup>, and Cr<sup>3+</sup>) are also present in Cr-Fo crystals, which were fabricated by the standard Czochralski technique. Presence of Cr<sup>2+</sup>, and Cr<sup>3+</sup> in the crystals results in worsening of their spectroscopic and laser properties. The general aim of our research is to reduce the content of parasitic chromium ions in the crystals, and to increase the Cr<sup>4+</sup> concentration, by perfection the crystals fabrication technology. In this presentation we report the results of usage the non-stoichiometric (MgO enriched) melts for the crystals growth, and of application the prolonged high-temperature oxidizing annealing of the as-grown Cr-Fo crystals.

In the frame of the work we have grown the series of high-quality Cr-Fo single crystals by Czochralski from the melts containing 0 to 2 wt. % MgO excess in standard slightly oxidizing atmosphere. The concentrations of Cr<sup>4+</sup>, Cr<sup>2+</sup>, and Cr<sup>3+</sup> ions in the samples were determined from the polarized optical absorption spectra, acquired in the range from 300 to 2000 nm. The spectra were decomposed for 24 elementary Gaussians with use of specially developed set. It was revealed, that contents of Cr<sup>4+</sup> continuously rises with increase of MgO content, and, simultaneously, the concentration of Cr<sup>3+</sup> passes through a maximum within this series of the crystals.

We have also measured the crystals densities by hydrostatic weighting and the unit cell parameters - by XRD analysis. These results allowed us to calculate the actual molar weights of the crystals. The calculated values were found to gradually increase, approaching the theoretical value of 140,7 g/mol. with increase of MgO excess in the parent melt, but they do not reach it. It means that MgO excess in the melt leads to reduction the content of vacancies (magnesium or oxygen ones) in the crystals rather than to introduction of the excess Mg<sup>2+</sup> ions, say, in interstitials. The possible mechanisms of influence of these defects onto Cr<sup>4+</sup> and Cr<sup>3+</sup> contents in the crystals are discussed in the presentation.

Besides that, the prolonged high-temperature annealing of several Cr-Fo single crystals grown in different conditions had been performed at 1300 °C in air. The evolution dynamics of Cr<sup>4+</sup>, Cr<sup>2+</sup>, and Cr<sup>3+</sup> concentrations in the samples during their annealing was studied. It was found that content of Cr<sup>2+</sup> exponentially reduces and after ~ 900 hours of annealing becomes negligible. Concentration Cr<sup>3+</sup> increases during the first 200-300 hours of the annealing, then reduces during the following 500-600 hours. Then the reduction stops, and Cr<sup>3+</sup> concentration becomes insensitive for the further annealing. The concentration of tetravalent chromium increases during the first stages of annealing, but this increment stops simultaneously with stopping the reduction of Cr<sup>3+</sup> content (i.e., after 800-900 hours of the annealing). The values of changes the Cr<sup>4+</sup>, and Cr<sup>3+</sup> concentrations in the crystals during the annealing appeared to be very sensitive to the conditions of preliminary crystal growth (the growth atmosphere, and introduction of the additional codopants into the crystal). The observed dependencies and trends are discussed in the presentation, and compared with the previously obtained results [1-4]. This research has been supported by Russian Fund for Basic Research (grant 18-33-01200), and by the Russian Scientific Fund (grant 18-12-00517)

[1] Y. Yamaguchi, K. Yamagishi, Y. Nobe, J. Crystal Growth vol. 128 pp. 996-1000 (1993).

[2] W.Chen, G.Boulon.- Optical Materials vol. 24 pp. 163-168 (2003).

[3] Yinchun Hou, Hongbin Thu, Shenghui Yan, Sitinh Wang, Bin Hu.- Proc. SPIE vol. 1863, p. 84-89

[4] K.A.Subbotin, V.V.Slavkina, D.A.Lis, O.N.Lis, and E.V.Zharikov, J. Crystal Growth, 468 (2017) 718-723

# 100 kHz, dual-beam, KTA-based noncollinear OPA delivering angular dispersion compensated 50 fs, CEP-stable idler pulses at 3.1 $\mu\text{m}$

**M. Mero<sup>1</sup>, V. Petrov<sup>1</sup>, M. J. J. Vrakking<sup>1</sup>, Z. Heiner<sup>2,3</sup>**

*1- Max Born Institute for Nonlinear Optics and Short Pulse Spectroscopy, Berlin 12489, Germany*

*2- School of Analytical Sciences Adlershof SALSA, Humboldt-Universität zu Berlin, Berlin 12489, Germany*

*3- Department of Chemistry, Humboldt-Universität zu Berlin, Berlin 12489, Germany*

*mero@mbi-berlin.de, heinerzs@hu-berlin.de*

The generation and amplification of few-cycle optical pulses at the short wavelength edge of the mid-infrared, MIR (i.e.,  $\sim 2.7\text{-}4\ \mu\text{m}$ ) benefit a wide range of applications from ultrafast vibrational spectroscopy to strong-field physics and high-harmonic generation. Optical parametric amplifiers (OPAs) pumped by high-repetition-rate ( $\gg 10\ \text{kHz}$ ), ps Yb and Nd lasers can directly satisfy the requirements for large spectral bandwidths and average power scalability in this spectral region. Bulk  $\text{KNbO}_3$  was identified as the best material for amplifying broadband, high average power MIR pulses near  $3\ \mu\text{m}$  utilizing the conventional noncollinear amplifying geometry, where the seed is free from angular dispersion [1]. Compared to  $\text{KNbO}_3$ ,  $\text{KTiOAsO}_4$  (KTA) is a more attractive material for low-gain boosters due to its higher resistance to laser-induced damage, thermal shock, photodarkening, and photorefractive effects, and its significantly reduced OH absorption [2,3]. The disadvantage of KTA is that the conventional noncollinear amplification scheme broadens the phase-matching bandwidth only with near-infrared (NIR) seeding resulting in angularly dispersed MIR idler pulses. Therefore, in the MIR range, KTA has only been considered so far for use in collinear geometry [2,4].

Here we demonstrate a white-light-seeded, dual-beam infrared OPA based on noncollinear amplification in KTA and straightforward angular dispersion compensation of the idler beam. We show that the corrected idler beam exhibits diffraction-limited quality, is astigmatism-free, and compressible to its transform-limited, 5-cycle pulse duration. In a benchmark experiment on beam quality, the corrected idler pulses were successfully used for generating high-harmonics in a crystalline solid up to the 9th order. Pumped by only  $40\ \mu\text{J}$  pulses at  $1.03\ \mu\text{m}$ , our parametric source delivers  $7.8\ \mu\text{J}$ , 38 fs,  $1.53\ \mu\text{m}$  signal pulses and  $2.3\ \mu\text{J}$ , 53 fs,  $3.1\ \mu\text{m}$  idler pulses with sub-100-mrad carrier-envelope phase (CEP) jitter at a repetition rate of 100 kHz. The pump-to-signal and pump-to-idler energy conversion efficiency in the KTA stage exceed 27% and 12%, respectively, without deteriorating the beam quality or the CEP stability. The measured  $M^2$  values of both the signal and idler beams are below 1.4. The scheme provides a promising route to scale the pulse energy and average power beyond collinear periodically-poled  $\text{LiNbO}_3$  (PPLN)- or KTA-based OPA architectures. Thanks to the high conversion efficiencies, our compact, small-scale OPA system constitutes a promising source not only for high-repetition-rate broadband sum-frequency generation spectroscopy [5], but also for high-harmonic spectroscopy of solids.

**Funding:** The European Union's Horizon 2020 research and innovation programme under grant agreement no. 654148; Deutsche Forschungsgemeinschaft (DFG), No. GSC 1013 SALSA.

[1] U. Elu, M. Baudisch, H. Pires, F. Tani, M. H. Frosz, F. Köttig, A. Ermolov, P. St.J. Russell, and J. Biegert, "High average power and single-cycle pulses from a mid-IR optical parametric chirped pulse amplifier," *Optica*, vol. 4, pp. 1024-1029, (2017).

[2] M. Mero, F. Noack, F. Bach, V. Petrov, and M. J. J. Vrakking, "High-average-power, 50-fs parametric amplifier front-end at  $1.55\ \mu\text{m}$ ," *Opt. Express*, vol. 23, pp. 33157-33163, (2015).

[3] M. Mero and V. Petrov, "High-power, few-cycle, angular dispersion compensated mid-infrared pulses from a noncollinear optical parametric amplifier," *IEEE Phot. J.*, vol. 9, pp. 3200408, (2017).

[4] G. M. Archipovaite, S. Petit, J.-C. Delagnes, and E. Cormier, "100 kHz Yb-fiber laser pumped  $3\ \mu\text{m}$  optical parametric amplifier for probing solid-state systems in the strong field regime," *Opt. Lett.*, vol. 42, pp. 891-894, (2017).

[5] Z. Heiner, V. Petrov, and M. Mero, "Compact, high-repetition-rate source for broadband sum-frequency generation spectroscopy," *APL Photonics*, vol. 2, pp. 066102, (2017).

# Passive Q-switching of fs-Laser-Written Thulium Waveguide Lasers by Graphene and MoS<sub>2</sub>

**E. Kifle<sup>1,\*</sup>, J. R. Vázquez de Aldana<sup>2</sup>, C. Romero<sup>2</sup>, A. Ródenas<sup>1,3</sup>, P. Loiko<sup>4</sup>, H. Yu<sup>5</sup>, H. Zhang<sup>5</sup>, Y. Chen<sup>5</sup>, M. Aguiló<sup>1</sup>, F. Díaz<sup>1</sup>, U. Griebner<sup>6</sup>, V. Petrov<sup>6</sup> and X. Mateos<sup>1</sup>**

*1-Universitat Rovira i Virgili, Departament Química Física i Inorgànica, Física i Cristal·lografia de Materials i Nanomaterials (FiCMA-FiCNA)-EMaS, Campus Sescelades, E-43007, Tarragona, Spain*

*2-Aplicaciones del Láser y Fotónica, University of Salamanca, 37008 Salamanca, Spain*

*3-Istituto di Fotonica e Nanotecnologie, Consiglio Nazionale delle Ricerche (IFN-CNR), 20133 Milano, Italy*

*4-ITMO University, 49 Kronverkskiy pr., 197101 St. Petersburg, Russia*

*5-State Key Laboratory of Crystal Materials & Institute of Crystal Materials, Shandong University, 250100 Jinan, China*

*6-Max-Born-Institute for Nonlinear Optics and Short Pulse Spectroscopy, Max-Born-Str. 2a, 12489 Berlin, Germany*

\*Email address: [mail2esrom@yahoo.com](mailto:mail2esrom@yahoo.com)

There is continuing interest in the development of compact and short-pulse lasers emitting at  $\sim 2 \mu\text{m}$ . This has stimulated the study of new saturable absorbers (SAs) with suitable nonlinear properties in this spectral range. Graphene and molybdenum disulfide (MoS<sub>2</sub>) are emerging as promising SAs [1,2]. In the present work, we have employed graphene and MoS<sub>2</sub> as SAs in femtosecond direct laser writing (fs-DLW) fabricated channel waveguide lasers based on monoclinic Tm:KLu(WO<sub>4</sub>)<sub>2</sub> (Tm:KLuW) crystals, for the first time, to the best of our knowledge.

A depressed-index channel waveguide with a circular cladding and a core diameter of  $40 \mu\text{m}$  was fabricated by fs-DLW in a 3 at.% Tm:KLuW bulk crystal. The waveguide was characterised by confocal laser microscopy, Fig. 1(a). A commercial chemical vapor deposition (CVD) graphene and a MoS<sub>2</sub> film prepared by pulsed laser deposition (PLD) both deposited on a quartz substrate were used as SAs. A Ti:Sapphire laser tuned to  $\sim 802 \text{ nm}$  was used as a pump source. The waveguide propagation losses were estimated from the Caird analysis as  $\sim 1.0 \pm 0.3 \text{ dB/cm}$ . Spatial profiles of the laser mode were well fitted with a Gaussian intensity profile, Fig. 1(b).

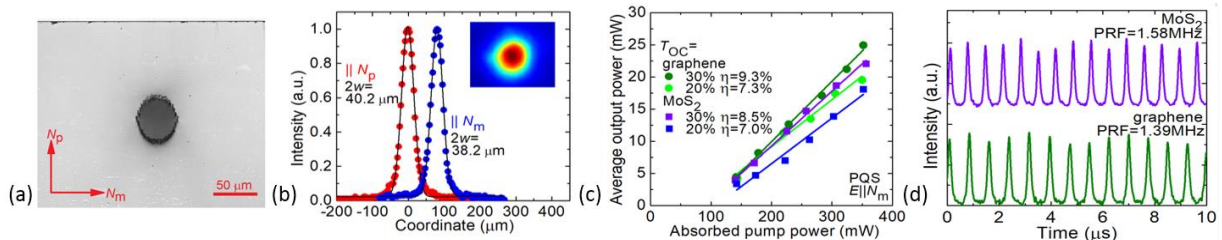


Fig. 1. (a) Confocal laser microscope images of the polished end-face of the fs-DLW Tm:KLuW waveguide; (b) The intensity profiles of the laser mode at the output facet of the waveguide: *inset* – 2D mode profile (graphene SA,  $T_{OC} = 30\%$ ,  $P_{abs} = 0.35 \text{ W}$ ); (c) Input-output dependences in passively Q-switched (PQS) operation mode,  $\eta$  – slope efficiency; (d) Oscilloscope traces of the typical pulse trains.

In the CW operation mode, the laser generated  $210 \text{ mW}$  at  $1851.4 \text{ nm}$  with a slope efficiency  $\eta$  of  $40.8\%$  (with respect to the absorbed pump power  $P_{abs}$ ). The laser threshold was as low as  $P_{abs} = 42 \text{ mW}$ . Using an output coupler with a transmission  $T_{OC}$  of  $30\%$  and the graphene-SA, this laser generated a maximum average output power of  $25 \text{ mW}$  at  $1844.8 \text{ nm}$  with  $\eta = 9.3\%$ , Fig. 1(c). The pulse characteristics (duration / energy) are  $84 \text{ ns} / 18 \text{ nJ}$  at a pulse repetition frequency (PRF) of  $1.39 \text{ MHz}$ , Fig. 1(d). For the MoS<sub>2</sub>-SA, slightly shorter pulses ( $72 \text{ ns} / 14 \text{ nJ}$ ) are obtained at a higher PRF of  $1.58 \text{ MHz}$ .

In conclusion, 2D materials (graphene and few-layer MoS<sub>2</sub>) are promising as SAs for waveguide lasers emitting at  $2 \mu\text{m}$ . They enable the generation of sub-100 ns pulses with nJ pulse energies at high repetition rates (MHz-range). Surface channel waveguides directly coated with such 2D-materials for evanescent field interaction seem also promising for PQS and future work is planned in this direction, too.

[1] Q. Bao, H. Zhang, Y. Wang, Z. Ni, Y. Yan, Z. X. Shen, K. P. Loh, and D. Y. Tang, "Atomic-layer graphene as a saturable absorber for ultrafast pulsed lasers," *Adv. Funct. Mater.*, vol. 19, pp. 3077–3083 (2009).

[2] J. M. Serres, P. Loiko, X. Mateos, H. Yu, H. Zhang, Y. Chen, V. Petrov, U. Griebner, K. Yumashev, M. Aguiló, and F. Díaz, "MoS<sub>2</sub> saturable absorber for passive Q-switching of Yb and Tm microchip lasers," *Opt. Mater. Express*, vol. 6, pp. 3262–3273 (2016).

# Comparing the different Yb<sup>+</sup> doped host crystal for their suitability for high power laser amplification

**M. Schmid<sup>1</sup>, E. Wyss<sup>2</sup>, A. El-Sayed<sup>1</sup>, Y. Zhang<sup>1</sup>, V. Romano<sup>1</sup>**

*1- Bern University of Applied Science, Institute of Advances in Laser, Photonics and Surface Technology*

*2- Bern University of Applied Science, Hochschule für Agrar-, Forst- und Lebensmittelwissenschaften HAFL*

*marc.schmid@bfh.ch*

In the past decade MOPA setup have proven to be the first choice for high power laser systems with good beam quality. When designing laser amplifiers of several tens of watts or even few hundred watts the thermal and optical properties like heat conductivity, absorption and emission cross section are of great importance. They must be harmonized carefully with the pump power, pump geometry and the seed beam. Additionally, Yb<sup>+</sup> doped laser materials have been of great interest for laser and amplifier material in the NIR region due to its high quantum efficiency [1-5]. But for Yb<sup>+</sup> doped laser crystals the thermal management is crucial due to the thermal population of the lower laser level (approx. 5.5% at room temperature [6]). On the other hand, the different host crystals for Yb<sup>+</sup> have a great influence on the absorption and emission cross section of the Yb<sup>+</sup>, the beam propagation and therefore on the whole amplification process [7-9].

In this paper we will report on our simulation study of different Yb<sup>+</sup> doped host crystals like YAG, KKY, CALGO, CaF<sub>2</sub>, LuAG and LuO and their suitability for high power laser amplifiers. The simulation includes the thermal dependency of the absorption and emission cross sections, thermal population of the lower laser level, temperature dependent refractive index, thermal lensing as well as the beam propagation through the crystal of the seed and the pump beam. The modelling has been verified previously by simulating the experimental data for different crystals available from the literature. In the main study we compare optimized configurations for the different host material by changing doping concentration, crystal rod geometry, pump and seed power as well as beam properties. The investigation covers the small signal gain region as well as the saturated gain region and is suitable for CW-amplifiers and pulsed systems with high repetition rates, respectively.

- [1] X. Delen, A. Aubourg, L. Deyra, F. Lesparre, I. Martial, J. Didierjean, F. Balembois, P. Georges, Single crystal fiber for laser sources, Proc. Of SPIE vol. 9342, pp. 934202-1 – 934202-88 (2015).
- [2] W. F. Krupke, Ytterbium Solid-State Lasers—The First Decade, IEEE J. selected. Topics in QE, vol.6 no. 6, pp. 1287-1296 (2000).
- [3] F. Pirzio, S. D. Di Dio Cafiso M. Kemnitzer, A. Guandalini, F. Kienle, S. Veronesi, M. Tonelli, J. Aus der Au, A. Agnesi, Sub-50-fs widely tunable Yb:CaYAlO<sub>4</sub> laser, pumped by 400-mW single-mode fiber-coupled laser diode, Opt. Exp. Vol. 23, no. 8, (2015).
- [4] G. Machinet G. Andriukaitis P. Se´villa no, J. Lhermite D. Descamps A. Pugzˆlys, A. Baltusˆka E. Cormier, High-gain amplification in Yb:CaF<sub>2</sub> crystals pumped by a high-brightness Yb-doped 976 nm fiber laser, Appl. Phys. B, pp. 495-500 (2013).
- [5] G. Toci, A. Pirri, J. Li, T. Xie, Y. Pan, M. Nikl, V. Babin, A. Beitlerova, M. Vannini, First laser operation and spectroscopic characterization of mixed garnet Yb:LuYAG ceramics, Proc. SPIE Vol. 9726, pp. 9726-01 9726N-8 (2015).
- [6] W. Koechner, Solid-State Laser Engineering (Springer) Chapter 2.6 Yb:YAG, (1999).
- [7] J. Koerner, Ch. Vorholt, H. Liebetrau, M. Kahle, D. Kloepfel, R. Seifert, J. Hein, M. C. Kaluza, Measurement of temperature-dependent absorption and emission spectra of Yb:YAG, Yb:LuAG, and Yb:CaF<sub>2</sub> between 20 °C and 200 °C and predictions on their influence on laser performance, J. Opt. Soc. Am. B, vol. 29 no. 9, pp.2493-2502 (2012).
- [8] P. A. Loiko, K. V. Yumashev, R. Schödel, M. Peltz, C. Liebald, X. Mateos, B. Deppe, C. Kränkel, Thermo-optic properties of Yb:Lu<sub>2</sub>O<sub>3</sub> single crystals, Appl. Phys. B, pp. 601-607 (2015).
- [9] D. C. Brown, C. D. McMillen, Ch. Moore, J. W. Kolis, V. Envid, Spectral properties of hydrothermally-grown Nd:LuAG, Yb:LuAG and Yb:Lu<sub>2</sub>O<sub>3</sub> laser materials, J. of. Luminescence, pp. 26-32 (2014).

# Compact optical frequency comb source based on microresonators and semiconductor laser diodes

**A. S. Voloshin<sup>1</sup>, S. E. Agafonova<sup>1,2</sup>, A. S. Gorodnitskiy<sup>1,2</sup>, R. R. Galiev<sup>1,3</sup>,  
G. V. Likhachev<sup>1,3</sup>, N. M. Kondratiev<sup>1</sup>, M. L. Gorodetsky<sup>1,3</sup>**

*1- Russian Quantum Center, Skolkovskoe shosse 45, Moscow, Russia*

*2- Moscow Institute of Physics and Technology, Moscow, Russia*

*3- Lomonosov Moscow State University, Moscow, Russia*

*a.voloshin@rqc.ru*

Optical frequency combs are a powerful tool of modern photonics as they can be used in the field of spectroscopy, optical communication, metrology and distance ranging. Commercially available frequency comb sources utilize bulky laser sources, while integrated photonics creates new opportunities for development of compact laser sources and techniques of frequency comb generation. In that regard, Kerr-frequency combs in microresonators have recently attracted a growing interest [1-5]. In comparison with femtosecond systems used for frequency comb generation, the microresonators manufactured by a variety of different platforms provide broadband low-noise states and high repetition rates. Significant advantage of microresonator-based combs is their compact footprint and possibility of further integration.

Recent developments include packaged devices based on the crystalline cavity and novel coupling methods. Different attempts have been made to demonstrate compact source of optical frequency comb source [2]. The distributed feedback (DFB) laser was operating in self-injection locking regime and was used to generate optical frequency comb in a crystalline micro-resonator [3]. The compact external-cavity diode laser enabled the generation of a single-soliton state in a silica micro-resonator [4]. Although a fully integrated device remains a challenge.

In this report, we demonstrate the compact integrated photonic device generating the optical frequency comb. Combination of different platform allows developing the integrated narrow-linewidth laser based on a low-loss ring resonator, which can be used for frequency comb generation.

The first platform is semiconductor laser diodes. A multi-frequency Fabry-Pérot InP laser diode serves as a laser light source. The center wavelength is 1535 nm, the CW power is up to 100 mW. Different longitudinal modes of the laser diode cover the range of tens nanometers with a line spacing 35 GHz; the linewidth of each mode is 20 MHz.

The second platform is CMOS-compatible Si<sub>3</sub>N<sub>4</sub> chips. The Si<sub>3</sub>N<sub>4</sub> microresonator with a free spectral range of 1 THz is manufactured with the optimized Damascene process [1]. The average linewidth of microresonator modes in strongly overcoupled regime is 1.5 GHz corresponding to intrinsic Q-factor 10<sup>6</sup>. The precise control of waveguide characteristics and group velocity dispersion (GVD) engineering allows to provide generation of low-power wide optical frequency combs, particular, dispersive Kerr solitons. Also the Si<sub>3</sub>N<sub>4</sub> bus waveguides are used to study Fabry-Perot interferometer formed by chip end faces.

Various regimes of the comb source operation are possible. First, the laser diode can be self-injection locked [5] to the Si<sub>3</sub>N<sub>4</sub> microresonator. The laser diode is converted to a single-frequency source with linewidth below 100 kHz. Characteristics of the stabilized laser are compared to theoretical estimations. In the second regime, the Kerr-frequency comb generation is observed. The Kerr comb with a line spacing 1 THz spanned over 300 nm.

[1] Martin H.P. Pfeiffer, et al. "Octave-spanning dissipative Kerr soliton frequency combs in Si<sub>3</sub>N<sub>4</sub> microresonators", *Optica*, vol. 4, issue 7, pp. 684-691 (2017).

[2] N. G. Pavlov, et al., "Kerr soliton combs with regular multifrequency diode lasers", *European Conference on Lasers and Electro-Optics (CLEO)*, paper CD\_11\_5 (2017).

[3] W. Liang, et al. "High spectral purity Kerr frequency comb radio frequency photonic oscillator", *Nat. Commun.* 6:7957 (2015).

[4] Nicolas Volet, et al., "Micro-Resonator Soliton Generated Directly with a Diode Laser", *Laser & Photonics Reviews*, vol. 12, issue 5, 1700307, (2018).

[5] Nikita Kondratiev, et al. "Self-injection locking of a laser diode to a high-Q WGM microresonator", *Optics Express*, vol. 4, issue 23, pp. 28167-2817 (2017).

# Temperature-wavelength dependence of the Verdet constant of dysprosium sesquioxide ceramics ( $\text{Dy}_2\text{O}_3$ )

O. Slezak<sup>1</sup>, R. Yasuhara<sup>2</sup>, H. Furuse<sup>3</sup>, D. Vojna<sup>1,4</sup>, A. Lucianetti<sup>1</sup>, T. Mocek<sup>1</sup> and M. Cech<sup>4</sup>

1 - HiLASE Centre, Institute of Physics ASCR v.v.i., Za Radnici 828, 25241 Dolni Brezany, Czech republic  
 2 - National Institute for Fusion Science, National Institutes of Natural Sciences, 322-6, Oroshi-cho, Toki, Gifu, 509-5292, Japan  
 3 - Kitami Institute of Technology, 165 Koen-cho, Kitami, Hokkaido, Japan  
 4 - Department of Physical Electronics, Faculty of Nuclear Sciences and Physical Engineering, Czech Technical University in Prague, Brehova 7, 115 19 Prague, Czech republic

Main-author email address: slezako@fzu.cz

A further development of the high power lasers and their numerous applications is world-widely struggling with the high-power-associated thermal effects, which are severely degrading the performance of a laser [1–3]. Optical isolators (OIs), the key optical components enabling safe operation of high power lasers, are particularly affected with the thermal effects, because of the relatively high absorption of the currently available magneto-optical elements (MOEs) [3,4]. This limitation could be overcome via investigation of novel magneto-optical materials possessing: high Verdet constant, high transparency, excellent thermal properties and scalability to large apertures; such properties enable reduction of the heat generated in a MOE.

Several material candidates suitable for high power laser OIs have been identified in the recent years. For the visible and near-infrared laser wavelengths, highly desirable for high power laser applications, terbium gallium garnet (TGG) represents the most commonly used magneto-optical material [3,4]. However, there has been an increasing trend in investigating new materials, which could supersede TGG, exhibiting even better magneto-optical properties. In this manner, an attention was brought towards the rare-earth (RE – Tb, Dy, and Ho) sesquioxides ( $\text{RE}_2\text{O}_3$ ) [5–8], containing much higher concentration of the highly magnetically active  $\text{RE}^{3+}$  ions. Compared to the effort put into the investigation of TGG successors, arguably less effort is being put into the research of magneto-optical materials suitable for mid-infrared wavelengths, especially around  $2\ \mu\text{m}$  [9], although several corresponding laser sources [10, 11] with numerous applications [12] have been already reported.

We report on comprehensive experimental characterization of the Verdet constant of the dysprosium sesquioxide ( $\text{Dy}_2\text{O}_3$ ) ceramics in a broad spectral range from 0.6 to  $2.2\ \mu\text{m}$  and for temperatures from 300 down to 20 K. The obtained results revealed that  $\text{Dy}_2\text{O}_3$  ceramics is not only a potential high-power-OI-material candidate for the visible wavelengths ( $V = 340\ \text{rad/Tm}$ , at  $0.633\ \mu\text{m}$ , room temperature), but it might be a suitable material for  $2\ \mu\text{m}$  as well. The obtained value for the Verdet constant at  $2\ \mu\text{m}$  was equal to  $10.5\ \text{rad/Tm}$  at room temperature. The measured transmittance of our sample at  $2\ \mu\text{m}$  was equal to  $\sim 72\%$  and could be further improved by optimization of the sintering conditions. Based on these results, a  $\text{Dy}_2\text{O}_3$ -based OI for a high-power  $2\text{-}\mu\text{m}$  laser could be designed.

- [1] H. Kiriya et al., *High-Contrast, High-Intensity Petawatt-Class Laser and Applications*, IEEE J. of Sel. Top. Quantum Electron. 21(1), 232-249, (2015).
- [2] O. Slezak et al., *Thermally induced depolarization in terbium gallium garnet ceramics rod with natural convection cooling*, J. of Opt. 17(6), 065610, (2015).
- [3] J. Huynh et al., *Femtosecond Yb:YAG ceramic slab regenerative amplifier*, Opt. Mater. Express 8, 615-621, (2018).
- [4] O. Slezak et al., *Temperature-wavelength dependence of terbium gallium garnet ceramics Verdet constant*, Opt. Mater. Express 6, 3683-3691, (2016).
- [5] A. Ikesue et al., *Polycrystalline  $(\text{Tb}_x\text{Y}_{1-x})_2\text{O}_3$  Faraday rotator*, Opt. Lett. 42, 4399-4401, (2017).
- [6] J. R. Morales et al., *Magneto-optical Faraday effect in nanocrystalline oxides*, J. Appl. Phys. 109(9), 093110, (2011).
- [7] H. Furuse et al., *Magneto-optical characteristics of holmium oxide ( $\text{Ho}_2\text{O}_3$ ) ceramics*, Opt. Mater. Express 7, 827-833, (2017)
- [8] D. Vojna et al., *Faraday effect measurements of holmium oxide ( $\text{Ho}_2\text{O}_3$ ) ceramics-based magneto-optical materials*, High Power Laser Science and Engineering 6, (2018).
- [9] G. Stevens et al., *Integrated disruptive components for  $2\ \mu\text{m}$  fibre lasers (ISLA): project overview and passive component development*, Proc. SPIE 9730, 973001, (2016).
- [10] C. Krankel et al., *Rare-earth-doped sesquioxides for diode-pumped high-power lasers in the 1, 2, and  $3\ \mu\text{m}$  spectral range*, IEEE J. of Sel. Top. Quantum Electron. 21(1), 250-262, (2015).
- [11] P. A. Ryabochkina et al., *Two-micron lasing on diode-pumped  $\text{Y}_2\text{O}_3:\text{Tm}$  ceramics*, Quantum Electron 46, 597-600, (2016).
- [12] K. Scholle et al.,  *$2\ \mu\text{m}$  laser sources and their possible applications*, Frontiers in Guided Wave Optics and Optoelectronics, B. Pal, Ed. London, U.K., InTech, (2010).

# Growth, spectroscopy and laser operation of novel “mixed” $\text{Tm}^{3+}:\text{Ca}(\text{Gd},\text{Lu})\text{AlO}_4$ crystals for mode-locked lasers

Z. Pan<sup>1,2</sup>, J. M. Serres<sup>3</sup>, E. Kifle<sup>3</sup>, P. Loiko<sup>4,\*</sup>, H. Yuan<sup>1</sup>, X. Dai<sup>1</sup>, H. Cai<sup>1</sup>, Y. Wang<sup>2</sup>,  
Y. Zhao<sup>2,5</sup>, M. Aguiló<sup>3</sup>, F. Díaz<sup>3</sup>, U. Griebner<sup>2</sup>, V. Petrov<sup>2</sup> and X. Mateos<sup>3</sup>

<sup>1</sup>Institute of Chemical Materials, China Academy of Engineering Physics, Mianyang, 621900, China

<sup>2</sup>Max-Born-Institute for Nonlinear Optics and Short Pulse Spectroscopy, Max-Born-Str. 2a, D-12489 Berlin, Germany

<sup>3</sup>Universitat Rovira i Virgili, Depart. Química Física i Inorgànica, FiCMA-FiCNA-EMaS, Campus Sescelades, E-43007, Tarragona, Spain

<sup>4</sup>ITMO University, 49 Kronverkskiy Pr., 197101 Saint-Petersburg, Russia

<sup>5</sup>Jiangsu Key Laboratory of Advanced Laser Materials and Devices, Jiangsu Normal University, 221116 Xuzhou, China

\*Email address: [kinetic@tut.by](mailto:kinetic@tut.by)

Tetragonal calcium rare-earth aluminates  $\text{CaLnAlO}_4$  (where  $\text{Ln} = \text{Gd}$  or  $\text{Y}$ ) are well-known disordered laser crystal hosts for  $\text{Yb}^{3+}$ -doping [1]. They feature high thermal conductivity, weak and positive thermal lensing. The structural disorder originates from random distribution of  $\text{Ca}^{2+}$  and  $\text{Ln}^{3+}$  ions over a single type of site ( $\text{C}_{4v}$ ). This leads to inhomogeneous broadening of the absorption and emission bands of the  $\text{Yb}^{3+}$  dopant making them attractive for sub-100 fs mode-locked (ML) lasers at  $\sim 1 \mu\text{m}$  [1]. Recently, a  $\text{Tm}^{3+}$ -doped  $\text{CaGdAlO}_4$  crystal has been implemented in continuous-wave (CW) and ML lasers at  $\sim 2 \mu\text{m}$  [2].

In the present work, we aimed to grow and study the spectroscopic and laser properties of a novel “mixed” calcium aluminate crystal,  $\text{Tm}:\text{Ca}(\text{Gd},\text{Lu})\text{AlO}_4$ . The addition of the optically passive  $\text{Lu}^{3+}$  ions is expected to provide compositional disorder leading to a further spectral broadening [3], which is attractive for fs pulse generation in  $\sim 2 \mu\text{m}$  ML lasers.

A 5 at.%  $\text{Tm}^{3+}$ -doped  $\text{CaGd}_{0.9}\text{Lu}_{0.1}\text{AlO}_4$  crystal was grown by the Czochralski method. Its structure was confirmed by XRD and Rietveld refinement. The polarized Raman spectra were also measured. The transition probabilities were analyzed using the Judd-Ofelt theory. The luminescence spectra are shown in Fig. 1(a) and compared with those for  $\text{Tm}:\text{CaGdAlO}_4$ . The introduction of  $\text{Lu}^{3+}$  indeed leads to additional spectral broadening. For  $\sigma$ -polarization, the emission bandwidth is  $>200 \text{ nm}$ . The absorption,  $\sigma_{\text{abs}}$ , and stimulated-emission (SE),  $\sigma_{\text{SE}}$ , cross-sections for the  ${}^3\text{F}_4 \leftrightarrow {}^3\text{H}_6$   $\text{Tm}^{3+}$  transition were determined, see Fig. 1(b). A compact diode-pumped  $\text{Tm}:\text{Ca}(\text{Gd},\text{Lu})\text{AlO}_4$  laser generated 1.83 W at 1945 nm with a slope efficiency of 28.4%, Fig. 1(c).

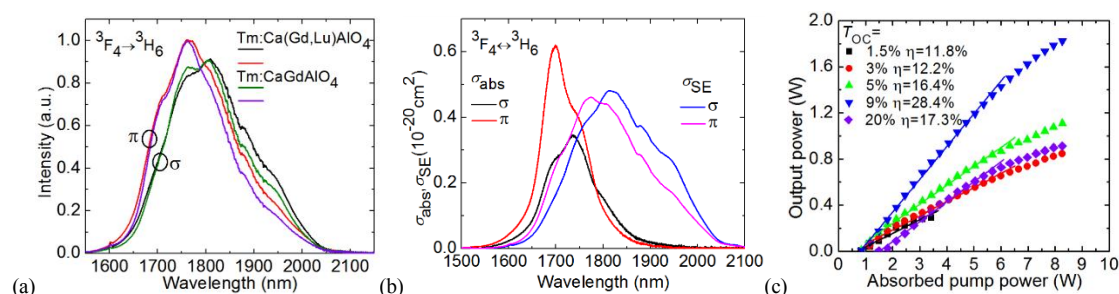


Fig. 1. (a,b) Spectroscopy of  $\text{Tm}^{3+}$  in the  $\text{Ca}(\text{Gd},\text{Lu})\text{AlO}_4$  crystal: (a) luminescence spectra for the  ${}^3\text{F}_4 \rightarrow {}^3\text{H}_6$  transition; the spectra for  $\text{Tm}:\text{CaGdAlO}_4$  are given for comparison,  $\lambda_{\text{exc}} = 802 \text{ nm}$ ; (b) absorption,  $\sigma_{\text{abs}}$ , and stimulated-emission,  $\sigma_{\text{SE}}$ , cross-sections for the  ${}^3\text{F}_4 \leftrightarrow {}^3\text{H}_6$  transition. The light polarizations are  $\pi$  and  $\sigma$ . (c) Input-output dependences of a compact diode-pumped  $\text{Tm}:\text{Ca}(\text{Gd},\text{Lu})\text{AlO}_4$  laser,  $\eta$  – slope efficiency. The laser polarization is  $\sigma$ .

[1] Y. Zaouter, J. Didierjean, F. Balembois, G. Lucas Leclin, F. Druon, P. Georges, J. Petit, P. Goldner, and B. Viana, "47-fs diode-pumped  $\text{Yb}^{3+}:\text{CaGdAlO}_4$  laser," *Opt. Lett.*, vol. 31, pp. 119-121 (2006).

[2] Y. Wang, G. Xie, X. Xu, J. Di, Z. Qin, S. Suomalainen, M. Guina, A. Härkönen, A. Agnesi, U. Griebner, X. Mateos, P. Loiko, and V. Petrov, "SESAM mode-locked  $\text{Tm}:\text{CaGdAlO}_4$  laser at  $2 \mu\text{m}$ ," *Opt. Mater. Express*, vol. 6, pp. 131-136 (2016).

[3] Q. Hu, Z. Jia, A. Volpi, S. Veronesi, M. Tonelli, and X. Tao, "Crystal growth and spectral broadening of a promising  $\text{Yb}:\text{CaLu}_x\text{Gd}_{1-x}\text{AlO}_4$  disordered crystal for ultrafast laser application," *Cryst. Eng. Comm.*, vol. 19, pp. 1643-1647 (2017).

# Tm:GdVO<sub>4</sub> laser Q-switched by a thin film Sb<sub>2</sub>Te<sub>3</sub> saturable absorber

**J. M. Serres<sup>1,2,\*</sup>, P. Loiko<sup>1,3</sup>, J. Bogusławski<sup>4,5</sup>, E. Kifle<sup>1</sup>, M. Kowalczyk<sup>4</sup>, J. Sotor<sup>4</sup>,  
R. Zybala<sup>6</sup>, K. Mars<sup>7</sup>, A. Mikula<sup>7</sup>, K. Kaszyca<sup>8</sup>, U. Griebner<sup>9</sup>, V. Petrov<sup>9</sup>, M. Aguiló<sup>1</sup>,  
F. Díaz<sup>1</sup> and X. Mateos<sup>1</sup>**

*1-Universitat Rovira i Virgili, Departament Química Física i Inorgànica, Física i Cristal·lografia de Materials i Nanomaterials (FiCMA-FiCNA)-EMaS, Campus Sescelades, E-43007 Tarragona, Spain*

*2-Eurecat, Centre Tecnològic de Catalunya, Unitat Advanced Manufacturing Systems (AMS), Campus Sescelades, E-43007 Tarragona, Spain*

*3-ITMO University, 49 Kronverkskiy pr., 197101 St. Petersburg, Russia*

*4-Laser & Fiber Electronics Group, Faculty of Electronics, Wrocław University of Science and Technology, Wybrzeże S. Wyspiańskiego 27, 50-370 Wrocław, Poland*

*5-Institute of Physical Chemistry, Polish Academy of Sciences, Kasprzaka 44-52, 01-224 Warsaw, Poland*

*6-University Research Centre, Functional Materials, Warsaw University of Technology, Wołoska 141, 02-507 Warsaw, Poland*

*7-Faculty of Material Science and Ceramics, AGH University of Science and Technology, A. Mickiewicza 30, 30-059 Kraków, Poland*

*8-Institute of Electronic Materials Technology, Wolczynska 133, 01-919 Warsaw, Poland*

*9-Max Born Institute for Nonlinear Optics and Short Pulse Spectroscopy, Max-Born-Str. 2a, D-12489 Berlin, Germany*

\*Email address: [josepmaria.serres@urv.cat](mailto:josepmaria.serres@urv.cat); [josepmaria.serres@eurecat.org](mailto:josepmaria.serres@eurecat.org)

In recent years, various novel 2D materials, like graphene, transition-metal dichalcogenides (TMDs), black phosphorus (BP) or topological insulators (TIs), have been developed and turned out to be promising ultrafast broadband saturable absorbers (SAs) for lasers emitting in the near-IR [1]. A TI (e.g., Bi<sub>2</sub>Te<sub>3</sub>, Bi<sub>2</sub>Se<sub>3</sub> or Sb<sub>2</sub>Te<sub>3</sub>) behaves like an insulator in the bulk material but it has conducting states at the surface [2]. The band structure of these surface states is similar to that of graphene, showing a Dirac-like linear band dispersion.

In the present work, we studied the continuous wave (CW) and passively Q-switched (PQS) laser operation of a Tm:GdVO<sub>4</sub> crystal with antimony telluride (Sb<sub>2</sub>Te<sub>3</sub>) as a SA. The 3–15 nm-thick Sb<sub>2</sub>Te<sub>3</sub> films were deposited on glass substrates by pulsed magnetron sputtering and they were studied by SEM, Fig. 1(a), X-ray diffraction, Raman and optical spectroscopy. The Sb<sub>2</sub>Te<sub>3</sub> films are characterized by a broadband absorption in the near-IR (0.8-2.2 μm). The saturable absorption of the Sb<sub>2</sub>Te<sub>3</sub> film was confirmed at 1.56 μm for ns-long pulses revealing low saturation intensity of 0.17 MW/cm<sup>2</sup>, Fig. 1(b).

In the CW mode, the diode-pumped compact Tm:GdVO<sub>4</sub> laser generated 3.54 W at 1908-1917 nm with a slope efficiency  $\eta$  of 36%. The laser output was linearly polarized ( $\sigma$ -polarization). When the Sb<sub>2</sub>Te<sub>3</sub> SAs with a thickness of 3 nm (#1) and 5 nm (#2) were inserted into the laser cavity at normal incidence, stable PQS operation was achieved, Fig. 1(c). In the former case, the laser generated 0.70 W at 1913 nm with  $\eta = 36\%$  and PQS conversion efficiency as high as 90%. The pulse energy and duration at maximum  $P_{\text{abs}}$  were 3.5 μJ and 223 ns, respectively, at a repetition rate of 200 kHz. A typical pulse train from the PQS laser is shown in Fig. 1(d), exhibiting intensity instabilities <15%. Sb<sub>2</sub>Te<sub>3</sub> thin films are promising SAs for PQS Tm waveguide lasers based on evanescent-field coupling.

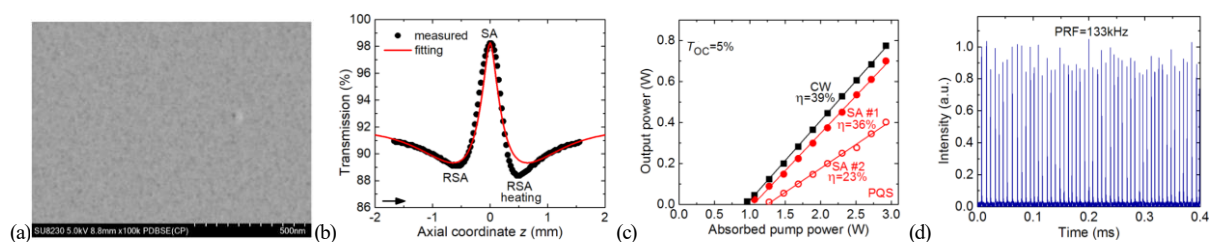


Fig. 1. (a) SEM image of the surface of a 15-nm-thick Sb<sub>2</sub>Te<sub>3</sub> film on a glass substrate; (b) open-aperture Z-scan curve for 15 nm-thick Sb<sub>2</sub>Te<sub>3</sub> SA at 1560 nm; (c) input-output dependences of the Tm:GdVO<sub>4</sub> laser PQS by Sb<sub>2</sub>Te<sub>3</sub> SAs with a thickness of 3 nm (#1) and 5 nm (#2) ( $\eta$  – slope efficiency); (d) oscilloscope trace of the pulse train from this laser and SA #1,  $P_{\text{abs}} = 2.3$  W.

[1] Z. Sun, A. Martínez, and F. Wang, “Optical modulators with 2D layered materials,” *Nature Photon.*, vol. 10, pp. 227-238 (2016).

[2] H. Zhang, C. X. Liu, X. L. Qi, X. Dai, Z. Fang, and S. C. Zhang, “Topological insulators in Bi<sub>2</sub>Se<sub>3</sub>, Bi<sub>2</sub>Te<sub>3</sub> and Sb<sub>2</sub>Te<sub>3</sub> with a single Dirac cone on the surface,” *Nat. Phys.*, vol. 5, pp. 438-442 (2009).

# System for Continuous Laser-Induced Forward Transfer of Materials

**I. Cornago<sup>1</sup>, J. Morentin<sup>1</sup>, S. Zabala<sup>1</sup>, F. Varela<sup>1</sup>**

*1- Naitec, Foundation for r+d on automotive and mechatronics, C/ Tajonar 20, 31006, Pamplona (Spain)*

*icornago@naitec.es*

Light-induced deposition process was first introduced long time ago [1], but it is only recently that industrial applications are being developed. Laser-Induced Forward Transfer (LIFT) is a technique to deposit a wide range of materials on a substrate, called receiver substrate, by means of a previous interaction of a laser radiation with the material in a donor substrate. The material is previously deposited onto the donor substrate, which is placed opposed to the receiver substrate separated a determined distance. The laser is then focused in the interface between the material film and the donor substrate and the material is transferred from the donor to the receiver substrate (see figure 1). In this work, an IR pulsed laser source is used (1064 nm of wavelength, 20 W of nominal power and 4-200 ns of pulse width). The possibility of tuning its parameters, such as its power, frequency of pulse width, allows exploring different densities of energy and conditions for the formation of drops in the LIFT process.

The preparation of the donor substrate is one of the main reasons for the lack of industrial applications of this technology. Here we present a system for a continuous feeding of material to a LIFT area for transferring this material to receiver substrates in a continuous way [2]. The system is mainly composed of 6 rollers, a material dispenser and a conveyor belt, transparent to the laser radiation, which acts as donor substrate (see 3D design in figure 2). The material dispenser applies a film of material onto the belt and rollers drive it to place the material opposed to the receiver substrate in the LIFT area. Then, the rest of rollers bring the belt to its initial position where it can be coated again with new material, forming a closed circuit in a U-shaped configuration.

Due to this system configuration, the space above the LIFT area is free and the use of laser heads with a long focal length is possible. This enables the laser to scan and perform the LIFT process over large areas. Furthermore, the whole system is rotated a small angle around a vertical axis so the advance direction of the belt in the LIFT area is oblique with respect to a laser linear scanning, allowing the laser to interact continuously with “fresh” material. These features, together with an advance movement of the receiver substrate perpendicular to the laser scanning direction, allows the system to perform large area LIFT processes in a continuous way.

Multiple materials can be used with this system, being appropriated for different applications such as printed electronics, decorative or other functional printing features.

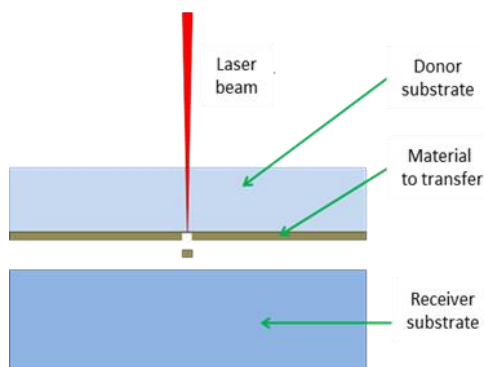


Fig. 1. Schematics of the LIFT process

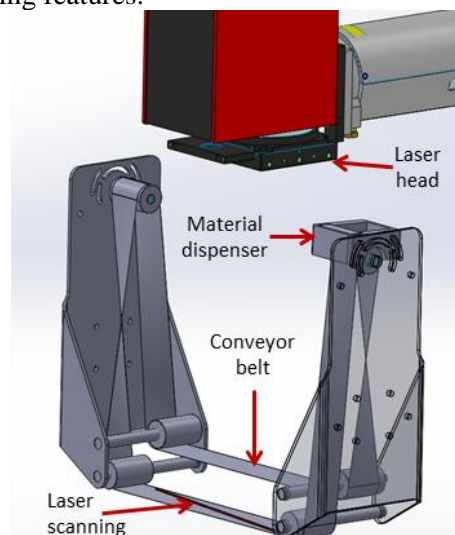


Fig. 2. 3D design of the system

[1] J. Bohandy, B.F. Kim and F. J. Adrian, Metal deposition from a supported metal film using an excimer laser, *Journal of Applied Physics*, 60, 1538, (1986).

[2] F. Varela, I. Cornago and J. Morentin, Continuous laser induced forward transfer of material system, EP18382193.3, April 2018.

## 2 W Cr: CdSe CW single mode laser

**M.K. Tarabrin<sup>1,2</sup>, D.V. Ustinov<sup>1</sup>, S.M. Tomilov<sup>1,2</sup>, V.A. Lazarev<sup>1</sup>,  
Yu.V. Korostelin<sup>2</sup>, M. P. Frolov<sup>2</sup>, Ya.K. Skasyrsky<sup>2</sup>, V.I. Kozlovsky<sup>2,3</sup>**

1 – Bauman Moscow State Technical University, Moscow 105005, Russia;

2 – P.N. Lebedev Physical Institute of RAS, Moscow 119991, Russia;

3 – National Research Nuclear University MEPhI, Moscow 115409, Russia;

[tarabrinmike@gmail.com](mailto:tarabrinmike@gmail.com)

Mid-infrared (mid-IR) solid-state lasers have drawn great scientific and technological interest [1]. Mid-IR lasers have been employed for a wide range of purposes, among which are spectroscopic gas analysis of atmosphere [2], medicine [3], optical frequency metrology [4] etc. High-power solid-state mid-IR Cr: CdSe lasers [5-7] are of great interest since its radiation spectrum covers a region near 3  $\mu\text{m}$ , which is important for medical applications [8-9], but power scalability for Cr: CdSe laser is still an urgent task.

We report on new experimental results for mid-IR Cr: CdSe single crystal laser. The Cr: CdSe crystal was grown by physical vapor transport [10]. Tm-doped fiber laser with an emission wavelength of about 1908 nm was used as the pump source.

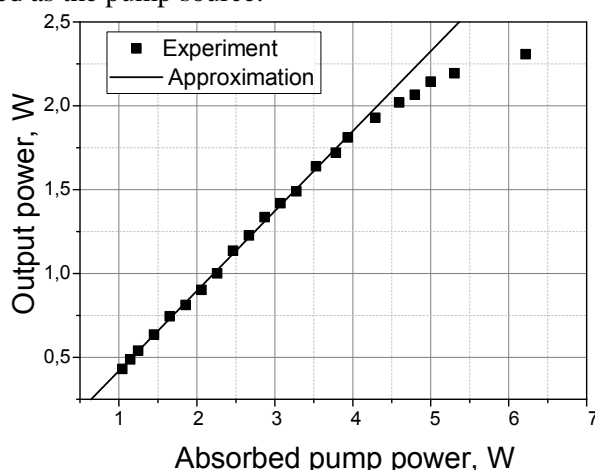


Fig. 1. Output power of the cw Cr: CdSe laser.

The almost concentric cavity of the Cr: CdSe laser consisted of a spherical dichroic input mirror ( $R_{in}=100$  mm) and a output coupler ( $R_{OC} = 50$  mm). A lens with a focal length of 75 mm focused the beam of the pump Tm fiber laser. The Cr: CdSe crystal laser CW output power as a function of absorbed pump power is shown in figure 1. The maximum output power was 2.3 W at 2650 nm, corresponding to an absorbed pump power of 6.2 W, and the absorbed power slope efficiency was 47.6 %. The threshold absorbed pump power was 0.12 W.

The authors acknowledge the Russian Science Foundation support, project No. 17-79-20431.

- [1] S. Mirov et al., *IEEE J. Sel. Top. Quantum Electron.* in press (2018).
- [2] F. Tittel et al., *Top. Appl. Phys.* **89**, 445-458 (2003).
- [3] V. Serebryakov et al., *J. of Opt. Tech.* **77**(1), 6-17 (2010).
- [4] M. Tarabrin et al. *J. Quant. Spectrosc. Radiat. Transfer* **177**, 241-247 (2016).
- [5] T. Fernandez et al., *Opt. Mater. Express* **7**, 3815-3825 (2017).
- [6] V. Lazarev et al., *Las. Phys. Lett.* **12**(12), 125003 (2015).
- [7] V. Lazarev et al., *J. Phys.: Conf. Ser.* **673**(1), 012015 (2016).
- [8] T. Lin et al. *Lasers in Surgery and Medicine* **48**(10), 965-977 (2016).
- [9] M. Tarabrin et al., *Proceedings SPIE Saratov Fall Meeting* **10717**, 1071707 (2017).
- [10] V. Akimov et al., *Phys. Status Solidi C* **3**(4), 1213-1216 (2006).

# Nanocrystals of CsYb(WO<sub>4</sub>)<sub>2</sub>: polymorphism with temperature and temperature dependence of its photoluminescence

**J. M. Gómez-Fernández, M. C. Pujol, J. J. Carvajal, F. Díaz and M. Aguiló,**

*Universitat Rovira i Virgili, Departament Química Física i Inorgànica, Física i Cristal·lografia de Materials i Nanomaterials (FiCMA-FiCNA) – EMaS, Campus Sescelades, E-43007, Tarragona, Spain*

*josemaria.gomez@estudiants.urv.cat*

The research on high temperature sensor and chromatic based thermometry is a focus of interest in the last years for their possible application in fields like industrial engineering. On the contrary to the nano-thermometers for biological applications, in which the temperature range of interest is below the 373K [1]; for this field higher temperatures <1073 K are being used [2, 3]. A common strategy for the phosphors applied in this field, it is to use the transition metals emission and to take profit of their high interaction with the crystal field, and to use a temperature phase transition, irreversible or reversible to modify the luminescence. In this work, despite of the low influence of the crystal field in the lanthanide emissions, the effect of a crystalline phase transition in the lanthanide based thermometry is explored.

It is reported in the literature that CsYb(WO<sub>4</sub>)<sub>2</sub> (hereafter CYbW) has polymorphism with the temperature. At 298 K CYbW is monoclinic, at 753 K has its first phase transition becoming an unknown monoclinic crystalline phase and at 1183 K, has a second transition phase to a trigonal phase [4]. Besides, the constituent ytterbium allows to study its luminescence dependence with temperature, and its known role of sensitizer facilitates the doping with other lanthanides to be used as activators for obtaining upconversion under infrared excitation.

The aims of the present work are to prepare CYbW nanocrystals of this material by Pechini's method, (this method has been broadly studied in FiCMA-FiCNA in the recent years [5]); the study of its first crystalline phase transition by high temperature X-ray diffraction and finally to study the temperature dependence of the luminescence to evaluate its potential as luminescent based thermometer.

The synthesized product crystallizes in the monoclinic low temperature phase  $\gamma$ -CsYb(WO<sub>4</sub>)<sub>2</sub>, confirmed with Pawley refinement in the space group *P2/c* with  $a = 9.3443(1)\text{\AA}$ ,  $b = 5.1574(1)\text{\AA}$ ,  $c = 7.3095(2)\text{\AA}$  and  $\beta = 95.670(1)^\circ$ . Differential thermal analysis of the obtained microcrystals shows two reversible phase transitions at 757 and 1172 K in agreement with Trunov *et al.*[6] High temperature X-ray diffraction confirmed this first crystalline phase transition. The effect of temperature in the photoluminescence was studied in the Yb<sup>3+</sup> active host and in an Er<sup>3+</sup> doped sample in the temperature range RT till 773 K. The Yb<sup>3+</sup> Stokes emission shows a decrease of the intensity during the heating due to nonradioactive effects. The anti-Stokes Er<sup>3+</sup> visible upconversion emission shows an intensity increase during heating, being the maximum at 623K. The Er<sup>3+</sup> visible upconversion emission has been also largely studied as base for a luminescent thermometer; by calibrating the intensity ratio of the emissions from the <sup>2</sup>H<sub>1/2</sub> and <sup>4</sup>S<sub>3/2</sub> thermally coupled levels [7]. Applying this conventional treatment, preliminary values of relative thermal sensitivity around 2.2 % K<sup>-1</sup> at 298 K and 0.7% K<sup>-1</sup> at 523 K were obtained, showing promising results for the use of these crystals as luminescent temperature sensors.

[1] Quintanilla M., Liz-Marzán L.M. Guiding rules for selecting a nanothermometer, *Nanotoday*, vol. 19, pp.126-145, (2018).

[2] G. Salek, A.Devoti, E.Lataste, A.Demourgues, A.Garcia, V. Jubera, M.Gaudon, Optical properties versus temperature of Cr-doped  $\gamma$ - and  $\alpha$ -Al<sub>2</sub>O<sub>3</sub>: Irreversible thermal sensors application, *Journal of Luminescence*, vol 179, pp. 89–196, (2016).

[3] M. L. Chepyga, A. Osveta, C. J. Brabeb, M. Batentschuk, High-temperature thermographic phosphor mixture YAP/YAG:Dy<sup>3+</sup> and its photoluminescence properties, *Journal of Luminescence*, vol. 188, pp. 582–588, (2017).

[4] V. A. Isupov, Binary Molybdates and Tungstates of Monoand Trivalent Elements as Possible Ferroelastics and Ferroelectrics. *Ferroelectrics*, vol. 321, pp. 63–90, (2005).

[5] M. Galceran, M. C. Pujol, M. Aguiló, F. Díaz, Sol-gel modified Pechini method for obtaining nanocrystalline KRE(WO<sub>4</sub>)<sub>2</sub> (RE = Gd and Yb), *Journal of Sol-Gel Science Technology*, vol. 42, pp. 79–88, (2007).

[6] V. K. Trunov, V. K. Rybakov, Double tungstates of Caesium and the rare earth elements, *Russian Journal of Inorganic Chemistry*, Vol. 19, pp. 347-352 (1974).

[7] S.A. Wade, S.F. Collins, G.W. Baxter, Fluorescence intensity ratio technique for optical fiber point temperature sensing, *Journal of applied Physics*, vol. 94, pp. 4743-4756, (2003).



# Single crystal growth and spectroscopic characterization of cerium and praseodymium single doped type III KGd(PO<sub>3</sub>)<sub>4</sub>

**I. Adell, R. Solé, M. C. Pujol, M. Aguiló, F. Díaz**

*Universitat Rovira i Virgili, Departament de Química Física i Inorgànica, Física i Cristal·lografia de Materials i Nanomaterials (FiCMA-FiCNA), Campus Sescelades, c/ Marcel·lí Domingo, 1, E-43007 Tarragona, Spain.*

*Email address: irina.adell@urv.cat*

Scintillators are materials which convert the high energy of an UV, X-ray or  $\gamma$ -ray photon into several visible or near visible photons, which can be easily detected with conventional detectors. These materials can also be used to detect accelerated particles, as neutrons, protons or electrons, with the emission of a flash of light as a result of the interaction of these particles with the scintillator [1-3]. They are used in a variety of applications as medical imaging (positron emission tomography, computed tomography, etc.), high energy physics, astrophysics and dosimetry [4].

Type III KGd(PO<sub>3</sub>)<sub>4</sub> (hereafter KGdP) is a deep-ultraviolet nonlinear optical material that allows to incorporate different lanthanide ions to its structure, among them Ce<sup>3+</sup> and Pr<sup>3+</sup>, with fast radiative emissions with decay times of the order of ns based on  $5d \rightarrow 4f$  electronic transitions.

In this work, Ce:KGdP and Pr:KGdP single crystals have been grown from high temperature solutions using the Top Seeded Solution Growth - Slow Cooling technique. The crystal growth was carried out from self-flux solutions to avoid the incorporation of foreign ions into the crystalline structure. The single crystals obtained were transparent and free from inclusions.

The optical characterization of these crystals show that the absorption bands of Ce<sup>3+</sup> and Pr<sup>3+</sup> ions from its ground state to the  $5d$  levels, are located in the UV region in this host. The luminescence of Ce:KGdP and Pr:KGdP exciting in the VUV-UV region shows down-shifting properties with decay times of the order of 16 ns in the case of Ce<sup>3+</sup> and 6 ns for Pr<sup>3+</sup>, of high interest for scintillation applications. Radiative emissions based on down-conversion processes are also observed when these crystals are excited under X-ray radiation.

[1] M. Nikl and A. Yoshikawa, Recent R&D Trends in Inorganic Single-Crystal Scintillator Materials for Radiation Detection, *Advanced Optical Materials*, 3, pp. 463-481 (2015).

[2] G. Blasse, *Scintillator Materials. Chemistry of Materials*, 6, pp. 1465-1475 (1994).

[3] P. Lecoq, A. Annenkov, A. Gektin, M. I. Korzhik, C. Pedrini, *Inorganic Scintillators for Detector Systems: Physical Principles and Crystal Engineering* (Springer), Scintillation and inorganic scintillators, (2006).

[4] P. A. Rodnyi, *Physical Processes in Inorganic Scintillators* (CRC Press), Scintillators requirements in various applications, (1997).

# Epitaxial porous GaN layer grown by CVD characterized by optical means

**J. Mena<sup>1</sup>, J. J. Carvajal<sup>1</sup>, F. Díaz<sup>1</sup>, M. Aguiló<sup>1</sup>, O. Martínez<sup>2</sup>, J. Jiménez<sup>2</sup>, V. Z. Zubialevich<sup>3</sup>, P. J. Parbrook<sup>3,4</sup>**

1- Física I Cristal·lografia de Materials I Nanomaterials (FiCMA-FiCNA) and EMaS, Universitat Rovira I Virgili (URV), Tarragona, Spain

2- GdS-Optronlab group, Dpto. Física de la Materia Condensada, Univ. de Valladolid, Valladolid, Spain

3- Tyndall National Institute, Lee Maltings, Dyke Parade, Cork, Ireland

4- University College Cork, Cork, Ireland

Main author email address: josue.mena@urv.cat

Porous GaN has attracted attention in recent years for the development of light emitting diodes (LEDs) with enhanced light extraction efficiency due to multiple reflections on the pores and an effective reduced refractive index alleviating the high refraction index contrast between GaN and air [1]. It has also been attractive to develop sensors and biosensors with improved sensitivity induced by the larger surface area of the porous structures [2]. Another attractive application of porous GaN is its use as a buffer layer to reduce the structural defects in non-porous GaN grown on foreign substrates, by alleviating the strain due to the lattice mismatch [3].

However, the residual structural strain existing on epitaxial porous layers has not been analyzed up to now. Taking into account the effects that this residual strain might induce in the potential applications of this porous semiconductor (LEDs, sensors and buffer layers), it is important to characterize

Here we analyze the optical and structural properties of homoepitaxial *n*-type porous GaN layers grown in a single step by CVD in non-porous GaN deposited on sapphire substrates under different deposition times [4], paying special attention to the role played by the layer porosity on the residual strain. Experimental results obtained by photoluminescence (PL) and resonant Raman scattering, as well as by cathodoluminescence (CL), show the existence of tensile strain for low deposition times (resulting in layer thickness below  $\sim 1 \mu\text{m}$ ). This residual tensile strain is reduced for increasing deposition time, as the porous layer becomes thicker, becoming nearly strain free for a thickness of  $1.7 \mu\text{m}$ . The analysis of the experimental data point to the existence of vacancy complexes as the main source of the tensile strain, which are formed in higher concentration at the interface between the substrate and the epitaxial porous layer.

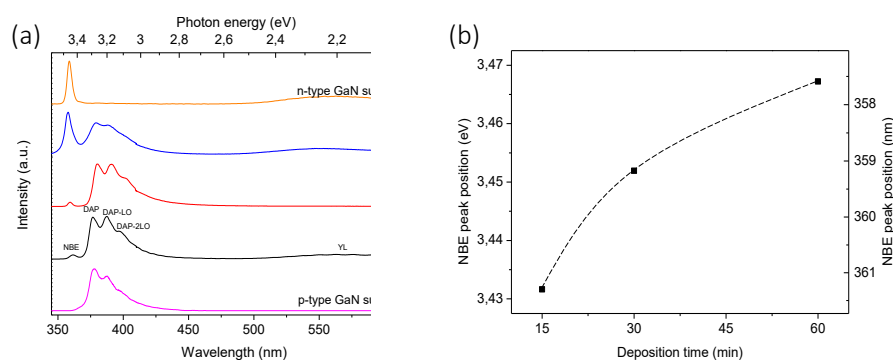


Figure 1. (a) PL spectra recorded at 80 K for porous GaN samples, the spectrum of the non-porous *p*-type substrate on which the porous layers are grown and a non-porous *n*-type GaN are also included. (b) Evolution of the position of the NBE band against the deposition time.

[1] C.F. Lin, K.T. Chen, C.M. Lin and C.C. Yang, InGaN-Based Light-Emitting Diodes With Nanoporous Microhole Structures, IEEE Electron Device Lett., 30, 1057-1059, (2009)

[2] A. Ramizy, Z. Hassan, and K. Omar, Sens. Actuators B, 155, 699-708, (2011)

[3] B.K. Ghosh, T. Tanikawa, A. Hashimoto, A. Yamamoto and Y. Ito, Reduced-stress GaN epitaxial layers grown on Si (1 1 1) by using a porous GaN interlayer converted from GaAs, J. Cryst. Growth, 249, 422-428, (2003)

[4] O.V. Bilousov, J.J. Carvajal, J. Mena, O. Martínez, J. Jiménez, H. Geaney, F. Díaz, M. Aguiló, C. O'Dwyer, Epitaxial growth of (0001) oriented porous GaN layers by chemical vapour deposition, CrystEngComm, 16, 10255-10261, (2014)

# High-Concentration Er<sup>3+</sup> Composite Fiber for Compact All-Fiber Devices

**B.I.Denker<sup>1</sup>, O.N.Egorova<sup>2</sup>, B.I.Galagan<sup>1</sup>, V.A.Kamynin<sup>1</sup>, A.A.Ponosova<sup>1,3</sup>, S.E.Sverchkov<sup>1</sup>, S.L.Semjonov<sup>2</sup>, V.B.Tsvetkov<sup>1,4</sup>, I.V.Zhluktova<sup>1</sup>**

*1- General Physics Institute, Russian Academy of Sciences, GPI RAS, Moscow, Russia*

*2- Fiber Optics Research Center, Russian Academy of Sciences, FORC RAS, Moscow, Russia*

*3- Perm Scientific Industrial Instrument-Making Company, Perm, Russia*

*4- National Research Nuclear University MEPhI, Moscow, Russia*

*E-mail: [nastya-aleksi@mail.ru](mailto:nastya-aleksi@mail.ru)*

Active fiber media with high optical gain over a short length are in the focus of the investigations. Phosphate glasses are able to accommodate an order of magnitude higher rare-earth dopant's concentration compared to the most common silica-based fibers [1, 2] without clustering. A substantial drawback of phosphate fibers is their degradation under exposure to air moisture. We report experimental results on high-concentration Er-doped fibers with phosphate core and silica cladding, which takes advantages of both silica and phosphate glasses.

The initial laser phosphate glasses for the fiber core were doped with about 1 wt.% and 3 wt.% of Er<sup>3+</sup> ions. The fiber blanks were fabricated by "rod-in-tube" technique. The drawn fibers were single mode at 1.5  $\mu$ m. The glass component distribution across the fiber core-sections was studied using SEM. The small-signal absorption at pump wavelength near 980 nm was about 0.46 dB/cm in 1 wt.% Er-doped fiber and it was 1.25 dB/cm in 3 wt.% Er-doped fiber.

The fibers were used in several schemes of all-fiber devices. The slope efficiency of 1.536  $\mu$ m continuous-wave fiber laser about 38.8 % was achieved while using extremely short (about 15 cm) 3wt.% Er-doped fiber.

Erbium-doped fiber amplifier with co-propagating pumping at 980 nm was used for gain characterization of investigated composite fibers. The achieved small-signal gain per unit-length of CW signal at 1536 nm was about 1.8 dB/cm for 3wt.% Er-doped fiber. Ultrashort pulses amplification was measured in EDFA based on 20-cm of 1wt.% Er-doped fiber. Pulse duration before amplification was about 486 fs with repetition rate being about 83 MHz. After amplification (fig.1,c), a change in the spectral characteristics of the pulsed radiation was observed, while the duration of the pulses remains unchanged within the error of the measuring equipment. The gain coefficient was about 10 dB.

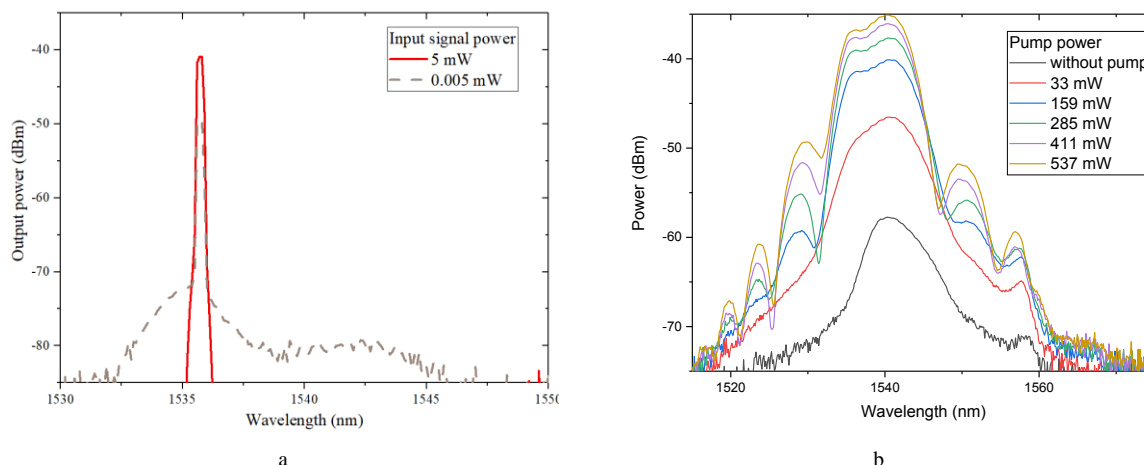


Fig.1. Spectral characteristics of the amplified CW(a) and pulsed (b) signal

The investigation demonstrate that high-concentration Er-doped phosphate core silica cladding fiber allows to significantly shortening of active fiber length. Russian Foundation for Basic Research RFBR (18-32-01010) funded the reported study of fiber properties. The reported study of fiber amplifying performances was funded by Russian Science Foundation (RSF) (17-12-01564).

# Temperature Effect on the Performance of Diode Pumped Nd- Yag Solid State Laser System

**M. Atta Khedr, E.Salam, G. E. Khalil, A. M. Abou-Elmagd**

*National Institute of Laser Enhanced Science (NILES) Cairo University Giza, Egypt.*

[makdr@yahoo.com](mailto:makdr@yahoo.com)/ [matta@niles.edu.eg](mailto:matta@niles.edu.eg)

We had used a compact Nd:YAG solid state laser in our laser system which consists of: pumping diode laser, collimating lens, dichroic mirror, Nd:YAG crystal, saturable absorber, Q-switching, KTP crystal, infrared filter , output coupler mirror, heater, power meter and spectrometer.

Measurements were carried out for power and intensity of the emitted laser beam together with the input power. The spectrum and the power of the diode excitation source has been examined before carrying out the experiment. Temperature effect was examined using a small oven for heating the laser Nd: YAG laser compact system using high accuracy temperature controller. We measured the output laser power and spectrum profile of laser wavelength at 532 nm and 536.1 nm the second harmonic of 1064nm of Nd :YAG laser crystal at different temperatures 30-65cenegrate. We obtained relation between temperature and laser power which reveals that we had an optimum output laser power at 35and 40 degree centigrade .The optimum spectrum was found at the same pervious degrees. We obtained the laser efficiency at different temperatures.

# Photoluminescence study on the effect of Ga<sup>3+</sup> in Yb:YAG at cryogenic temperatures

S.P. David<sup>1</sup>, F. Yue<sup>1</sup>, V. Jambunathan<sup>1</sup>, M. Mika<sup>2</sup>, A. Lucianetti<sup>1</sup>, T. Mocek<sup>1</sup>

1- HiLASE Centre, Institute of Physics CAS, Za Radnici 828, 25241 Dolní Brežany, Czech Republic  
2- Department of Glass and Ceramics, University of Chemistry and Technology, Prague, Technická 5, 16628 Prague, Czech Republic

Main author email address: Samuel-Paul.David@hilase.cz

At cryogenic temperature, Yb: Y<sub>3</sub>Al<sub>5</sub>O<sub>12</sub> (YAG) shows narrow emission spectrum at laser wavelength which limits the generation of ultrashort pulses to few picosecond pulse durations. To overcome this issue, we propose to modify the nature of the gain media by introducing extra cations such as Ga<sup>3+</sup> into the regular lattice and make a disordered structure. In this way, one can achieve inhomogeneous spectrum broadening at cryogenic temperature [1]. In order to study the effect of Ga<sup>3+</sup> in Yb:YAG at cryogenic temperatures, we prepared mixed garnets by solid state reaction method with different Ga<sup>3+</sup> concentration in YAG and maintaining a fixed Yb<sup>3+</sup> concentration. We measured the photoluminescence of all the samples by pumping at 940 nm and emission was collected from 950 – 1100 nm from room temperature down to 20K in step size of 40K.

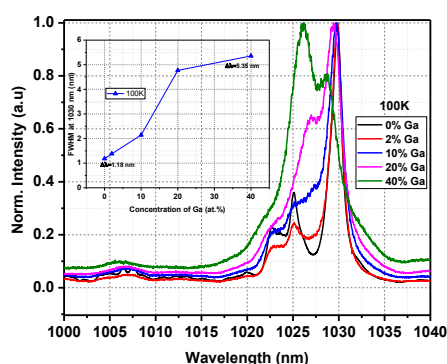


Fig. 1. Emission width at 1030 nm for different Ga<sup>3+</sup> concentration

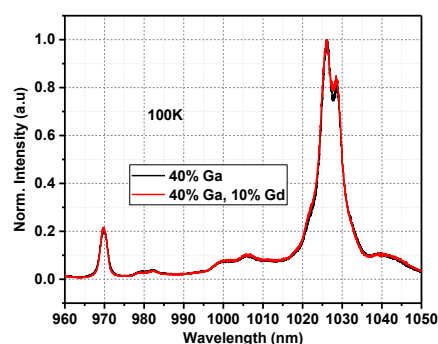


Fig. 2. Emission spectra of Ga and Gd admixed garnet

Compared to Yb:YAG, Yb:Y<sub>3</sub>Ga<sub>2</sub>Al<sub>3</sub>O<sub>12</sub> shows five times broadening for the emission peak centered at ~1030 nm at 100K as shown in Fig. 1. We also prepared a couple of samples incorporating Gd<sup>3+</sup> resulting in a multicomponent garnet. Addition of Gd<sup>3+</sup> does not show a significant effect on the broadening at 1030 nm as can be seen in Fig. 2.

Gd<sup>3+</sup> and Yb<sup>3+</sup> ions occupy dodecahedron site whereas Al<sup>3+</sup> ions can occupy two different sites: octahedral and tetrahedral. Replacing Al<sup>3+</sup> by Ga<sup>3+</sup> in one of the sites results in different crystal field strength on Yb<sup>3+</sup> ion [2]. Such varied field leads to inhomogeneous broadening of the spectrum in Ga admixed samples. The role of site symmetry and occupancy results in broadening mechanism whereas difference in ionic radius between Al<sup>3+</sup> and Ga<sup>3+</sup> results in wavelength shifts. The resulting change in energy level diagrams with corresponding shifts at different Ga/Gd concentration will be discussed in detail based on the emission analysis.

- [1] V. Jambunathan, L. Horackova, T. Miura, J. Sulc, H. Jelinkova, A. Endo, A. Lucianetti and T. Mocek, Spectroscopic and lasing characteristics of Yb:YAG ceramic at cryogenic temperatures, *Opt. Mater. Exp.*, vol. 5, pp. 1289 – 1295 (2015)  
[2] B. M. Walsh, N. P. Barnes, R. L. Hutcheson, R. W. Equall, and B. Di Bartolo, Spectroscopy and lasing characteristics of Nd-doped Y<sub>3</sub>Ga<sub>x</sub>Al<sub>(5-x)</sub>O<sub>12</sub> materials: application toward a compositionally tuned 0.94- $\mu$ m laser, *J. Opt. Soc. Am. B*, vol. 15, pp. 2794–2801 (1998).

# Exploration of Langasite family in Mid-infrared Applications

**Haichao Lan<sup>1</sup>, Haohai Yu<sup>2</sup>, Huaijin Zhang<sup>3</sup>, Jiyang Wang<sup>4</sup>**

*State Key Laboratory of Crystal Materials and Institute of crystal Materials, Shandong University, 27 Shanda Nanlu, Jinan 250100, China*

*lanhaichao999@163.com*

With the rapid development of laser diode-pumped solid-state laser technology, the coherent light produced by this technology has been widely used in the fields of medicine, materials processing and information communication such as photo-lithography. The strong interests of intense mid-infrared (mid-IR) lasers has forced considerable efforts to develop the light source. Unfortunately, due to the lack of gain media and limited power scaling, the wavelengths required for these applications are not always directly generated from convenient laser sources, but the important method is to use nonlinear optical (NLO) materials through frequency conversion (eg, second harmonic generation (SHG)). NLO materials extend the available electromagnetic spectrum of solid-state lasers from ultraviolet (UV) to infrared (IR). In 1982, Kaminsky and Sarkisov first reported langasite  $\text{La}_3\text{Ga}_5\text{SiO}_{14}$  (LGS) and its laser properties [1]. After this, the important langsite family has been found, which contains different element compositions, including  $\text{Ba}_3\text{Ga}_4\text{Ge}_2\text{O}_{14}$  (BGG),  $\text{Ca}_3\text{TaGa}_3\text{Si}_2\text{O}_{14}$  (CTGS),  $\text{La}_3\text{Ga}_{5.5}\text{Ta}_{0.5}\text{O}_{14}$  (LGT),  $\text{La}_3\text{Ga}_{5.5}\text{Nb}_{0.5}\text{O}_{14}$  (LGN), and so on. These crystals are characterized by a combination of piezoelectric, laser and acoustic abilities at first [2]. The langasite family belongs to the trigonal 32 point group, space group P321, which is the same as quartz. There are four cationic sites in this structure that can be represented by the chemical formula  $\text{A}_3\text{BC}_3\text{D}_2\text{O}_{14}$  [3]. The above analysis demonstrates that the A and B sites have the greatest effect on SHG, while the B and D sites determine the IR absorption edge in langasite materials.

In this paper, based on theoretical understanding and rational molecular design, combined with experimental synthesis and photoelectronic property characterization, the new compound  $\text{La}_3\text{SnGa}_5\text{O}_{14}$  (LGSn), one member of langsite family, was investigated. Centimeter-sized LGSn crystals possess the widest transparent region (0.27-11.0  $\mu\text{m}$ ) among known oxides, highest laser damage threshold (LDT) (846  $\text{MW}/\text{cm}^2$ ) in the known NLO material, and strongest SHG effect among langasites. The discovery of LGSn actually triggers the new application of oxides as good NLO crystal, into the mid-IR spectral region beyond 10  $\mu\text{m}$ .

[1] Kaminsky AA, Sarkisov S E. [J]. Reports of the USSR Academy of Science, 1982, 264(1):93.

[2] A. A. Kaminskii, E. L. Belokoneva, B. V. Mill et al., "Pure and  $\text{Nd}^{3+}$ -doped  $\text{Ca}_3\text{Ga}_2\text{Ge}_4\text{O}_{14}$  and  $\text{Sr}_3\text{Ga}_2\text{Ge}_4\text{O}_{14}$  single crystals, their structure, optical, spectral luminescence, electromechanical properties, and stimulated emission," *Physica Status Solidi (A)—Applications and Materials Science*, vol.86, no.1, pp.345–362, 1984.

[3] H. Takeda, R. Aoyagi, S. Okamura, and T. Shiosaki, "Cation distribution and melting behavior of  $\text{La}_3\text{Ga}_5\text{M}_4\text{O}_{14}$  (M = Si, Ti, Ge, Zr, Sn, and Hf) crystals," *Ferroelectrics*, vol. 295, no. 1, pp.67–76, 2003.

## Ca<sub>3</sub>TaGa<sub>3</sub>Si<sub>2</sub>O<sub>14</sub> single crystals and their optical characterization

O. Buzanov,<sup>1</sup> A. Kozlova,<sup>2</sup> N. Kozlova,<sup>2</sup> D. Spassky,<sup>3</sup> E. Zabelina<sup>2</sup>

1- JSC Fomos-Materials, Buzheninova 16, Moscow 107023, Russia

2- National University of Science and Technology "MISIS", 4, Leninskiy pr. 119049, Moscow, Russia

3- Skobeltsyn Institute of Nuclear Physics, M.V. Lomonosov Moscow State University, 1(2), Leninskie gory, GSP-1, 119991, Moscow, Russia

Kozlova\_nina@mail.ru

Catungasite Ca<sub>3</sub>TaGa<sub>3</sub>Si<sub>2</sub>O<sub>14</sub> (CTGS) are crystals with calcium-gallogermanate structure. CTGS crystallize in the P321 space group with formulae A<sub>3</sub>BC<sub>3</sub>D<sub>2</sub>O<sub>14</sub>, where A is decahedron position, B – octahedral position, C and D – large and small tetrahedral positions [1]. In contrast to the isostructural to CTGS langasite and langatate, which are of disordered type, the structure of catungasite is ordered (Table 1) [2].

Table 1

Crystal	Type	Elements' Positions			
		A	B	C	D
La <sub>3</sub> Ga <sub>5.5</sub> Ta <sub>0.5</sub> O <sub>14</sub>	disordered	La <sup>3+</sup>	½ Ga <sup>3+</sup> (½ Ta <sup>5+</sup> )	Ga <sup>3+</sup>	Ga <sup>3+</sup>
La <sub>3</sub> Ga <sub>3</sub> SiO <sub>14</sub>	disordered	La <sup>3+</sup>	Ga <sup>3+</sup>	Ga <sup>3+</sup>	½ Ga <sup>3+</sup> (½ Si <sup>4+</sup> )
Ca <sub>3</sub> TaGa <sub>3</sub> Si <sub>2</sub> O <sub>14</sub>	ordered	Ca <sup>2+</sup>	Ta <sup>5+</sup>	Ga <sup>3+</sup>	Si <sup>4+</sup>

CTGS is a new laser frequency-doubling crystal [2-4] that may enrich very limited number of multi-functional self-frequency doubling nonlinear laser crystals and expand areas of their applications.

CTGS single crystals were grown at JSC "Fomos-Materials" by Czochralski method with RH heating using iridium crucible in argon atmosphere with admixture of 0.5-1% of pure O<sub>2</sub>.

We have investigated the optical activity, refractive index dispersion, transmittance and reflectance spectra of CTGS crystals. We observed transmittance spectra anisotropy and dichroism phenomenon for the samples, which were cut in the direction parallel to axis Z. These phenomena may be caused by the symmetry of the crystals' structure or by the anisotropy of defects such as color centers. Dichroism takes place in some crystals with specific structure and is most pronounced when p- or s-polarized light passes along directions perpendicular to the optical axis. Table 2 presents the obtained values of refractive indices and specific rotation in CTGS.

Table 2

λ, nm	260	300	350	400	450	500	550	600	650	700	750	800	850	900	940
n <sub>o</sub>	2,495	2,201	1,956	1,847	1,824	1,800	1,783	1,775	1,767	1,759	1,751	1,750	1,750	1,724	1,720
ρ <sub>s</sub> , deg/mm	245	168	114	83	60	49	38	33	27	24	20	18	15	14	13

Optical properties of catungasite were measured in the Accredited testing laboratory "Single Crystals and Stock on their Base" of the NUST "MISIS" by spectrophotometric methods using the spectrophotometer "Cary 5000" ("Agilent Technologies" company) with the automatic universal measurement accessory (UMA).

Luminescence properties of catungasite single crystals were studied as well and the results will be discussed in the presentation. The studies were performed in the temperature range 80-300 K under UV excitation.

[1] A. A. Kaminskii, Physics and Spectroscopy of Laser Crystals (Moscow:Nauka) (1986).

[2] N.S. Kozlova, A.P. Kozlova, D.A. Spassky and E.V. Zabelina, Influence of growth atmosphere on Ca<sub>3</sub>TaGa<sub>3</sub>Si<sub>2</sub>O<sub>14</sub> single crystals optical properties, IOP Conf. Series: Materials Science and Engineering, vol. 169, pp. 1-6, (2017).

[3] F. Chen, F. Yu, Sh. Hou, Y. Liu, Y.Zhou, X. Shi, H. Wang, Z. Wang and X. Zhao, Crystal growth and characterization of CTGS and Nd:CTGS for self-frequency-doubling applications, CrystEngComm, vol 16, pp. 10286-10291, (2014).

[4] X. Fu, E. G. Villora, Y. Matsushita, Y. Kitanaka, Y. Noguchi, M. Miyayama, K. Shimamura, N. Ohashi, Influence of growth conditions on the optical, electrical resistivity and piezoelectric properties of Ca<sub>3</sub>TaGa<sub>3</sub>Si<sub>2</sub>O<sub>14</sub> single crystals, Ceramic Society Japan, vol. 124, № 5, pp. 523-527, (2016).

# $\text{Ca}_3(\text{VO}_4)_2:\text{Tm}^{3+}/\text{Ho}^{3+}$ , New Crystalline Medium for Lasers of 2 $\mu\text{m}$ Spectral Range

**Ivleva L.I., Doroshenko M.E., Voronina I.S., Dunaeva E.E., A.G.Papashvili**

*Prokhorov General Physics Institute of the Russian Academy of Sciences, 119991 Moscow, Vavilov str.38, ,  
[ivleva@lst.gpi.ru](mailto:ivleva@lst.gpi.ru)*

Nowadays, scientists are looking for the modern materials with multifunctional characteristics. From the other side, solid-state lasers of 2- $\mu\text{m}$  range is interesting due to their possibility of wide application in medicine, biology, environment monitoring. Rare-earth-doped vanadates with the general formula  $\text{Ca}_{3-x}\text{M}_{2x}(\text{VO}_4)_2$ , where M is rare earth element, can be used as laser active media. At the same time,  $\text{Ca}_3(\text{VO}_4)_2$  is a potentially useful nonlinear material for the frequency conversion of broadband or tunable laser sources:  $\text{Ca}_3(\text{VO}_4)_2$  has nonlinear optical coefficients comparable to those of  $\text{KH}_2\text{PO}_4$  ( $d_{ij}/d_{36}(\text{KH}_2\text{PO}_4)$ :  $d_{31}=1.51 \pm 10\%$ ;  $d_{15}=1.29 \pm 10\%$ ); The crystals exhibit favourable phase matching conditions with respect to angular and spectral spread of the incident beam in the range between 2  $\mu\text{m}$  and 3  $\mu\text{m}$ . This crystal possesses high nonlinear-optical properties and can be used as for second harmonic generation as for Raman shifting of laser radiation. Also, the crystals are characterized by the high damage threshold. In our work we consider the possibilities of creation of effective laser-nonlinear media based on  $\text{Ca}_3(\text{VO}_4)_2$  doped with  $\text{Tm}^{3+}$  and  $\text{Ho}^{3+}$  ions.

The crystals were grown from the melt by Czochralski method using the Pt crucible in the air atmosphere. Melting point of  $\text{Ca}_3(\text{VO}_4)_2$  is 1430 $^\circ\text{C}$ . The RE dopants were added into the melt in the form of  $\text{Tm}_2\text{O}_3$  (up to 2 wt.%) and  $\text{Ho}_2\text{O}_3$  (0.7wt.%). Growth direction was 90 $^\circ$  to optical axis. Pulling rate was varied from 1.5 to 8 mm/h. Rotation rate: 30 rpm. Bulk crystallisation rate was decreased from 1.5  $\text{cm}^3/\text{h}$  for nominally pure material up to 0.24  $\text{cm}^3/\text{h}$  for heavy-doped crystals. Vertical thermal gradients was 60-90 $^\circ\text{C}/\text{cm}$  in the growth zone and 5-10 $^\circ\text{C}/\text{cm}$  in the annealing region. The values of anomalous birefringence in as-grown crystals were calculated based on the data of induced biaxiality, which can be registered by observation of conoscopic pictures along crystal length and cross-section. It was shown that the anomalous birefringence for as-grown crystal was not exceeded  $1.3 \times 10^{-5} \text{ cm}^{-1}$ . The  $\text{Ca}_3(\text{VO}_4)_2$  crystals obtained ( $d=20\text{mm}$ ,  $L=50\text{mm}$ ) had a color from slightly lemon to bright yellow and were optically homogeneous. Color variations in the crystals are associated with the lack of oxygen and the presence of vanadium ions with lowered valence  $\text{V}^{4+}$ . It was estimated that V/Ca ratio in the samples corresponds to stoichiometric composition (within the measurement error) using X-ray microanalysis. According to energy dispersive microanalysis the effective segregation coefficient of  $\text{Tm}^{3+}$  in the matrix is 0.8. In the case of  $\text{Tm}^{3+}/\text{Ho}^{3+}$  co-doping effective segregation coefficient for  $\text{Tm}^{3+}$  is 0.7, for  $\text{Ho}^{3+}$  -0.9. Ferroelectric domain structure was investigated by chemical etching. It was shown that form and sizes of domain strongly depend on crystal composition.

Polarized absorption and fluorescence spectra of  $\text{Tm}^{3+}$  ions in  $\text{Ca}_3(\text{VO}_4)_2$  crystal were measured. Based on absorption spectra Judd-Ofelt analysis was performed and intensity parameters:  $\Omega_2=8.89 \times 10^{-20}$ ;  $\Omega_4=1.71 \times 10^{-20}$ ;  $\Omega_6=2.54 \times 10^{-20}$  were determined. Using these intensity parameters radiative lifetime of  $^3\text{F}_4$  upper laser level was calculated to be 1.26 ms which is in very good agreement with measured lifetime for  $^3\text{F}_4$   $\text{Tm}^{3+}$  level in  $\text{Ca}_3(\text{VO}_4)_2$  crystals with different  $\text{Tm}^{3+}$  concentration and temperatures (1.3 ms). Using absorption and fluorescence spectra corresponding absorption and emission cross-sections were calculated. Emission cross-section for  $^3\text{F}_4 \rightarrow ^3\text{H}_6$  laser transition was found to be about twice different for light polarized perpendicular and along optical c axis. For E $\perp$ c polarization maximum emission cross-section was determined to be about  $1.3 \times 10^{-20} \text{ cm}^2$ . Laser generation at wavelength of 1972 nm was observed for  $\text{Ca}_3(\text{VO}_4)_2:\text{Tm}^{3+}(2\%)$  under standard laser diode pumping at 795 nm. Slope efficiency was about 3% for the transmittance of the output mirror of 0.3%. The output light was found to be elliptically polarized with orthogonal polarizations intensities ratio close to that for corresponding emission cross-sections. For  $\text{Ca}_3(\text{VO}_4)_2:\text{Tm}^{3+}(2\%)/\text{Ho}^{3+}(0.7\%)$  crystal practically full quenching of  $\text{Tm}^{3+}$  ions 2 micron fluorescence was observed and lasing of  $\text{Ho}^{3+}$  ions was obtained at wavelength of 2070 nm under pumping by laser diode at 795 nm (absorption band of  $\text{Tm}^{3+}$  ions). Slope efficiency was also about 3% with the same output mirror. In this case laser generation of thulium ions wasn't observed.

## Radiation hardness of Yb:LaSc<sub>3</sub>(BO<sub>3</sub>)<sub>4</sub> and Yb:LuYSiO<sub>5</sub> laser crystals

S.A. Kutovoi<sup>1</sup>, Yu.D. Zavartsev<sup>1</sup>, A.I. Zagumennyi<sup>1</sup>, Yu. L. Kalachev<sup>1</sup>, V. A. Mikhailov<sup>1</sup>,  
V.A. Kozlov<sup>2</sup>, M.V. Zaverlyaev<sup>2</sup>, I. A. Shcherbakov<sup>1</sup>

1- Prokhorov General Physics Institute, Russian Academy of Sciences, 119991, 38 Vavilov Str., Moscow, RF.

2- Lebedev Physical Institute, Russian Academy of Sciences, 119991, 53 Leninskiy Prospekt, Moscow, RF.

kalachev@kapella.gpi.ru

As the laser communications can be used in free space near Earth and Deep space and some other environments with strong radiation, the irradiation damages of the laser gain media should be carefully considered. Unfortunately, many fluoride and oxide crystals have weak or no resistance to the radiation, so it is important and necessary to develop novel laser crystals, which possess good radiation-resistant ability and can be applied in the strong radiation environment.

Radiation induced absorption of oxide material is well known. This absorption was studied particularly in the case of Nd<sup>3+</sup> doped crystals, as it lowers energy output from laser rods exposed to Ultra Violet (UV) irradiation of flash lamp light. Yellow or brown color of oxide YAG, YSGG, GSGG GGG crystals is attributed to the oxygen O- centre formation, which causes an increasing of absorption near 300-500 nm of spectral range.

We studied radiation hardness of Yb:LSB and Yb:LYSO crystals by comparing transmission spectra of the samples before and after irradiation using <sup>60</sup>Co source.

The oxides La<sub>2</sub>O<sub>3</sub>, Sc<sub>2</sub>O<sub>3</sub>, Y<sub>2</sub>O<sub>3</sub>, Lu<sub>2</sub>O<sub>3</sub>, B<sub>2</sub>O<sub>3</sub>, SiO<sub>2</sub> with the purity 99.99% and Yb<sub>2</sub>O<sub>3</sub> (99,95%) are used as starting component. The 70 mm long 4at.%Yb:LuYSiO<sub>5</sub> (Yb:LYSO) and 50 mm long 10at.%Yb, 25at.%Yb:LaSc<sub>3</sub>(BO<sub>3</sub>)<sub>4</sub> (Yb:LSB) laser crystals was grown by the Czochralski technique in a radio-frequency-heated new 40 mm in diameter crucibles having the iridium purity of 99.989%. From this crystal boules was produced both the thin-disc laser elements and polished 20 mm long rods for investigation the radiation hardness. The 25at.%Yb:LSB laser material in thin-disk (300-μm thick) configuration demonstrates output power 40 W for 95W of pump power at 974 nm [1,2].

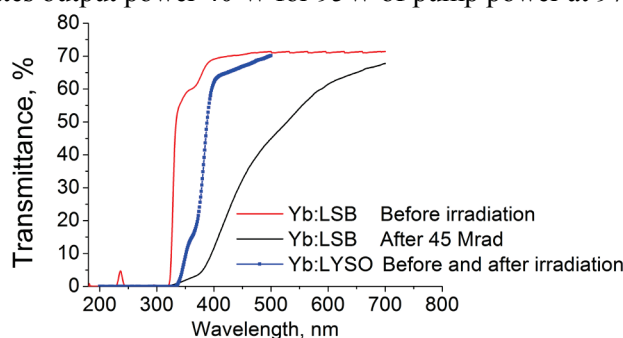


Fig.1. Transmittance of Yb:LSB and Yb:SSO crystals before and after 45 Mrad irradiation using <sup>60</sup>Co source

Measured radiation damage of Yb:LSB crystals and the degradation of optical transmission in the range 340-700 nm due to irradiation with the dose of 45 Mrad of <sup>60</sup>Co  $\gamma$ -rays was very significant (Fig.1). Yb:LSB crystals was colorless before irradiation, and the color was change to dark brown after irradiation. This radiation damage (dark brown color) of Yb:LSB crystal are stable in period up to 5 years. There is no observed a laser lasing of Yb:LSB crystal after radiation damage.

There was no reduction in transmission spectra for 4at.% Yb:LYSO after <sup>60</sup>Co  $\gamma$ -rays irradiation with the dose of 45 Mrad. Lasing property of this crystal remains rather good.

**Conclusion.** Our investigation shown that Yb:LSB crystal have problem with radiation hardness, in other hand the Yb:LYSO is radiation resistant crystal and capable of working under heavy radiation conditions during an extended period of time.

[1] K. Petermann, D. Fagundes-Peters, J. Johannsen, M. Mond, V. Peters, J.J. Romero, S. Kutovoi, J. Speiser, A. Giesen. Highly Yb-doped oxides for thin-disc lasers. *Journal of Crystal Growth* vol. 275, pp. 135–140, (2005)

[2] C. Krankel, J.Johannsen, R.Peters, K.Petermann, G. Huber. Continuous-wave high power laser operation and tunability of Yb:LaSc<sub>3</sub>(BO<sub>3</sub>)<sub>4</sub> in thin disk configuration. *Appl. Phys. B* vol. 87, pp. 217–220, (2007).

# Fabrication and characterization of $\text{KLu}(\text{WO}_4)_2/\text{SiO}_2$ taper waveguide platform for sensing applications

**Marc Medina<sup>1</sup>, Christian Haunhorst<sup>2</sup>, ....., Maria Cinta Pujol<sup>1,\*</sup>, Detlef Kip<sup>2</sup>, Jaume Masons<sup>1</sup>, Airán Rodenas<sup>3</sup>, Magdalena Aguiló<sup>1</sup>, Francisco Díaz<sup>1</sup>**

*1-Física i Cristal·lografia de Materials i Nanomaterials (FiCMA-FiCNA-EMaS), Departament de Química Física i Inorgànica (DQFI), Universitat Rovira i Virgili (URV), Campus Sescelades, C/Marcel·lí Domingo 1, E-43007, Tarragona, Spain*

*2-Faculty of Electrical Engineering, Helmut Schmidt University, D-22043 Hamburg, Germany*

*3-Istituto di Fotonica e Nanotecnologie - Consiglio Nazionale delle Ricerche, Piazza Leonardo da Vinci, 32, I-20133 Milano, Italy*

*marc.medina@urv.cat*

In the last decade scientific community has been doing a great effort to develop integrated photonic chips for different fields (purposes) like telecommunications, photonic computation or chemical and biochemical sensing. Optic sensors at chip scale have turned out as a promising solution for environmental monitoring and high throughput screening for biomedical discovery [1]. Most of those chips are silicon based, and fabrication approaches are mainly focused in bottom-up ideas. Nonetheless this research is aimed to move to non-Si based materials, e.g.  $\text{KLu}(\text{WO}_4)_2$ . Here a high throughput generic recipe for sensor chip fabrication based on a top-down approach is proposed. As a first study a high-index-contrast waveguides configuration is used with  $\text{KLu}(\text{WO}_4)_2$  as a core and  $\text{SiO}_2$  as a mechanical support and cladding compound.  $\text{KLuW}$  is chosen because of extensive experience with monoclinic double tungstates from our research groups in addition to its high absorption and emission cross-sections when doped with active lanthanide ions. It also provides a high refractive index contrast ( $\Delta n = 0.4$ ) with  $\text{SiO}_2$  and the possibility to operate at biological fingerprints due to its broad transmission window from visible up to  $5 \mu\text{m}$  [2]. Our generic recipe for chip fabrication is based on the combination of three techniques: chip bonding, taper cut with an ultra precise dicing saw machine [3] and Inductively Coupled Plasma Reactive Ion Etching (ICP-RIE) as a post processing step.

This work presents the first phase of the project consisting on design and fabrication of  $\text{KLuW}$  on silica taper waveguides for sensing applications together with first results in sensor proof of concept. Ultra precise dicing saw approach for the fabrication of taper waveguides has been shown as an optimal fabrication technique and around  $15 \mu\text{m} \times 15 \mu\text{m} \times 15 \text{mm}$  taper waveguides have been fabricated with high quality. The adhesive NOA81 has prove high quality bonding with  $\text{KLuW}$ . First optical characterization allows to obtain an estimation of propagation losses from taper waveguides at  $3.7 \mu\text{m}$  wavelength and they turn out to be around 3 dB/cm. Sensor proof of concept have been carried out successfully showing that our waveguides can detect the presence of ethanol.

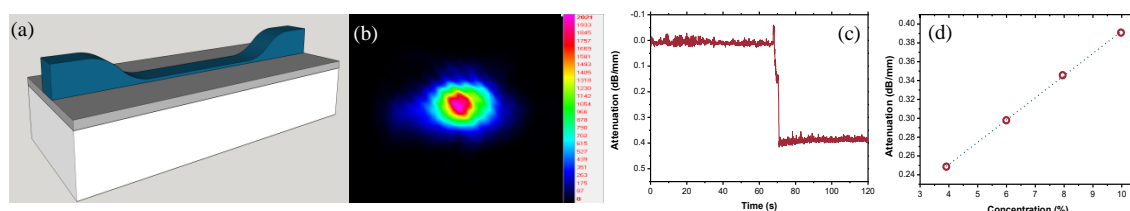


Fig.1. (a) shows a 3D design of taper waveguides concept, (b) is an output beam near field image from a taper waveguide, (c) sensor response to a 10% ethanol/water solution, (d) attenuation induced by different concentration of ethanol in water.

- [1] J. Tiening, *et al.*: *Real time and label free chemical sensor on a chip using monolithic Si-on-BaTiO<sub>3</sub> mid-infrared waveguides*, Sci.Rep., 7. 5836, 2017.
- [2] V. Petrov, M.C. Pujol, *et al.* *Growth and properties of  $\text{KLu}(\text{WO}_4)_2$ , and novel ytterbium and thulium laser based on this monoclinic crystalline host*, Laser and Photonics Rev., vol. 7. pp. 179-212, May 2007.
- [3] F. Martin, *et al.*: *Low loss ridge waveguides in lithium niobate thin film by optical grade diamond blade dicing*, Opt. Express, vol. 2. pp 1386-1391, 2016.

## Optical Cell Line Detection In Microfluidic Devices

**Eric Pedrol<sup>1</sup>, Javier Martínez<sup>1</sup>, Manuel Garcia-Algar<sup>2</sup>, Moritz Nazarenus<sup>2</sup>, Luca Guerrini<sup>2</sup>, Eduardo Garcia-Rico<sup>3</sup>, Ramón A. Álvarez-Puebla<sup>4,5,6</sup>, Magdalena Aguiló<sup>1</sup>, Francesc Díaz<sup>1</sup>, Jaume Massons<sup>1</sup>**

*1- Universitat Rovira i Virgili, Física i Cristal·lografia de Materials i Nanomaterials (FiCMA-FiCNA) and EMaS, Tarragona, Spain*

*2- Universitat Rovira i Virgili, Departament de Química Física i Inorgànica, Tarragona, Spain*

*3- Servicio de Oncología, Hospital Universitario Madrid-Torrelodones, Madrid 28250, Spain*

*4- Medcom Advance SA, Viladecans Bussines Park, Carrer de Bertran i Musitu, 83-85, 08840 Viladecans (Barcelona), Spain*

*5- Centro de Tecnología Química de Catalunya, Carrer de Marcel·lí Domingo s/n, 43007 Tarragona, Spain*

*6- ICREA, Passeig de Lluís Companys 23, 08010 Barcelona, Spain,*

*Main author email address: eric.pedrol@urv.cat*

One milliliter of blood from a person suffering metastatic cancer contains seven million white blood cells. Among them, there exist, on average, just one to ten cells prone to cause metastatic tumors in vital organs. We exploited the features of a microfluidic-based optical device produced in-house to perform a classification and quantification of cancerous cell lines, features that may allow to detect these incredibly rare cells when employed in patient's blood sample. Our approach makes use of specific cell line antibody expression to dye cells of interest in laboratory-prepared mixed cell line samples. The techniques employed in this device may contribute in the field of cancer research and diagnosis since it may allow to detect circulating tumour cells (CTC's) in early stages of the disease, before any symptoms arise or solid tumors show up in imaging scans, or during cancer treatment monitoring. Our device may also offer an interesting alternative to more invasive conventional exploration techniques such as traditional biopsy.

# **Channels Multiplexing in Spectral Encoded White Light Interferometry**

**I. G. Likhachev, V. I. Pustovoy, V. V. Svetikov, N.P.Khakamova,**

*Prokhorov General Physics Institute of Russian Academy of Sciences,*

*Russia, 19991, Moscow, Vavilov Str., 38*

*pustovoy@nsc.gpi.ru*

## **Abstract**

Simultaneous interrogation of the interferometric fiber optic sensors by means of spectral signal processing has been demonstrated. The method provides high accurate non incremental measurements of the optical path difference for each sensor in the network and consequently the external parameter affecting that sensor. . The combination of multiplexing techniques described results in several tens of sensors in the single network. Spectral signal processing technique can be used in fiber optic networks for numerous applications.

# Polarization Switching and Modulation in Graphene-Based Optical Waveguide Polarizer

**Jin Tae Kim\*** and Hongkyw Choi

*Creative Future Research Laboratory, Electronics and Telecommunications Research Institute (ETRI), Daejeon 34129, Republic of Korea*

*\*E-mail: jintae@etri.re.kr*

Numerous waveguide polarizers using graphene have been investigated theoretically and experimentally [1-8]. The extraordinary electro-optical characteristics of graphene make it expected that graphene-integrated waveguide polarizers act as a polarization-switchable device [9-11]. However, the feasibilities have yet to be demonstrated experimentally, and the possibility of realizing the device appears low. Thus, active polarization control in the graphene-based waveguide polarizer is an interesting subject worth investigating via different methods.

In this work, we propose and demonstrate a polarization-switchable graphene-based waveguide polarizer. The suppression of the unwanted polarization state is configured with the aid of mechanically movable graphene films embedded in a superstrate and placed on a waveguide core through elastomer spacers. The thickness of the graphene film plays a key role in selecting a polarization state: few-layer graphene suppresses the TE mode, making the device TM-passing, whereas many-layer graphene suppresses the TM mode, making the device TE-passing. In addition, by adjusting the air gap between the graphene-integrated superstrate and the waveguide core, the polarization extinction ratio is also tunable. A theoretical investigation of the designed polarization-switchable graphene-based waveguide polarizer exhibits good agreement with the experimental results.

To measure the dynamic characteristics of fabricated optical devices, the effect of step-wise pressure on the temporal behavior of the devices was measured. The intensity change of the optical output agrees with the temporal change of the mechanical pushing and releasing. The optical responses are timely corresponding to the mechanical pressing and releasing of the superstrate, indicating that the device serves as an optical modulator. Dynamic optical response to various stepped pressing and releasing forces on the superstrate is measured, revealing the capability of the device to serve as an optical attenuator.

- [1] J. T. Kim, C.-G. Choi, Graphene-based polymer waveguide polarizer, *Opt. Express*, vol. 20, pp. 3556–3562 (2012).
- [2] R. E. P. de Oliveira, J. S. de Matos, Graphene based waveguide polarizers: In-depth physical analysis and relevant parameters, *Sci. Report.*, vol. 5, p. 16949 (2015).
- [4] X. Yin, T. Zhang, L. Chen, X. Li, Ultra-compact TE-pass polarizer with graphene multilayer embedded in a silicon slot waveguide, *Opt. Lett.*, vol. 40, pp. 1733–1736 (2015).
- [5] R. Hao, W. Du, E. -P. Li, H. -S. Chen, Graphene assisted TE/TM-independent polarizer based on Mach-Zehnder interferometer, *IEEE Photon. Technol. Lett.*, vol. 27, pp. 1112–1115 (2015).
- [6] X. Yin, X. Ke, L. Chen, T. Zhang, J. Li, Z. Zhu, X. Li, Ultra-broadband TE-pass polarizer using a cascade of multiple few-layer graphene embedded silicon waveguides, *J. Lightwave Technol.*, vol. 34, pp. 3181–3187 (2016).
- [7] Y. Meng, S. Ye, Y. Shen, Q. Xiao, X. Fu, R. Lu, Y. Liu, M. Gong, Waveguide engineering of graphene optoelectronics—modulators and polarizers, *IEEE Photon. J.*, vol. 10, p. 6600217 (2018).
- [8] X. Hu, J. Wang, Ultrabroadband compact graphene-silicon TM-pass polarizer, *IEEE Photon. J.*, vol. 9, p. 7101310 (2017).
- [9] M. Liu, X. Yin, E. Ulin-Avila, B. Geng, T. Zentgraf, L. Ju, F. Wang, X. Zhang, A graphene-based broadband optical modulator, *Nature*, vol. 474, pp. 64–67 (2011).
- [10] B. J. Park, M. -K. Kim, and J. T. Kim, Analysis of a graphene-based silicon electro-absorption modulator in isotropic and anisotropic graphene models, *J. Korean Phys. Soc.*, vol. 70, pp. 967–972 (2017).
- [11] J. T. Kim, H. Choi, Y. Choi, J. H. Cho, Ion-Gel-Gated Graphene Optical Modulator with a Hysteretic Behavior, *ACS Appl. Mater. Interfaces*, vol. 10, pp. 1836–1845 (2018).

# Synthesis of SiC nanoparticles using CO<sub>2</sub> laser pyrolysis

L.Iskhakova<sup>1</sup>, I.Ershov<sup>1</sup>, V.Krasovskii<sup>1</sup>, N.Novikov<sup>1</sup>, V. Pustovoy<sup>1</sup>

1- Prokhorov General Physics Institute of Russian Academy of Sciences  
38, Vavilov st, Moscow, 119991, Russia

*pustovoy@nsc.gpi.ru*

The unique properties of SiC such as high thermal conductivity, high breakdown voltage, and wide bandgap has made it one of the most prominent materials for high power and high temperature electronic devices [1]. Various mature fabrication methods originating from silicon technology have been applied to SiC and fabrication of sophisticated nanostructures has been demonstrated [1]. By combining this with the unique properties of SiC, i.e. a wide bandgap for broadband optical access across the visible to infrared, SiC also has become a promising platform for nanophotonics [2]. Most recently, defects in SiC have attracted attention as potential host for quantum spin systems. Its weak spin-orbit coupling gives potential for long spin relaxation times [4,5]. Isolated electron spins are a promising platform for an array of new technologies, ranging from quantum communication [6] to nanoscale nuclear magnetic resonance [7,8] and intracellular sensing of magnetic, electric and thermal fields [9].

The results of silicon carbide nanoparticles synthesis by laser pyrolysis using a CO<sub>2</sub> laser are presented. The starting materials were SiF<sub>4</sub> and acetylene. The powder obtained were characterized by reflective electron microscopy. X-ray analysis of the samples obtained with a 5:3 ratio of monosilane and acetylene showed approximately 60% content of amorphous carbon and 5% oxide. The volume fraction of silicon carbide in the form of nanoparticles with an average diameter of about 6 nm was 30% with a laser power density of about 0.8 kW /cm.

This work was supported by the Russian Foundation for Basic Research (Grant No. 18-02-00786) and by the Presidium of RAS (Program I.7 "Modern problems of photonics, the probing of inhomogeneous media and materials")

- [1] Mizuochi, N. et al. Continuous-wave and pulsed EPR study of the negatively charged silicon vacancy with S=3/2 and C {3v} symmetry in n-type 4H-SiC. Phys. Rev. B 66, p.235202 (2002).
- [2] Soltamov, V. A., Soltamova, A. A., Baranov, P. G. & Proskuryakov, I. I. Room Temperature Coherent Spin Alignment of Silicon Vacancies in 4H- and 6H-SiC. Phys. Rev. Lett. 108, p.226402 (2012).
- [3] Menzel, R., Bachmann, T., Wesch, W. & Hobert, H. Maskless sub-mu m patterning of silicon carbide using a focused ion beam in combination with wet chemical etching. J. Vac. Sci. Technol. B Microelectron. Nanom. Struct. 16, pp.540–543 (1998).
- [4] Balasubramanian, G. et al. Ultralong spin coherence time in isotopically engineered diamond. Nat Mater 8, pp.383–387 (2009).
- [5] Cochrane, C. J., Lenahan, P. M. & Lelis, A. J. An electrically detected magnetic resonance study of performance limiting defects in SiC metal oxide semiconductor field effect transistors. J. Appl. Phys. 109, pp.14506–14512 (2011).
- [6] Bernien, H. et al. Heralded entanglement between solid-state qubits separated by three metres. Nature 497, pp.86-90 (2013).
- [7] Mamin, H. J. et al. Nanoscale Nuclear Magnetic Resonance with a Nitrogen-Vacancy Spin Sensor. Science 339, pp.557-560 (2013).
- [8] Staudacher, T. et al. Nuclear magnetic resonance spectroscopy on a (5-nm) cubed sample volume. Science 339, pp.561-565 (2013).
- [9] Toyli, D. M., Casas, C. F. d. l., Christle, D. J., Dobrovitski, V. V. & Awschalom, D. D. Fluorescence thermometry enhanced by the quantum coherence of single spins in diamond. Proc. Natl. Acad. Sci. USA 110, p8417 (2013).

# Synthesis and characterization of SiC nanoparticles using laser ablation of monocrystalline silicon in toluene

S.Rasmagin<sup>1</sup>, L.Apresyan<sup>1</sup>, V.Krasovskii<sup>1</sup>, A.Khomich<sup>1</sup>, N.Khakamova<sup>1</sup>, V. Pustovoy<sup>1</sup>

*1- Prokhorov General Physics Institute of Russian Academy of Sciences  
38, Vavilov st., Moscow, 119991, Russia*

*pustovoy@nsc.gpi.ru*

Recently, silicon carbide is considered as a promising material for nanophotonics [1]. Synthesis of SiC nanoparticles with single lattice defects allows to implement quantum spin systems with long spin relaxation time, as a consequence of a weak spin-orbit coupling [2]. The possibilities of application of such systems in quantum communication [3], in the measurement of nuclear magnetic resonance with nanometer resolution [4], in biomedical applications for intracellular sensing of electromagnetic and temperature fields [5] are demonstrated. SiC nanoparticles can be synthesized by chemical vapor deposition (CVD), sol-gel processes, laser gas-phase pyrolysis or laser evaporation processes.

In this paper, silicon carbide nanoparticles were synthesized by laser ablation of crystalline silicon in toluene using the frequency-doubled of Nd laser with a pulse duration of 20 ns, energy of single pulse of 1 mJ and a repetition rate of 10 Hz. The radiation was focused by a lens with a focal length of about 10 cm on the surface of silicon located in a cuvette under a layer of toluene. The duration of the surface treatment was 10 min. In the result, the SiC particles in toluene formed as a result of toluene decomposition and plasma-chemical reaction. Large particles were removed using centrifuge.

Nanoparticles were studied using transmission electron microscopy on graphite meshes. It was shown that the colloid contains nanoparticles of silicon and silicon carbide with an average size of about 10 nm. The composition elemental analysis showed the ratio of Si to SiC at about 1: 1. The Raman spectra of the initial silicon substrate were also measured and the photoluminescence spectrum of the colloid when excited at a wavelength of 455 nm in silicon carbide nanoparticles. A strong photoluminescence with a wide peak in the plate of 570 nm was detected (Fig.1). The work is supported by the Russian Foundation for Basic Research (Grant No. 18-02-00786).

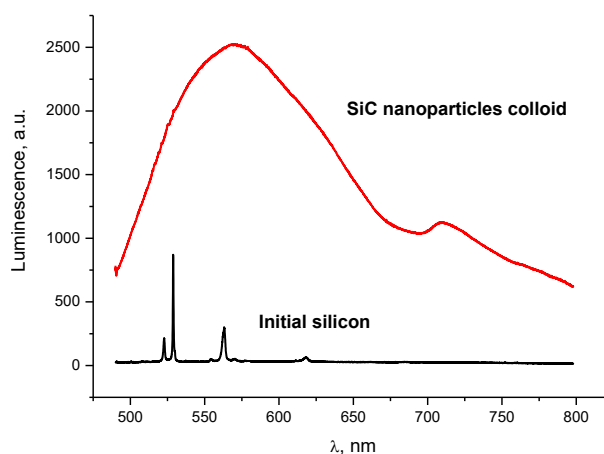


Fig.1. Raman spectrum of Si substrate (black line), photoluminescence spectrum of SiC colloid in toluene under 455 nm excitation

- [1]. Soltamov, V. A., Soltamova, A. A., Baranov, P. G. & Proskuryakov, I. I. Room Temperature Coherent Spin Alignment of Silicon Vacancies in 4H- and 6H-SiC. *Phys. Rev. Lett.* 108, p.226402 (2012).
- [2]. Balasubramanian, G. et al. Ultralong spin coherence time in isotopically engineered diamond. *Nat Mater* 8, pp.383–387 (2009).
- [3]. Bernien, H. et al. Heralded entanglement between solid-state qubits separated by three metres. *Nature* 497, pp.86-90 (2013).
- [4]. Mamin, H. J. et al. Nanoscale Nuclear Magnetic Resonance with a Nitrogen-Vacancy Spin Sensor. *Science* 339, pp.557-560 (2013).
- [5]. Toyli, D. M., Casas, C. F. d. l., Christle, D. J., Dobrovitski, V. V. & Awschalom, D. D. Fluorescence thermometry enhanced by the quantum coherence of single spins in diamond. *Proc. Natl. Acad. Sci. USA* 110, p8417 (2013).

# BIOPHOTONICS

# Photodynamic opening of blood-brain barrier: non-invasive approaches and new applications

**O. Semyachkina-Glushkovskaya<sup>1</sup>, E. Vodovosova<sup>2</sup>, E. Borisova<sup>1,3</sup>, A. Khorovodov<sup>1</sup>, A. Terskov<sup>1</sup>, I. Agranovich<sup>1</sup>, A. Mamedova<sup>1</sup>, M. Klimova<sup>1</sup>, C. Zhang<sup>4,5</sup>, W. Feng<sup>4,5</sup>, Yu. Li<sup>4,5</sup>, T. Yu<sup>4,5</sup>, D. Zhu<sup>4,5</sup>, V. Tuchin<sup>6,7,8</sup>**

1- Saratov State University, Department of Human and Animal Physiology, Astrakhanskaya Str. 83, Saratov 410012, Russian Federation

2- Shemyakin-Ovchinnikov Institute of Bioorganic Chemistry, Russian Academy of Sciences, Ul. Miklukho-Maklaya Str. 16/10, Moscow 117997, Russian Federation

3- Institute of Electronics, Bulgarian Academy of Sciences, Tsarigradsko Chaussee Blvd. 72, Sofia 1784, Bulgaria

4 - Britton Chance Center for Biomedical Photonics, Wuhan National Laboratory for Optoelectronics-Huazhong University of Science and Technology, Wuhan, Hubei 430074, China

5 - MoE Key Laboratory for Biomedical Photonics, Collaborative Innovation Center for Biomedical Engineering, School of Engineering Sciences, Huazhong University of Science and Technology, Wuhan, Hubei 430074, China

6- Saratov State University, Department of Optics and Biophotonics, 83Astrakhanskaya str., Saratov 410012, Russian Federation

7 - Tomsk State University, Laboratory of Biophotonics, 36 Lenin's Ave., Tomsk 634050, Russian Federation

8- Institute of Precision Mechanics and Control of RAS, Laboratory of Laser Diagnostics of Technical and Living Systems, 24 Rabochaya str., Saratov 410028, Russian Federation

Photodynamic (PD) diagnostics, a minimally invasive tool, has been an emerging option for intraoperative fluorescent imaging of malignant glioma. In our studies we demonstrate that PD also opens the blood-brain barriers (BBB) that is new important informative platform for development of perspective strategies for PD therapy (PDT) of glioma and brain drug delivery including liposomes as a good candidate for drug delivery system.

In the first step, using different doses of laser radiation (635 nm, 10-40 J/cm<sup>2</sup>) and photosensitizer (5-aminolevulinic acid – 5-ALA, 20 and 80 mg/kg, i.v.), we found that the optimal PDT for the reversible opening of the BBB is 15 J/cm<sup>2</sup> and 5-ALA, 20 mg/kg, exhibiting brain tissues recovery 3 days after PD. Further increases in the laser radiation or 5-ALA doses have no amplifying effect on the BBB permeability, but are associated with severe damage of brain tissues [1].

In the second step, we solved limitation of PD such as high scattering property of skull and small laser penetration using optical clearing window (OCW). Our results clearly show that application of OCW allows to perform PD-related BBB opening non-invasively with rapid recovery of BBB permeability. Using optimal PD-dose, in our *ex vivo* and *in vivo* experiments we showed efficiency of PD to open the BBB for high weight molecules and for GM1-liposomes 100 nm that passed the vascular endothelium, the basal membrane and distributed among astrocytes. These results indicate that OCW might be promising tool for non-invasive PD-related BBB opening for high weight molecules and liposomes that provides a novel useful tool for brain drug delivery and treatment of gliomas.

In the third step, we showed a new PD application as a technique of brain drug delivery and the brain clearing activation related with activation of the meningeal lymphatics as a novel drainage system in the brain layers [2].

This work was supported by Grant of Russian Science Foundation 17-15-01263 and the Foundation for Innovative Research Groups of the National Natural Science Foundation of China (Grant No. 61721092), and Director Fund of WNLO.

[1] O. Semyachkina-Glushkovskaya et al., Photodynamic opening of blood brain barrier, Biomedical Optics Express, <https://doi.org/10.1364/BOE.8.005040> (2017).

[2] O. Semyachkina-Glushkovskaya et al., Photodynamic opening of the blood-brain barrier and pathways of brain clearing, doi: 10.1002/jbio.201700287 (2018).

# Optical 3D microscopy for visualizing a chemotherapeutic agent

**Herbert Schneckenburger, Verena Richter, Petra Weber, and Michael Wagner**  
*Institute of Applied Research, Aalen University, Beethovenstr. 1, 73430 Aalen, Germany*

*E-Mail: [herbert.schneckenburger@hs-aalen.de](mailto:herbert.schneckenburger@hs-aalen.de)*

Doxorubicin, an anthracycline antibiotic, has been used as a cytostatic drug in cancer chemotherapy for many years. The drug is taken up by cells due to passive diffusion through their membrane and finally intercalates in DNA strands, where it causes chromatin condensation and initiates apoptosis. Due to its fluorescence properties doxorubicin has been localized within single cells, e.g. by wide-field microscopy, hyperspectral imaging or fluorescence lifetime imaging. Now physiological 3D cell cultures in combination with advanced microscopy techniques make it possible to study intracellular location and cytotoxic reactions in more detail.

Key parameters are lateral and axial resolution in single cells and in multi-cellular tumour spheroids (MCTS). Single layers in MCTS are assessed by confocal laser scanning microscopy as well as by light sheet fluorescence microscopy (LSFM), where LSFM has the great advantage that only those cell layers are exposed to light which are measured at the same time. So, LSFM can be used over long measuring periods at very low phototoxicity, proving e.g. uptake of doxorubicin in 3D spheroids of MCF-7 breast cancer cells within 48h, and cytotoxic reactions between 48h and 96h. In addition, Fluorescence Lifetime Imaging Microscopy (FLIM) permits to distinguish doxorubicin and its degradation product on the basis of their lifetimes of about 1.8 ns and 3.5 ns, respectively [1].

Axial rotation within a specific sample holder adapted to the microscope allows cells to be observed from different sides, and thus improves not only visualization of the fluorescent drug, but permits to use always the best (lateral) resolution [2]. Doubling of resolution can be obtained by Structured Illumination Microscopy (SIM), permitting to localize doxorubicin in the cell nucleus with a precision of about 100 nm and to obtain some information about nuclear architecture upon application of the chemotherapeutic drug [3].

- [1] V. Richter, P. Weber, M. Wagner, H. Schneckenburger: "3D visualization of cellular location and cytotoxic reactions of  
[2] V. Richter, S. Bruns, T. Bruns, P. Weber, M. Wagner, C. Cremer, H. Schneckenburger: "Axial tomography in live cell laser microscopy," *J. Biomed. Opt.* 22(9) (2017), 091505, doi: 10.1117/1.JBO.22.9.091505.  
[3] V. Richter, M. Piper, M. Wagner, H. Schneckenburger: "Structured Illumination for Live Cell Microscopy," *Proc. SPIE*, Vol. 10686, 2018, 10685-93.

**25 Years of Biomedical Optoacoustics:  
From Idea to Optoacoustic Theranostics**

Rinat Esenaliev, PhD

[riesenal@utmb.edu](mailto:riesenal@utmb.edu)

University of Texas Medical Branch, Galveston, Texas, USA

We proposed to use optoacoustics for biomedical applications and for more than 25 years have been working on it starting from idea and basic science; proposed a number of important diagnostic, therapeutic, and theranostic applications; developed and built optoacoustic systems; and performed animal and clinical optoacoustic studies. Recently, we built FDA-compliant, multi-wavelength, fiber-coupled, highly-compact laser diode-based optoacoustic systems. Optoacoustic theranostics is based on detection and analysis of optoacoustic waves induced in tissues via thermoelastic mechanism. It can be used for diagnostics (imaging, monitoring, and sensing), therapy, and monitoring of therapeutic response as well as for follow-up after the therapy. It can find a number of important clinical applications in large populations of patients such as diagnostics and management of traumatic brain injury (TBI), intracranial hematomas, circulatory shock, neonatal and fetal cerebral hypoxia, etc. Moreover, we proposed Nano-Pulse Laser Therapy (NPLT) which utilizes short optical pulses to generate optoacoustic waves in tissues. It is known that CW NIR light can be used for photobiomodulation. In the past few years, new works emerged on therapeutic effects of low-intensity ultrasound waves. The NPLT is based on irradiating tissue by low-level pulsed light and optoacoustic waves and combines merits of low-level light and ultrasound therapies. In this paper we present our major pre-clinical and clinical results on optoacoustic diagnostics and animal studies results on optoacoustic theranostics. Our medical-grade, nanosecond, tunable, near infrared (680-1064 nm), fiber-coupled systems were used for optoacoustic theranostics studies in rats with TBI. Our studies demonstrated that TBI results in cerebral hypoxia and intracranial hematoma formation, while transcranial application of NPLT significantly reduces negative (both acute and chronic) effects of TBI. The obtained results indicate that optoacoustic theranostics can be used for diagnostics and management of TBI and other disorders.

# **Spectral distortion measuring and correction in SD-OCT**

**G. Gelikonov**<sup>1</sup>

*1- Institute of Applied Physics Russian Academy of Sciences, 46 Uljanov str., Nizhny Novgorod, 603950 Russia*

*Main author email address: grgel@yahoo.com*

This work is devoted to method of overcoming SD OCT image worsening caused by distortion of measured spectral information. It is well known that low coherence interferometry is very sensitive to material and other kind of dispersion. Some in depth blurring of resulting OCT image is caused by dispersion factor. In the case of spectral domain methods of interference signal registration additional factors (such as non-equidistant frequency distribution over spectroscopic readouts) provide very similar blurring. Despite of different nature those factors hardly distinguished in many cases and may mislead researches. In this work methods of measuring and compensation are discussed. Results of experimental application of those methods are demonstrated on examples biological tissues including eye retina.

The work was supported by Ministry of Sciences RF (000000007417P3X0002)

# Perspectives of dual-wavelength photodynamic therapy controlled by optical monitoring

**M.Yu. Kirillin<sup>1</sup>, A.V. Khilov<sup>1</sup>, D.A. Loginova<sup>1</sup>, E.A. Sergeeva<sup>1</sup>, V.V. Perekatova<sup>1</sup>,  
M.A. Shakhova<sup>1,2</sup>, A.E. Meller<sup>1,2</sup>, D.A. Sapunov<sup>1,2</sup>, A.V. Shakhov<sup>1,2</sup>, N.Yu. Orlinskaya<sup>2</sup>,  
and I.V. Turchin<sup>1</sup>**

*1 - Institute of Applied Physics RAS, Nizhny Novgorod, Russia*

*2 – Privolzhsky Research Medical University, Nizhny Novgorod, Russia*

*Main author email address: mkirillin@yandex.ru*

Photodynamic therapy (PDT) is a modern treatment technique demonstrated its efficiency against both tumors and non-oncologic pathologies. Mechanisms of PDT include cytotoxic and antimicrobial effects of singlet oxygen produced upon light irradiation of photosensitizer (PS) selectively accumulated in treatment area. Fluorescent properties of PSs provide additional diagnostic opportunities. Employment of chlorin-based PS brings additional benefits to PDT performance due to two absorption peaks in blue and red ranges of the visible spectrum (402 and 662 nm, respectively). Deeper penetration of red light into biotissue relative to blue one allows selecting between superficial and deep impact or combining them, while blue light provides additional antimicrobial effect. Besides anti-tumor treatment, recent applications of PDT include treatment of chronic inflammatory diseases and skin rejuvenation.

Employment of non-invasive optical diagnostic techniques is a step towards implementation of personalized medicine. Dual-wavelength fluorescence imaging prior to and in course of PDT procedure permits monitoring of PS penetration and photobleaching. The ratio of fluorescence signals at two wavelength allows evaluating PS penetration depth, while the decay in fluorescence signal at both wavelength during irradiation indicates efficient photobleaching [1]. Monitoring of morphological and functional changes in tissue with optical coherence tomography (OCT) allows evaluating immediate and long-term response of tissue reaction to PDT. The difference in the distribution of absorbed dose within the tissue can be evaluated quantitatively in frames of Monte Carlo simulations that can serve for PDT planning [2].

In this paper we report on comparative analysis of different PDT regimens with chlorin-based PS employing irradiation at the wavelength of 405 and 660 nm, or their combination. The total delivered doses varied from 50 to 150 J/cm<sup>2</sup> that is typical for antibacterial and rejuvenation procedures and for treatment of chronic inflammatory diseases. The animal study was performed on an intact tissue of the inner surface of a laboratory rabbit ear. A custom-developed “Fluovizor” device [3] was employed for dual-wavelength fluorescence monitoring in course of PDT procedure. OCT-monitoring using OCT-1300E device (IAP RAS, Biomedtech, Russia) [4] capable of OCT-angiography was employed to monitor tissue structural and functional features prior to and after PDT procedure.

Monte Carlo simulation allowed to compare the distribution of absorbed dose at 405 nm and 660 nm within tissue for different concentrations of PS accounting for inhomogeneous distribution of PS.

Clinical study indicated the efficiency of PDT treatment of pharynx chronic inflammatory diseases with chlorin-based PS and irradiation at 405 nm. The treatment protocol included OCT-monitoring with the OCT-1300U device equipped with an endoscopic probe. Microbiological examination indicated elimination of the pathogenic flora in all patients that underwent PDT treatment.

The study is supported by Russian Science Foundation, project 17-15-01264.

[1] A. Khilov et al, Two-Wavelength Fluorescence Monitoring and Planning of Photodynamic Therapy, CTM, 9, 96–105 (2017).

[2] M. Shakhova et al, Photodynamic therapy with chlorin-based photosensitizer at 405 nm: numerical, morphological and clinical study, J. Biomed. Opt., 23, in print (2018).

[3] M. Kleshnin et al, Compact and fully automated system for monitoring photodynamic therapy, based on two LEDs and a single CCD. Laser Phys. Lett.; 12, 115602 (2015).

[4] A. Moiseev et al, OCT-based angiography device with real-time angiography B-scans visualization and hand-held probe for everyday clinical use, J. Biophotonics, e201700292 (2018).

## Biophotonics at Small Scales using Structure-mediated Light Robotics

**Jesper Glückstad**

*DTU Fotonik, Dept. Photonics Engineering, Techn. Univ. Denmark  
Ørsted Plads 343, DK-2800 Kgs. Lyngby, Denmark  
[jesper.gluckstad@fotonik.dtu.dk](mailto:jesper.gluckstad@fotonik.dtu.dk)  
[www.PPO.dk](http://www.PPO.dk) [www.OptoRobotix.com](http://www.OptoRobotix.com) [www.GPCphotonics.com](http://www.GPCphotonics.com)*

### Abstract

Light robotics combines the latest developments in a variety of disciplines to achieve an all-optical toolbox for probing micro- and nano-environments in real-time 3D, opening up new avenues of applications of structure-mediated control of tiny biological constituents. Dynamic optical trapping is used for e.g. on-site assembly or disassembly of larger structures into component parts as well as their actuation to pre-determined sites with high precision. The optically manipulated and controlled structures of Light Robotics can be used to carry loads that can as well be functionalized to perform specific and predefined tasks. Structure-mediated transport provides convenience over direct particle trapping without compromising how precise particles can be moved and positioned. In cell trapping or transport, for example, damage due to direct irradiation can be substantially minimised by loading the cell into a prefabricated platform that is illuminated and moved around instead. Not only does this lessen the negative impact of high-intense radiation, but it also adds the benefit of having up to six degrees-of-freedom control over the robotic structure, hence on the specimen itself.

### References

- [1] Glückstad, J., "Sorting particles with light", *Nature Materials* 3, 9 (2004).
- [2] Papagiakoumou, E., Anselmi, F., Begue, A., Sars, V., Glückstad, J., Isacoff, E., Emiliani, V., *Nature Methods* 7, 848 (2010).
- [3] Rodrigo, P., Gammelgaard, L., Bøggild, P., P.-Nielsen, I., Glückstad, J., *Opt. Express* 13, 6899 (2005)
- [4] Glückstad, J., "Sculpting the object", *Nature Photonics* 5, 7 (2011)
- [5] Palima, D., & Glückstad, J., "Gearing up for optical micro-robotics: synthetic microstructures actuated by optical trapping and optical manipulation", *Lasers & Phot. Reviews* 17, 478 (2013).
- [6] Villangca, M., Casey, D., Glückstad, J., "Optically-controlled platforms for single- and sub-cellular transfection and surgery," *Biophysical Reviews* 7, 379 (2015).
- [7] Villangca, M., Palima, D., Bañas, A., Glückstad, J., "Light-driven micro-tool equipped with a syringe function," *Light: Science & Applications*, *Nature Publ. Group*, 5 (9) e16148 (2016).
- [8] Glückstad, J. & Palima, D., "Light Robotics: structure-mediated nanobiophotonics", Elsevier Science, 482 pages (2017).

# A potential of optical coherence tomography and terahertz pulsed spectroscopy for intraoperative diagnosis of brain tumors

**K.I. Zaytsev<sup>1,2,3</sup>, I.N. Dolganova<sup>2,3,4</sup>, N.V. Chernomyrdin<sup>1,2,3</sup>,  
G.A. Komandin<sup>1</sup>, M.A. Schcedrina<sup>3</sup>, S.-I.T. Beshplav<sup>5</sup>, S.A. Goryaynov<sup>5</sup>,  
I.V. Reshetov<sup>3</sup>, A.A. Potapov<sup>5</sup>, and V.V. Tuchin<sup>6</sup>**

1 - Prokhorov General Physics Institute of RAS, Moscow 119991, Russia

2 - Bauman Moscow State Technical University, Moscow 105005, Russia

3 - Sechenov First Moscow State Medical University, Moscow 119991, Russia

4 - Institute of Solid State Physics of RAS, Chernogolovka 142432, Russia

5 - Burdenko Neurosurgery Institute, Moscow 125047, Russia

6 - Saratov State University, Saratov 410012, Russia

E-mail: [kirzay@gmail.com](mailto:kirzay@gmail.com)

Intraoperative diagnosis of brain tumors remains a challenging problem of modern neurosurgery [1]. A complete resection of tumor is the most important factor, determining an efficiency of its treatment [2]. An incomplete resection, caused by inaccurate detection of tumor margins, increases a probability of the tumor recurrence. The existing methods of the intraoperative neurodiagnosis of tumors are plagued with limited sensitivity and specificity; they remain laborious, time-consuming and/or rather expensive. Therefore, the development of novel methods for the intraoperative diagnosis of gliomas relying on modern instruments of medical imaging is a topical problem of medicine, physics, and engineering [3,4].

In our research, we study an ability of optical coherence tomography (OCT) [5,6] and terahertz (THz) pulsed spectroscopy [7–11] for intraoperative diagnosis of brain tumors, with a strong emphasize on a human brain gliomas featuring different grades. We perform experimental measurements of the frequency-dependent THz dielectric permittivity and OCT imaging of healthy (intact) and pathological brain tissues *ex vivo* in order to analyze the prospect for differentiation between various classes of tissues [12,13]. The observed results highlight a potential of these two instruments of tissue imaging in intraoperative neurodiagnosis relying on endogenous markers of tumor.

- [1] Q.T. Ostrom et al., *Neuro-Oncology* **18**, v1–v75 (2016).
- [2] S. Phuphanich et al., *The Journal of the Florida Medical Association* **80**, 181–184 (1993).
- [3] N. Pustogarov et al., *Molecular Neurobiology* **54**, 5699–5708 (2017).
- [4] A.A. Potapov et al., *Neurosurgical Review* **39**, 437 (2016).
- [5] O.M. Carrasco-Zevallos et al., *Biomedical Optics Express* **8**, 1607 (2017).
- [6] I.N. Dolganova et al., *Journal of Biomedical Optics* **23**, 091406 (2018).
- [7] K.I. Zaytsev et al., *Applied Physics Letters* **106**, 053702 (2015).
- [8] K.I. Zaytsev et al., *IEEE Trans. Terahertz Science and Technology* **5**, 817–827 (2015).
- [9] K.I. Zaitsev et al., *Optics and Spectroscopy* **119**, 404–410 (2015).
- [10] I. Reshetov et al., *European Journal of Cancer* **51**, S167–S167 (2015).
- [11] K.I. Zaytsev et al., *IEEE Trans. Terahertz Science and Technology* **6**, 576–582 (2016).
- [12] I.N. Dolganova et al., *Proceedings of SPIE* **10717**, 107171X (2018).
- [13] N.V. Chernomyrdin et al., *Proceedings of SPIE* **10716**, 107160S (2018).

# Medical Applications of THz and IR Imaging And Machine Learning

**Yu.Kistenev<sup>1,2</sup>, A.Borisov<sup>1,2</sup>, V.Nikolaev<sup>1</sup>, D.Vrazhnov<sup>1</sup>, N.Krivova<sup>1</sup>, A.Knyazkova<sup>1</sup>, E.Sandykova<sup>1,2</sup>**

<sup>1</sup>*Tomsk State University, Tomsk, Russia,*

<sup>2</sup>*Siberian State Medical University, Tomsk, Russia*

*Main author email address: yuk@iao.ru*

The cancer tissue diagnostics is known to be one of the main problems in medicine. Combination of tissue optical imaging and machine learning (ML) allows to construct predictive models, which can be used for further diagnostics. The advantage of ML approach being a subset of artificial intelligence provides ability to get an optimal task solution without explicit programming [1].

Typical ML pipeline includes image quality improving (denoising, smoothing, color and brightness normalization), image segmentation and region of interest selection, feature extraction, classification and diagnosis.

We plan to discuss applications of IR and THz imaging and machine learning methods for cancer tissue and post cancer treatment complications tissue diagnosis.

The first example will be connected with the classification of paraffin tissue blocks. Formalin-fixed paraffin-embedded (FFPE) tissue samples are widely used worldwide in diagnosis and research. The protocol for FFPE tissue samples sectioning has been developed to prevent cross-contamination and distributed between participating centers [2]. A consensus histopathology evaluation form was developed by an international panel of pathologists, as a result the histopathology evaluation of the cases assured the presence of the targeted tissue, identified the presence of other tissues that could disturb the molecular diagnosis and allowed the assessment of tissue quality. Thus, the protocol allows to process correctly FFPE tissue samples for study.

Difference in THz absorbance between malignant tumor and normal tissues can be useful for instrumental diagnosis [3]. To realize potential of THz imaging, efficient methods of automatic image content analysis should be created.

The results of application of machine learning approach in paraffin embedded cancer tissue THz 2d imaging analysis will be discussed in the report. Absorption spectra of paraffin blocks were measured using of Time-domain THz spectrometer (EKSPLA, Estonia) with tuning range 0.3-3 THz.

The second example will be connected with the secondary lymphedema analysis. This disease is acquired and can cause by a number of reasons, for example, by surgical removal of lymph nodes with malignant neoplasms [4].

The results of THz (EKSPLA, Estonia) and two-photon (MPTflex microscope, JenLab GmbH) imaging of lymphedema tissue imaging and applications of various methods of image analysis and classification, including edge detectors, method of the histogram of oriented gradients, and machine learning will be discussed.

The work was carried out under partial financial support of the Russian Fund of Basic Research (grant No.17-00-00186, grant No. 18-42-703012 p\_мол\_a).

[1] A. Samuel, Some Studies in Machine Learning Using the Game of Checkers, IBM Journal of Research and Development, 3, pp.210–229, (1959).

[2] M. Mena, B. Lloveras, S. Tous, J. Bogers, et. al., Development and validation of a protocol for optimizing the use of paraffin blocks in molecular epidemiological studies: The example from the HPV-AHEAD study, PLoS ONE, 12, pp.1-12, (2017).

[3] T.Bowman, Yo.Wu, J.Gauch, L. K. Campbell, M. El-Shenawee, Terahertz Imaging of Three-Dimensional Dehydrated Breast Cancer Tumors, J Infrared Milli Terahz Waves, 38, pp.766–786, (2017)

[4] B. B. Lee, J. Began, and S. G. Rockson, Lymphedema: A Concise Compendium of Theory and Practice, Springer, London (2011).

# Quantitative Phase Microscopy Spatial Signatures of Cancer Cells

**Natan T. Shaked**

*Department of Biomedical Engineering, Tel Aviv University, Tel Aviv, Israel*  
[nshaked@tau.ac.il](mailto:nshaked@tau.ac.il), [www.eng.tau.ac.il/~omni](http://www.eng.tau.ac.il/~omni)

Cancer is a leading cause of death worldwide. Flow cytometry of body fluids obtained by routine medical tests can identify circulating tumor cells. In flow cytometry, one evaluates cellular features through fluorescence markers. However, in addition to possible cytotoxicity, suitable markers might be not available for certain cell types. The internal morphology and texture of cancer cells change during oncogenesis. Without staining, however, biological cells are nearly transparent, resulting in a low image contrast. An inherent contrast mechanism that can be used when imaging cells without staining is their refractive index. Phase imaging methods use interference to record the delay of light passing through the cell due to a slightly higher refractive index compared with the cell surrounding. Contrary to qualitative phase contrast methods, interferometric phase microscopy (IPM) yields the optical path delay (OPD) map of the cell, which is equal to the integral of the refractive index values across the cell thickness. In addition, IPM allows calculating quantitative parameters, such as cell volume and dry mass, which were not available to clinicians so far. IPM is based on a mature technology for wavefront sensing, digital holography. However, till recently it could not be implemented in clinical settings due to its bulkiness and the requirement for specific optical skills to align and use it. In the last years, we made significant efforts to make these wavefront sensors affordable to clinical use ([1], for example). Our approach is based on using the microscopes already existing in medical clinics and attaching a portable interferometric module to their exit port. This wavefront sensor is compact, inexpensive and easy to operate, making this technology affordable to clinicians' direct use. Using stain-free IPM, we have recently compared the quantitative phase imaging-based features of healthy and cancer cells and of primary and metastatic cancer cells [2]. The cells were round and unattached to the surface to allow imaging during flow, and therefore most of the cells look alike, thus subjective pathological examination cannot be performed, even under IPM (see Fig. 1(a)). We therefore applied machine learning classifiers on 12 parameters extracted from the cell OPD maps (see examples in Fig. 1(b)), and obtained classification results (healthy/ cancer/metastatic) with 86% average sensitivity and 90% average specificity. This stain-free quantitative imaging technique shows a clinical potential for automatic cell flow cytometry.

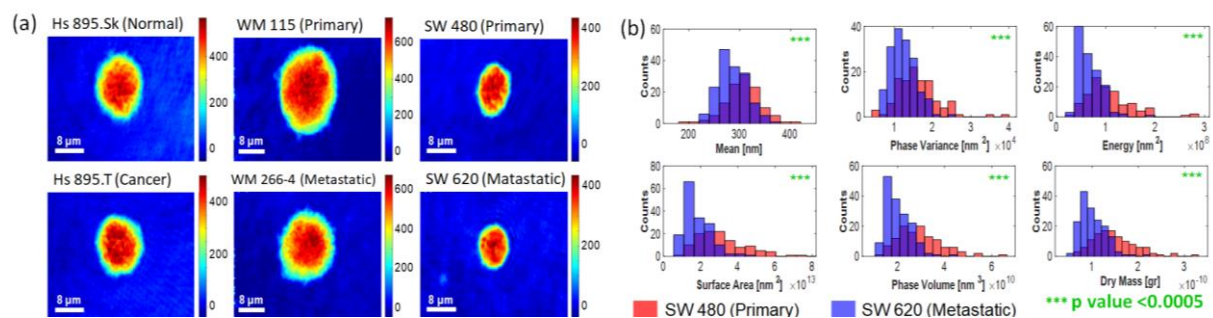


**Figure 1. Preliminary results [2]:** (a) OPD maps of human cells, demonstrating that even under IPM, unattached cells cannot be classified visually. Colorbars: OPD values in nm. (b) Examples of parameters extracted from the OPD maps that are used for classification due to great statistical difference.

- [1] P. Girshovitz and N. T. Shaked, Compact and portable low-coherence interferometer with off-axis geometry for quantitative phase microscopy and nanoscopy, *Optics Express*, vol. 21, 5701-5714 (2013).
- [2] D. Roitshain, L. Wolbromsky, E. Bal, H. Greenspan, L. Satterwhite, and N. T. Shaked, Quantitative phase microscopy spatial signatures of cancer cells, *Cytometry Part A*, vol. 91, pp. 482-493 (2017).

# Detecting Structural Alterations in Cancer Progression with Label-Free Spectroscopy

L. Zhang, V. Turzhitsky, U. Khan, Y. Zakharov, E. Vitkin, D. K. Pleskow, T. M. Berzin, M. Sawhney, J. D. Goldsmith, E. Yee, K. Kantekure, I. Itzkan, L. Qiu, L. T. Perelman

Center for Advanced Biomedical Imaging and Photonics  
Beth Israel Deaconess Medical Center  
Biological and Biomedical Sciences Program  
Harvard University

*lperelman@fas.harvard.edu*

Although subcellular organelles, such as the mitochondria, lysosomes, or Golgi bodies, and various types of cellular vesicles are known to be altered in cancer, the most important cancer hallmark is the structural abnormality of the cell nucleus. In addition, nanoscale subnuclear changes of chromatin packing have also been shown to play an important role in genetic and transcriptional alterations in cancer progression. Unfortunately, fundamental limitations of the existing imaging techniques, and mainly the lack of technologies for label-free nanoscale-sensitive measurements in live cells, prevent the study of these very early stage pre-cancerous structural alterations. Electron microscopy has the adequate resolution but cannot be utilized in living systems, involves extensive manipulations with the sample, and has minute field of view, while fluorescence microscopy can achieve targeted contrast for a limited number of specific organelles or proteins, however, most of its labels are to some extent cytotoxic. In order to overcome these shortcomings we have been developing the optical spectroscopic sensing technique which is based on the combination of confocal microscopy with light scattering spectroscopy [1,2], called confocal light scattering spectroscopic microscopy (see Fig. 1) [3-5]. It provides several advantages over the existing approaches: the ability to image live cells, no need for labels for nanoscale sensing, and the ability to image a large number of cells rapidly. Though the imaging resolution of this technique is diffraction limited, the spectral classification is not, and it is sensitive to scales as small as 10 nm. We employed the developed technique to monitor cancer progression in tumors and live cells at organelle and chromatin spatial scales and to study how the subcellular exosomes perform cell-independent microRNA biogenesis and promote tumorigenesis.

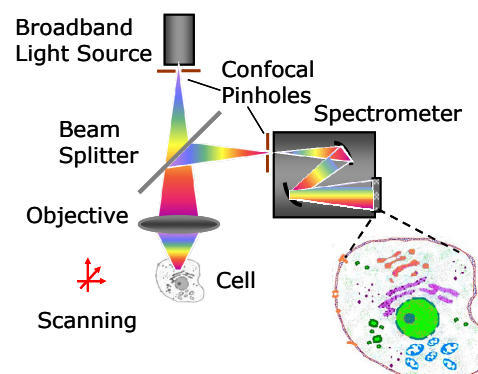


**Figure 1.** Concept of confocal light scattering spectroscopic microscopy.

This work was supported by the U.S. National Institutes of Health under grants R01 EB003472, R01 EB025173, R01 CA205431, and R01 CA218382 and U.S. National Science Foundation under grants EFRI-1240410, CBET-1402926 and CBET-1605116.

- [1] Perelman LT, Backman V, Wallace M, Zonios G, Manoharan R, Nusrat A, Shields S, Seiler M, Lima C, Hamano T, Itzkan I, Van Dam J, Crawford JM, Feld MS. Observation of Periodic Fine Structure in Reflectance from Biological Tissue: A New Technique for Measuring Nuclear Size Distribution. *Phys. Rev. Lett.* **80**, 627-630 (1998).
- [2] Backman V, Wallace M, Perelman LT, Arendt JT, Gurjar R, Müller MG, Zhang Q, Zonios G, Kline K, McGillican T, Shapshay S, Valdez T, Badizadegan K, Crawford JM, Fitzmaurice M, Kabani S, Levin HS, Seiler M, Dasari RR, Itzkan I, Van Dam J, Feld MS. Detection of Preinvasive Cancer Cells. Early-Warning Changes in Precancerous Epithelial Cells Can Now be Spotted In Situ. *Nature* **406**, 35-36 (2000).
- [3] Itzkan, I. Qiu L, Fang H, Zaman MM, Vitkin E, Ghiran IC, Salahuddin S, Modell MD, Andersson C, Kimerer LM, Cipolloni PB, Lim K-H, Freedman SD, Bigio IJ, Sachs BP, Hanlon EB, Perelman LT. Confocal light absorption and scattering spectroscopic microscopy monitors organelles in live cells with no exogenous labels. *Proc. Natl. Acad. Sci. USA.* **104**, 17255-17260 (2007).
- [4] Qiu L, Turzhitsky V, Chuttani R, Pleskow DK, Goldsmith JD, Guo LY, Vitkin E, Itzkan I, Hanlon EB, Perelman LT. Spectral Imaging With Scattered Light: From Early Cancer Detection to Cell Biology. *IEEE J. Sel. Top. Quant. Elect.* **18**, 1073-1083 (2012).
- [5] Turzhitsky V, Qiu L, Itzkan I, Novikov AA, Kotelev MS, Getmanskiy M, Vinokurov VA, Muradov AV, Perelman LT. Spectroscopy of Scattered Light for the Characterization of Micro and Nanoscale Objects in Biology and Medicine. *Appl. Spect.* **68**, 133-154 (2014).

# Plasmon-enhanced Raman detection of neurodegenerative biomarkers

**P. Matteini, C. D'Andrea, M. Cottat, M. Banchelli, M. De Angelis, R. Pini**

*Institute of Applied Physics, National Research Council of Italy (CNR), Florence, Italy*

*r.pini@ifac.cnr.it*

Plasmon-enhanced spectroscopies such as surface-enhanced Raman spectroscopy (SERS) concern the detection of enhanced optical responses of molecules in close proximity to plasmonic structures, which results in a strong increase in sensitivity.

We develop reliable methods based on SERS for determining chemical identity and structural information from given proteins and biomarkers in trace concentration. The unique combination of sensitivity, selectivity and spectral multiplexing of SERS coupled with the use of powerful signal-enhancing plasmonic substrates represents a valuable option for the effective analysis of biomolecules.

These species may include different forms of the amyloid beta ( $A\beta$ ) protein, which impair the cognitive function of Alzheimer's disease (AD) patients. This aberrant protein aggregation typically starts from 10 to 20 years before the AD symptoms become evident, so that the detection of  $A\beta$  oligomers at low concentration plays a key role for early diagnosis.

Here we will present a review on different strategies we are pursuing in our lab for this purpose [1-4]:

1. SERS with isolated Ag nanocubes, providing high reproducibility, quantitative detection and limit of detection at nanomolar concentration.
2. Assembled plasmonic nanostructures for rapid and cost-effective SERS analysis, such as: 2a) SERS with quasi-ordinated assemblies of Concave Au nanoCubes; 2b) SERS with randomly assembled Ag nanowires.
3. An advanced optofluidic system for protein detection based on Raman signal amplification *via* dewetting and molecular gathering within temporary mesoscale assemblies.

[1] Matteini P et al. *Nanoscale* 8 3374 (2015)

[2] Banchelli M et al. *ACS Appl Mater Interfaces* 8 2628 (2016)

[3] Matteini P et al. *ACS Nano* 11 918-926 (2017)

[4] Matteini P et al. *Sci Rep* 8, 1033 (2018)

# Advanced Laser-Optic Techniques for the Study of Blood Structure and Dynamics

**Alexander Priezzhev<sup>1,2</sup>, Andrei Lugovtsov<sup>1,2</sup>, Alexey Semenov<sup>1,2</sup>, Kisung Lee<sup>2,3</sup>,  
Sergey Nikitin<sup>1,2</sup>, Vladislav Ustinov<sup>4</sup>, Yuri Gurfinkel<sup>5</sup>, Evgeny Shirshin<sup>1,2</sup>.**

*1 - International Laser Center, Lomonosov Moscow State University, Moscow, Russia.*

*2 - Physics Faculty, Lomonosov Moscow State University, Moscow, Russia.*

*3 - Currently with Ulsan National Institute of Science and Technology, Ulsan, Republic of Korea*

*4 - Faculty of Comput. Mathematics and Cybernetics, Lomonosov Moscow State University, Moscow, Russia.*

*5 - Medical Research and Education Center, Lomonosov Moscow State University, Russia*

[avp@biomedphotonics.ru](mailto:avp@biomedphotonics.ru)

Blood composition as well as the parameters characterizing the structure and dynamics of blood and tissues surrounding the blood microvessels are the factors that determine blood fluidity and efficiency of performing the functions of transporting and delivering the gases (oxygen and carbon dioxide) and nutrients all throughout the human body. Age-related changes in the organism and most of socially important diseases are followed and highly determined by the alteration of these parameters from normal values. Thus the ability to measure and monitor these parameters in norm and their alterations in pathology is essential for adequate estimation of the patients' state, the ways to improve the treatment procedure and to correct the patients' hemorheology.

In our work, we combined several laser and optical techniques to perform a complex study of various parameters related to blood structure and dynamics by means of imaging and measurement. In particular we used: diffuse light scattering (DLS); laser diffractometry (LD); optical trapping and manipulation (OT), videocapillaroscopy (VC) and two-photon tomography (TPT) and fluorescence life-time imaging (FLIM)). Three former techniques were used for *in vitro* measurements with fresh samples of blood stabilized with EDTA drawn from either healthy donors or patients suffering from various diseases such as hypertension, heart failure and/or diabetes mellitus. Three latter techniques were used for *in vivo* measurements and imaging. We also measured the parameters related to erythrocyte aggregation in model solutions of certain blood plasma proteins known as aggregation agonists or inhibitors. In particular, we measured the forces of aggregation and disaggregation of individual erythrocytes with OT [1,2], as well as the aggregation index, characteristic half-time of aggregation and the critical shear stress with a whole blood aggregometer implementing the DLS technique. We used the conventional LD technique (ektacytometry) to measure the average value of deformability of the erythrocytes in the sample and upgraded the technique to enable measuring the parameters of deformability distribution, which is essential for clinical application of the technique [3]. We performed *in vivo* imaging of the blood flows in nailfold capillaries and the perivascular zone (PZ) around them with high resolution VC technique. TPT and FLIM was used to investigate the PZ composition, and this enabled us to clearly demonstrate that PZ corresponds to the border of viable epidermis and it was suggested that the PZ size variations were due to the different amounts of interstitial fluid [4]. The obtained results allow to suggest that the PZ size measured with nailfold VC can be used as a novel quantitative non-invasive marker sensitive of the severity of such diseases as heart failure.

This work was supported by the grant of the Russian Science Foundation № 18-15-00422.

[1] K. Lee, A.V. Danilina, A.V. Priezzhev et al. Probing the red blood cells aggregating force with optical tweezers. IEEE Journal of Selected Topics in Quantum Electronics, 22(3), 7000106 (2016). DOI: 10.1109/JSTQE.2015.2477396.

[2] K. Lee, Ch. Wagner, A.V. Priezzhev. Assessment of the "cross-bridge"-induced interaction of red blood cells by optical trapping combined with microfluidics. Journal of Biomedical Optics, 22(9), p. 091516 (2017). DOI: 10.1117/1.JBO.22.9.091516.

[3] S.Yu. Nikitin, V.D. Ustinov, Yu.S. Yurchuk. New diffractometric equations and data processing algorithm for laser ektacytometry of red blood cells. Journal of Quantitative Spectroscopy & Radiative Transfer 178, 315–324 (2016). DOI: 10.1016/j.jqsrt.2016.02.024.

[4] E.A. Shirshin, Y.I. Gurfinkel, S.T. Matskeplishvili, et al. In vivo optical imaging of the viable epidermis around the nailfold capillaries for the assessment of heart failure severity in humans. J. Biophotonics. 2018; e201800066. DOI: 10.1002/jbio.201800.

# Kinetics of optical properties of human colorectal tissues during optical clearing – a comparative study between normal and pathological tissues

I. Carneiro<sup>1</sup>, S. Carvalho<sup>1</sup>, V. Silva<sup>2</sup>, R. Henrique<sup>1,3</sup>, L. Oliveira<sup>2,4</sup>, V. V. Tuchin<sup>5,6,7</sup>

1- Department of Pathology and Cancer Biology and Epigenetics Group-Research Centre, Portuguese Oncology Institute of Porto, Rua Dr. António Bernardino de Almeida S/N, 4200-072 Porto, Portugal

2- Centre of Innovation in Engineering and Industrial Technology, ISEP, Rua Dr. António Bernardino de Almeida N° 431, 4200-072 Porto, Portugal

3- Department of Pathology and Molecular Immunology, Institute of Biomedical Sciences Abel Salazar – University of Porto (ICBAS-UP), Rua de Jorge Viterbo n° 228, 4050-313 Porto, Portugal

4- Physics Department, School of Engineering, Polytechnic of Porto, Rua Dr. António Bernardino de Almeida, n° 431, 4200-072 Porto, Portugal

5- Research-Educational Institute of Optics and Biophotonics, Saratov State University (National Research University of Russia), 83 Astrakhanskaya str., Saratov 410012, Russia

6- Laboratory of Laser Diagnostics of Technical and Living Systems, Precision Mechanics and Control Institute of the Russian Academy of Sciences, 24 Rabochaya, Saratov 410028, Russia

7- Laboratory of Femtomedicine, ITMO University, 9 Lomonosova street, St. Petersburg 191002, Russia

Main author email address: lmo@isep.ipp.pt

The optical immersion clearing method creates a temporary increase in light penetration depth and in image contrast through the reduction of light scattering in tissues [1]. Measurements performed from *ex vivo* tissues during clearing have allowed to estimate agent's diffusion properties [2], and pathology discrimination through the evaluation of the free water content [3]. The study of the kinetics of tissue's optical properties during treatment is also important, since it allows to evaluate the clearing efficiency [4]. Using only thickness and collimated transmittance measurements made from normal and pathological colorectal tissues during treatment with glucose-water solutions we estimated the kinetics of tissue's optical properties. A significant decrease in the scattering coefficient ( $\mu_s$ ) was obtained for both tissues – see Fig. 1.

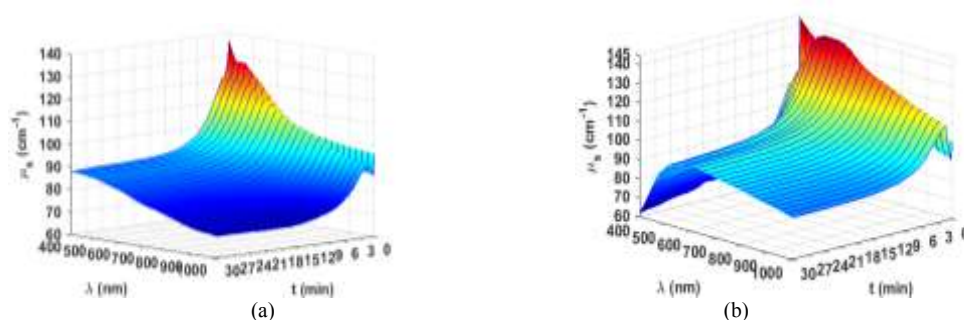


Fig. 1. Kinetics of the  $\mu_s$  for normal (a) and pathological (b) human colorectal mucosa during treatment with glucose-water solutions.

Pathological tissue shows higher magnitude decrease in  $\mu_s$  at short wavelengths, indicating a possible window for tumor removal with laser surgery. The kinetics of the other optical properties were also estimated and compared, again showing some differences. The model used in these calculations has also predicted a mean scatterer size for pathological tissue  $\sim 3.5x$  higher than in normal tissue.

[1] A. Yu. Sdobnov *et al*, Recent progress in tissue clearing for spectroscopic application, *Spect. Acta Part A*, vol. 197, pp. 216-229, (2018).

[2] L. Oliveira *et al*, The characteristic time of glucose diffusion measured for muscle tissue at optical clearing, *Las. Phys.*, vol. 23, pp. 075606-1-6, (2013).

[3] I. Carneiro *et al*, Water content and scatterers dispersion evaluation in colorectal tissues, *J. Biomed. Phot. & Eng.*, vol. 3, pp. 04301-1-10, (2017).

[4] I. Carneiro *et al*, Kinetics of optical properties of colorectal muscle during optical clearing, *IEEE J. Sel. Top. Quant. Elect.*, doi: 10.1109/JSTQE.2018.2840346.

# Photodetection of Stress-induced Gastrointestinal Neoplasia in Laboratorial Animals

**E. Borisova<sup>1,2</sup>, Ts. Genova<sup>1</sup>, A. Khorovodov<sup>2</sup>, I. Agranovich<sup>2</sup>, I. Angelov<sup>3</sup>, V. Mantareva<sup>3</sup>,  
M. Kanevsky<sup>2</sup>, N. Navolokin<sup>4</sup>, O. Semyachkina-Glushkovskaya<sup>2</sup>, L. Avramov<sup>1</sup>**

1- Institute of Electronics, Bulgarian Academy of Sciences, Tsarigradsko Chaussee 72, Sofia 1784, Bulgaria

2- Saratov State University, Astrakhanskaya Str. 83, Saratov 410012, Russia

3 - Institute of Organic Chemistry with Center of Phytochemistry, Bulgarian Academy of Sciences, Acad. G. Bontchev str. Bl. 9, 1113 Sofia, Bulgaria

4 - Saratov State Medical University, Saratov 410010, Russia

borisova@ie.bas.bg

Our research objective is a development of innovative optical technologies for sensitive diagnosis of early stages of development of stomach and intestine cancer and monitoring of stress-induced appearance and development of tumors of the gastrointestinal tract by applying endogenous and exogenous fluorescence spectroscopy modalities. Exogenous fluorescent markers used are from the family of photosensitizers – porphyrins and phthalocyanines, which are the most popular photosensitive drugs applied in experimental and preclinical practice. Other important advantage related to usage of photosensitizers as exogenous fluorophores is their applicability as therapeutic drugs for forthcoming photodynamic therapy of the lesions induced in the gastrointestinal tract.

Different mechanisms solely and in combination for evaluation of the joint impact of bioenvironmental factors (stress, *Helicobacter pylori*, exotoxins in the food, water, soil and air) were applied to induce gastrointestinal tract (GIT) neoplasia in rats. The transformation of damaged areas of the stomach mucosa into malignancies in all parts of gastrointestinal tract were detected initially using fluorescence detection technique using excitation at 405 nm. Histological analysis of all suspicious areas investigated spectroscopically was made as well and used as a “gold standard” for comparison with the optical results received.

Exogenous fluorescence detection of photosensitizers - 5-aminolevulinic acid/ protoporphyrin IX (5-ALA/PpIX), zinc phthalocyanine (ZnPc) and galactose- zinc phthalocyanine (GalZnPc) was used. Fluorescent maps of different organs (liver, spleen, lungs, brain) were developed as well – to evaluate the distribution of the photosensitizers in the whole body on the second hour after photosensitizer application. 5-ALA was applied per os on a dose of 20 mg/kg, and phthalocyanines were applied intravenously on a dose of 1 mg/kg. Fiber-optic probe was used to measure all organs investigated. Fluorescence spectra were detected by microspectrometer USB4000 (OceanOptics Inc., USA), and FS405 LED source on 405 nm (Polironik Ltd., Russia) was used as excitation source.

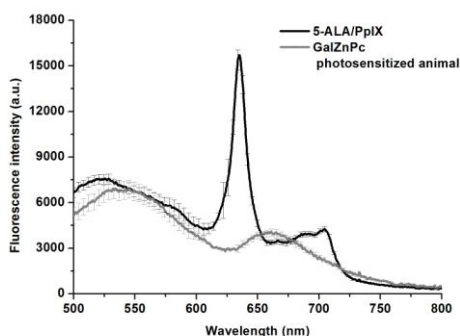


Fig. 1. Fluorescence spectra of photosensitized rats with 5-ALA/PpIX and GalZnPc. Spectral region 500-600 nm is related to mucosal autofluorescence of the stomach, Maxima at 635 and 704 nm are associated to 5-ALA/PpIX signal and maximum at 680-685 nm is associated with phthalocyanine signal.

Acknowledgments: The work was supported by the bilateral project, funded by NSF-MES-Bulgaria and RFBR-Russia “Development of new optical technologies for improvement of diagnostics quality of gastric cancer”-2016 and by project #DFNI-B02/9/2014 “Development of biophotonics methods as a basis of oncology theranostics”,

## Fluorescence imaging for stem cell research and tissue engineering

E. Zagaynova<sup>1</sup>, A. Meleshina<sup>1</sup>, D. Kuznetsova<sup>1</sup>, O. Rogovaya<sup>2</sup>, V. Dudenkova<sup>1</sup>,

S. Roddimova<sup>1</sup>, M. Sirotkina<sup>1</sup>, E. Vorotelyak<sup>1,2</sup>

<sup>1</sup> Privolzhsky Research Medical University; 603005 Nizhny Novgorod, Minin and Pozharsky Square, 10/1

<sup>2</sup> Koltzov Institute of Developmental Biology of Russian Academy of Sciences; 119334 Moscow, Vavilova St., 26

<sup>3</sup> Pirogov Russian National Research Medical University; 117997 Moscow, Ostrovityanova St., 1

*e-mail: [ezagaynova@gmail.com](mailto:ezagaynova@gmail.com)*

Regenerative medicine includes two main fields: cell therapy and tissue engineering. For cell therapy doctors and researchers strongly needed: label free analysis of stem cells differentiation state before transplantation, estimation of regenerative potential of organ before cell therapy or stimulation regeneration. For tissue engineering there are also some main tasks: estimation of tissue equivalent before transplantation: matrix and cells differentiation, noninvasive diagnosis of tissue formation in the body and estimation of seeded cells function.

To solve these problems we used some fluorescence imaging techniques: laser scanning microscopy (Zeiss 580) with FLIM module (Becker and Hickl), Multiphoton tomography (MPT Flex) and Optical coherence tomography (OCT). Such unique techniques allow to visualize the individual cells embedded in the constructs, their migration, proliferation, and also to study the cell differentiation processes. The study of the epigenetic mechanisms of stem cell (mesenchymal stromal cells (MSC), induced pluripotent stem cells (iPS)) differentiation is an actual problem. So using fluorescence lifetime imaging microscopy (FLIM) the metabolic switch from glycolysis to oxidative phosphorylation was shown during MSC differentiations by the lifetimes changing of NAD(P)H. A cholestatic liver disease presents one of the most common liver diseases and can potentially progress to cirrhosis or even cholangiocarcinoma. Conventional techniques are insufficient to precisely describe the complex internal structure, heterogeneous cell populations and the dynamics of biological processes of the liver. Multiphoton and FLIM microscopy do not need additional staining of samples or the incorporation of any markers to study metabolism, lipid composition, microstructure analysis, evaluation of fibrous structures. These parameters have pronounced changes in hepatocytes of liver with common pathological diseases. Thereby in this study we investigated metabolic changes in the healthy and cholestatic liver based on the fluorescence of the metabolic co-factors NAD(P)H and FAD by multiphoton microscopy combined with FLIM. The data can be used to develop new criteria for the identification of hepatic pathology at the level of hepatocyte changes directed to personalized medicine in the future.

Despite the significant progress in developing of skin equivalents (SEs) a problem of non-invasively assessing the quality of the cell components and the collagen structure of living SEs both before and after transplantation remains. Using the methods of optical coherence tomography, multiphoton tomography and FLIM, the structure and quality of dermal SEs before transplantation, and remodeling of collagen matrix and microcirculation in the wound healing after dermal SEs transplantation were studied. Thus, the methods of optical imaging and genetic labeling are a powerful tool for the solving a huge number of problems in both the tissue engineering and the biomedicine in general.

This work has been financially supported by Russian Foundation of Basic Research (grants No. 15-29-04851).

# Optical properties of rat brain tissue in the normal state and at the different stages of glioma development

**Elina A. Genina<sup>1,2</sup>, Alexey N. Bashkatov<sup>1,2</sup>, Daria K. Tuchina<sup>1,2</sup>, Polina A. Timoshina<sup>1,2</sup>,  
Oxana V. Semyachkina-Glushkovskaya<sup>1</sup>, Valery V. Tuchin<sup>1-3</sup>**

*1- Saratov State University, Astrakhanskaya str. 83, 410012 Saratov, Russia*

*2 - Tomsk State University, Lenin's av. 36, 634050 Tomsk, Russia*

*3 - Institute of Precision Mechanics and Control RAS, Rabochaya str. 24, 410028 Saratov, Russia*

*eagenina@yandex.ru*

Glioma is a type of tumor that occurs in the brain and spinal cord. Gliomas are one of the most common types of primary brain tumors [1]. For diagnostics of low grade glioma, the detailed knowledge about optical parameters in the different stages of development of the malignancy is important. However, in literature there is lack of information on optical properties of gliomas. The absorption coefficients of paraffin-embedded mice brain glioma and normal brain tissues have been measured in the terahertz spectral range, 0.2- to 2.0-THz [2]. The absorption coefficient, the scattering coefficient, and anisotropy factor of a human glioma have been calculated in the range from 350 to 1100 nm [3, 4]. Light penetration depth in this spectral range has been evaluated in Ref. [4]. The absorption and transport scattering coefficients of intracranial glioma in rats at some wavelengths in the visible range have been presented in Ref. [5].

In this paper, we are presenting results of measurements of optical parameters (diffuse reflectance and total transmittance) of brain tissues in healthy rats and rats with model glioma (7, 10, and 30 days) which were performed using a UV-3600 spectrophotometer (Shimadzu, Japan) with an integrating sphere of LIRS-3100 in the spectral range of 350-2500 nm. Basing on the measured parameters, the values of the absorption coefficient and the transport scattering coefficient of the tissues were reconstructed.

It was obtained that the 10-days development of glioma led to the increase in the absorption coefficient, which was associated with the water content increasing in the tumor. However, further development of the tumor (formation of the necrotic nucleus) led to the decrease in the water content and the corresponding decrease in the absorption coefficient. The dependence of the transport scattering coefficient on the different grades of glioma was more complex. Light penetration depth in the healthy brain and in tumor was evaluated.

[1] C.J. Fisher and L. Lilge, Photodynamic therapy in the treatment of intracranial gliomas: a review of current practice and considerations for future clinical directions, *Journal of Innovative Optical Health Sciences*, vol. 8(1), 1530005, (2015).

[2] K. Meng, T.-N. Chen, T. Chen, L.-Q. Zhu, Q. Liu, Z. Li, F. Li, S.-C. Zhong, Z.-R. Li, H. Feng, and J.-H. Zhao, Terahertz pulsed spectroscopy of paraffin-embedded brain glioma, *J. Biomed. Opt.*, vol. 19(7), 077001, (2014).

[3] H.-J. Schwarzmaier, F. Eickmeyer, V.U. Fiedler, and F. Ulrich, Basic principles of laser induced interstitial thermotherapy in brain tumors, *Medical Laser Application*, vol. 17, pp. 147-158, (2002).

[4] H.J.C.M. Sterenborg, M.J.C. van Gemert, W. Kamphorst, J.G. Wolbers, and W. Hogervorst, The spectral dependence of the optical properties of human brain, *Lasers Med. Sci.*, vol. 4, pp. 221-227, (1989).

[5] M. Sibai, C. Fisher, I. Veilleux, J.T. Elliott, F. Leblond, D.W. Roberts, B.C. Wilson, Preclinical evaluation of spatial frequency domain-enabled wide-field quantitative imaging for enhanced glioma resection, *J. Biomed. Opt.*, vol. 22(7), 076007, (2017).

# Quantitative techniques for extraction of blood oxygenation from multispectral optoacoustic measurements

V. Perekatova<sup>1</sup>, M. Kirillin<sup>1</sup>, D. Loginova<sup>1</sup>, A. Orlova<sup>1</sup>, I. Turchin<sup>1</sup>, P. Subochev<sup>1</sup>

1- Institute of Applied Physics, Russian Academy of Sciences, 46 Ulyanov Street, Nizhny Novgorod 603950, Russia

V. Perekatova: ValeriyaPerekatova@gmail.com

Biomedical optoacoustic (OA) or photoacoustic imaging is a hybrid modality combining the benefits of optical contrast and ultrasonic resolution. Due to high absorption of blood in visible range as compared to surrounding biotissues OA imaging is efficient for *in vivo* angiography [1, 2]. However, functional information provided by multispectral optoacoustic measurements of blood oxygen saturation is rather more important, as it significantly broadens the range of biomedical optoacoustic applications. Two approaches to reconstruct the oxygen saturation value from OA measurements can be highlighted, both based on differences in absorption spectra of oxy- and deoxyhemoglobin.

The first, traditional approach is based on extraction of blood oxygenation from OA signal amplitudes in blood vessels acquired at multiple optical wavelengths [3]. As long as OA pressure is proportional to the optical fluence at a given point that depends on the wavelength of the laser illumination, this approach requires the account for the optical fluence distribution in biotissue. Since the value is extracted from the resultant OA image, the algorithms for acoustic and optical reconstruction and precise calibration of the whole system should be applied prior to saturation determination.

To perform acoustic reconstruction from raw OA B-scan we use a reconstruction algorithm comprising improved synthetic aperture focusing technique (SAFT) algorithm [4] accounting for both the spatial response of the acoustic antenna and the spatial distribution of optical fluence. For optical fluence compensation we employ 3D Monte Carlo code previously customized for simulation of light transport in medium with optical properties typical for biotissues accounting for complex geometry of OA system illumination unit [5]. The proposed technique of combined SAFT and fluence compensation was employed for both phantom objects and *in vivo* imaging demonstrating significant enhancement of image quality.

The second approach to saturation determination is based on evaluation of the OA signal effective attenuation coefficient  $\mu_{\text{eff}}(\lambda)$  in given blood-containing vessel at multiple probing wavelengths [6]. This calibration-free method demands for broadband registration of OA pulses including low frequency band. Wideband ultrasonic detectors based on polyvinylidene difluoride (PVDF) films are beneficial for these measurements [7].

The first approach was employed for *in vivo* 2D OA measurements in rat, and reconstructed distribution of optical absorption  $\mu_a$  allowed to differentiate between artery and vein.

The second approach was initially applied for phantom experiment employing estimations of  $\mu_{\text{eff}}(\lambda)$  of OA signal in the blood *in vitro* in the range of 532-1064 nm. The *in vitro* results demonstrated the potential of wideband (0.1-50 MHz) PVDF ultrasonic detector for calibration-free quantitative optoacoustic measurements of  $\mu_{\text{eff}}(\lambda)$ , since the results of 1D OA measurements were in agreement with gold standard spectrophotometry measurements of the same diluted blood sample. The second approach was also tested at two 3D OA data sets, which were consecutively acquired from the superficial vasculature of the rabbit ear *in vivo* at 532 nm and 1064 nm wavelengths. Both approaches allowed to differentiate between artery and vein in full agreement with anatomical data.

The work was supported by the Russian Science Foundation, project no. 14-15-00709-II.

[1] P. Subochev, A. Orlova, E. Smolina, A. Kirillov, N. Shakhova, I. Turchin, Raster-scan optoacoustic angiography reveals 3D microcirculatory changes during cuffed occlusion, *Laser Physics Letters*, vol. 15, pp. 045602 (2018).

[2] X. L. Deán-Ben and D. Razansky, Functional optoacoustic human angiography with handheld video rate three dimensional scanner, *Photoacoustics*, vol. 1, pp. 68-73, (2013).

[3] Z. Guo, C. Favazza, A. Garcia-Urbe, L.V. Wang, Quantitative photoacoustic microscopy of optical absorption coefficients from acoustic spectra in the optical diffusive regime, *Journal of Biomedical Optics*, vol. 17, pp. 0660111-0660116 (2012).

[4] C.-K. Liao, M.-L. Li, and P.-C. Li, Optoacoustic imaging with synthetic aperture focusing and coherence weighting, *Optics letters*, vol. 29, pp. 2506-2508, (2004).

[5] M. Kirillin, V. Perekatova, I. Turchin, and P. Subochev, Fluence compensation in raster-scan optoacoustic angiography, *Photoacoustics*, vol. 8, pp. 59-67, (2017).

[6] J. Laufer, C. Elwell, D. Delpy, P. Beard, In vitro measurements of absolute blood oxygen saturation using pulsed near-infrared photoacoustic spectroscopy: accuracy and resolution, *Physics in medicine and biology*, vol. 50, pp. 4409 (2005).

[7] P. Subochev, M. Prudnikov, V. Vorobiev, A. Postnikova, E. Sergeev, V. Perekatova, A. Orlova, V. Kotomina, I. Turchin, Wideband linear detector arrays for optoacoustic imaging based on polyvinylidene difluoride films, *Journal of Biomedical Optics*, in press (2018).

## Is it possible to combine photodynamic therapy and application of dinitrosyl iron complexes in the wound treatment?

**Anna B. Solovieva, Anatoly F. Vanin, S.F. Timashev**

*N.N.Semenov Institute of Chemical Physics, 4 Kosygin St., Moscow, 119991, Russia  
ann.solovieva@gmail.com*

The interest to short-living biologically active simple molecules, in particular, to nitric oxide and reactive oxygen species (ROS) arises from the fact that such substances perform a function of regulators at different levels of live species organization [1]. Nitric oxide is a multifunctional signal molecule controlling intra- and intercellular processes in animal, bacterial and plant organisms and having both promoting (regulatory, protective) and inhibiting effects on the metabolism [2]. In turn, ROS are necessary components of the cell life activity and of an organism as a whole and in fact comprise a separate system in a body, participating both in a number of physiological functions and in many pathological processes. The most important ROS are superoxide radical  $O_2^{\bullet-}$ , singlet oxygen  $^1O_2$ , hydroxyl  $OH^{\bullet}$  and peroxide  $H_2O_2$  radicals, hydrogen peroxide  $H_2O_2$ , peroxide ion  $HO_2^-$ , hypochlorite  $HOCl$ . The average ROS concentration in human tissues is 8–10 mM [3]. Since ROS photogeneration represents a basis for oxidative destruction of pathological cells and tissues (malignant and benign tumors, purulent wounds, trophic ulcers) upon photoexcitation of a photosensitizer administered to a lesion (photodynamic therapy, PDT), a new possibility arises for the search of PDT combination with the DNIC action. This work is dedicated to the consideration of some aspects of ROS interaction with nitric oxide derivatives. We analyze a possibility of the simultaneous application of effects of singlet oxygen (produced in the conditions of photoexcitation of porphyrin photosensitizers (PPS)) with DNIC and nitrosogluthatione effects. We have studied the effect of interactions between dinitrosyl iron complexes with thiol-containing ligands (DNIC-TL) and diglucamine salt of chlorine e6 (photoditazine, PD) on the rate of photosensitized oxidation of a model organic substrate – tryptophan – in the presence and absence of an amphiphilic polymer, Pluronic F127, as well as on the DNIC-TL and PD photostability. Using EPR and UV spectroscopy, we determined the rate constants for photodegradation of mono- and dinuclear DNIC-TL and PD, respectively. The presence of the photosensitizer and Pluronic F127 has been shown to have a negligible effect on the rate of photodestruction of mono- and dinuclear DNIC-TL, taking into account the changing DNIC-TL and PD concentrations in the photoexcitation conditions. At the same time, in the DNIC-TL presence, the rate of PD photodestruction increases, however, addition of Pluronic 127 leads to a decrease in the rate constant of PD photodestruction. The latter circumstance creates an opportunity for a simultaneous application of DNIC-TL and photodynamic therapy in the wound treatment without losing the PDT efficiency. We believe that the results of this study open new opportunities in antimicrobial photodynamic therapy, since they uncover the conditions in which the application of photosensitizers in the solubilized state (provided by polymer surfactants, in particular, Pluronic F127) efficient in the treatment of complicated wounds [28] may be combined with the application of DNIC without the loss of the PDT efficiency.

This work was supported by Russian Scientific Foundation (Grant No.16-10295, preparation of dinitrosyl iron complexes and kinetics of photodestruction of PD and mono- and dinuclear DNIC forms) and Russian Foundation for Basic Research (Grant No. 17-02-00294, kinetics of tryptophan photooxidation).

1. A.F.Vanin. Dinitrosyl-iron complexes with thiol-containing ligands. Physicochemistry, biology, medicine. M., Izhevsk. 2015, 219P.
2. Murad F. Discovery of some of the biological effects of nitric oxide and its role in cell signaling. Biosci Rep 1999; 19: 133-154.
3. Magder Sheldon. Reactive oxygen species: toxic molecules or spark of life? // Crit. Care. 2006. Vol. 10:208 (doi:10.1186/cc3992).

# Imaging through reconnectable fiberscopes for *in vivo* deep-brain endoscopy

**M.S. Pochechuev<sup>1,2,3</sup>, I.V. Fedotov<sup>1,2,3,4</sup>, O.I. Ivashkina<sup>1</sup>, A.B. Fedotov<sup>1,2,3,4</sup>, K.V. Anokhin<sup>1</sup> and A.M. Zheltikov<sup>1,2,3,4,5</sup>**

1- Kurchatov Institute National Research Center, pl. akad. Kurchatova 1, Moscow 123182, Russia

2- Physics Department, International Laser Center, M.V. Lomonosov Moscow State University, Moscow 119992, Russia

3- Russian Quantum Center, ul. Novaya 100, Skolkovo, Moscow Region, 143025 Russia

4- Kazan Quantum Center, A.N. Tupolev Kazan National Research Technical University, Kazan, Russia,

5- Department of Physics and Astronomy, Texas A&M University, College Station, TX 77843, USA

Author e-mail address: matveymoo@mail.ru

Fiber-based methods are widely used in modern neurosciences [1,2]. They allow cell specific optogenetic stimulation and fluorescence detection in freely moving animals, helping correlate neural activity and animal behaviour. While single-core fibers provide averaged information about a region of interest, bundles of optical fibers enable fluorescence imaging [3] and spatially selective photoactivation [4] in freely behaving mice.

In this work, image formation using reconnectable fiber bundles is studied theoretically and experimentally. The concept of reconnectable fiberscopes [5] is an extension of the idea of reconnectable implantable single-fiber optical neurointerfaces [6,7]. Because it is practically impossible to accurately position thousands of cores of two multicore fibers in order to effectively couple them, random connection is used. It is shown, that connection of two multicore fibers with random relative orientation and lateral shift leads to appearance of moire patterns (Fig 1A, B). These patterns are similar to undersampling artifacts and can lead to wrong interpretation of biological images when background signal and noise are high. To suppress the artifacts, a transparent spacer is placed between two randomized multicore fibers. This results in decreased amplitude of artifacts, while preserving the optical resolution, measured as visibility of simulated grid with 10  $\mu\text{m}$  period (Fig. 1C). Resolution and field uniformity in single fiber bundle and reconnectable fiber bundles modalities are compared. Suitability of the proposed method for fluorescence microscopy *in vivo* is analyzed and a special case of calcium imaging is discussed.

This work was funded by RFBR according to the research project № 18-32-00892.

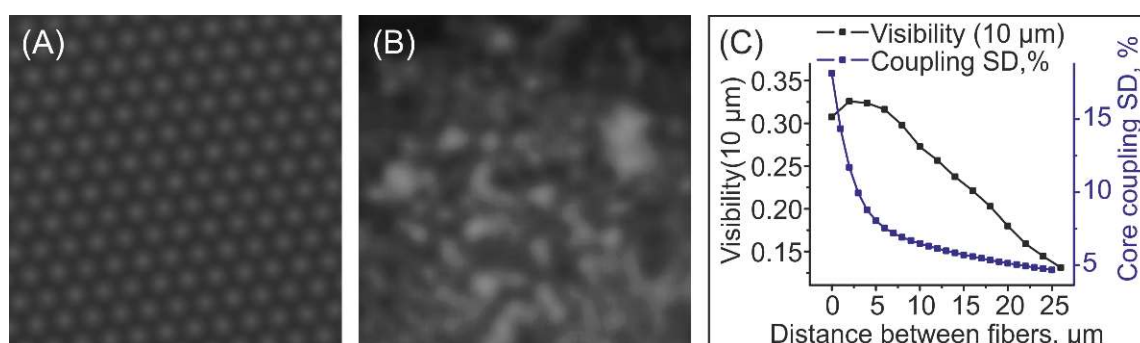


Fig. 1. Moire patterns appearing when two regular (A, simulation) and randomized (B, experiment) multicore fibers are connected. (C) Increasing distance between fibers reduces randomness (standard deviation) in core to core coupling, while preserving 10  $\mu\text{m}$  grid visibility.

[1] E.S. Boyden et al. "Millisecond-timescale, genetically targeted optical control of neural activity," *Nature Neuroscience* 8, 1263–1268 (2005).

[2] I. Diester et al. "An optogenetic toolbox designed for primates," *Nature Neuroscience* 14, 387–397 (2011).

[3] P. Vincent et al. "Live imaging of neural structure and function by fibred fluorescence microscopy," *EMBO Rep.* 7, 1154–1161 (2006).

[4] V. Szabo, C. Ventalon, V. De Sars, J. Bradley, V. Emiliani, *Neuron* 2014, 84, 1157

[5] M.S. Pochechuev et al. "Reconnectable fiberscopes for chronic *in vivo* deep-brain imaging," *Journal of Biophotonics*, 2017.

[6] D.R. Sparta et al. "Construction of implantable optical fibers for long-term optogenetic manipulation of neural circuits," *Nature Protocols* 7, 12–23 (2012).

[7] G.D. Stuber et al. "Excitatory transmission from the amygdala to nucleus accumbens facilitates reward seeking," *Nature* 475, 377–380 (2011).

# Thyroid nodule capsules: structural characterization with texture analysis of second harmonic generation images

**R. Hristu<sup>1</sup>, B. Paun<sup>2</sup>, L. Eftimie<sup>1,3</sup>, S.G. Stanciu<sup>1</sup>, G. A. Stanciu<sup>1</sup>**

*1- Center for Microscopy-Microanalysis and Information Processing, University Politehnica of Bucharest, 313 Splaiul Independentei, 060042, Bucharest, Romania*

*2- Faculty of Automation and Computer Science, Technical University of Cluj-Napoca, 26-28 George Baritiu St, 40002, Cluj-Napoca, Romania*

*3- Central University Emergency Military Hospital, Pathology Department, 134 Calea Plevnei, 010825, Bucharest, Romania*

*radu.hristu@physics.pub.ro*

Despite their low incidence rate, thyroid carcinomas represent nonetheless a challenging problem as their differentiation from the much more frequent benign pathologies is often times difficult. This is also related to the fact that the vast majority of thyroid nodules are benign, and only a small percentage of thyroid lesions that come to medical attention are malignant. Consequently, diagnostic approaches that can differentiate between malignant and benign thyroid nodules in a quantitative manner would be of great benefit for addressing thyroid related pathologies.

In this study we have used quantitative second harmonic generation (SHG) microscopy [1] to investigate collagen organization in the fibrillar capsules of human benign and malignant thyroid nodules. By combining SHG microscopy with quantification parameters for image texture analysis provided by the histogram analysis, gray level co-occurrence matrix, fractal analysis and Helmholtz analysis applied on the collagenous capsule surrounding the thyroid gland, follicular adenoma as benign pathology and papillary thyroid carcinoma as malignant pathology, we were able to differentiate between capsules surrounding benign and malignant nodules. Our findings indicate that SHG microscopy can provide quantitative information about the collagenous capsule surrounding both the thyroid and thyroid nodules, which may complement current histopathology and cytopathology procedures for thyroid cancer diagnosis.

[1] R. Hristu, S. G. Stanciu, D. E. Tranca, G. A. Stanciu, Improved quantification of collagen anisotropy with polarization-resolved second harmonic generation microscopy, *Journal of Biophotonics*, vol. 10(9), pp. 1171-1179 (2017).

# Nonlinear Microscopy Imaging of Stroma Reorganization in Breast Lesions

**E.Sergeeva<sup>1</sup>, V.Dudenkova<sup>2</sup>, M.Kirillin<sup>1</sup>, S.Kuznetsov<sup>2</sup>, M.Pavlov<sup>2</sup>,  
N.Orlinskaya<sup>2</sup>, and N.Shakhova<sup>1</sup>**

*1- Institute of Applied Physics RAS, Nizhny Novgorod, Ulyanov str., 46, Russia*

*2- Privolzhskiy Research Medical University, Nizhny Novgorod, Russia*

[sea@ufp.appl.sci-nnov.ru](mailto:sea@ufp.appl.sci-nnov.ru)

Breast cancer and benign pathologies are the leading case of lesions in women worldwide. Recent trends in breast lesion diagnostics are aimed at immediate characterization of large volumes of tissue at cellular level, which first of all allows for intraoperative resection line monitoring during organ-preserving surgeries. Currently, optical biopsy techniques are showing high potential in distinguishing various tissue pathologies without additional staining, thus providing the advantage of a time-saving diagnostic tool. Among such techniques is nonlinear microscopy (NLM) which allows for imaging tissue stroma structure by second harmonic generation (SHG) in collagen and two-photon autofluorescence (TPAF) of elastin [1]. Though NLM provides rather limited information on tumor cells themselves, it can be anyway used for distinguishing breast pathologies due to the fact that benign and malignant pathologies of breast are always accompanied by changes in stroma organization [2].

In our study we used NLM to image fresh biopsy samples of breast tissue in norm and pathology. Biopsy specimens were obtained during planned diagnostic procedures and imaged without staining within 60 minutes after dissection. Visualization setup included Carl Zeiss laser scanning microscopy system based on inverted microscope with 1.3-NA oil-immersion objective and a Mai Tai HP pulsed femtosecond laser operating at the wavelength of 800 nm. Registration of tissue nonlinear response was performed in spectral ranges of 370-420 nm (SHG by collagen) and 460-660 nm (TPAF of elastin and, in some cases, cells). After NLM, the samples were sent to histological examination with hematoxylin&eosin staining as well as specific stroma staining (Van Gieson's staining, Mallory's staining). Stroma organization is characterized by fibers orientation, thickness and concentration. We demonstrate that stroma organization in normal tissue significantly differs from that in fibroadenoma (benign breast lesion) and cancer. In order to design an algorithm for breast tissue pathologies differentiation, development of numerical criteria based on the above-mentioned parameters (alignment, thickness and concentration of fibers) was initiated. To evaluate the degree of collagen disorganization in various pathologies, we performed 2D Fourier transformation of SHG images. Collagen disorganization factor (CDF) ranging from 0 to 1 was calculated as the inverse aspect ratio of the transformed images indicating tendency to alignment (CDF=0) or to randomization (CDF=1) of collagen fibers. Combination of CDF with the information on fibers thickness makes it possible to construct an algorithm for discrimination of cancer from fibrous and normal breast tissue.

This study was supported by Russian Foundation for Basic Research (grants 16-02-00974 and 18-42-520041).

[1] M. Weinigel, H. Breunig, A. Uchugonova, K. König Multipurpose nonlinear optical imaging system for in vivo and ex vivo multimodal histology, *Journal of Medical Imaging*, 2(1), 016003 (2015).

[2] A. G. Clark and D. M. Vignjevic, Modes of cancer cell invasion and the role of the microenvironment, *Current Opinion in Cell Biology*, 36, 13-22 (2015).

# Monte Carlo-based dual-wavelength PDT planning

**D.A. Loginova<sup>1</sup>, A.V. Khilov<sup>1</sup>, E.A. Sergeeva<sup>1</sup>, M.Yu. Kirillin<sup>1</sup>**

*1 - Institute of Applied Physics RAS, Nizhny Novgorod, Russia*

*Main author email address: [vekfy@inbox.ru](mailto:vekfy@inbox.ru)*

Photodynamic therapy (PDT) is a photochemistry-based treatment technique that is widely used in different medical areas including oncology, dermatology and otolaryngology. The PDT procedure includes injection of a photosensitizer (PS), which is accumulated selectively in tissues with increased circulatory activity, such as tumors, and its subsequent activation by light irradiation at a certain wavelength. Photochemical reactions initiated as a result of the procedure are accompanied by the release of cytotoxic products, such as singlet oxygen, causing cell death [1]. Chlorin-based PS with two absorption peaks at 402 and 662 nm provide possibility for dual-wavelength PDT performance consisting in combination of PDT treatment effects at two wavelengths [1].

The efficacy of PDT procedure depends on several parameters including PS in-tissue distribution and the light dose absorbed during the procedure. Light propagation in tissue is determined by its local optical properties which differ for various wavelengths within one tissue types and vary from patient to patient. To achieve an optimal effect of PDT treatment it is important to perform an appropriate procedure planning accounting the patient individual features and character of light propagation at different wavelengths, thus, implementing the principles of personalized medicine and dual-wavelength PDT.

In this work we suggest an approach to planning dual-wavelength PDT treatment procedure based on Monte Carlo modeling of light propagation in tissue in combination with optical properties reconstruction modalities. Modeling was performed in the context of 405 and 660 nm corresponding to the wavelengths of the radiation sources used in the PDT procedure with chlorin-based PS.

Monte Carlo technique implies modeling of a large number of random photon trajectories in turbid media followed by statistical processing. In this study a custom developed MATLAB-based implementation of Monte Carlo algorithm was employed simultaneously processing  $10^7$  photon trajectories. As a result of Monte Carlo simulation, absorbed light dose maps were derived for given parameters, such as the initial PS concentration and the total light dose, and uneven in-tissue distribution of PS. The maps allow to analyze the distribution of the absorbed dose over depth and estimate the treatment area (Fig.1).

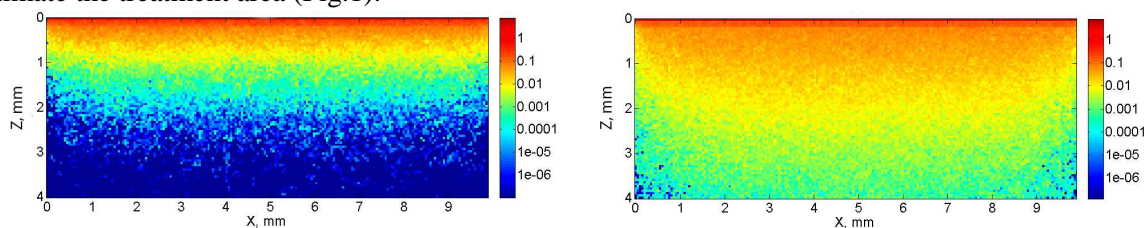


Fig.1. Distribution maps of absorbed light dose density for skin at a wavelength of 405 nm (left) and 660 nm (right).

For Monte Carlo modeling the exact optical properties of the studied tissue is of great importance. In this work two methods for optical properties reconstruction are suggested. The first one consists of *in vitro* spectrophotometric measurements of the transmitted and reflected radiation followed by optical properties reconstruction by means of Monte Carlo-based lookup table. The second one is based on *in vivo* measurements using optical diffusion reflectometry with employment of structured illumination and approximation of experimental intensity profiles with an analytic function.

The study is supported by Russian Science Foundation, project 17-15-01264.

# Acousto-optical laser beam shaping for design of an annular optical trap

**K.B. Yushkov, V.Ya. Molchanov**

*National University of Science and Technology MISIS, 4 Leninsky Prospekt, Moscow 119049, Russia*

*konstantin.yushkov@misis.ru*

Optical traps and tweezers are used for precise microparticle manipulation with the main application in biophotonics. A simple optical trap contains one laser beam tightly focused by a large-NA lens. Multiple-spot traps can be obtained by time-domain sharing of the laser beam. More complicated trapping fields are achieved by means of diffractive optics, e.g. using digital holography.

In this report we propose a novel concept of using a noncollinear acoustooptical tunable filter (AOTF) as a spatial beam shaping device for obtaining an annular trap. The symmetry of the AOTF transfer function is used to provide a ring-shaped intensity distribution. This research demonstrates the first application of noncollinear AOTFs for direct  $k$ -space laser beam shaping and its application to optical trapping.

Noncollinear AOTFs can be used for spatial filtering of light beams and visualization of phase objects [1-3]. Transfer function of an AOTF has a ring shape with variable diameter depending on the frequency of ultrasound as shown in Fig. 1. This feature is used to provide annular trapping field with variable diameter in the focal plane of a microscope objective.

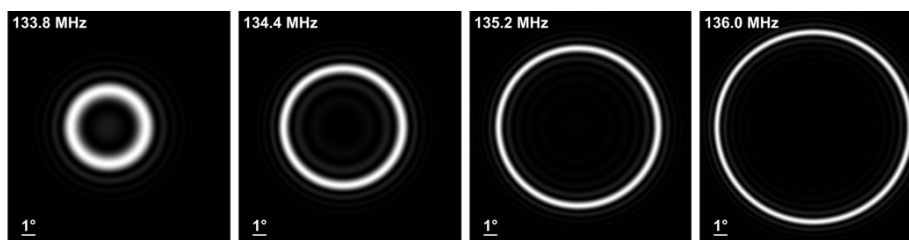


Fig. 1. Transfer function of a noncollinear acousto-optical tunable filter. The scale bar shows angle in the air at the AOTF output.

The prototype of the optical trap has been built with a 532 nm laser (Coherent Inc., Verdi V-5) and a custom-built paratellurite AOTF (Acousto-Optical Research Center, MISIS). Operating frequency of the AOTF was  $\sim 135$  MHz. The optical scheme (Fig. 2) consists of a laser, a Keplerian telescope for beam diameter adjustment, a focusing lens converting spatial field distribution into the  $k$ -space, an AOTF as a tunable spatial filter, a relay lens scaling the diffracted field, and a large-NA microscope objective lens. Thus, direct shaping of the beam angular spectrum by the AOTF is converted into spatial shaping at the focal plane of the objective lens.

Switching between different diameters of the trapping field ring can be performed with 100 kHz rate. A method to adjust instantaneous ring width and synthesize simultaneous multiple rings is developed based on tailored chirped-waveform controlling of the AOTF.

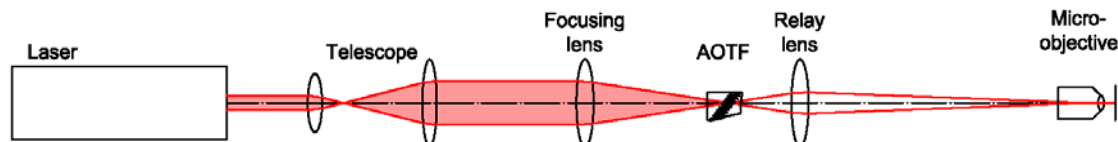


Fig. 2. A setup for annular beam shaping

The research was supported by the RFBR (Project 18-07-00674) and by the Ministry of Education and Science of the Russian Federation (Project 02.A03.21.0004 / Grant K2-2017-079).

[1] K.B. Yushkov and V.Ya. Molchanov, Hyperspectral imaging acousto-optic system with spatial filtering for optical phase visualization, *Journal of Biomedical Optics*, vol. 22, p. 066017 (2017).

[2] V.I. Balakshy, Acousto-optic visualization of optical wavefronts, *Applied Optics*, vol. 57, pp. C56-C63 (2018).

[3] K.B. Yushkov, V.Ya. Molchanov, and V.I. Balakshy, Acousto-optical transfer functions as applied to laser beam shaping [Invited paper], *Proc. SPIE*, vol. 10744 (2018).

## Self-assessed photothermal agents based on Ho,Tm:KLu(WO<sub>4</sub>)<sub>2</sub> nanocrystals

**Albenc Nexha, Joan J. Carvajal, Maria Cinta Pujol, Francesc Díaz, Magdalena Aguiló**

*Universitat Rovira i Virgili, Departament Química Física i Inorgànica, Física i Cristal·lografia de Materials i Nanomaterials (FiCMA-FiCNA) – EMaS, Campus Sescelades, E-43007, Tarragona,*

*Spain*

*albenc.nexha@urv.cat*

Short-wavelength infrared (SWIR) emissions of Ho<sup>3+</sup> and Tm<sup>3+</sup> doped lutetium double tungstate are being investigated as basis for a potential luminescent nanothermometer to be used in biomedical applications. Working in this region of the electromagnetic spectrum where scattering of light is reduced, while absorption from biological tissues is moderate, allows for higher penetration depths. These luminescent nanothermometers also release heat due to the energy transfer processes between the two ions and the non-radiative relaxation processes generated using the phononic structure of the material, becoming efficient photothermal agents. Thus, by combining these two properties, we can develop photothermal agents in which the temperature that they reach can be controlled by the emission generated by themselves, constituting in this case self-assessed photothermal agents.

KLu<sub>1-x-y</sub>Ho<sub>x</sub>Tm<sub>y</sub>(WO<sub>4</sub>)<sub>2</sub> nanocrystals with different molar concentrations were synthesized via the modified sol-gel Pechini method, using ethylenediaminetetraacetic acid (EDTA) as the chelating agent, and polyethyleneglycol (PEG) (MW=400g/mol) as the esterification agent. Different doping levels were implemented with the goal to determine the optimal ratio for maximizing the intensity of their optical emission, but at the same time, equilibrate the intensity of the emissions arising from the two ions in the SWIR region. The other goal was to maximize the photothermal conversion efficiency of the photothermal agents.

The KLu<sub>1-x-y</sub>Ho<sub>x</sub>Tm<sub>y</sub>(WO<sub>4</sub>)<sub>2</sub> nanocrystals exhibit a monoclinic structure and an irregular morphology, with a crystalline size of ~100 nm.

The nanocrystals were excited at 808 nm and the photoluminescence spectrum in the SWIR region consisted of three main manifolds: <sup>3</sup>H<sub>4</sub>→<sup>3</sup>F<sub>4</sub> (1.45 μm) and <sup>3</sup>F<sub>4</sub>→<sup>3</sup>H<sub>6</sub> (1.8 μm) of Tm<sup>3+</sup> and <sup>5</sup>I<sub>7</sub>→<sup>5</sup>I<sub>8</sub> (1.96 μm) of Ho<sup>3+</sup>.

The temperature dependency evolution of the three emissions was recorded in the physiological range of temperatures from 293-333K displaying a significant slope for the intensity ratio of the bands located at 1.45μm/1.96μm and 1.8μm/1.96μm as the temperature increased, for which the highest relative thermal sensitivity was obtained for the doping level of x=0.01 and y=0.1 with a value of 0.92% K<sup>-1</sup> (R<sup>2</sup>=0.98) and the lowest relative thermal sensitivity 0.07% K<sup>-1</sup> (R<sup>2</sup>=0.88) for x=0.075 and y=0.05.

With these particles it was possible to monitor the increase of temperature induced *ex-vivo* in chicken breast meat, with an experimental thermal resolution of ~ 0.5 K, below the theoretical value of 0.8 K predicted for particles operating in this spectral region, and at a penetration depth of at least 0.5 cm. These results demonstrate that KLu<sub>1-x-y</sub>Ho<sub>x</sub>Tm<sub>y</sub>(WO<sub>4</sub>)<sub>2</sub> nanocrystals might be a potentially efficient photothermal agent.

# Diffuse optical spectroscopy monitoring of experimental tumor oxygenation during growth and under treatment

**A.G. Orlova<sup>1</sup>, A.V. Maslennikova<sup>1,2</sup>, G.Yu. Golubiatnikov<sup>1</sup>, M.Yu. Kirillin<sup>1</sup>,  
M.S. Kleshnin<sup>1</sup>, Yu.P. Ivanova<sup>3</sup>, and I.V. Turchin<sup>1</sup>**

*1- Institute of Applied Physics RAS, 46 Ulyanov Street, Nizhniy Novgorod, Russia*

*2- Privolzhskiy Research Medical University, 10/1 Minin & Pozharsky sq., Nizhny Novgorod, Russia*

*3- Lobachevsky State University of Nizhny Novgorod, 19 Gagarin Avenue, Nizhniy Novgorod, Russia*

*orlova@ufp.appl.sci-nnov.ru*

Tumor oxygen state is considered to be one of the key factors affecting the malignant tumor prognosis and treatment effectiveness [1]. Estimation of tumor oxygenation in the course of therapy may be of great importance for treatment efficiency control. Besides, the effects of oxygen modifiers aimed at hypoxia suppression are to be monitored. The goal of the current study was to monitor the oxygenation of experimental tumor models during their natural growth and to study the biological effects of different types of therapy and oxygen-modifying. Diffuse optical spectroscopy (DOS) was employed for *in vivo* assessing the tumor oxygenation in course of treatment. This technique is capable to provide information concerning the concentration of hemoglobin and blood oxygen saturation [2].

Two DOS modalities were used for experiments. The first modality is a frequency domain system with parallel plane geometry and three probing wavelengths, allowing for whole-tumor imaging and mapping of main tissue chromophores concentrations. The second modality is a continuous wave fiber probe based system in reflectance configuration, that provides fast measurement of diffuse optical spectra in a single area of animal body surface. The experiments were carried out on white outbred rats, as well as balb/c and balb/c-nude mice. Pliss's lymph sarcoma (PLS) of rats, murine colon carcinoma (CT26), and human breast adenocarcinoma (SKBR-3) transplanted subcutaneously were used as tumor models. Cyclophosphan in the dose of 50 mg/kg was used for chemotherapy, single-dose irradiation in the dose of 10 Gy for radiation therapy, and oxygen modifier pentoxifylline (Ptx) in the dose of 10 mg/kg for improvement of tumor microcirculation.

DOS allows observing the dynamics of tissue oxygen saturation in the process of tumor natural growth, as well as after different treatment approaches. In the course of a natural growth, tumors demonstrated a pronounced decrease of blood saturation [3]. Radiation and chemotherapy cause the increase of the blood oxygen saturation. Such effect may be explained by inhibition of tumor cells division and their death, decrease in interstitial pressure leading to increased oxygen availability, decrease in oxygen consumption, and improvement of oxygen supply of the tumor [4, 5]. Ptx treatment also induces substantial raise of blood oxygen saturation [6], probably due to enhancement of the capillary blood content and increase in the oxygen supply to tissues.

Our research demonstrated the capabilities of the DOS modalities for *in vivo* noninvasive monitoring of experimental tumors, for estimation of their blood oxygen saturation level in response to chemotherapy, radiotherapy and oxygen-modifiers action. This method may be employed both in experimental oncology for development of new approaches to cancer treatment and in clinical practice for investigation of tumor oxygenation dynamics in course of therapy.

This work was supported by Russian Foundation for Basic Research (project No. 15-29-04884).

[1] P. Vaupel, Hypoxia and aggressive tumor phenotype: implications for therapy and prognosis, *Oncologist*. 13(suppl. 3), 21–26, (2008).

[2] T. Durduran, R. Choe, W.B. Baker and A.G. Yodh, Diffuse optics for tissue monitoring and tomography, *Rep. Prog. Phys.*, 73, 076701, (2010).

[3] A. Orlova, M. Kirillin, A. Volovetsky, et al., Diffuse optical spectroscopy monitoring of oxygen state and hemoglobin concentration during SKBR-3 tumor model growth, *Laser Phys. Lett.*, 14, 015601 (2016).

[4] H. Poptani, N. Bansal, W.T. Jenkins, et al., Cyclophosphamide Treatment Modifies Tumor Oxygenation and Glycolytic Rates of RIF-1 Tumors: <sup>15</sup>C Magnetic Resonance Spectroscopy, Eppendorf Electrode, and Redox Scanning, *Cancer Res.*, 63(15), 8813-8820, (2003).

[5] N. Crokart, B.F. Jordan, C. Baudelet, et al., Early reoxygenation in tumors after irradiation: determining factors and consequences for radiotherapy regimens using daily multiple fractions, *Int. J. Radiation Oncology Biol. Phys.*, 3, 901–910, (2005).

[6] T.I. Kalganova, A.G. Orlova, G.Yu. Golubiatnikov, et al., Dynamic influence of pentoxifylline on the oxygen status of Pliss's lymph sarcoma in rat, *Frontiers of Optoelectronics*, 10(3), 317-322, (2017).

# Estimation of photosensitizer penetration depth with dual-wavelength fluorescence imaging prior to PDT procedure with chlorin-based photosensitizers

**A.V. Khilov<sup>1</sup>, M.Yu. Kirillin<sup>1</sup>, D.A. Loginova<sup>1</sup>, and I.V. Turchin<sup>1</sup>**

*1 - Institute of Applied Physics RAS, Nizhny Novgorod, Russia*

*Main author email address: alhil@inbox.ru*

Photodynamic therapy (PDT) is a modern technique proved as a highly efficient antitumor and antibacterial treatment method [1]. PDT is based on the light absorption by fluorescent photosensitizers (PS) inducing generation of singlet oxygen. Thus, PDT can be treated as a theranostics technique when the applied agents serve both for diagnostic and treatment purposes. The evaluation of the in-depth distribution of PS in tissue is of high importance both for PDT planning and performance.

Previously the ratio of fluorescence signals registered at different emission wavelengths was shown to allow evaluating the depth of fluorescent object localization [2]. Employment of chlorin-based PS provides additional benefits due to two pronounced peaks in the fluorescence excitation spectrum at 402 and 662 nm. The difference in tissue optical properties and PS absorption at these wavelengths allows evaluating PS penetration depth via probing the tissue with different excitation wavelengths [3].

We present numerical model of fluorescence response of PS distributed within the superficial tissue layer based on Monte Carlo (MC) simulation for multispectral PS excitation. The method for the estimation of PS penetration depth based on fluorescence signals ratio (FSR) analysis is proposed.

Previously reported MC algorithm for multi-layered media was applied for simulation of fluorescence signals. In MC simulations, the tissue was divided into two layers while PS was assumed to be distributed uniformly in the top layer only. The first step was the calculation of the absorption map for planar wave irradiation. At the second step the absorption map was employed as the source of fluorescence emission for calculation of fluorescence response at tissue surface. The procedure was performed for both excitation wavelengths of 662 nm and 402 nm. PS penetration depth can be estimated upon the analysis of FSR corresponding to 662 nm and 402 nm.

In order to confirm the results of MC simulations, a phantom experiment was designed. Agar biotissue phantoms were prepared consisting of water, 20% Lipofundin and red ink ("Koh-I-Noor", Czech Republic) to ensure optical properties close to that of biotissues. Fluorescent phantoms were prepared the same way with the addition of chlorin-based PS "Revixan" (Revixan-Derma, Russia) in concentration typical for PS accumulation in tissues. Optical properties of phantoms were measured by spectrophotometry approach and employed for MC simulations. Fluorescence images during phantom experiment were obtained with an in-house fluorescence imaging device [4] equipped with two LED sources at  $405\pm 10$  nm and  $660\pm 10$  nm for two-wavelength PS excitation synchronized with the CCD camera.

The results of MC simulations were in good agreement with experimental data. It was shown that FSR can serve as an indicator fluorescent layer thickness. The comparison of the results of MC modeling with phantom experiment proved the proposed approach to be sensitive to the PS-containing layer thickness in the range below 3 mm; this limit is determined by tissue optical properties and PS concentration. It was demonstrated that FSR is quite stable to variations in tissue optical properties. FSR increases both for the increase in tissue optical properties (absorption and scattering) and the increase in PS concentration in PS-containing layer. FSR variations remained within  $\pm 10\%$  while tissue optical properties were varied within  $\pm 30\%$ .

The study is supported by Russian Science Foundation, project 17-15-01264.

[1] J. P. Celli et al., Imaging and photodynamic therapy: mechanisms, monitoring and optimization, *Chem. Rev.* 110, 2795–2838 (2010).

[2] J. Svensson, and S. Andersson-Engels, Modeling of spectral changes for depth localization of fluorescent inclusion, *Optics Express* 13(11), 4263-4274 (2005).

[3] A. V. Khilov et al., Two-wavelength fluorescence monitoring and planning of photodynamic therapy, *CTM* 9(4), 96–105 (2017).

[4] M. S. Kleshnin et al., Compact and fully automated system for monitoring photodynamic therapy, based on two LEDs and a single CCD, *Laser Phys. Lett.* 12, 115602 (2015).

# Optical Spectroscopy of Rare Earth Vanadates for Temperature Sensors Based on Green Down and Up-conversion Emissions

**N. Bhirir<sup>1,2\*</sup>, M. Dammak<sup>2</sup>, M. C. Pujol<sup>1</sup>, J. J. Carvajal<sup>1</sup>, M. Aguiló<sup>1</sup>, F.c Díaz<sup>1</sup>**

*1- Universitat Rovira i Virgili, Departament de Química Física i Inorgànica, Física i Cristal·lografia de Materials i Nanomaterials (FiCMA-FiCNA) and EMaS, Marcel·li Domingo 1, Tarragona, 43007, Spain*

*2- Université de Sfax, Laboratoire de Physique Appliquée, Groupe de Physique des matériaux luminescents, Faculté des Sciences de Sfax, Département de Physique, BP 1171, Université de Sfax, 3018 SFAX, Tunisie. Main author email address: bhirinisin92@gmail.com*

The non-contact thermometry methods based on the fluorescence intensity ratio (FIR) approach between two thermally adjacent emitting energy levels have garnered lots of attention and have widely developed in view of their unique advantages; sufficient accuracy, and simplicity of readout and calibration [1]. The sensing medium usually used are the lanthanide ( $\text{Ln}^{3+}$ ) ion-doped materials and the triply ionized erbium ( $\text{Er}^{3+}$ ) is the most suitable one for optical thermometry in the visible due to its intense two green emission bands arising from the two thermally coupled levels  ${}^2\text{H}_{11/2}$  and  ${}^4\text{S}_{3/2}$  which may be populated under either down-conversion (DC) or up-conversion (UC) excitation mechanism [2-3]. In this work,  $\text{Er}^{3+}$  /  $\text{Er}^{3+}$ - $\text{Yb}^{3+}$  doped / co-doped  $\text{GdVO}_4$  microcrystals have been synthesized by high temperature solid-state reaction.  $\text{Er}^{3+}$ - $\text{Yb}^{3+}$ : $\text{GdVO}_4$  nanocrystals have also been synthesized by a hydrothermal procedure. The X-ray diffraction patterns indicated that the obtained materials were pure tetragonal phase. The photoluminescence thermometric behavior under DC and UC processes have been studied using the self-referenced fluorescence intensity ratio technique in the whole temperature of 300-453 K. The calculated temperature sensitivity values of the as-prepared vanadates showed high and similar sensitivities for the microcrystals ranging from 1.08 to 0.90%  $\text{K}^{-1}$ . While, for 1 at.% Er, 20 at.% Yb:  $\text{GdVO}_4$  nanocrystals, it found to be 0.55%  $\text{K}^{-1}$ . Compared to other  $\text{Er}^{3+}$  single doped and  $\text{Er}^{3+}$ / $\text{Yb}^{3+}$  pair doped materials [4-6], the analyzed materials acquired excellent results that reveals their potential applications as optical thermometer.

This work also aims to discriminate in the different performance of these luminescent thermometers in terms of thermal sensitivities and temperature uncertainties when operated under conditions of Stokes or anti-Stokes emissions.

- [1] C.D.S. Brites, A.Millán, L.D. Carlos, Lanthanides in Luminescent Thermometry, Handbook on the Physics and Chemistry of Rare Earths, 49, pp. 339-427, (2016).
- [2] H. Zheng, B. Chen, H. Tu, J. Zhang, J. Sun, X. Li, M. Sun, B. Tian, S. Fu, H. Zhong, B. Dong, R. Hua, H. Xia, Microwave-assisted hydrothermal synthesis and temperature sensing application of  $\text{Er}^{3+}/\text{Yb}^{3+}$  doped  $\text{NaY}(\text{WO}_4)_2$  microstructures, J. Colloid and Interface Science, 420, pp. 27-34, (2014).
- [3] W. Cheng, Z. Jia-Zhong, X. Hai-Ping, F. Zhi-Gang, J. Dong-Sheng, Z. Jian, G. Xue-Mei, Z. Jian-Li, J. Hao-Chuan, C. Bao-Jiu, Cooperative downconversion of  $\text{Er}^{3+}/\text{Yb}^{3+}$  co-doped- $\text{NaYF}_4$  single crystals, Optik, 127, pp. 2608-2612, (2016).
- [4] O. A. Savchuk, J. J. Carvajal, C. Cascales, M. Aguiló, F. Díaz, ACS Applied Materials and Interfaces, 8, pp. 7266-7273, (2016).
- [5] T. V. Gavrilovic, D. J. Jovanovic, V. Lojpur, M. D. Dramicanin, Sci Rep-Uk, 4, (2014).
- [6] W. Xu, X.Y. Gao, L.J. Zheng, P. Wang, Z.G. Zhang, W.W. Cao, Optical Thermometry through Green Upconversion Emissions in  $\text{Er}^{3+}/\text{Yb}^{3+}$ -Codoped  $\text{CaWO}_4$  Phosphor Applied Physics Express, 5, pp. 72201-72203, (2012).

# Determination of stress-related characteristics of blood vessels using endoscopic optical coherence elastography

A. Potlov, S. Frolov, S. Proskurin<sup>1</sup>

Tambov State Technical University

<sup>1</sup>spros@tamb.ru

Endoscopic optical coherence tomography (OCT) is modification of OCT method characterized by removable sample arm, which is made as endoscopic probe [1-4]. Endoscopic OCT, as well as classical OCT, has harmless near-infrared radiation and a micron spatial resolution. However, endoscopic OCT can be used not only for obtaining structural images, but also to obtain Doppler images and elasticity maps. The purpose of this work is to increase the efficiency and reliability of determination of the stress-related properties for soft biological tissues, such as blood vessels [2, 4].

Structural OCT images of the blood vessel wall at the moments of systole and diastole were obtained using endoscopic OCT system with forward-side probe. Structural images were filtered in the temporal and frequency domains for noise removal. Then, the displacements (figure 1) of the internal structures on the OCT images were estimated using sets of the pairs of test points [2].

The Young's modulus and Poisson's ratio were determination using classical equations. At that, normal component of the deforming force was approximately calculated as difference in systolic and diastolic pressure. Longitudinal and transversal displacements of the internal structures of the blood vessel were calculated as projections of displacement vectors for each pair of test points per ordinate and per abscissa axis, respectively [2].

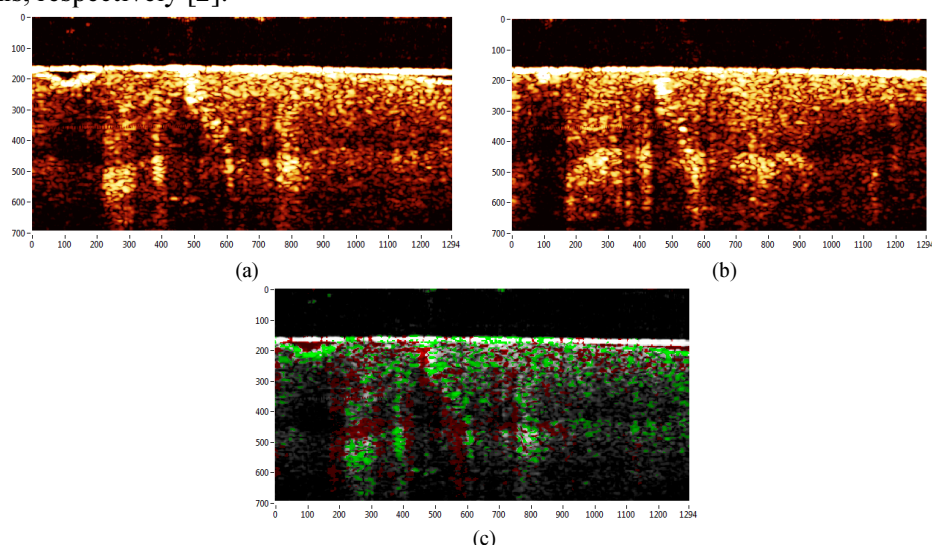


Figure 1 Structural OCT images of soft biological tissue phantom before (a) and after (b) the compression and cumulative displacements on OCT images (c)

Thus, the original method for increasing the efficiency and reliability [4] of the stress-related properties evaluation for blood vessels using endoscopic OCT is proposed. Key feature of the described method is application of a pulse wave as a deforming force. A series of experiments with blood vessel phantoms [3] have demonstrated good agreement of evaluated stress-related properties with the real clinical data [2, 4].

This work was supported by Russian Science Foundation (Project 16-15-10327).

- [1] S. Wang and K.V.Larin, Optical coherence elastography for tissue characterization: a review, *Journal of Biophotonics*, Vol. 8, Is. 4, pp. 279-302 (2015).
- [2] S.V. Frolov, A.Yu. Potlov and S.V. Sindeev, Selection of flow-diverter stent models using optical coherence tomography and mathematical modeling of hemodynamics, *Biomedical Engineering*, Vol. 51, Is. 6, pp. 381-384 (2018).
- [3] B.W. Pogue and M.S. Patterson, Review of tissue simulating phantoms for optical spectroscopy, imaging and dosimetry, *Journal of Biomedical Optics*, Vol. 11, Is. 4, No. 041102 (2006).
- [4] A.Yu. Potlov, S.V. Frolov and S.G. Proskurin, An algorithm for improving the quality of structural images of turbid media in endoscopic optical coherence tomography, *Optical Technologies in Biophysics and Medicine XIX - Proceedings of SPIE*, Vol. 10716, No. 1071609 (2018).

## **Application of laser scanning confocal fluorescent microscopy for visualization microglia morphology in mouse local cerebral ischemia**

Glyavina M.M.<sup>1,3</sup>, Loginov P.A.<sup>1</sup>, Dudenkova V.V.<sup>2</sup>, Shirokova O.M.<sup>1</sup>, Reunov D.G.<sup>2</sup>, Karpova A.O.<sup>1,3</sup>, Prodanets N.N.<sup>1</sup>, Korobkov N.A.<sup>3</sup>, Zhuchenko M.A.<sup>4</sup>, Mukhina I.V.<sup>1,3</sup>

*1- Central Research Laboratory of the Privolzhsky Research Medical University, Russian Federation, Nizhny Novgorod, Gagarin Avenue 70*

*2- Institute of Biomedical Technologies, Privolzhsky Research Medical University, , Russian Federation, Nizhny Novgorod, Gagarin Avenue 70*

*3 - Department of neurotechnology, Institute of biology and biomedicine, Lobachevsky State University, Russian Federation, Nizhny Novgorod, Gagarin Avenue 23-1*

*4 - Faculty of Applied Mathematics and Control Processes, Saint Petersburg State University, Russian Federation, Saint Petersburg, Peterhof, Universitetskii Avenue 35*  
*4- PHARMAPARK LLC, Moscow, Russia.*

*mariyannov@gmail.com*

Microglia is a unique example of immunocompetent cell in central nervous system that is capable protecting the brain from ischemic injury. One of microglia membrane's receptors is common receptor subunit ( $\beta$ -cR), which in the presence of a ligand can form a dimeric complex with erythropoietin. Carbamylated darbopoietin (CdEPO) (PHARMAPARK LLC, Moscow) was used as an agonist for this receptor. Laser radiation is used to image the dynamic of changing microglia morphological phenotypes. The objective of this work is to study the proportion of microglia phenotype and their morphological characteristic after of the middle cerebral artery occlusion (MCAO) and CdEPO treatment, because this is important for assessing the development of ischemic damage. The report presents the results of microglia phenotype distribution in the somatosensory cortex of the mouse brain in the early postischemic period in the MCAO model.

One-hour exposure on C57BL/6 mice was proceeded by a 7-0 microfilament (Doccol Corporation) under isoflurane anesthesia. CdEPO was injected intravenously in 1, 3, 6, 12, 24, 48 hours after OCMA at 50 mkg/kg. Locomotor activity and work memory was studied with Open Field LE800S test and Shuttle Box LE916. Brain is fixed in 4% paraformaldehyde (PFA). Microglia was marked with primary Iba-1 antibodies (Rabbit polyclonal) and secondary antibody with fluorescent agant AlexaFluor 555. Visualization was carried out by a ZEISS LSM 880 laser scanning confocal fluorescents microscope with an 40x immersion objective and a yellow-green spectrum filter. Paraffin coronal sections of the brain (5  $\mu$ m thick) were studied. The images were processed using ImageJ and Python 3 software.

The somatosensory cortex is studied on the 4th day after the ischemia. The number of microglial cells in the zone with ischemic damage decreased in control group. In the group with CdEPO injection there is an opposite situation: number of microglial cells approximated the intact values. The area of microglial cells decreased on the 4th day after the MCAO in the control group and in the group with injection of CdEPO. On the 4th day after MCAO, there was a decline in the number of ramified microglia in the control group as well as in generation of active and amoeboid microglia in both hemispheres. In the group with CdEPO injection, the number of resting microglia had not changed but the amount of activated microglia increased. Change in microglia phenotypes and their morphology characteristic proportion in the group with CdEPO injection correlated with improved functional state of the animals after one-hour exposure: their motor activity restored, stress level decreased and their memory was preserved. The ongoing research on regulation of microglia phenotypes proportion with CdEPO allows considering it as a promising neuroprotector giving a positive impact on the organism recovery in early post-ischemic period.

The reported study was funded by RFBR according to the research project № 18-34-00877

# Upconversion luminescent nanoparticles for tumor visualisation

**I. Yanina<sup>1,2</sup>, N. Navolokin<sup>3</sup>, E. Sagaydachnaya<sup>1</sup>,  
V. Kochubey<sup>1,2</sup>, V. Tuchin<sup>1,2,4</sup>**

<sup>1</sup> - Saratov State University (National Research University), Research-Educational Institute of Optics and Biophotonics, 83 Astrakhanskaya str., Saratov 410012, Russia

<sup>2</sup> - Tomsk State University (National Research University), Interdisciplinary Laboratory of Biophotonics, 36 Lenin's av., Tomsk 634050, Russia

<sup>3</sup> - Saratov State Medical University, Department of Pathological Anatomy, 112 B Kazachaya str., Saratov 410012, Russia

<sup>4</sup> - Institute of Precision Mechanics and Control RAS, Laboratory of Laser Diagnostics of Technical and Living Systems, 24 Rabochaya, Saratov 410028, Russia

e-mail: irina-yanina@list.ru

The upconversion nanoparticles (UCNPs) hold promise as novel luminescent probes for numerous applications in nanobiophotonics [1,2]. Small size of UCNPs enables the particles to bypass the biological barriers, thus allowing deep tissue penetration and the accumulation of the particles in a number of organs. In addition, particles are known to possess high surface chemical reactivity as well as a large surface-to-volume ratio, which may seriously affect their biocompatibility [3]. UCNPs can be used both as biosensors for temperature control and for monitoring the state of the tissue. The aim of the work was to develop a method for targeted delivery of UCNPs in the tumor biological tissue with thermal control.

0.5 mL of 25% tumor cell suspension of alveolar liver cancer — cholangiocarcinoma PC-1, obtained from the bank of tumor strains of Russian Cancer Research Center n.a. N.N. Blokhin (Moscow, Russia), was implanted subcutaneously in rats. When the tumor reached a diameter of  $3 \pm 0.3$  cm, the animals were randomly divided into three groups (6 rats in each group): group 1 without any exposure (control group), group 2 with intratumoral administration UCNPs and laser irradiation of the tumor (see Fig.1), group 3 with intratumoral administration of conjugate of UCNPs with folic acid and laser irradiation of the tumor. Prior to any medical procedure or treatment, the rats were anaesthetized with Zoletil 50 (Virbac, France) in dose of 0.05 mg/kg.

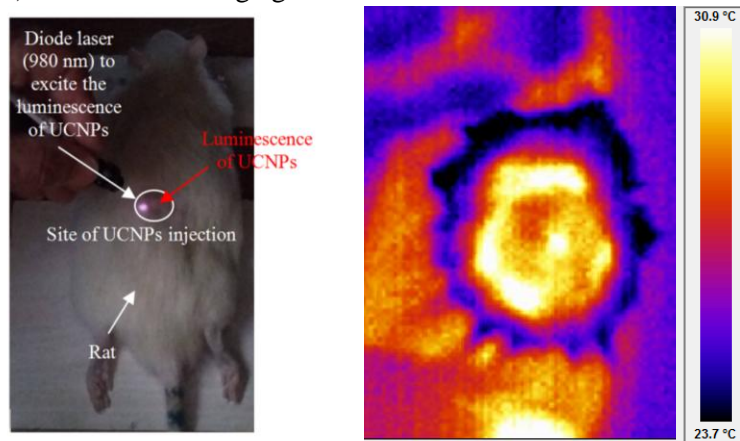


Fig. 1. Experimental animal and obtained thermal field in cancer region after UCNPs injection.

It was found that inflammatory reaction is developing in the skin when UCNPs are introduced. The particles do not diffuse and dissolve, but remain at the introduction site.

[1] D. Dong, L. Zheng, L. Sun, Z. Zhang, and C.-H. Yan, Lanthanide Nanoparticles: From Design toward Bioimaging and Therapy, *Chemical Reviews*, vol. 115, no. 19, pp.10725–10815, (2015).

[2] K. Y. Dong, S. N. Sitansu, K. Kwangmeyung and T. S. Subramanian, Recent progress in nanotechnology for stem cell differentiation, labeling, tracking and therapy, *J. Mater. Chem. B*, vol. 5, pp. 9429-9451, (2017).

[3] I. Yu. Yanina, E. K. Volkova, E. A. Sagaidachnaya, N. A. Navolokin, D. A. Mudrak, A. M. Zakharevich, V. I. Kochubey, V. V. Tuchin, Interaction of upconversion luminescent nanoparticles with tissues and organs, *Proc. SPIE. Biophotonics: Photonic Solutions for Better Health Care VI*, vol. 10685, pp. 106852X-1-10 (2018).

# Autofluorescence differentiation of lower gastrointestinal tract benign and malignant lesions using synchronous spectroscopy technique

**Ts. Genova<sup>1</sup>, E. Borisova<sup>1,2</sup>, N. Penkov<sup>3</sup>, B. Vladimirov<sup>3</sup>, Al. Zhelyazkova<sup>1</sup>, L. Avramov<sup>1</sup>**

<sup>1</sup>*Institute of Electronics, Bulgarian Academy of Sciences, 1784 Sofia, Bulgaria*

<sup>2</sup>*Interdisciplinary Center of Critical Technologies in Medicine, Saratov State University, Saratov, Russian Federation*

<sup>3</sup>*University Hospital "Tsaritsa Yoanna-ISUL", 1527 Sofia, Bulgaria  
ts.genova@gmail.com*

The current status of autofluorescence spectroscopy in clinical diagnostics of gastrointestinal cancer is of a "red flag" technique. Since it has the potential of painless, rapid and sensitive diagnostic technique, its further implementation as a stand-alone diagnostic modality is quite desirable. However it requires improvement of the existing equipment and more precise diagnostic indicators. In order to define more reliable diagnostic criteria for differentiation between cancerous and healthy tissue we have focused on the investigation of fluorescence spectral peculiarities of lower tract gastrointestinal of benign, pre-cancerous and cancerous tissues that could be diagnostically valuable, specific and lead to accurate differentiation between cancerous and healthy tissue.

Ex vivo samples of healthy and abnormal tissues originating from different parts of the lower gastrointestinal tract (GIT) were examined through synchronous fluorescence spectroscopy. Tissue samples were excised during standard surgical procedure for tumour removal and transported in safe-keeping solution and isothermal conditions. Synchronous fluorescence spectroscopy (SFS) allows observation of tissue autofluorescence with reduced maxima overlapping and enables the evaluation of specific spectral peculiarities that could be diagnostically valuable in a manner superior to standard fluorescence spectroscopy [1]. This method is based on simultaneous scan with a constant shift on both excitation and emission wavelengths. In our study the excitation was the reference in the range of 280-720nm and the constant offset varied in the range of 10-280 nm with step of 10 nm. Particularly the SFS for offsets of 60nm, 90nm and 120nm, which consist of diagnostically meaningful endogenous fluorophores were evaluated not only for comparison between cancerous and healthy tissue but also for precancerous abnormal tissues and lesions from different parts of the lower GIT.

The primary difference between the lesions emission was contributed to their stage of development and not on their side of origin in the GIT. The comparison between the fluorescence characteristics of healthy, precancerous and cancerous tissues demonstrate gradual alteration towards typical for cancer fluorescence hallmarks.

Acknowledgments: This work was carried out in the frames of projects #DNTS/Russia 01/7-23/06/2017 "Development of new optical technologies for improvement of diagnostics quality of gastric cancer" and #DFNI-B02/9/2014 "Development of biophotonics methods as a basis of oncology theranostics" of NSF-MES.

[1] Q. Liu, G. Grant and T. Vo-Dnh, Investigation of Synchronous Fluorescence Method in Multicomponent Analysis in Tissue, IEEE J SEL TOP QUANT 16(4), 927 (2010).

## Photoacoustic spectroscopy in human space application

C. Achim (Popa)<sup>1</sup>, M. Mogildea<sup>2</sup>, G. Mogildea<sup>3</sup>, A. M. Bratu<sup>4</sup>, M. Petrus<sup>5</sup>

1- National Institute for Laser, Plasma and Radiation Physics, 409 Atomistilor St., PO Box MG-36,  
077125, Romania

2-Institute of Space Science, 077125, Bucharest, Romania

*cristina.achim@inflpr.ro*

The role of oxidative stress (OS) and antioxidants in cardiovascular adaptation to space flight is currently being studied on International Space Station (ISS) [1-7].

The study was initiated on ISS in September 2013 and aims to accomplish this goal, evaluating oxidative damage during flight by measuring biomarkers of blood and urine [2,4] as indicators of lipid peroxidation (LP) and DNA damage.

OS is a multifaceted issue and represents a social and health care problem because it affects many systems. At astronauts can accelerate the atherosclerosis, the risks of kidney stones, acceleration of age-related changes similar to osteoporosis, impact muscles and also can change the cardiovascular physiology [1-4].

A new way to measure noninvasively OS in humans is to measure free radical damage by analyzing early byproducts of oxidation like exhaled hydrocarbons (e.g. ethylene). Among the health care approaches of NASA and ESA our research can give an important contribution, the main objective being the research in the possibility of the application of an instrument in the analysis of breath gases at astronauts [1-4].

With the advantages of high sensitivity and accuracy, photoacoustic spectroscopy (PAS) has been proven to be one promising sensing technology for trace gas recognition. Such instrument can be realized using an innovative, sensitive trace gas detection platform based on photoacoustic spectroscopy [5-7].

In this research, a tunable PAS experimental system based on a CO<sub>2</sub> laser was proposed for detection of different gases. Relationships between the PA signal and gas pressure, laser power and ethylene gas concentration were measured and discussed in detail, respectively [5-7].

### Acknowledgments

We acknowledge the financial support of the Space Technology and Advanced Research-ESA, project (C3 2016) no. 153, ID. 603 „Development of an Instrument for Monitoring of the Astronauts Health” (Acronym: IMAH).

[1]. Jeffery C. Chancellor, Graham B. I. Scott, Jeffrey P. Sutton, *Life (Basel)*, 4(3): 491–510, (2014).

[2]. <<http://www.nasa.gov/feature/nasa-nsbri-select-proposals-to-support-astronaut-health-on-long-duration-space-exploration>>

[3]. Versari S, Longinotti G, Barenghi L, Maier JA, Bradamante S., *FASEB J*.27(11):4466-752013(2013).

[4]. [http://www.nasa.gov/mission\\_pages/station/research/news/heart\\_health\\_cardio\\_ox](http://www.nasa.gov/mission_pages/station/research/news/heart_health_cardio_ox)

[5]. A. M. Bratu, M. Petrus, C. Popa, *Microchemical Journal* 138, 203–208, (2018).

[6]. D. C. Dumitras, D. C. Dutu, C. Matei, A. M. Magureanu, M. Petrus, C. Popa, *JOAM*, Vol 9, No. 12, pp: 3655-3701 (2007).

[7]. C. Popa, “Human respiration in wavelengths”, ISBN: 978-3-659-61401-9, LAP Lambert Academic Publishing (2014).

# **Optical monitoring of fluorescent glioma progression and blood-brain barrier permeability**

**A.Terskov<sup>1</sup>, M.Klimova<sup>1</sup>, A.Dubrovskij<sup>1</sup>, A. Khorovodov<sup>1</sup>, A.Mamedova<sup>1</sup>, A.Namykin<sup>1</sup>,  
N.Navolokin<sup>2</sup>, A.Shirokov<sup>3</sup>, O.Semyachkina-Glushkovskaya<sup>1</sup>.**

*1 - 83 Astrakhanskaya street, Saratov State University, 410012, Russia*

*2 - 112 Bolshaya Kazachya street, Saratov State Medical University, 410010, Russia*

*3 - 13 Prospekt Entuziastov, Institute of Biochemistry and Physiology of Plants and Microorganisms, Russian Academy of Sciences (IBPFM RAS), 410049, Russia*

*terskow.andrey@gmail.com*

Malignant gliomas are highly invasive tumors that use cerebral vessels for invasion due to high vascular fragility of the blood-brain barrier (BBB). On one hand, glioma is characterized by the BBB disruption, on the other hand, drug brain delivery via the BBB is a big challenge in glioma therapy. The limited information about vascular changes associated with glioma growth is a reason of slow progress in prevention of glioma development.

Here we present *in vivo* and *ex vivo* study of the BBB disruption and glioma cell (GC) migration in rats using fluorescence and confocal microscopy. We discovered a local breach in the BBB in the main tumor mass but not within the border of normal and malignant cells (GCs), where the BBB was impermeable for high weight molecules. The migration of GC observed via the cerebral vessels with the intact BBB and macrophages infiltration was found around tumor mass.

The mechanisms underlying glioma progression remain unknown but there is evidence that the sympathetic nervous system via activation of vascular beta2-adrenoreceptors (B2-ADRs) can play an important role in tumor metastasis. Our results clearly show an increase in the expression of vascular B2-ADRs and production of the beta-arrestin-1 – co-factor of B2-ADRs signaling pathway in rats with glioma. Pharmacological blockade of B2-ADRs reduces the BBB disruption, macrophages infiltration, GCs migration and increases survival rate.

These data suggest that the blockade of B2-ADRs may be a novel adjuvant therapeutic strategy to reduce glioma progression and prevent metastasis.

The research was supported by grant of Russian Science Foundation № 17-75-20069.

## **Optical monitoring of brain clearing via the meningeal lymphatics**

**M. Klimova 1, A. Abdurashitov 1, D. Bragin 2, O. Bragina 2, A. Dubrovsky1, O. Semyachkina-Glushkovskaya 1.**

*1 - 83 Astrakhanskaya street, Saratov State University, 410012, Russia*

*2-University of New Mexico School of medicine, Department of Neurosurgery, Albuquerque*

*mari-1997@mail.ru*

The meningeal lymphatic vessels were discovered three years ago as the drainage system involved in mechanisms underlying the clearance of brain from waste products but extremely limited information about mechanisms underlying these processes.

To answer the question: "What are mechanisms underlying brain clearing?", we created the innovative approaches for in vivo monitoring of brain clearing in mice from substances coming to the brain through the opening of blood-brain barrier (BBB) using optical coherent tomography (OCT), confocal and two-photon imaging.

We showed that the opening of BBB is accompanied by the brain clearing from dextran and gold nanoparticles, which crossed the BBB, via the meningeal lymphatic vessels and then accumulated in the deep lymph nodes (during 5 min) in the neck as a first anatomical station for the exit of cerebrospinal fluid from the brain to the peripheral lymphatics.

We first demonstrate successful application of OCT for imaging of changes in the meningeal lymphatic vessels after opening of BBB that might be a new useful strategy for non-invasive analysis of effectiveness of lymphatic drainage in daily clinical practice.

The research was supported by grant of Russian Science Foundation № 17-75-20069.

# **The study of the lymphatic system using optical coherence tomography by means of analyzing the accumulation of gold nanorods in the deep lymph node of a laboratory mouse**

**Dubrovskiy A., Abdurashitov A., Shushunova N., Semyachkina-Glushkovskaya O.**

*3<sup>rd</sup> year student, Bachelor's program "Biotechnical systems and technologies", Saratov Chernyshevsky State University*

*flat 12, 99/109a Chapaeva st., Saratov, Russia*

*paskalkamal@mail.ru*

Optical coherence tomography (OCT) is a method for studying weakly scattering layered objects, which is based on the principles of low-coherence interferometry, using broadband radiation sources. The OCT method works on ballistic photons that have experienced a single scattering at the interface between two media with different refractive indexes. Multiple scattering significantly reduces the depth of sounding and degrades the signal-to-noise ratio.

The lymphatic system plays the key role in the fluid drainage in the peripheral blood circulation. Despite discovery of the meningeal lymphatic vessels, the role of this lymphatic system in brain cleansing remains unknown.

In our studies we used the commercial OCT Thorlabs GANYMEDE and gold nanorods as a contrast agent for dynamic visualization of lymphatic vessels. Two distinct accumulation dynamics were clearly visible during the experiment, within the first ten minutes there was a significant increase in the average OCT signal and the second stage was a slow growth with a lower coefficient.

In sum, our results clearly show that the meningeal lymphatics is pathway for brain fluid drainage and clearing. The gold nanorods as good contrast agents for optical imaging of the meningeal lymphatic system in the near infrared range.

The research was supported by grant of Russian Science Foundation № 17-75-20069.

## 2-photon polymerization of the polylactide acrylate derivatives for preparation of 3D structures for regenerative medicine

**N.A. Aksenova<sup>1,2</sup>, V.T. Shashkova<sup>1</sup>, I.A. Matveeva<sup>1</sup>, N.N. Glagolev<sup>1</sup>, N.V. Minaev<sup>3</sup>,  
T.S. Zarkhina<sup>1</sup>, P.S. Timashev<sup>1,2,3</sup>, A.B. Solovieva<sup>1</sup>**

*1 - N.N. Semenov Institute of Chemical Physics, Russian Academy of Sciences, 119991, Russian Federation, Moscow, ul.Kosygina, 4*

*2 - Institute for Regenerative Medicine, Sechenov University, 119991, Russian Federation, Moscow, Trubetskaya ul., 8*

*3 - Institute of Photonic Technologies, Research center "Crystallography and Photonics", 108840, Russian Federation, Troitsk, Moscow, Pionerskaya ul., 2*

*E-mail: naksenova@mail.ru*

Poly lactides (PLA) are biodegradable polymers which are widely used in two most important spheres of the mankind activities – medicine and environmental protection<sup>1</sup>. In particular, bone-plastic mineral-filled composites for implantology are made on the polylactide basis, primarily, for creation of artificial joints or their parts (for example, in the maxillofacial osteoplastics). The duration of their degradation is one to five years, depending on the molecular weight and porosity of the polymer. The use of PLA and their copolymers in the tissue engineering is of particular interest, primarily, in the bone tissue engineering, in which a 3D structure is formed from a biodegradable material, autologous stem cells are seeded on that structure, and formation of a new tissue occurs upon embedding such a construct into a bone defect, due to the cells' growth and differentiation. To increase the adsorption activity of polylactide and to enhance polymer mechanical properties as well as to increase the rate of the polymer degradation and enhance its processability the polymer is chemically modified. In this study acrylate derivatives of polylactide have been synthesized. Such chemical modification is one of the promising approaches for controlled variation of the physico-chemical properties of biodegradable PLA. For formation of implants spatially cross-linked structures have been prepared by photopolymerization of polylactide derivatives. In this study we created 3D-structures using the method of 2 photon polymerization (laser stereolithography) [1,2]. Laser stereolithography allows the fabrication of 3D scaffolds with well-defined architectonics [3]. Being a technique of additive manufacturing, laser stereolithography relies on layer-by-layer building of the materials by local solidification under laser-induced reactions. As a function of the features of the laser beam, resolution can reach submicron levels. For example, two-photon stereolithography based on focused femtosecond laser pulses allows the creation of structures with a sub-diffraction limit of resolution, as well as overcoming local overheating [3]. So, formation of 3D-structures proceeded without deformations and shrinkage, which allows consideration of the developed approach for creation of precise biodegradable structures. Thus, we have demonstrated a possibility of lactic acid polymers modification by each of the functional groups, with obtaining polymerizable acrylic derivatives of PLA, which can be used for formation of cross-linked films and 3D-structures.

This study was financially supported by the Russian Scientific Foundation (Grant No. 16-15-00042) and Russian Foundation for Basic Research (Grant No 18-29-06019, 18-07-01052).

[1] A. Koroleva, A. Deiwick, A. Nguyen, S. Schlie-Wolter, R. Narayan, P. Timashev, V. Popov, V. Bagratashvili, B. Chichkov, Osteogenic differentiation of human mesenchymal stem cells in 3-D Zr-Si organic-inorganic scaffolds produced by two-photon polymerization technique. *PLoS ONE*, 10, pp. 1-18, (2015).

[2] T. S. Demina, K. N. Bardakova, E. A. Svidchenko, N. V. Minaev, G. I. Pudovkina, M. M. Novikov, D. V. Butnaru, N. M. Surin, T. A. Akopova, V. N. Bagratashvili, A. N. Zelenetskii, P. S. Timashev, Fabrication of microstructured materials based on chitosan and D,L-lactide copolymers using laser-induced microstereolithography, *High Energy Chemistry*, vol. 50, 5, pp 389–394 (2016).

[3] A.I. Ciuciu; P.J. Cywinski, Two-photon polymerization of hydrogels—Versatile solutions to fabricate well-defined 3D structures, *RSC Adv.*, 4, pp. 45504–45516, (2014).

# **LASER DIAGNOSTICS AND SPECTROSCOPY**

# In Vivo Study of Intracellular Processes in Animal Embryo with Stimulated Raman Imaging

**M. Veres, L. Himics, I. Rigó, S. Tóth, P. Baranyai, A. Czitrovsky, T. Váci**

*1- Wigner Research Centre for Physics, Hungarian Academy of Sciences, Budapest, Hungary*

*veres.miklos@wigner.mta.hu*

Raman spectroscopy gives information on vibrational modes and so on the structural properties of the investigated medium affecting them (composition, bonds, functional groups, presence of impurities etc.). In general, Raman scattering has low probability, but several techniques can be used to enhance the efficiency of the method, like resonant Raman scattering or surface enhanced Raman scattering. With state of the art instrumentation non-linear Raman methods, like stimulated Raman spectroscopy (SRS) or coherent anti-Stokes Raman scattering can be used even for video rate imaging and real time monitoring of cellular activity, biochemical reactions etc.

While the spontaneous Raman scattering is an inelastic light scattering process, in which a part of the energy of the monochromatic incident light goes for the excitation of fundamental vibrations of the medium, SRS utilizes two coherent, temporally and spatially synchronized light sources (the so-called Stokes and pump beams having lower and higher energies, respectively). When the energy difference of the two beams is equal to the energy of a vibrational transition of the medium, stimulated excitation of the vibration takes place. The intensity of the scattered light at the pump wavelength experiences a stimulated Raman loss while that at the Stokes wavelength experiences a stimulated Raman gain. The probability of the SRS process is a few orders of magnitudes higher than that of the spontaneous Raman scattering resulting is much higher sensitivity. SRS microscopy is capable of high-speed spectral imaging of different samples ranging from single cells to tissues.

In this work SRS was used to map the distribution and temporal evolution of different biomolecules with subcellular resolution in order to in vivo study processes related to cell division in zebrafish embryo. A dual output Coherent Chameleon Discovery femtosecond laser was used as light source for the SRS measurements, which was coupled into a Femtonics FemtoSmart two-photon scanning microscope. The SRS optics incorporated between the laser and the microscope consists of a motorized delay line in the Stokes beam for temporal synchronization, an acousto-optic modulator for the pump beam and a dichroic mirror used for collinear alignment of the two beams. A 3 MHz modulation of the pump beam was utilized for lock-in detection. A 20x water immersion scanning objective was used to illuminate the samples. After the sample the pump beam was filtered with long-pass filter and the intensity of the scattered Stokes beam was recorded with a photodiode in transmission geometry. In addition to the SRS data two-photon images were also recorded simultaneously. Series of SRS spectra of zebrafish embryo were recorded on sub-cellular level in order to determine the characteristic bands of the embryo cells. Based on these data SRS imaging was performed at certain selected wavenumbers related to cellular lipids, proteins and DNA. The in vivo study of the processes was performed at these wavenumbers and the results were analyzed using image analysis and statistical methods.

This work was supported by the European Commission through the H2020 FET-OPEN project NEURAM (grant agreement 712821) and H2020 MSCA-RISE-2016 project VISGEN (grant agreement: 734862), as well as by the NVKP 16-1-2016-0043 and KFI\_16-1-2016-0055 projects. Projects no. NVKP 16-1-2016-0043 and KFI\_16-1-2016-0055 have been implemented with the support provided from the National Research, Development and Innovation Fund of Hungary

## Measurements of surgical smoke using optical methods

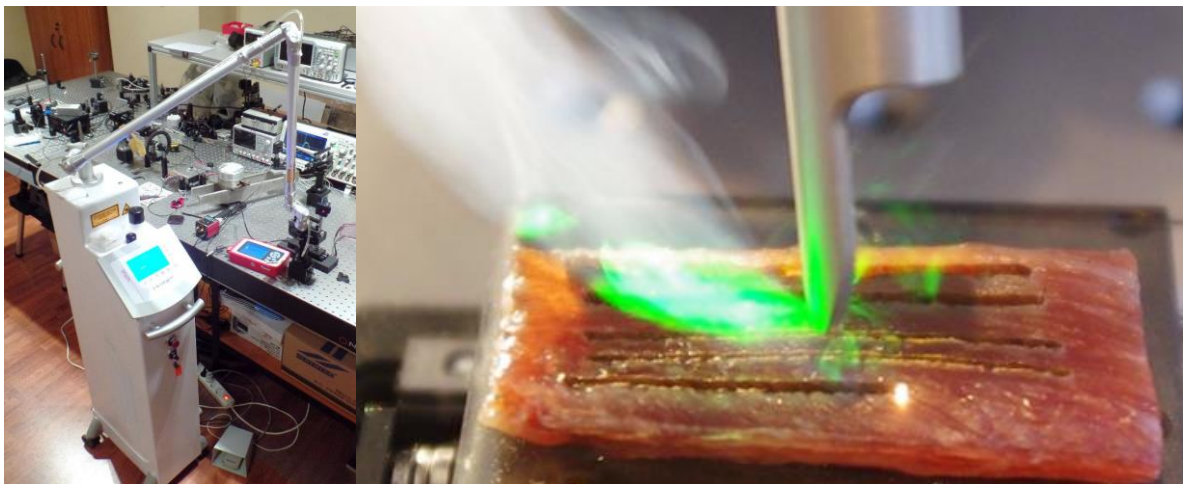
**A. Czitrovsky<sup>1</sup>, A. Nagy<sup>1</sup>, M. Veres<sup>1</sup>, Sz. Kugler<sup>1</sup>, I. Kreis<sup>2</sup>, I. Vass<sup>2</sup>, I. Rigó<sup>1</sup>**

<sup>1</sup>Wigner Research Centre for Physics of the Hungarian Academy of Sciences,  
Institute for Solid State Physics and Optics, P.O. Box 49., Budapest, Hungary

<sup>2</sup>Lasram Engineering Ltd., H-1044 Budapest, Ezred u.2.B2/2. Hungary

Czitrovsky.Aladar@wigner.mta.hu

Surgical smoke is the by-product of using energy-generating devices that raise intracellular temperatures higher 100 °C. It contains toxic biological and viral aerosols and gases from tissue destruction, among them more than 150 chemicals, including 16 that are listed as “priority pollutants” by the EPA. An estimated 500,000 health care workers are exposed to potentially dangerous surgical smoke each year. Unfortunately, many OR nurses are unaware of the harm that inhaling surgical smoke, could be causing to their health. For mitigation of the hazards of surgical smoke transmitting viruses and disease, including cancer, proper evacuation and filtration, determination of the concentration, size distribution, spreading, sedimentation and velocity of flow profile is especially important. Our aim was to determine these parameters of surgical smoke using optical and laser techniques, and study of the methods of mitigation of their health risk for medical workers. Recently we have developed a system to generate surgical smoke by laser evaporation of different tissues and measurement of particle formation and spreading. In this system we used a 30 W LASRAM CO<sub>2</sub> laser generating in CW, pulse and superpulse regime. Using a fast imaging system and a laser Doppler velocimeter (LDV) system developed previously for determination of aerodynamic parameters of spreading of surgical smoke, we can elaborate more precise conditions for evacuation and filtration of toxic aerosols. The short sampling time of the aerosol instruments and LDV makes possible to perform real time measurements in large volume covering the formation and spreading of aerosols. Beside the above mentioned methods we use also optical microscopy and Raman spectroscopy to investigate the morphology and composition of collected and sedimented aerosol samples. All of these methods have their own advantages in terms of speed and precision of the measurement. Analysing the results of the above mentioned measurements we calculated the kinetic energy distribution of aerosol particles determining their spreading parameters and elaborated evacuation and filtration methods to mitigate the hazard for operating personnel and also patients. These results under implementation in operating theater of the Otolaryngology department of Semmelweis University clinic (SOTE).



The research was supported by the Hungarian National Research, Development and Innovation Fund under grant No. KFI\_16-1-2016-0055.

# Characterization of the aerosol plume released during laser tissue interactions

**A. Nagy<sup>1</sup>, A. Czitrovsky<sup>1</sup>, M. Veres<sup>1</sup>, Sz. Kugler<sup>1</sup>, I kreisz<sup>2</sup>, I. Vass<sup>2</sup>, I. Rigó<sup>1</sup>**

<sup>1</sup>*Wigner Research Centre for Physics of the Hungarian Academy of Sciences,  
Institute for Solid State Physics and Optics, P.O. Box 49., Budapest, Hungary*

<sup>2</sup>*Lasram Engineering Ltd., H-1044 Budapest, Ezred u.2.B2/2. Hungary*

*nagy.attila@wigner.mta.hu*

It is widely recognized that the smoke which is generated during laser surgery is potentially harmful to both operating theatre personnel and patients. The risks include airway irritation and inflammation, micro toxicity in the alveolar region of the lung, virus, bacteria and cancer spread through aerosolized cells. It is of crucial importance to recognize the potential hazards and provide a safe environment for the exposed persons. Cutting soft tissues by laser produces large numbers of particles. Surgical smoke consists of 95% water and 5% other stuff, gaseous toxic compounds, bio-aerosols, like cellular material, viruses, bacteria, and carbonized tissue, where water vapor acts as a carrier of other dangerous compounds. The size distribution of the produced particles depends on the applied laser (power density, wavelength, pulsed or cw, focusing), the tissue and the applied cutting method. The mean aerodynamic size in case of laser tissue ablation is typically around 300nm.

This study was aimed to characterize airborne particles released when a model tissue was cut by a CO<sub>2</sub> surgical laser. Different instruments were used to measure the size distribution, concentration and composition of the generated particles. The number and mass concentrations of the particles were measured by an optical particle counter, a condensation particle counter, and an aerodynamic particle sizer. The particles were also sampled by a cascade impactor and Raman spectroscopy was utilized to analyze their composition.

Physical and chemical properties of the sampled particles depend highly on the properties of the applied laser pulses (power density, wavelength, pulse duration, etc.). A typical measured size distribution is shown on Fig. 1. The generated smoke contains a considerable amount of ultrafine particles, where the filtration requires special techniques.

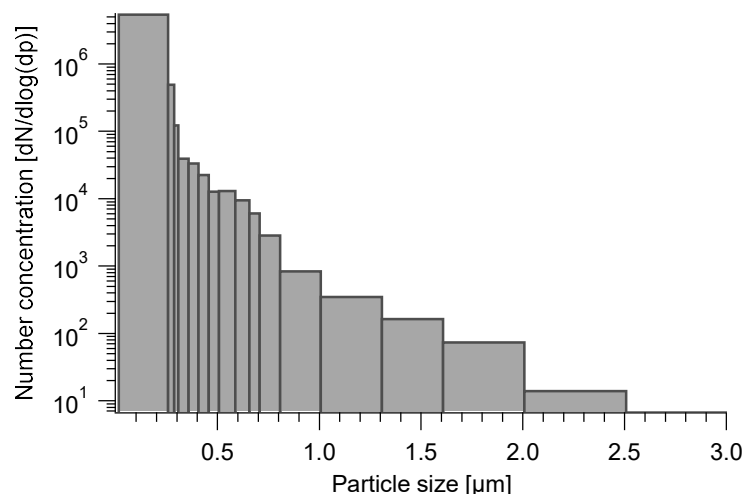


Fig.1. Typical measured size distribution of aerosol particles generated by laser-cutting of sample tissue

The research was supported by the Hungarian National Research, Development and Innovation Fund under grant No. KFI\_16-1-2016-0055.

# Optical Spectroscopy and Kinetics of Photoinduced Carriers of 2D Transition Metal Dichalcogenides

S.D. Lavrov, A.P. Shestakova, A.V. Kudryavtsev, L.Q.K. Pham, N.A. Ilyin, E.D. Mishina

*MIREA-Russian Technological University, Vernadsky ave. 78, 119454 Moscow, Russia*

*mishina\_elen57@mail.ru*

Monolayers of transition metal dichalcogenides (TMDs), such as MoS<sub>2</sub>, WS<sub>2</sub>, MoSe<sub>2</sub>, WSe<sub>2</sub> are direct bandgap semiconductors. This fact provides their unique properties and makes them very good complement to graphene. Several optoelectronic devices were suggested and assembled using pure TMDs as well as TMD/graphene heterostructures: phototransistors [1], field-effect transistors [2] and others. Carrier dynamics is one of the most important properties in semiconductor devices, such as high electron mobility transistor and field-effect transistor, both of which are capable for realizing terahertz ultrahigh-speed operation.

Here we report the results of optical characterization of TMD monolayers. Monolayers were commercial fabricated (SixCarbon Technology) by chemical vapor deposition technique on SiO<sub>2</sub>(285nm)/Si substrate. Optical confocal microscope was used to obtain reflectivity, luminescence and optical second harmonic images, which were complemented by atomic force microscopy. Visualization of the thin layers was based on the optical properties of high refractive index layer (TMD) on top of Fabry-Perot cavity, the thickness of SiO<sub>2</sub> layer is chosen in order to provide minimal reflectivity accompanied by maximal contrast. However, it is not possible by this method to distinguish between 1-3 monolayers (ML). The latter can be achieved by photoluminescence (PL) microscopy on wavelength of excitonic resonance. Due to exponential dependence of PL intensity on the thickness, only ML flakes will be seen as bright spots, the method is proved to be even more precise than conventional AFM. SHG microscopy controls the quality of the flakes (it is also quite useful for large area CVD layers due to their polycrystallinity), in particular edge effects, consisting in increasing or decreasing SHG intensity at the edges due to higher concentration of defects, including absorption of extrinsic molecules [3].

To measure the relaxation time for hot photocarriers in monolayer, the two-color pump-probe experiment was performed at room temperature using the amplified Ti-sapphire laser and frequency doubler. The wavelength of the pump was fixed at 400 nm (pulse widths of 50 fs). The wavelength of the probe was varied in the range of 1200-1500 nm. The differential reflectivity of a WSe<sub>2</sub> monolayer was obtained and fitted within the two-time relaxation model which is commonly used for direct band semiconductors [4]. The relaxation time constants were found to be slightly dependent on wavelength and to be of the order of magnitude of  $t_1 \sim 1.5$  ps, and  $t_2 \sim 10$  ps. Resonant behavior of the transient reflectivity amplitudes was observed at 0.83 eV. This value doubled coincides with the luminescence peak position of 1.67 eV. This means that two photon process takes place for the probe in the pump-probe experiment.

Finally, the model was suggested to describe the obtained results based on the spectral dependence of time evolution of complex refractive index for semiconductor with photoexcited carriers. Numerical calculation of the reflectivity dependence on carrier concentration along with the calculation of the temporal dependence of carrier concentration allows to simulate time dependence of reflectivity.

The work is supported by Russian Science Foundation (Grant 14-12-01080) and Ministry of Education and Science (State task for the Universities).

[1] W. Zhang, C.-P. Chuu, J.-K. Huang, et al, Ultrahigh-Gain Photodetectors Based on Atomically Thin Graphene-MoS<sub>2</sub>Heterostructures, *Scientific Reports* Vol. 4, p. 3826 (2014).

[2] R.J. Chang, H. Tan, X. Wang, et al, High-Performance All 2D-Layered Tin Disulfide: Graphene Photodetecting Transistors with Thickness-Controlled Interface Dynamics, *ACS Appl. Mater. Interfaces*. Vol. 10, pp.13002-13010 (2018).

[3] E. Mishina, N. Sherstyuk, A. Shestakova, et al, Edge effects in second-harmonic generation in nanoscale layers of transition-metal dichalcogenides, *Semiconductors* Vol. 49, pp. 791-796 (2015).

[4] V.G. Morozov, C. Dekeyser, N. Ilyin, E. Mishina, Photocarrier-phonon relaxation in highly excited monolayer transition metal dichalcogenides, *Solid St. Commun.* Vol. 251, pp.32-34 (2017).

# Effect of Polymer on Photoluminescence of CdSe Quantum Dots in Amorphous and Liquid-Crystal Matrices

A. V. Elopov<sup>1</sup>, V. B. Zaytsev<sup>1</sup>, D. M. Zhigunov<sup>1</sup>, G. A. Shandryuk<sup>2</sup>, A. A. Ezhov<sup>1,2</sup>,  
A. S. Merekalov<sup>2</sup>, L. A. Golovan<sup>1</sup>

1- Faculty of Physics, M. V. Lomonosov Moscow State University, Moscow 119991, Russia

2- A. V. Topchiev Institute of Petrochemical Synthesis RAS, Moscow 119991, Russia

Semiconductor quantum dots - particles with 3D restriction of the carrier movement – are subject of various studies since they open up possibilities to produce novel materials. The idea to form QD-based nanocomposite media for laser generation is of extreme attraction [1]. In particular, this can be done with the help of II-VI QD (i.e. CdSe) and polymer. Employment of liquid-crystal polymers (LCP) is very promising since they allow formation of ordered QD arrays and high QD concentration. Measurement of QD-LCP nanocomposite photoluminescence (PL) spectra and PL kinetics is the first stage of study of such nanocomposites. It would be also very instructive to compare results obtained both for LCP and amorphous polymer matrices.

In this paper, we employed dried CdSe QD sol and nanocomposite based on smectic BA-6PA and amorphous PMBA-6A polymers with various CdSe QD mass fractions (up to 30%). QD diameter was 4.1 nm. PL measurement were carried out under excitation by picosecond pulses of 532 nm. PL spectra were registered with the help of Princeton Instrument Acton 2500i spectrometer equipped by gated CCD camera. PL and PL excitation spectra were also obtained by Perkin Elmer LS 55 spectrometer.

PL spectra contain two bands (2.15 and 1.70 eV) (Fig. 1) corresponding to exciton radiative recombination and radiative recombination in defects (traps) at QD-matrix interface [2]. The latter band intensity increases in LCP matrix in comparison with QD sol and amorphous matrix. The most effective excitation is at 370 nm. In LCP matrix exciton band prevails for QDs with 30 mass. % concentration, whereas for less concentrations defect band PL is more intensive. The exciton PL band is characterized by less PL lifetime than defect one. Increase of QD concentration results in PL lifetime decrease. If amorphous polymer matrix is used, PL signal decreases almost twice in comparison with LCP nanocomposite with the same QD mass concentration.

In conclusion, measurements of the excitation and emission spectra of PL of CdSe quantum-size nanoparticles embedded in the polymer matrices, as well as the kinetics of their PL, indicate that the use of a LCP as a matrix makes it possible to increase the lifetime of PL and the quantum yield of this process.

This work was supported by Russian Foundation for Basic Research (grant 18-02-00548), synthesis of QDs and polymer matrices was carried out in framework of the State Assignment for IPS (AAAA-A18-118011990207-1).

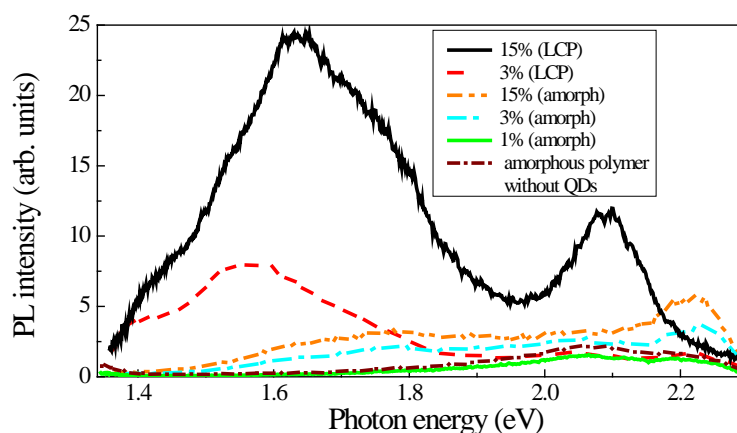


Fig. 1. PL spectra for QDs in LCP and amorphous polymer matrices.

[1] V. Klimov and M. Bawendi, Ultrafast Carrier Dynamics, Optical Amplification, and Lasing in Nanocrystal Quantum Dots. MRS Bulletin, vol.26, pp.998-1004. (2001).

[2] G. I. Tselikov, V. Y. Timoshenko, L. A. Golovan, et al., Role of the Polymer Matrix on the Photoluminescence of Embedded CdSe Quantum Dots. ChemPhysChem, vol. 16 pp. 1071-1078. (2015).

## TERS spectroscopy of CdSe nanocrystals on Au nanostructured surfaces

**A.G. Milekhin<sup>1,2</sup>, M. Rahaman<sup>3</sup>, K.V. Anikin<sup>1</sup>, I.A. Milekhin<sup>1</sup>, T.A. Duda<sup>1</sup>,  
E.E. Rodyakina<sup>1,2</sup>, V.M. Dzhagan<sup>4</sup>, A.V. Latyshev<sup>1,2</sup>, D.R.T. Zahn<sup>3</sup>**

*1- A.V. Rzhanov Institute of Semiconductor Physics, 630090, Novosibirsk, Lavrentjev av. 13*

*2- Novosibirsk State University, Novosibirsk, 630090, Pirogov str., 1*

*3- Technische Universität Chemnitz, Chemnitz, 09126, Reichenhainer Straße 70*

*4- V.E. Lashkaryov Institute of Semiconductor Physics, UA-03028 Kiev, Ukraine*

*milekhin@isp.nsc.ru*

We present the results of tip-enhanced Raman scattering (TERS) study of CdSe nanocrystals (NCs) on nanostructured plasmonic Au surfaces with nanometer spatial resolution.

Commercial surface-enhanced Raman scattering (SERS) substrates (Klarite) as well as specially designed Au nanocluster arrays were used to realized gap-plasmon TERS by optical phonons in CdSe NCs. Klarite substrates represent the arrays of the Si inverted pyramids covered with Au nanoclusters with a size of 50-100 nm. The arrays of Au nanoclusters with a size of about 80 nm on a Si substrate were fabricated using nanolithography.

SERS substrates were covered by sub-monolayers of CdSe NCs with a size of 5-6 nm using the Langmuir-Blodgett technology. The structural parameters of plasmonic and semiconductor nanostructures (size and morphology of NCs and Au nanoclusters) were determined by means of scanning electron and atomic force microscopies (SEM and AFM). The energy of localized surface plasmon in the SERS substrates which is located in the visible spectral range and depends on the size and morphology of Au nanoclusters was chosen in that way to match the energy of interband transitions in CdSe NCs.

We observed a giant plasmonic enhancement of the Raman scattering by longitudinal optical (LO) phonons in CdSe NCs (near  $214\text{ cm}^{-1}$ ) placed in the gap between the TERS tip apex and Au nanoclusters. Additional features at  $230\text{-}250\text{ cm}^{-1}$  evidence the formation of Se nanoclusters due to photodegradation of CdSe NCs.

TERS maps for LO phonon mode in CdSe NCs deposited the on Au nanostructures were obtained with a spatial resolution down to 2.3 nm. The TERS signal from CdSe NCs deposited on Au nanocluster arrays forms the pattern of ordered rings similar to those observed for MoS<sub>2</sub> monolayers [1]. A superposition of the TERS image on the corresponding AFM topography shows that the rings perfectly coincide with the edges of the Au nanoclusters. This indicates that the TERS signal predominantly originates from the edges of the Au nanoclusters. For a Klarite substrate, the maxima of EM field are located at the corners of inverted pyramids [2,3]. Comparison of AFM and TERS images shows that the most intense TERS signal is observed from CdSe NCs at the pyramid corners. The giant enhancement of Raman response allowed us the observation of the Raman response from single CdSe NCs.

The reported study was funded by Volkswagen Foundation and RFBR according to the research project № 18-02-00615.

[1] A.G. Milekhin, M.Rahaman, E.E. Rodyakina, A.V. Latyshev, V.M. Dzhagan and D.R.T. Zahn, Giant Gap-Plasmon Tip-Enhanced Raman Scattering of MoS<sub>2</sub> Monolayers on Au Nanocluster Arrays, *Nanoscale*, 10, 2755 - 2763 (2018).

[2] N.M.B. Perney, J.J. Baumberg, Tuning localized plasmons in nanostructured substrates for surface-enhanced Raman scattering, *Optics express*, 14, 847-857 (2006).

[3] D. Meneses-Rodríguez, E. Ferreira-Vila, P. Prieto, J. Anguita, M. U. González, J.M. García-Martín, A. Cebollada, A. García-Martín, and G. Armelles, Probing the Electromagnetic Field Distribution within a Metallic Nanodisk, *Small*, 7, 3317-3323 (2011).

## Spectroscopic studies of III-V nanostructures for optoelectronic applications

**N. Ben Sedrine<sup>1,®</sup>, J. Cardoso<sup>1</sup>, J. Rodrigues<sup>1</sup>, J. P. Teixeira<sup>1</sup>, A. Alves<sup>1</sup>, R. Ribeiro-Andrade<sup>2,3</sup>,  
A. Gustafsson<sup>4</sup>, J. Bourgard<sup>1</sup>, P. M. P. Salomé<sup>2</sup>, J. C. González<sup>3</sup>, D. Nd. Faye<sup>5</sup>,  
M. Belloeil<sup>6</sup>, B. Daudin<sup>6</sup>, M. Bockowski<sup>7</sup>, V. Hoffmann<sup>8</sup>, M. Weyers<sup>8</sup>, E. Alves<sup>5</sup>, K. Lorenz<sup>5,9</sup>,  
A. J. Neves<sup>1</sup>, J. P. Leitão<sup>1</sup>, M. R. Correia<sup>1</sup>, and T. Monteiro<sup>1</sup>**

<sup>1</sup>*Departamento de Física e I3N, Universidade de Aveiro, Portugal*

<sup>2</sup>*INL – International Iberian Nanotechnology Laboratory, Braga, Portugal*

<sup>3</sup>*Departamento de Física, Universidade Federal de Minas Gerais, Brazil*

<sup>4</sup>*Solid State Physics and NanoLund, Lund University, Sweden*

<sup>5</sup>*IPFN, Instituto Superior Técnico, Campus Tecnológico e Nuclear, Bobadela LRS, Portugal*

<sup>6</sup>*Univ. Grenoble Alpes and CEA, INAC-PHELIQS "Nanophysics and semiconductors" group, Grenoble, France*

<sup>7</sup>*Institute of High Pressure Physics, Polish Academy of Sciences, Warsaw, Poland.*

<sup>8</sup>*Ferdinand-Braun-Institut, Leibniz-Institut für Höchstfrequenztechnik, Germany*

<sup>9</sup>*INESC-MN, Instituto de Engenharia de Sistemas de Computadores, Lisboa, Portugal*

® [nbensedrine@ua.pt](mailto:nbensedrine@ua.pt), [bsnebiha@yahoo.fr](mailto:bsnebiha@yahoo.fr)

Since the successful development of quantum well lasers in the 1970s, one of the richest areas of application of semiconductor nanostructures is the area of optoelectronics, such as lasers and detectors [1]. The most widely used semiconductors for optoelectronic applications are the compounds formed by group III and group V elements. For instance, GaAs and related compounds are mostly used for optical fiber communications, near infra-red and visible light emitting diodes (LEDs) as well as laser diodes. While, GaN and AlGaIn are used for LEDs, solid-state lasers and color displays [2], in the short wavelength range. Furthermore, optoelectronic devices based on novel semiconductor nanostructures are foreseen to revolutionize nowadays technology in terms of superior performance and efficiency, as well as the reduction of costs and material consumption.

The use of semiconductor nanostructures integrated in devices is governed by the realization and control of p-n junctions, obtained by the p and n-type doping of the base materials. In addition to n and p-type doping, the semiconductor nanostructure emission can be tuned by incorporating rare earth ions by implantation and post-growth annealing. Doping can be performed by intentionally adding dopants during the growth (*in-situ*) or after the growth (*ex-situ*) by diffusion and ion implantation. However, several issues and controversies still need to be investigated in order to access/control semiconductor properties at the nanoscale level.

In this work, we present our recent research on semiconductor nanostructures such as: *i*)  $\text{Al}_x\text{Ga}_{1-x}\text{N}$  ( $0 \leq x \leq 1$ ) NWs grown by molecular beam epitaxy on Si (111) substrate implanted with europium (Eu) ions and subject to rapid thermal annealing, *ii*) AlGaIn/GaN superlattice-based diode structures grown by metalorganic chemical vapor deposition implanted with two Eu fluences and subject to high temperature and high pressure annealing [3], and *iii*) silicon-doped GaAs NWs with four nominal silicon doping levels [4]. The optical and vibrational properties of these nanostructures, of utmost importance for optoelectronic applications, will be assessed mainly using photoluminescence and micro-Raman spectroscopy.

[1] Semiconductor Nanostructures for Optoelectronic Applications, Todd Steiner ARTECH HOUSE, INC, Chapter 1 (2004).

[2] Wakahara, A.; Sekiguchi, H.; Okada, H.; Takagi, Y. Current Status for Light-Emitting Diode with Eu-Doped GaN Active Layer Grown by MBE. *J. Lumin.* 2012, 132 (12), 3113–3117.

[3] Ben Sedrine, N.; Rodrigues, J.; Cardoso, J.; Faye, D. N.; Fialho, M.; Magalhães, S.; Martins, A. F.; Neves, A. J.; Alves, E.; Bockowski, M.; Hoffmann V.; Weyers M.; Lorenz K.; Correia M. R.; Monteiro T.: Optical Investigations of Europium Ion Implanted in Nitride-Based Diode Structures. *Surf. Coat. Technol.* 2018, No. 10.1016/j.surfcoat.2018.02.004, 10.1016/j.surfcoat.2018.02.004.

[4] Ben Sedrine N.; Ribeiro-Andrade R.; Gustafsson A.; Soares M. R.; Bourgard J.; Teixeira J. P.; Salomé P. M. P.; Correia M. R.; Moreira M. V. B.; De Oliveira A. G.; González J. C.; Leitão J. P.: "Fluctuating potentials in GaAs:Si nanowires: critical reduction of the influence of polytypism on the electronic structure", *Nanoscale*, 10, 3697 (2018).

# Anisotropy of light scattering by liquid foams

D. Zimnyakov<sup>1</sup>, O. Ushakova<sup>1</sup>, S. Yuvchenko<sup>1</sup>

1- Yury Gagarin State Technical University of Saratov, Saratov, 410054, Russia

s\_sov@rambler.ru

Studies of peculiarities of the radiation transfer in foamed liquids in the dependence on their characteristics (the average radius of gas bubbles ( $\langle R \rangle$ ) and the volume fraction of liquid phase in a foam  $\varepsilon$ ) are carried out by many research groups. Optical and structural properties of foams were systematically studied by D. Durian with co-workers beginning from the nineties of the last century using the diffusing wave and diffuse transmittance spectroscopies [1-4]. They used the diffusion approximation to describe the transfer of probe radiation in foams and achieved impressive results in describing the relationship between structural and optical properties of foamed substances. But on the other hand, the diffusion approximation does not take into account the features of the “single-particle” interaction of light with scatterers (in particular, the value of the scattering anisotropy parameter  $g$  for a probed medium). D. Durian with co-workers estimated  $g$  on the base of the angular distributions of light outgoing from foam layers with the low content of the liquid phase; they found that the value of the scattering anisotropy parameter was approximately equal to 0.5 [2]. This is a questionable point since the  $g$  value can vary depending on the degree of correlations of the mutual positions of scattering centers.

The goal of this work is to analyze the behavior of the scattering anisotropy of foamed liquids during the “wet-to-dry” transition. Experimental studies of the optical transport parameters (the mean transport free path and the mean scattering free path) in samples of foamed liquids in the wavelength range from 500 nm to 900 nm are presented. The obtained results allow us to suggest that at early stage of foam aging, the values of the mean scattering free path  $l$  are comparable with the corresponding values of the mean transport free path  $l^*$  (see Fig. 1) and the regime of light propagation with close-to-zero or even negative values of the scattering anisotropy parameter occurs.

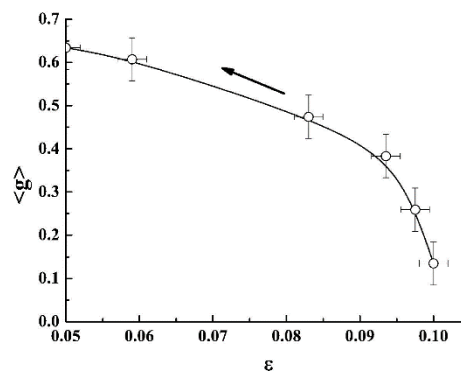


Fig. 1. Dependence of the averaged parameter of scattering anisotropy on the liquid content in foam samples. Averaging was carried out over the spectral range 500 nm – 900 nm. The fitting curve was obtained using the B-spline interpolation. Standard deviations are equal  $\pm 0.16$  for  $g$  estimates and  $\pm 0.02$  for  $\varepsilon$  estimates.

The closeness of the values of scattering anisotropy parameter to 0 at early stages of aging is due to the effect of a strong correlation of the spatial positions of the scattering centers (gas bubbles in the liquid-phase matrix). The increase of the scattering anisotropy parameter in the course of foam aging is due to the effect of "optical" inversion (transition from the regime of light scattering by gas bubbles in the liquid matrix to the regime of scattering by Plateau-Gibbs channels (PGC) and vertices of the PGC net).

[1] D.J. Durian, D.A. Weitz, D.J. Pine, Multiple light-scattering probes of foam structure and dynamics, *Science*, vol. 252, № 5006, pp. 686-688, (1991).

[2] M.U. Vera, A. Saint-Jalmes, D.J. Durian, Scattering optics of foam, *Applied Optics*, vol. 40, № 24., № 24. pp. 4210- 4210 (2001).

[3] A.S. Gittings, R. Bandyopadhyay, D.J. Durian, Photon channelling in foams, *Europhys. Lett.*, vol. 65, № 3. pp. 414-419. (2004).

[4] A.S. Gittings, D.J. Durian, Gaussian and non-Gaussian speckle fluctuations in the diffusing-wave spectroscopy signal of a coarsening foam, *Applied Optics*, vol. 45, № 10, pp. 2199 - 2204 (2006).

# Speckle-correlometry techniques in diagnostics of the functional and structural properties of multi-phase systems

E.A. Isaeva<sup>1,2</sup>, A.A. Isaeva<sup>1,2</sup>, D.A. Zimnyakov<sup>1,2</sup>

1- Yuri Gagarin Saratov State Technical University, Saratov, Russia

2- Institute of Precision Mechanics and Control RAS, Saratov, Russia

27isaevaea@mail.ru

One of the actual direction of modern science is the development of laser methods for analyzing the rheological, structural, and transport properties of porous polyphase structures during their synthesis, including using supercritical and near-critical technologies. The topicality of this direction is caused by the wide application of two-phase structured systems in various areas of industry and biomedicine: as functional membranes [1-2], three-dimensional porous matrices in tissue engineering [3], porous - polymer separators in fuel energy [4], filters in geophysics [5] et.al.

The analysis of the laser light scattered by a multiphase system allows to obtain information about the structural topology of the object (concentration and form of inhomogeneities, the features of structure organization and its dynamic evolution) and to determine the functional and rheological properties.

Dynamic light scattering demonstrated good results in determining the coefficient of translational diffusion of particles or the particle size and the components distribution in the continuous phase [6, 7].

At present time, the fundamental regularities of the formation of the ensembles of the liquid-crystal domains in LC polymer composites at the UV-induced polymerization of liquid crystal-prepolymer mixtures have been established using the full-field speckle-correlometry method [8].

It is shown that the characteristic time of intensity fluctuations correlations in the recorded signal is an informative parameter describing the kinetics and dynamics of mass transfer processes in two-phase foamed systems under the conditions of drainage of the liquid component of the system and local structural rearrangements (collapse of gas bubbles) under conditions of temperature change of the system [9].

In this paper, the results of the analysis of the structural and transport properties of two-phase disperse systems in the process of their structural evolution by use of the diffuse optical spectroscopy are presented. The behavior of intensity correlation function of laser light scattered by porous system during a transition from a wet to a dry foam is analyzed. The values of the statistical and correlation characteristics of dynamic speckles obtained at the different stages of foam aging are compared with the structural parameters (porosity, stability of foam-like structures, the ratio of the liquid and gas phases) of mesoporous multiphase systems in the course of their evolution.

[1] N. Li, Y. Fu, Q. Lu and C. Xiao, Microstructure and Performance of a Porous Polymer Membrane with a Copper Nano-Layer Using Vapor-Induced Phase Separation Combined with Magnetron Sputtering, *Polymers*, 9, pp. 524-527, (2017).

[2] Y. Chen, Y. Zhang, J. Liu, Preparation and antibacterial property of polyethersulfone ultrafiltration hybrid membrane containing halloysite nanotubes loaded with copper ions, *Chem. Eng. J.*, 210, pp. 298-308 (2012).

[3] V. R. Hokmabad, S. Davaran, A. Ramazani, R. Salehi, Design and fabrication of porous biodegradable scaffolds: a strategy for tissue engineering, *J. Biomater. Sci. Polym.*, 28, pp. 1797-1825 (2017).

[4] Z. H. Li, H. P. Zhang, P. Zhang, G. C. Li, Y. P. Wu, and X. D. Zhou, Effects of the porous structure on the conductivity of nanocomposite polymer electrolyte for lithium ion batteries, *J. Membr. Sci.*, 322, pp. 416-422 (2008).

[5] J.M. Prado, G. H.C. Prado, M. A. A. Meireles, Scale-up study of supercritical fluid extraction process for clove and sugarcane residue, *J. Supercritical Fluids*, 3, pp. 231-237 (2011).

[6] S.P. Cadogan, C.J. Hahn, M.H. Rausch, A.P. Fröba AP, Study on the applicability of dynamic light scattering (DLS) to microemulsions including supercritical carbon dioxide-swollen micelles, *J. Colloid Interface Sci.*, 499, pp. 202-208 (2017).

[7] T. Koga, S. Zhou, and B. Chu, Dynamic light-scattering study of self-assembly of diblock copolymers in supercritical carbon dioxide, *Applied Optics*, 40, pp. 4170-4178 (2001).

[8] D.A. Zimnyakov, S.P. Chekmasov, O.V. Ushakova, E.A. Isaeva, V.N. Bagratashvili, S.B. Yermolenko, Laser speckle probes of relaxation dynamics in soft porous media saturated by near-critical fluids, *Applied Optics*, 53, pp. B12-B21 (2014).

[9] Zimnyakov D.A., Isaeva A.A., Isaeva E.A., Ushakova O.V., Chekmasov S.P., Yuvchenko S.A., Analysis of the scatter growth in dispersive media with the use of dynamic light scattering, *Applied Optics*, 51, pp. C62-C69 (2012).

## Sum frequencies of multi-line CO laser for gas analysis applications

**A.A. Ionin<sup>1</sup>, I.O. Kinyaevskiy<sup>1</sup>, Yu.M. Klimachev<sup>1</sup>, A.A. Kotkov<sup>1</sup>, Yu.M. Andreev<sup>2,3</sup>**

*1- Lebedev Physical Institute of the Russian Academy of Sciences, 53 Leninskiy Ave., 119991 Moscow, Russia*

*2- Institute of Monitoring of Climatic and Ecological Systems of the Siberian Branch of Russian Academy of Sciences, 10/3 Akademicheskii Ave., 634055 Tomsk, Russia*

*3- Siberian Physical Technical Institute of Tomsk State University, 1 Novosobornaya Sq., 634050 Tomsk, Russia*

*kigor@sci.lebedev.ru*

The mid-IR range is the “molecular fingerprint” region. Therefore, a development of mid-IR laser sources is very important for gas analysis and remote detection of air pollutants. For atmosphere sensing and pollutions concentration measurement, a differential absorption technique has the advantages of high sensitivity, relative simplicity, and minimal beam power [1]. However, it requires proper multi-wavelength (or multi-line) laser sources. Another important problem is an absorption line profile measurement of atmospheric gases, e.g. for measuring temperature and/or pressure of these gases. A rough estimate for air-broadened spectral half width of gases is  $0.1 \text{ cm}^{-1} \text{ atm}^{-1}$  to all atmospheric components [2]. Therefore, to measure absorption line profile, fine frequency tuning or a pack of close emission lines with spectral resolution better than  $\sim 0.1 \text{ cm}^{-1}$  are required.

Very attractive laser source for atmosphere sensing is multi-line CO laser with frequency conversion of its radiation in nonlinear crystals [3, 4]. An opportunity of  $\text{CO}_2$  and  $\text{N}_2\text{O}$  absorption measurement by this laser source was experimentally demonstrated in [4]. It was found in present research that broadband sum frequencies radiation of multi-line Q-switched CO laser is very attractive source not only for the atmosphere gases concentration measurement in the wavelength range of 2.5-4.0  $\mu\text{m}$  by differential absorption technique but also for the absorption line profile measurement.

A detailed study of broadband sum-frequency generation of multi-line CO laser radiation in  $\text{ZnGeP}_2$  crystal demonstrated that sum frequencies spectrum is significantly (about an order of magnitude) richer than previously reported because of its fine substructure. By other words, sum-frequency spectrum of multi-line CO laser has complicated structure like a broadband (up to  $1000 \text{ cm}^{-1}$ ) comb of multi-line groups having their own substructure. A spectral distance between multi-line groups is about  $5 \text{ cm}^{-1}$  that can be applied for multi-component gas analysis by a differential absorption technique. These groups consist of about dozens narrow (linewidth is about  $10^{-4} \text{ cm}^{-1}$ ) lines with average distance of  $\sim 0.05 \text{ cm}^{-1}$ , which can be applied for absorption line profile measurement, i.e. for measuring temperature and/or pressure of these gases. The possibility of absorption line profile measuring of  $\text{CO}_2$  molecule by means of the sum frequencies radiation was experimentally demonstrated. We suppose that the advanced broadband slab RF discharge CO laser combined with nonlinear frequency converters will result in high performance characteristics of such laser system suitable for atmosphere sensing.

The research was supported by the RFBR (Project No. 18-32-00209).

[1] D.C. O'Shea and L.G. Dodge, “NO<sub>2</sub> Concentration Measurements in an Urban Atmosphere Using Differential Absorption Techniques”, *APPLIED OPTICS*, vol. 13, pp. 1481-1486, (1975).

[2] L.S. Rothmana, I.E. Gordona, Y. Babikov, et al., “The HITRAN2012 molecular spectroscopic database”, *Journal of Quantitative Spectroscopy and Radiative Transfer*, vol. 130, pp. 4-50, (2013).

[3] Yu.M. Andreev, A.A. Ionin, I.O. Kinyaevskiy, et al., “Broadband carbon monoxide laser system operating in the wavelength range of 2.5 – 8.3  $\mu\text{m}$ ”, *Quantum Electronics*, vol. 43, pp. 139-143, (2013).

[4] O.V. Budilova, A.A. Ionin, I.O. Kinyaevskiy, et al., “Absorption of the CO laser sum frequency radiation obtained in a nonlinear crystal  $\text{AgGaSe}_2$ ”, *Journal of Physics: Conference Series*, vol. 769, pp. 012042, (2016)

# Speckle-based low-coherence reflectometry in applications to media structure characterization

A.A. Isaeva, E.A. Isaeva, S.A. Yuvchenko, D. A. Zimnyakov  
Yuri Gagarin State Technical University of Saratov, Saratov, Russia  
*isanna.1987@mail.ru*

The method of reference-free reflectometry is used to analyze the stochastic interference of fluorescence radiation emitted by a laser-pumped dye-doped random medium, such as densely packed silica layers saturated by rhodamine 6G and pyridine.

At the present time, coherence-domain optical techniques are widely used for characterization of structural and dynamic properties of various complex systems [1-3]. In particular, modifications of the optical coherence tomography are commonly applied for examination of weakly scattering media with the stratified structure. In this case the interference between the reference and the object low-coherent beams is applied for recovery of the depth distributions of the local values of reflection coefficient inside an examined medium [3-4]. Application of the spectral selection of diffusively backscattered broadband probe light combined with the statistical analysis of intensity fluctuations in speckle-modulated detected light allows the improvement of the functional capabilities of the reflectometric probing and can serve as a basis for the development of a variety of novel diagnostic approaches in biomedicine and materials science [5].

In the experiments, fluorescent coarse-grained silica layers with rhodamine 6G or pyridine solutions were pumped by the CW laser radiation at 532 nm. The volume fraction of submicrometer-sized silica particles dioxide in the probed layers was approximately equal to 0.35. A confocal detection scheme with the narrow-band spectral selection of detected light was used to provide the stochastic interference in the detected signal. The detection of fluorescence radiation was performed in the scanning mode at various position of the confocal unit and various scan depths. The experimentally obtained fluorescence spectra at various scan positions were used to calculate the second- and third-order moments of intensity fluctuations in random interference patterns:

$$M_2(\lambda) = \langle I^2_\lambda \rangle / \langle I_\lambda \rangle^2 ;$$

$$M_3(\lambda) = \langle I^3_\lambda \rangle / \langle I_\lambda \rangle^3 ,$$

where  $\langle I_\lambda \rangle$  is the mean value of detected intensity for the selected wavelength. Analysis of the obtained experimental data has shown the ergodicity and the statistical homogeneity of intensity distributions along the scan traces. The method for recovery of the optical transport parameters and structure properties of examined media from the spectral dependencies  $M_2(\lambda)$  and  $M_3(\lambda)$  is proposed. This method is based on application of the inverse Monte-Carlo technique and the model of stochastic interference establishing the relationships between the pathlength distributions of probe light in the medium and the experimentally measured diagnostic parameters.

This work was supported by grant # 16-19-10455 from the Russian Science Foundation.

- [1] L. Brunel, A. Brun, P. Snabre, and L. Cipelletti, Adaptive speckle imaging interferometry: a new technique for the analysis of microstructure dynamics, drying processes and coating formation, *Opt. Exp.*, vol. 15 (23), pp.15250–15259 (2007).
- [2]. P. Zakharov, F. Cardinaux, and F. Scheffold, Multispeckle diffusing-wave spectroscopy with a single-mode detection scheme, *Phys. Rev. E Stat. Nonlin. Soft Matter Phys.*, vol. 73 (1), pp. 011413-011416 (2006).
- [3]. B. Liu, and M. E. Brezinski, Theoretical and practical considerations on detection performance of time domain, Fourier domain, and swept source optical coherence tomography, *J. Biomed.Opt.*, vol. 12 (4), pp. 044007- 0440011 (2007).
- [4]. D. A. Zimnyakov, J. S. Sina, S. A. Yuvchenko, E. A. Isaeva, S. P. Chekmasov, and O. V. Ushakova, Lowcoherence interferometry as a method for assessing the transport parameters in randomly inhomogeneous media, *Quant.Electron.*vol. 44 (1), pp. 59–64 (2014).
- [5]. D. A. Zimnyakov, I. A. Asharchuk, S. A. Yuvchenko, and A. P. Sviridov, Stochastic interference of fluorescence radiation in random media with large inhomogeneities, *Opt. Commun.*,vol 387, 121–127 (2017).

# Calculations on Gold Coated Arrays for Surface Enhanced Raman Scattering

I. Rigó<sup>1</sup>, M. Veres<sup>1</sup>, O. Hakkel<sup>2</sup>, P.R. Rigó<sup>3</sup>, P. Fürjes<sup>2</sup>

<sup>1</sup>*Institute for Solid State Physics and Optics, Wigner Research Centre for Physics, HAS, Budapest, Hungary*

<sup>2</sup>*Institute of Technical Physics and Materials Science, Centre for Energy Research, HAS, Budapest, Hungary*

<sup>3</sup>*Budapest University of Technology and Economics, Budapest, Hungary*

*rigo.istvan@wigner.mta.hu*

Raman spectroscopy has many applications in life sciences, biology and other domains. Raman scattering is inherently weak, that is why it cannot be used for the detection analysis of analytes having relatively low- concentration analytes. However, Raman sensitivity can be improved by applying surface- enhanced Raman scattering (SERS) [1]. It has been observed in many cases that by using SERS, the degree of achievable sensitivity can reach attomolar ( $10^{-18}$  M) concentrations. But this requires careful design and fabrication of SERS active substrates, the first step of which is modeling. In the latter non-linear optimization problems arise and for their numerical solutions the primal-dual Newton interior-point algorithms can be used [2].

A novel type of SERS substrates providing high enhancement rates was tested recently, consisting of inverse pyramid arrays filled with gold nanoparticles [3]. In this work near-field intensity distributions of such substrates were studied by finite-difference time-domain (FDTD) simulations using the Lumerical FDTD Solutions v.8.15.736 software. In order to model the array geometry, we have chosen periodic boundary conditions in the directions parallel to the substrate surface, together with perfectly matched layer (PML) boundary conditions in the perpendicular direction. We have used silicon as substrate material and a 200 nm gold coating was placed on that. The software's built in material parameter set from the Handbook of Optical Constants of Solids I was used for the silicon substrate and from CRC Handbook of Chemistry and Physics for the gold layer. The simulation grid was defined by the built-in automesh algorithm with an accuracy level of 4. The inverse pyramid array was illuminated using a broadband (400–900 nm) plane wave having normal incidence to the array surface and polarization parallel to the base of the pyramid. We have recorded near-field profiles using two monitors placed along the two symmetry planes of the pyramid, being parallel to its base and a third one placed above being parallel to the array surface (Fig. 1).

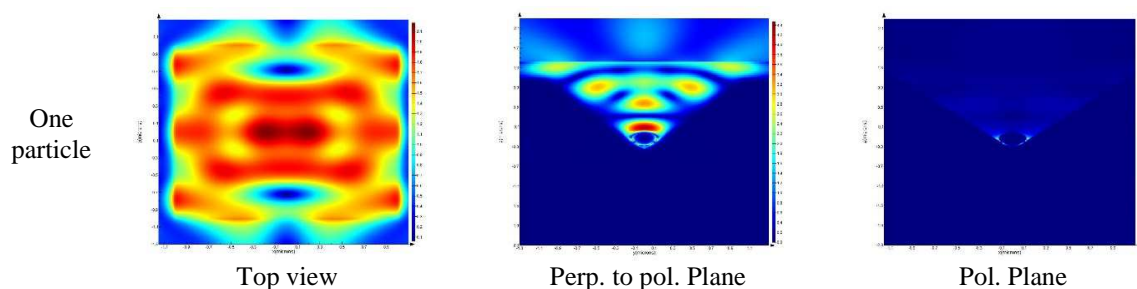


Fig. 1. Near-field intensity distribution of arrays of inverse pyramids being filled with 1 gold nanoparticle monitored in three different planes.

[1] A.G. Ryder, Surface enhanced Raman scattering for narcotic detection and applications to chemical biology. *Curr. Opin. Chem. Biol.* 9 489-493. (2005).

[2] R. H. W. Hoppe, S. I. Petrova, Primal-dual Newton interior point methods in shape and topology optimization, *Numerical Linear Algebra with Applications*, 11, 413-429, (2004).

[3] Rigó, I., Veres, M., Himics, L., Vácsi, T., & Fürjes, P. Preparation and Characterization of SERS Substrates of Different Morphology. In *Advanced Nanotechnologies for Detection and Defence against CBRN Agents* (pp. 63-68). Springer, Dordrecht.. (2018).

[4] I. Rigó, M. Veres, P. Fürjes, SERS active periodic 3D structure for trapping and high sensitive molecular analysis of particles or cells, *Proceedings*, 1(4), 560, (2017);

[5] I. Rigó, M. Veres, L. Himics, S. Tóth, A. Czitrovsky, A. Nagy, P. Fürjes, Comparative analysis of SERS substrates of different morphology, *Procedia Engineering* 168, 371-374. (2016)

# Investigation of Raman scattering spectra of aqueous solutions of high dilution

I.A. Ershov, M.A. Kononov, V.I. Pustovoy, V.V. Svetikov

A.M. Prokhorov General Physics Institute, Russian Academy of Sciences, Vavilov str., 38, 119991, Moscow, Russia

[ershov@nsc.gpi.ru](mailto:ershov@nsc.gpi.ru)

Different methods are used to study aqueous solutions with a low concentration of the analyte. Among them are methods based on plasmon spectroscopy [1] and Raman scattering. A highly sensitive method of research is also a method combining plasmon spectroscopy and Raman scattering. The aim of the presented studies is preliminary determination of the spectral displacements in Raman scattering, which are of interest in the study of small analyte concentrations in water. For this purpose, two samples were investigated by the Raman spectroscopy method: distilled water ( $\rho \sim 0.6 \text{ M}\Omega \cdot \text{cm}$ ) and deionized water ( $\rho \sim 1.2 \text{ M}\Omega \cdot \text{cm}$ ).

For both water samples, the spectra were measured by focusing the exciting radiation in the water volume (approximately at a distance  $h \sim 5 \text{ mm}$  below the surface). For deionized water, an additional measurement was made when focusing on the water surface. The excitation was carried out by laser radiation with a wavelength of  $\lambda = 473 \text{ nm}$  and a power  $P = 10 \text{ mW}$ .

The results of the measurements are shown in Fig.1. It is noteworthy that the intensity of the Raman spectrum for distilled water as a whole repeats the spectrum for deionized water. However, there were differences in the regions  $\nu = 175; 400\text{-}700$  and  $3200\text{-}3600 \text{ cm}^{-1}$  (in Fig. 1 these areas are surrounded by a green dotted line). According to [2], the presence of additional ions in water leads to a decrease in the intensity of the oscillatory level  $\nu_{h2}$  ( $175 \text{ cm}^{-1}$ ).

In addition, there is a change in the slope of the spectral dependences in the region  $\nu = 400\text{-}700 \text{ cm}^{-1}$ . In the region  $\nu = 3200\text{-}3600 \text{ cm}^{-1}$ , an increase in the intensity of Raman radiation for deionized water is observed in comparison with distilled water.

The spectrum features for the case of measurement from the water surface in this series of experiments were observed for the frequencies  $\nu_{11}$  and  $\nu_{12}$ . The spectra for the water surface have less pronounced amplification in the region of these frequencies. According to the results of these experiments, when investigating Raman scattering from solutions with small analyte concentrations, special attention should be paid to the investigation of spectral windows  $\nu = 175; 400\text{-}700$  and  $3200\text{-}3600 \text{ cm}^{-1}$ .

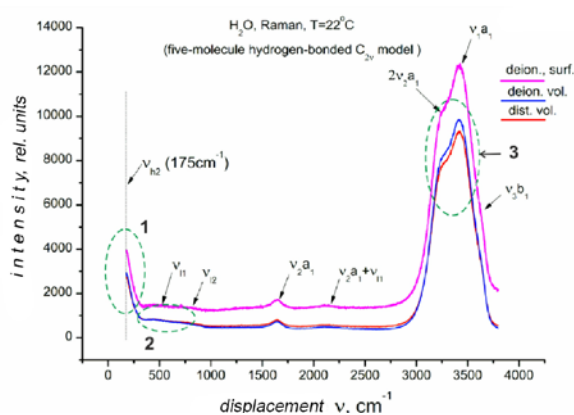


Рис.1 – Raman spectra of water (red curve - distilled water, measurement in volume, blue curve - deionized water, measurement in volume, crimson curve - deionized on the surface)

[1] Vinogradov S.V., Kononov M.A., Pustovoi V.I., Svetikov V.V. "Plasmonic spectroscopy of the water solutions of the copper phthalocyanine adsorbed on a silver surface", *Prikladnaya Fizika (Applied Physics, Russia)*, v.1, pp.69-73 (2018)

[2] G.E. Walrafen, "Raman Spectral Studies of Water Structure", *The Journal of Chemical Physics*, v.40, no.11, pp.3249-3256 (1964)

# Multi-Wavelengths Fluorescence and Raman Spectroscopic Study of The SiV Center Containing Diamond Nanostructures

**L. Himics<sup>1</sup>, M. Veres<sup>1</sup>, M. Koós<sup>1</sup>, S. Tóth<sup>1</sup>, I. Rigó<sup>1</sup>, P. Baranyai<sup>1</sup>, T. Váczi<sup>1</sup>, A. Czitrovsky<sup>1</sup>, A. Nagy<sup>1</sup>, R. Holomb<sup>1,2</sup>, D. Oszetzky, N. Felgen<sup>3</sup>, C. Popov<sup>3</sup>**

*1- Wigner Research Centre for Physics, Hungarian Academy of Sciences, HU-1121 Budapest, Hungary, Konkoly-Thege M. St. 29-33*

*2-Uzhhorod Uzhhorod National University, UA-88000 Uzhhorod, Ukraine, Universytets'ka St. 14*

*3- University of Kassel, DE-34125 Kassel, Germany, Mönchebergstraße 19*

*himics.laszlo@wigner.mta.hu*

Optically active point defects or so called “color centers” in diamond nanostructures are very promising nano-objects and they are attracted the interest of many researchers and companies in the last decades. Some diamond color centers, like nitrogen-vacancy (NV) or silicon-vacancy (SiV) have unique physical and optical properties like intensive, stable and narrow emission band, single photon emission and optically addressable and readable spin state at room temperature. The mentioned properties in combination with the unique nature of diamond nanostructures can significantly contribute to the development of such nowadays intensively studied fields like quantum information processing, nanophotonics, nanobiology and nanomedicine [1].

In high quality diamond crystals - due to the strong covalent bond between the carbon atoms and the well-packed nature of the diamond lattice - the impurity related optically active defect centers behave as individual molecule and the luminescence spectrum of a color center consists of a narrow zero phonon line (ZPL - which is the pure electronic transition of the defect) and a broad phonon sideband (PSB - which is the phonon assisted replica of the pure transition). But the diamond lattice of nanostructures – more interesting for novel applications – can be partially destroyed or may contain non-diamond fragments, which can affect the spectral characteristics and the emitted light intensity of the color centers embedded in this structures [2].

In this paper we report about the experimentally studied effect of different diamond nanostructures on the emission intensity and spectral parameters (peak position and full width at half maximum) of the embedded SiV centers, being one of the most intensively studied impurity related optically active defect in diamond.

SiV centers were created in isolated diamond nanocrystals, nanodiamond films and diamond nanopillars by using the hot filament chemical vapor deposition (HFCVD), the microwave enhanced chemical vapor deposition (MWCVD) and the combination of HFCVD and electron beam lithography techniques, respectively.

Photoluminescence (PL) spectroscopy was used to detect the created SiV centers within the nanostructures and to determine their spectral parameters, while the bonding structure in surrounding of the centers was investigated by Raman spectroscopy. All measurements were performed on a Renishaw micro-Raman spectrometer attached to a Leica microscope and using 325, 488, 532, 635 nm laser lines for excitation.

The results of our experiments show that the created diamond nanostructures with different amount of non-diamond content in form of amorphous and graphitic carbon have significant effect on the emission intensity and on the spectral characteristics of the SiV centers, but the shape and size of the nanostructures are also important. Most tentatively, for the SiV center containing nanodiamond films and nanopillars the grain boundary related internal stress, while for the individual nanocrystals the graphitic carbon shell is the main source of the differences observed in the SiV PL parameters.

This work was supported by the VEKOP-2.3.2-16-2016-00011 grant, which is co-financed by the European Union and European Social Fund.

[1] I. Aharonovich et al. Nature Photonics 5(2011), 397.

[2] L. Himics et al. Optical and Quantum Electronics, 48(2016), 394.

# Synthesis, reversible laser modification and structural characterization of As-S based functional media for ultrafast photonics

**R. Holomb<sup>1,2,\*</sup>, M. Veres<sup>2</sup>, O. Kondrat<sup>1</sup>, I. Rigo<sup>2</sup>, L. Himics<sup>2</sup>, A. Czitrovszky<sup>2</sup>, A. Csik<sup>3</sup>, V. Takats<sup>3</sup> and V. Mitsa<sup>1</sup>**

*1- Uzhhorod National University, Pidhirna Str., 46, 88000 Uzhhorod, Ukraine*

*2- Wigner Research Centre for Physics, Hungarian Academy of Sciences, 1121 Budapest, Hungary*

*3- Institute for Nuclear Research, Hungarian Academy of Sciences, H-4001 Debrecen, Hungary*

\* e-mail: holomb@gmail.com

Non-crystalline chalcogenides with high infrared transparency, have stood out as materials of choice for infrared optics. Research into the physical properties of these materials revealed their unique and remarkable structural, electronic, optical properties and large functionality, and has attracted significant attention, representing an important scientific and technological challenge. In addition to their intrinsic infrared properties, they offer wide possibilities in domains such as information technologies (optical data storage, ultrafast optical transmission and information processing), photolithography, renewable energy technologies (high efficiency solar cells, solid electrolytes), medicine, thermal imaging, sensing and biosensing *etc.* thanks to the advantageous combination of infrared properties, optical activity, structural photosensitivity and high third-order optical non-linearity. Recent progress in photonics shows that amorphous chalcogenides are among the best candidates as active optical media for ultrafast *all-optical* processing systems [1].

We report the results of investigation of As-S chalcogenide thin films prepared by thermal evaporation of target  $\text{As}_2\text{S}_3$  glass and by gold-catalyzed thermally initiated chemical vapor deposition. The crucial difference between the structure and properties of these films was observed. The structure of as-deposited  $\text{As}_2\text{S}_3$  film prepared by thermal evaporation method contain large concentration of photosensitive realgar-like  $\text{As}_4\text{S}_4$  inclusions in comparison with the structure of bulk  $\text{As}_2\text{S}_3$  glass as confirmed by the Raman spectra (Fig. 1, curves 1 and 2). Recently, using synchrotron radiation photoelectron spectroscopy the reversible transformation of the structure of As-S films prepared by thermal deposition in "laser irradiation"- "thermal annealing" cycles was detected [2].

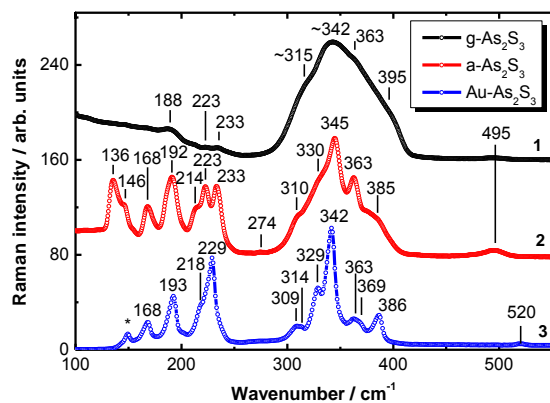


Fig. 1. Raman spectra of bulk  $\text{As}_2\text{S}_3$  glass (1), amorphous  $\text{As}_2\text{S}_3$  film prepared by thermal deposition (2) and  $\text{As}_2\text{S}_3$  nanolayers synthesized by using gold catalysis (3).

In contrast, the growth of molecular nanocrystals on the surface of  $\text{As}_2\text{S}_3$  films synthesized with using gold-catalysis were observed. The formation of crystallites, their size and shape on the surface of  $\text{As}_2\text{S}_3$  films are well defined by electron microscopy. These crystallites are built from a new type of cage-like molecules. Surface enhanced Raman spectra (Fig. 1, curve 3) of crystallites used together with the results of density functional theory (DFT) calculations of Raman active modes of different cage-like As-S nanoclusters [3] let us to identify the  $\text{As}_4\text{S}_5$  cage-like molecules, which form the tetra-arsenic pentasulfide (uzonite).

The structure formation, laser induced modification of the structure and properties of As-S chalcogenide thin films prepared by different methods as well as their application in modern photonics are discussed.

[1] B.J. Eggleton, B. Luther-Davies, and K. Richardson, Chalcogenide photonics, *Nat. Photonics*, Vol. 5, pp. 141-148 (2011).

[2] O. Kondrat, R. Holomb, N. Popovich, V. Mitsa, M. Veres, A. Csik, A. Feher, N. Tsud, M Vondráček, V. Matolín, and K.C. Prince. In situ investigations of laser and thermally modified  $\text{As}_2\text{S}_3$  nanolayers: synchrotron radiation photoelectron spectroscopy and density functional theory calculations, *Journal of Applied Physics*, Vol. 118, pp. 225307(1-7) (2015).

[3] R.M. Holomb, First-principles calculations and characterization of  $\text{As}_4\text{S}_m$  and  $\text{As}_4\text{Se}_m$  ( $m=1-6$ ) type molecular clusters, *Uzhhorod University Scientific Herald. Series Physics*, Vol. 33, pp. 30-35 (2014).

# Third-Harmonic Generation in Silicon Nanowire Arrays

A.S. Ustinov<sup>1</sup>, L.A. Osminkina<sup>1</sup>, A.I. Efimova<sup>1</sup>, S.V. Zaboltnov<sup>1,2,3</sup>, L.A. Golovan<sup>1</sup>

1- Physics Department, M.V. Lomonosov Moscow State University, Moscow, 119991, Russia

2- National Research Center 'Kurchatov Institute', Moscow, 123182, Russia

3- FNBIC, Moscow Institute of Physics and Technology, Moscow, 123098, Russia

lexa97.ustinov@yandex.ru

An important direction of modern photonics is the study of metamaterials - artificial media formed by particles, whose dimensions are comparable with the wavelength in the medium. The use of materials with a high refractive index makes it possible to ensure the concentration of the electromagnetic wave field in the particle. The ensembles of such particles can, in addition, exhibit strong light scattering accompanied by a significant increase in the photon lifetime in such a medium. The interaction of these two effects is of great interest. To study it, one can use methods of nonlinear optics that are highly sensitive to local fields.

Arrays of silicon nanowires (SiNWs) with a diameter of about 100 nm and a length of 0.1 — 100  $\mu\text{m}$  as a metamaterial are of great interest because of their unusual optical properties and the prospects of their use in various devices. Such arrays can be obtained, for example, using the method of metal-assisted chemical etching (MACE) [1]. Among the optical properties of SiNW arrays, it should be noted extremely low reflection and almost complete absorption of visible radiation, a large amount of reflection in the near infrared range, as well as an increase in the efficiency of Raman scattering and interband photoluminescence [2]. These effects are explained by an increase in the lifetime of photons in SiNW arrays, due to strong light scattering in them [3]. On the other hand, the size of SiNWs, comparable to the wavelength in silicon, allows us to consider their arrays as a dielectric metamaterial [4]. In this connection, one would expect the relationship between the structural characteristics of SiNW arrays and their optical properties.

To study this relationship, it is worthwhile to use the method of third harmonic (TH) generation, which is very sensitive to the values of the local field. In the present work we used SiNW ensembles formed by the MACE method on the surface of crystalline silicon with a surface orientation (110), while the SiNWs are inclined at an angle of 45° to the surface of the substrate. Measurements of the orientation dependences of the TH signal were made when the sample was pumped by radiation of the femtosecond laser on Cr:forsterite crystal (1250 nm, 80 fs, 150 mW, 80 MHz).

As it turned out, the efficiency of TH generation and its orientation dependences are significantly conditional on the direction of incidence of the pump radiation, along the SiNWs or perpendicular to them. In the latter case, the TH signal is several times higher than the TH signals for the SiNW arrays in the case of a incidence of radiation along them and for crystalline silicon. In this case, a complete change in the orientation dependences is observed. Also TH generation measurements reveals that with the wires oriented in the vertical direction there is a difference between the TH signal for incident radiation with right circular polarization and left circular polarization. Thus, achiral SiNW arrays demonstrate circular dichroism. The sign of the chirality reverses by switching the direction of the wires from upward to downward, consequently demonstrating extrinsic nature of chirality.

Despite strong light scattering by SiNW arrays and its depolarization, TH signal demonstrates its significant anisotropy. In the case of incidence of radiation along the SiNWs a complete change in the orientational dependences is observed. For a crossed polarizer and analyzer, the TH signal in the SiNW arrays is an order of magnitude greater than the TH signal for crystalline silicon. The efficiency of TH generation increases with increasing thickness of the SiNWs layer. The observed effects are due, on the one hand, to light scattering in SiNWs arrays and, on the other hand, to the orientation of the SiNWs along one direction. Thus, it is shown that the generation of TH is sensitive to local fields inside the elements of the scattering medium.

This work was supported by the Russian Foundation for Basic Research (grant № 15-29-01185).

[1] V. A. Sivakov *et al.*, "Realization of vertical and zigzag single crystalline silicon nanowire architectures", *J. Phys. Chem. C.*, 114., pp. 3798–3803, (2010).

[2] L. A. Osminkina *et al.*, "Optical properties of silicon nanowire arrays formed by metal-assisted chemical etching: evidences for light localization effect", *Nanoscale Research Lett.*, 7., p. 524, (2012).

[3] A. Efimova *et al.*, "Enhanced photon lifetime in silicon nanowire arrays and increased efficiency of optical processes in them", *Optical and Quantum Electronics*, 48., pp. 232–240, (2016).

[4] S. Jahani *et al.*, "All-dielectric metamaterials", *Nature Nanotechnology*, 11., pp. 23–36, (2016).

# Control of the Raman scattering efficiency by elastic scattering in suspensions

O.I. Sokolovskaya<sup>1</sup>, N.B. Tkachenko<sup>1</sup>, L.A. Golovan<sup>1</sup>, V.V. Yakovlev<sup>2</sup>

<sup>1</sup> Faculty of Physics, Lomonosov Moscow State University, Moscow, 119991, Russia

<sup>2</sup> Texas A&M University, College Station, Texas 77843, USA

*E-mail: oi.sokolovskaja@physics.msu.ru*

Elastic light scattering is a well-studied phenomenon intrinsic to random media. It is well known that controlled elastic scattering in photonic materials give them completely new properties [1]. In random media this phenomenon can lead to increase in the volume of light-matter interaction (in comparison with homogeneous medium) and even to achieve lasing in such kind of samples [2-4].

It would be instructive to perform a deeper study of how incoherent effects lead to the output signal amplification in random medium. Is it possible to increase spontaneous Raman scattering efficiency by utilizing only scattering properties of medium itself or by adding scatterers in a controlled manner?

In this work numerical simulation and experimental study of the effect that elastic scattering in suspensions has on photon lifetime and Raman scattering efficiency have been carried out. The samples of interest were suspensions of rutile particles with 0.5  $\mu\text{m}$  diameter and GaP particles with diameter of 3  $\mu\text{m}$  in dimethyl sulphoxide (DMSO). Each type of suspension has been prepared with various volume fraction of scatterers.

Exploiting Monte Carlo method the numerical simulation of light propagation in suspensions has been carried out. It has been shown that with the rutile powder addition to DMSO the photon average path length increases. For the volume fractions of scatterers of the order of 0.1 the increase of average photon's pathlength was threefold. The total number of Raman scattering acts also increased as average photon pathlength increases – up to 2.6 times. In the study of Raman efficiency in suspensions of interest by their excitation with the radiation of 1064 and 532 nm the increase in Raman signal was observed and was fourfold and threefold respectively. Therefore, the simulation results had a qualitative agreement with the experimental results. If GaP powder is added to DMSO, the average photon's pathlength and Raman intensity strongly decreased with the growth of their volume fraction. The corresponding experiments confirmed these results.

By means of optical heterodyning method scattering dynamics in suspensions was studied. Cr:forsterite laser radiation (80 fs, 1250 nm) were used. The dependence of photon lifetime on volume fraction of scatterers turned out to be non-monotonic. The maximum increase in photon lifetime was up to 1.5 ps. The results of the corresponding numerical simulation of temporal dynamics of pulse propagation in suspensions have a good agreement with the experimental study.

Thus, the numerical simulation of light propagation in suspensions of rutile in DMSO and the results of corresponding experiment have shown the possibility of Raman intensity increase while scattering grows in the medium of interest – up to 4 times. Nevertheless, high volume fractions of scatterers (above 0.001) result in weak photon penetration in the depth of sample and their faster reflection in backward direction; as a result the volume of light-matter interaction decreases. The numerical simulation of light propagation in suspensions of GaP in DMSO and the results of corresponding experiments have shown strong decrease in Raman efficiency in presence of scatterers due to absorption.

This work was supported by the Russian Foundation for Basic Research (grant № 15-29-01185).

[1] D.S. Wiersma, The physics and applications of random lasers, *Nature Physics*, vol. 4, pp. 359-367, (2008).

[2] V.S. Letokhov, Generation of light by a scattering medium with negative resonance absorption, *Soviet Journal of Experimental and Theoretical Physics*, vol. 26, p. 835, (1968).

[3] H. Cao, Y.G. Zhao, H.C. Ong, et. al., Ultraviolet lasing in resonators formed by scattering in semiconductor polycrystalline films, *Appl. Phys. Lett.*, vol. 73, pp.3656-3658, (1998).

[4] B.H.Hokr, J.N. Bixler, M.T. Cone, et al. Bright emission from a random Raman laser. *Nature communications*, vol. 5 pp. 4356-1 -4356-5, (2014).

## Surface optical sensitization in the operation of sensors

**S.I. Valyanskii<sup>1</sup>, S.V. Vinogradov<sup>2</sup>, M.A. Kononov<sup>2</sup>, V.I. Pustovoy<sup>2</sup>,  
V.V. Svetikov<sup>2</sup>, V.V. Savranskii<sup>2</sup>, V.V. Tishkov<sup>3</sup>.**

<sup>1</sup> *National Research Technological University «MISiS», Leninskiy prospekt 4, 119049, Moscow, Russia*

<sup>2</sup> *A.M. Prokhorov General Physics Institute, Russian Academy of Sciences, ul. Vavilova 38, 119991, Moscow, Russia*

<sup>3</sup> *Moscow Aviation Institute (National Research University), Volokolamskoe shosse, 4, 125993, Moscow, Russia*

*mike@kapella.gpi.ru, serge-vin@yandex.ru.*

Using the optical scheme of excitation of surface plasmon, structural photochemical changes of silver iodide nanocrystals in the process of surface optical sensitization caused by weakly volatile dye molecules located in the gas phase were studied.

Chemical and biochemical sensors and sensory systems for the purposes of express analysis have long attracted scientific and technological interest. Among all the diversity of methods, an approach should be distinguished with the use of optical technologies, primarily laser ones. This is due to the fact that in most cases, optical measurement methods allow you to obtain data in a non-destructive manner in real time. In general, the sensory chemical system can be conditionally divided into two subsystems: sensitive and recording. In the sensitive part, reversible or irreversible changes occur under the influence of chemical or biochemical reactions, and the recording part, respectively, records the changes that have occurred either physically or chemically. With this approach, one of the ways to increase the signal-to-noise ratio of the sensor system is the transition from the volume to the planar geometry of the sensitive part. In accordance with this approach, the authors develop a technique based on resonant optical excitation of surface plasmon in thin multilayer structures [1, 2]. The basis of the sensitive element in our case is a polycrystalline film of nanocrystals of silver iodide. Under normal conditions, silver iodide nanocrystals are not sensitive to visible radiation, which allows experiments without additional complications and determines the possibility of further technological use of this material. The process that determines the changes in the above-mentioned polycrystalline film of silver iodide nanocrystals is surface optical sensitization. In general, optical sensitization is the process of sensing a substance to a certain wavelength range of electromagnetic radiation. Usually, the result of exposure to radiation during optical sensitization is the various photochemical transformations of this substance. Accordingly, sensitizers are called sensitizer substances. Arsenazo III is a naphthalenedisulfonic acid and is widely used in photometric methods for the purpose of determining a wide range of metals, so that the techniques are characterized by high selectivity and sensitivity. In our studies, it was shown that arsenazo III is an optical sensitizer. The photo induced reaction in our experiments was carried out on the surface of the solid phase of a multilayer thin-film structure. The number of arsenazo III molecules was at the density level at the saturated vapor pressure of the substance under normal conditions. The first phase of research aimed at creating an optical chemical sensor with optical spectral selectivity was performed by the experiments. The next step would be to conduct studies to determine the reaction conditions of arsenazo III with metal atoms on the surface of a polycrystalline silver iodide film. It is probably possible to assume that arsenazo III, being a chemical analytic, but used in solutions, being on the surface of a polycrystalline film, can enter into a chemical reaction with metal atoms.

[1] Vinogradov S.V., Kononov M. A., Kononov V. M., Savransky V.V. // Bulletin of the Lebedev physics institute . **42**, (1), 30, (2015).

[2] Vinogradov S.V., Kononov M.A., Savranskii V.V., Valyanskii S.I., Urbaitis M.F. //Quantum Electronics. **33**. (8). 711, (2003 ).

# Investigation of the adsorption of copper phthalocyanine from aqueous solutions on the metal surface by the plasmon resonance method

M.A. Kononov, N.P. Khakamova, V.I. Pustovoy, V.V. Svetikov

A.M. Prokhorov General Physics Institute, Russian Academy of Sciences, ul. Vavilova 38, 119991, Moscow, Russia  
[pustovoy@nsc.gpi.ru](mailto:pustovoy@nsc.gpi.ru)

One of the most sensitive methods for determining low concentrations of liquids dissolved in a liquid is a method based on measuring the excitation parameters of surface plasmon (SP) at the metal/analyte interface. When the refractive index of the analyzed varies, for example, due to the presence of impurities, the SP wave vector has to change. That change may be registered by monitoring of SP launching conditions.

In our work, we investigated the adsorption of dyes from an aqueous solution onto the metal surface by excitation of surface plasmon resonance (SPR) [1]. To study aqueous solutions of copper phthalocyanine ( $C_{32}H_{16}CuN_8$ ), a measurement scheme was constructed using a fixed wavelength of the laser. The excitation parameters in this case are determined from the dependence of the intensity of the reflected radiation on its angle of incidence on the investigated interface.

Two series of experiments were conducted in which surface electromagnetic waves (SEW) were excited on the surface of a silver film contacting with aqueous solutions of phthalocyanine of various concentrations. There were studied twelve samples of water dilutions (C1-C12) of the original solution Copper (II) phthalocyanine-tetrasulfonic acid tetrasodium salt (Sigma-Aldrich) at initial concentration of 0.001 M.

The overall aim of the experiments was to find the dependence of the reflection contrast (Height) and the angular width at the half height (width) of the reflected laser radiation when the SP is launched depending on the degree of aqueous dilution. To measure the reflection contrast, a value equal to the difference between the maximum and minimum in the reflection of the laser beam was used. The experimental results (fig.1) demonstrate the dependence of the excitation parameters of the surface plasmon: the width of the excitation line of the surface plasmon (red curve) and the magnitude of the change in the intensity of the reflected radiation (blue curve) on the concentration of solutions.

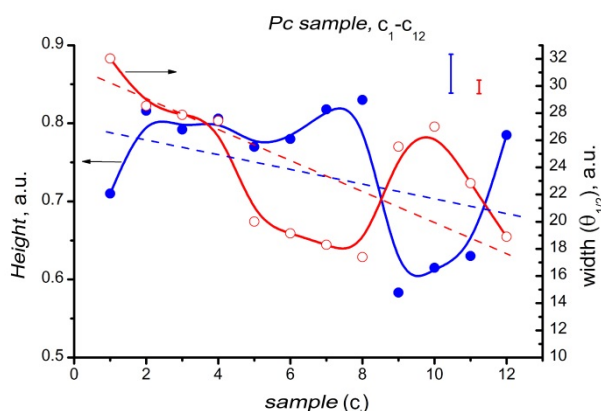


Fig.1. Dependence of the depth of the dip (blue curve) and the angular width at half-height (red curve) of the light reflection curves for the excitation of PP in aqueous solutions of phthalocyanine. Dotted lines-approximation by linear dependence.

The linear approximation of the measured curves shows the general trend of the measured dependences on the solution number.

At the same time, the experimental curves show local deviations from the linear dependence, which require further investigation.

[1] Vinogradov S.V., Kononov M.A., Pustovoi V.I., Svetikov V.V. "Plasmonic spectroscopy of the water solutions of the copper phthalocyanine adsorbed on a silver surface", *Prikladnaya Fizika (Applied Physics, Russia)*, v.1, pp.69-73 (2018)

# Investigation of island films by surface plasmon spectroscopy method

M.A. Kononov, V.I. Pustovoy, V.V. Svetikov

A.M. Prokhorov General Physics Institute, Russian Academy of Sciences, ul. Vavilova 38, 119991, Moscow, Russia

[svetikov@nsc.gpi.ru](mailto:svetikov@nsc.gpi.ru)

It is known that modern technological operations in microelectronics, integral photonics, and also in modern biomedical research require precise measurements of the geometric and dielectric parameters of nanoscale layers. In some cases, due to the specificity of the formation of nanometer layers, consisting of the island growth mechanism in the initial stages, the use of traditional optical methods does not allow obtaining objective information. The present article is devoted to the investigation of application of the plasmon spectroscopy method for monitoring the formation parameters of cluster nanometer films.

To study the island film growth aqueous solutions of copper phthalocyanine were used in our experiments. This was due to the fact that the adsorption of phthalocyanine on the metal surface leads to the formation of polymer aggregates, which include a very large number of molecules. To investigate the process of adsorption of a dye on the substrate surface, a method of surface plasmon spectroscopy was used. The surface plasmon (SP) in our experiments was excited on the surface of silver in the Kretschmann geometry [1]. Typical curves of the intensity of reflection upon excitation of a surface plasmon is presented in the fig.1.

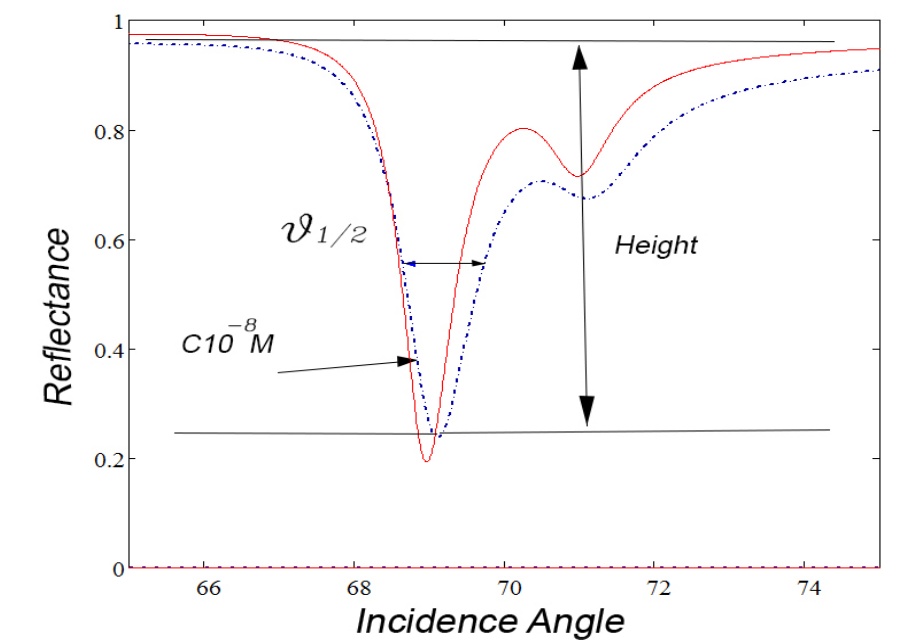


Fig.1. Typical curves of the intensity of reflection upon excitation of a surface plasmon..

It was shown that the process of adsorption of phthalocyanine molecules from an aqueous solution of  $10^{-6}$ - $10^{-8}$  M on the surface of the substrate (in our case, the substrate was the silver surface) was fragmentary with the formation of dye islands. The degree of surface filling by molecular clusters, their thickness and dielectric constant were determined by the numerical simulation of excitation of SEW.

[1] Kretschmann E, Raether H (1968) Z Naturforsch P.2135.

# Spectroscopic Study of Breath Ethylene in People with Schizophrenia and Autism

A. Bratu<sup>1</sup>, C. Popa<sup>1</sup>, M. Petrus<sup>1</sup>, D. C. Dumitras<sup>1</sup>

*1-National Institute for Laser, Plasma and Radiation Physics, Department of Lasers, 409 Atomistilor St., 077125 Magurele, Ilfov, Romania*

*ana.magureanu@inflpr.ro*

Analysis of exhaled breath is a noninvasive sampling technique easy to perform and safe for the patients, having no undesirable side effects. The results are achieved in near real time and data are immediately available to the clinicians, helping in the treatment decision-making process, reducing the number of visits to the clinic.

Oxidative stress has been proposed as one factor that plays a potential role in the etiopathogenesis of neurodegenerative disorders. The understanding of the oxidative stress and the potential role of lipid peroxidation - a degradation of cell membrane by free radicals- in the etiopathogenesis of schizophrenia and autism would be very useful for therapeutic or preventive strategies into clinical settings. Breath ethylene has been associated with oxidant stress. Analysis of breath biomarkers is still in an exploratory area presenting challenges in the field of research and the progress is closely related with the detection techniques.

CO<sub>2</sub> laser photoacoustic spectroscopy is a well known technique for measure trace gases at ppm (parts-per-million) or ppb (parts-per-billion) level. Analysis of exhaled breath using laser-based spectrometer is suitable for molecular identification and quantification to provide the pathophysiological status of the body. The present study uses CO<sub>2</sub> laser photoacoustic spectroscopy to compare the level of oxidative stress (given by the exhaled ethylene) from people with schizophrenia and autism with the level of oxidative stress from individuals with healthy physiological state.

First, we analyzed the breath ethylene of patients with schizophrenia before and after the treatment with Levomepromazine, and we compared the results with the exhaled breath of normal controls. Levomepromazine (Methotrimeprazine) is a phenothiazine that was first introduced in treatments in 1956. From the results of this study, the ethylene of schizophrenia patients were identified in higher concentrations when we compared to the healthy group. So our findings confirm previous determinations that oxidative stress is increased in schizophrenia and that this is unlikely to be a consequence of antipsychotic medications because the breath biomarkers after the treatment were not significantly increased. The results also reveal that the ethylene levels can be considered as a measure of oxidative stress index in people with schizophrenia.

Breath ethylene was also studied from the young adults with autism and results were compared with the exhaled breath of normal controls. In addition to ABA therapy, our subjects were receiving antioxidants and neurostimulative treatment. Treatment with Vitamin B-Complex, Tonotil-N, Neuro Optimizer® 60cps and Cod Liver Oil was instituted for 3 consecutive months. The results indicated that the breath ethylene from people with autism was not significantly increased compared to the healthy group.

The purpose of this study was to determine if ethylene biomarker from the breath of patients with different neurological disorders have different levels compared with a healthy control groups. In conclusion, the data from this study support the hypothesis of the oxidant/antioxidant balance as a key component that may contribute to different pathologies.

[1] T. Risby, S. Sehnert, Clinical application of breath biomarkers of oxidative stress status, *Free Rad Biol Med* 27 (11-12), 1182–1192, (1999)

[2] J. J. Bradstreet, S. Smith, M. Baral, D.A. Rossignol, Biomarker-guided interventions of clinically relevant conditions associated with autism spectrum disorders and attention deficit hyperactivity disorder, *Alternat. Med. Rev.* 15, 15–32, (2010).

[3] D. Pavlovic, V. Tamburic, and I. Stojanovic, "Oxidative stress as marker of positive symptoms in schizophrenia," *Facta Univ.* 9(2), 157–161, (2002).

# The effect of the lack of synchronisation between pMDI activation and inhalation on the lung deposition of aerosol drugs

**Sz. Kugler<sup>1</sup>, A. Kerekes<sup>1</sup>, A. Nagy<sup>1</sup>, A. Czitrovsky<sup>1</sup>**

*1- Department of Applied and Nonlinear Optics, Institute for Solid State Physics and Optics, Wigner Research Centre for Physics of the H.A.S., Budapest, 1121, Hungary*

*Main author email address: kugler.szilvia@wigner.mta.hu*

According to the WHO (World Health Organization) in 2016 approximately 251 million people suffered from COPD (Chronic obstructive pulmonary disease) and 235 million people were affected by asthma. Both diseases can be treated by pressurized metered dose inhalers (pMDI-s) using the proper inhalation techniques. In case of the pMDI-s the inhalation volume capability does not influence the lung deposition of the drug, while the synchronization of the inhalation and the actuation of the device can affect it. The purpose of this work is to study how the lack of synchronization influences the lung deposition efficiency of the pMDI.

The measurement setup consists of a pulmonary waveform generator and an actuator, an induction port, a vacuum pump with a critical flow controller and an Aerosol Particle Sizer (APS) Spectrometer. The applied APS provides accurate number size distributions for aerosol particles with aerodynamic diameters from 0.5 to 20 micron in 52 channels.

26 healthy adult volunteers were examined to see how their inhalation profile changes due to the selected pMDI. Two groups were defined according to the length of their inhalation time (4 and 6 seconds). From each group the 50th percentile inhalation curve was considered [1] and the waveforms were programmed into the pulmonary waveform generator accordingly. The applied time shift started from -0.6 s till 4 or 6 s and the size distributions and the concentrations of the drug particles were measured with the APS.

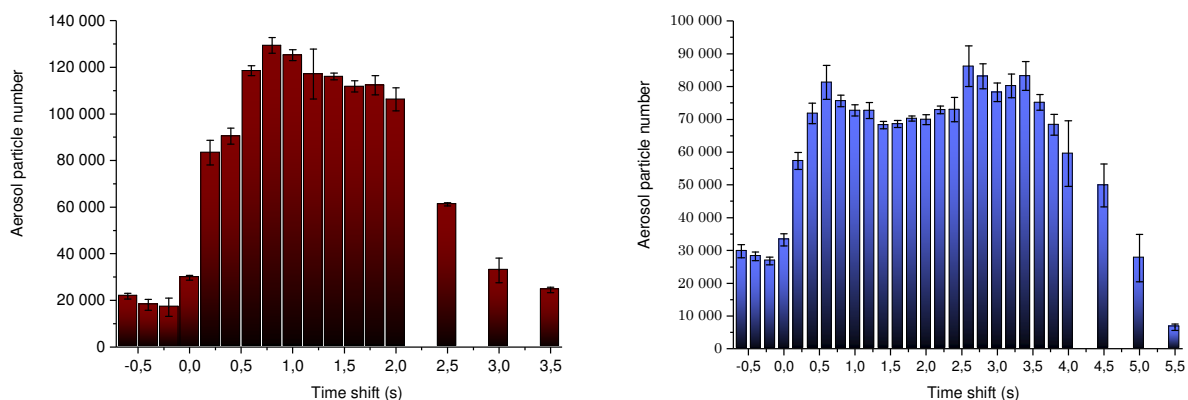


Fig. 1.: Mean aerosol particle number and its standard deviation at different time shifts

According to Fig. 1 early actuation of the pMDI results to the fact that only a small part (maximum 30%) of the emitted aerosol particles can reach the lung. The length of the puff is 0.2 seconds and it remains in the mouthpiece with deposition by impaction. In case of the late actuation the first half of the time shift (maximum up to 3 seconds) results to the optimal deposition in the lung.

[1] D. Casaro, G. Brambilla, I. Pasquali, In vitro aerosol performances of NEXThaler® using representative inhalation profiles from asthmatic patients, *Respir. Drug Delivery*, vol. 2, pp. 375–379 (2014).

[2] Á. Farkas, A. Horváth, A. Kerekes, A. Nagy, Sz. Kugler, L. Tamási, G. Tomisa, Effect of delayed pMDI actuation on the lung deposition of a fixed-dose combination aerosol drug, *International Journal of Pharmaceutics*, vol. 547, pp. 480–488 (2018)

## **Spectral assessment of ultrasound process influence during production of the implants based on dura mater**

**P.E. Timchenko<sup>1</sup>, E.V. Timchenko<sup>1</sup>, L.T. Volova<sup>2</sup>, O.O. Frolov<sup>1</sup>**

<sup>1</sup>*Samara National Research University, 443086, Russia, Samara, Moscow highway, 34*

<sup>2</sup>*Experimental Medicine And Biotechnologies Institute of the Samara State Medical University, 443079, Russia, Samara, Gagarin Street, 20*

[laser-optics.timchenko@mail.ru](mailto:laser-optics.timchenko@mail.ru)

The prevalence of gingival recession increases with age from 38% in the age group 30-39 to 90% in the age group 80-90 [1]. One way of dealing with gingival recession is using the allogenic human dura mater, made by original "Lioplast®" method (TU- 9398-001-01963143-2004), as plastic material. The success of such surgeries depends on the material quality and technologies of production maintaining the necessary biological components of extracellular matrix (EM), such as collagens, glycosaminoglycans (GAG), proteoglycans [2] and removing cellular components (DNA, RNA) and lipids. The application of grafts is impossible without the preclinical estimation of their biological effect. For the estimation of their quality histological, biochemical and immunological methods are used. The main disadvantage of those methods is their destructive influence on the analyzed samples along with their high cost and complexity. From this point of view the Raman spectroscopy can be effective for estimation of EM basic components of the grafts obtained from the dura mater.

The subjects of the research were the samples of dura mater 10\*10 mm in size. All samples were divided into two groups: the first group was treated by ultrasound (UN); the second group was formed by the samples without ultrasonic treatment (BN). In the process of production of grafts from the dura mater by "Lioplast®" method, the first stage of graft production includes the special ultrasonic cleaning from antigenic structures for primary sterilization of the material and viral inactivation.

Using the method of spectral contour selection and Gaussian function deconvolution the nonlinear regressive analysis of Raman spectrums was made using the MagicPlotPro software, consisting of their spectrum decomposition. The principal component analysis (PCA) providing visual presentation of relationship between the sampling and variables was used for the multidimensional analysis of the obtained data.

The comparative spectral estimation of component composition of surfaces of the dura mater based graft samples made by "Lioplast®" method with ultrasonic treatment and without it was conducted.

Spectrum deconvolution by selection of spectral contour and chemometric analysis by the principal component method (PCA) allows conducting the extended componential qualitative and quantitative analysis of the dura mater based grafts, of content of basic biomatrix indicators: collagens, proteins, glycosaminoglycans, proteoglycans, DNA / RNA and determining the most representative parameters affecting the graft quality during the rapid assessment.

It was determined that the main differences occurred at 1440, 1738, 1660  $\text{cm}^{-1}$  (lipids & fatty acid), 856 and 929  $\text{cm}^{-1}$  (proline), 1062 and 1167  $\text{cm}^{-1}$  (GAG, CSPG), 1204  $\text{cm}^{-1}$  (tyrosine).

The coefficients were implied and the two-dimensional analysis, showing that the treatment preserves the basic biomatrix components and removes lipids and fats (fatty acid), improving the quality of material, providing good clinical effect of multiple gingival recession treatment, was conducted.

[1] M.K. Moawia, The etiology and prevalence of gingival recession, Journal of the American Dental Association, vol. 134, pp. 220-225, (2003).

[2] H. Chen, P. W. Xu, N. Broderick, In vivo spinal nerve sensing in MISS using Raman spectroscopy, In Proceedings of SPIE, vol. 9802, pp. 98021L, (2016).

# Spectral analysis of the normal bone tissue, the tissue affected by experimental osteoporosis and its prevention using the biotechnology products

**E.V. Timchenko<sup>1</sup>, P.E. Timchenko<sup>1</sup>, E.V. Pisareva<sup>1</sup>, M.Y. Vlasov<sup>2</sup>, L.T. Volova<sup>2</sup>,  
A.S. Tyumchenkova<sup>1</sup>, J.V. Fedorova<sup>1</sup>**

<sup>1</sup> Samara National Research University, 443086, Russia, Samara, Moscow highway, 34

<sup>2</sup> Experimental Medicine And Biotechnologies Institute of the Samara State Medical University, 443079, Russia, Samara, Gagarin Street, 20

[laser-optics.timchenko@mail.ru](mailto:laser-optics.timchenko@mail.ru)

An osteoporosis result in the increase of bone fragility and bone fracture risk and is a common reason of disability and early death of elderly people [1]. Treatment of such patients is time consuming and requires considerable financial expenses. In spite of the fact that there are many groups of medications for osteoporosis treatment and prevention, the problem of effective treatment and diagnostics is a pressing issue today [2]. For their development and the improvement of present methods it is necessary to create the methods of estimation of bone tissue pathological changes at different stages of the disease.

The aim of this work is a spectral estimation of the normal bone tissue, the tissue affected by experimental osteoporosis and its prevention using allogenic biomaterial.

The mature female rats at the age of 6-9 months with a mass of 180-230 grams were used as the samples in the research. The animals were divided into three groups. The first group (control) is a group of healthy animals. The second group (cortisone) is a group of rats, in which the model of osteoporosis was created by cortisone injections. The third group (cortisone + HA) is a group of animals in which the model of osteoporosis was made by injection of cortisone with the subsequent course of treatment using the powder of allogenic hydroxyapatite (HA). The amount of the injected drugs per rat mass estimated 10 mg/kg and 40 mg/kg (the second and third groups were divided into two subgroups).

The research was conducted with the use of stand, implementing the method of Raman spectroscopy. The stand included the high-resolution digital spectrometer Shamrock sr-303i with the spectral range of 200-1200 nm, with the built-in cooling chamber DV420A-OE, the fiber optic probe RPB-785 used for Raman spectroscopy combined with the laser module LuxxMaster LML-785.ORB-04 with the laser wavelength of 785 nm and with the bandwidth of 0.2 nm [3].

More over all samples of the research were analyzed for mechanical breaking and bending strength.

As a result of the research the Raman spectrum decomposition (the Gaussian function was used) using the MagicPlotPro 2.7.2 was conducted. Spectral changes were detected on the wavenumbers of 857 cm<sup>-1</sup>, 956 cm<sup>-1</sup>, 1033 cm<sup>-1</sup>, 1389 cm<sup>-1</sup>, 1430 cm<sup>-1</sup> and 1660 cm<sup>-1</sup> for the groups of samples (control group, group with the model of osteoporosis and group with the model of osteoporosis after the HA treatment).

The coefficients allowing estimating the efficiency of treatment of the cortisone osteoporosis model (10 mg/kg) using HA were introduced. There were no changes during the HA treatment of the model with cortisone of 40 mg/kg, which in this case indicates that treatment of this osteoporosis development model is ineffective.

The results of the research using the Raman spectroscopy method were confirmed by mechanical breaking and bending strength tests.

[1] Lesnyak O.M., Benevolenskaya L.I. Osteoporosis. Diagnostics, prevention and treatment. GEOTAR-Media- vol. 2, pp. 122-141 (2010).

[2] Nasonov E.L. Osteoporosis in a physician practice. Independent journal for practicing doctors. №4 (2011).

[3] P.E. Timchenko, E V Timchenko, E V Pisareva, M Yu Vlasov, N A Red'kin and O O Frolov Spectral analysis of allogeneic hydroxyapatite powders // IOP Conf. Series: Journal of Physics: Conf. Series 784 (2017)

# Optical method of identification and certification of cell tissue graft components during their production

**P.E. Timchenko<sup>1</sup>, E.V. Timchenko<sup>1</sup>, L.T. Volova<sup>2</sup>, O.O. Frolov<sup>1</sup>**

<sup>1</sup> Samara National Research University, 443086, Russia, Samara, Moscow highway, 34

<sup>2</sup> Experimental Medicine And Biotechnologies Institute of the Samara State Medical University, 443079, Russia, Samara, Gagarin Street, 20

[laser-optics.timchenko@mail.ru](mailto:laser-optics.timchenko@mail.ru)

Bone grafts are used in reconstructive surgery to restore bone structural integrity and increase the osteogenic potential of bone fabric [1]. Both cadaveric and vital resective biomaterials are used for production of cell and tissue grafts. The cadaveric tissue harvesting, together with legal problems, leads to a number of difficulties caused by high virus hazard and posthumous hemolysis provoking undesirable serological reactions. The use of vital biomaterials in the graft production can reduce the risk of recipient infection considerably [2]. Also after adoption of the Federal Law N 180-Φ3, dated 23 of June 2016, "On biomedical cell products" the use of allogeneic biomedical cell products on the basis of vital donor materials becomes relevant for many reasons. The use of bone biomaterials as cell carriers imposes high demands on them. Thus, the effective control of biomaterial quality is a relevant issue.

The method of Raman spectroscopy was used as a basic method of cell-tissue graft estimation during its production.

The samples of cancellous bone grafts in a form of 5\*5\*5 mm cubes, made by "Lioplast®" method (TU- 9398-001-01963143-2004), were used as research materials. The samples were divided into four groups. The first group was made by the demineralized samples obtained from cadaveric tissue. The second group was made by the mineralized samples from the same source. The third group was formed by the demineralized samples taken from the heads of femur obtained intraoperatively during hip replacement. The fourth group was formed by the mineralized samples from the same source. On the first stage of bone graft production the low-frequency ultrasonic treatment (24-40 kHz during 2-3 minutes) was conducted, which caused the sample degreasing and removal of all bone marrow from the space between the trabeculae ossea.

Using the method of spectral contour selection and Gaussian function deconvolution the nonlinear regressive analysis of Raman spectrums was made using the MagicPlotPro software, consisting of their spectrum decomposition. Average value of the determination coefficient of the result spectrum, generated by spectral contours, from the original Raman spectrum for area 750-2050 cm<sup>-1</sup>, amounted R<sup>2</sup>=0.99. The principal component analysis (PCA) providing visual presentation of relationship between the sampling and variables was used for the multidimensional analysis of the obtained data.

The comparative spectral estimation of component composition of surfaces of the investigated bone graft samples made by "Lioplast®" method with ultrasonic treatment, demineralization and without processing was conducted.

Spectrum deconvolution by selection of spectral contour and chemometric analysis by the principal component method (PCA) allows conducting the extended componential qualitative and quantitative graft analysis of content of basic mineral and organic components: hydroxyapatites, collagens, proteins, glycosaminoglycans, DNA / RNA.

It was found that during demineralization and ultrasonic treatment the main differences of the investigated sample groups occur at 959 cm<sup>-1</sup> (HAP), 1068 cm<sup>-1</sup> (carbonate) 1440 cm<sup>-1</sup>, 1738 cm<sup>-1</sup> (lipids & fatty acid), 856 cm<sup>-1</sup> and 870 cm<sup>-1</sup> (proline & hydroxyproline).

The implied coefficients allowed confirming that the content of basic graft components necessary for implementation of their osteoinductive and osteoconductive properties appeared to be similar, both in the mineralized and demineralized samples obtained intraoperatively from the heads of femur and in the samples made from cadaveric material.

The two-dimensional analysis of the implied coefficients, allowing estimating the quality of the bone grafts made using different methods, was conducted.

[1] Kirilova I.A., Demineralized bone graft as a osteogenesis stimulant: modern concepts, vol. 3, pp. 105-110, (2004).

[2] Grudyanov A.I., Chupakhin P.V. The method of tissue directed regeneration. Transplant material. - Medical information agency, Moscow, p. 64 (2007).

# **NONLINEAR OPTICS AND PHOTONICS**

# Broadband In-Line 2D Imaging With Different Data Processing

**A.A. Ushakov<sup>1,2</sup>, P.A. Chizhov<sup>2</sup>, V.V. Bukin<sup>2</sup>, A.B. Savel'ev<sup>1</sup>, S.V. Garnov<sup>2</sup>**

*1- M.V. Lomonosov Moscow State University, Moscow, 119991 Russia*

*2- A.M. Prokhorov General Physics Institute RAS, Moscow, 119991 Russia*

*ushakov.aleksandr@physics.msu.ru*

Since 1995 various imaging techniques in the THz range have actively been developed [1]. Imaging with applying of few-cycle pulsed sources and electro-optical sampling allows analyzing THz field waveform and extracting information about delay and phase shift of THz radiation in the studying sample [2–4]. In this paper we implement the large-aperture focal-plane broadband THz in-line imaging for visualization of transparent objects, that allows to increase frame rate in the contrast to raster imaging.

The source of the optical radiation is a Ti:Sapphire laser (central wavelength 775nm, repetition rate 10 Hz, pulse duration 150 fs, pulse energy 2.8 mJ, Gaussian beam diameter 12 mm on the 1/e<sup>2</sup> level, horizontal polarization). The main part of the radiation is used for the THz radiation generation in the THz source, based on the optical rectification of the femtosecond radiation with tilted front of amplitude in LiNbO<sub>3</sub> crystal [5]. THz radiation from the source is collimated by PTFE lens with focal length 10 cm. The studying object is introduced in the beam, thereafter this object is depicted onto the wide-aperture crystal surface ZnTe (10x10x0.5 mm<sup>3</sup>) by PTFE lens with focal length 6 cm. The second part of laser radiation – probe pulse – is propagated through delay line, quarter wave plate, filters and expanding the beam lens. Thereafter the THz and optical beams are combined on the pellicle and directed to the ZnTe crystal. The surface of the detecting crystal is depicted by the telescope onto the digital camera. The polarizer is mounted before the telescope on the probe beam path. The presence of the THz field in the crystal causes the enlightenment or the shading of the crystal image on the digital camera due to linear electro-optical effect [6].

From the obtained images of ZnTe crystal from the digital camera background (THz beam is passed through free space) and signal (THz beam goes through object under investigation) the spatio-temporal distributions of THz field has been received. The subsequent processing of the received 3D spatial-temporal distributions of the THz field has been realized in three different ways: (i) by detecting displacement of the maximum peak position of the THz pulse due to phase delay in the object under study; (ii) by using a cross-correlation function analysis; (iii) by a Fourier transformation of a THz waveform and subsequent extraction the phase difference at each THz frequency. We analyze key parameters for the applying imaging techniques: noise level, image contrast and spatial resolution. The noise level for the THz direct time-of-flight or the THz cross-correlation time-of-flight imaging is noise is error in the delay determination. For the phase imaging we defined the noise level as the RMS recalculated in delay units from the phase difference acquired by pulses passed through the free space and through the object at a certain frequency. Image contrast was defined as the ratio of image brightness with and without the sample near its edge. For the three different techniques in the sequence order as it was mentioned at the beginning of this chapter noise level (in the picoseconds) are 0.06, 0.015, 0.075; Image contrast are 14, 80, 6; spatial resolutions (in  $\mu\text{m}$ ) are 300, 300 and 700 correspondingly.

[1]. X.-C. Zhang and J. Xu. "Introduction to THz wave photonics", Springer, 2010.

[2]. L. Zhang, Y. Zhang, C. Zhang, Y. Zhao and X. Liu, "Terahertz multiwavelength phase imaging without  $2\pi$  ambiguity", Optics Letters, vol. 31, pp. 3668, 2006.

[3]. D.M. Mittleman, S. Hunsche, L. Boivin and M. C. Nuss, "T-ray tomography", Optics Letters, vol. 22, pp. 904-906, 1997.

[4]. J.L. Johnson, T.D. Dorney and D.M. Mittleman, "Enhanced depth resolution in terahertz imaging using phase-shift interferometry", Applied Physics Letters, vol. 78, pp. 835-837, 2001.

# Generation and Control of Dissipative Kerr Solitons in Optical Microresonators by Pump Modulation

**V.E. Lobanov<sup>1</sup>, A.V. Cherenkov<sup>1,2</sup>, A.E. Shitikov<sup>1,2</sup>, N.M. Kondratiev<sup>1</sup>, G.V. Lihachev<sup>1</sup>,  
N.G. Pavlov<sup>1,3</sup>, A.S. Gorodnitskiy<sup>1,3</sup>, M.L. Gorodetsky<sup>1,2</sup>**

*1- Russian Quantum Center, 143025, Skolkovo, Russia*

*2- Faculty of Physics, Moscow State University, 119991, Moscow, Russia*

*3- Moscow Institute of Physics and Technology, 141700, Dolgoprudny, Russia*

*v.lobanov@rqc.ru*

As it was demonstrated for the first time in 2007, microresonators can be used to generate optical frequency combs, i.e. regularly spaced optical laser lines, from a continuous wave (c.w.) laser [1]. It was revealed that the generation of frequency combs in nonlinear microresonators results from the cascaded four-wave mixing process. To date such frequency combs were demonstrated in many types of microstructures of different geometries made of different materials.

Dissipative Kerr soliton correspond to a low-noise frequency comb having smooth envelope in a spectral domain [2]. Wide range of approaches have been elaborated to generate optical frequency in microresonators. The conventional method is based on slow variation of a pump frequency or by a pump power pulsed modulation. In this work we show that the additional pump modulation adds more flexibility to the generation process and may provide the efficient method of tuning of dissipative Kerr solitons properties.

First of all, in several earlier works it was shown that the number of generated solitons is probabilistic and a single-soliton generation is difficult to achieve directly. Single-soliton combs are of specific interest for many applications due to the highly coherent, spectrally smooth and low noise resulting frequency comb. We reveal that the effective single-soliton generation in optical microresonators with an anomalous dispersion can be realized by the frequency scanning method augmented with the phase or amplitude pump modulation [3]. It was found that the efficiency of this approach depends on the frequency scan rate and the modulation depth. The modulation frequency must be equal to one free spectral range (FSR) of microresonator for the effective single-soliton generation, which is the inverted round-trip time of light in the cavity, the modulation depth must be large enough and the frequency scan rate should be small enough. The relevance of the proposed method was confirmed experimentally in MgF<sub>2</sub> microresonator.

Besides that, one may control a soliton repetition rate using pump modulation due to the injection locking effect. If modulation frequency is close enough to the microresonator FSR soliton repetition rate follows modulation frequency. As this effect has been already shown and investigated analytically for the phase modulation [4], we studied numerically the case of pump amplitude modulation and showed that the tuning range is proportional to the modulation depth. One may also use the modulation frequencies divisible by FSR that may expand the repetition range tuning range. Also, in contrast to the case of the phase modulation at amplitude modulation tuning range depends on the mismatch of pump frequency from microresonator eigenfrequency.

Also, it should be noted, that besides conventional solitons corresponding to an anomalous group velocity dispersion one may use the amplitude modulation of the pump for generation of flat-topped dissipative solitonic pulses, “platicons”, and corresponding frequency combs in optical microresonators with a normal group velocity dispersion (GVD) [5] that is quite important since material GVD in the visible and near IR is mostly normal.

This work was supported by the Russian Foundation for Basic Research (Project No. 17-02-00522).

[1] P. Del’Haye, et al., Optical frequency comb generation from a monolithic microresonator, *Nature*, vol. 450, pp. 1214–1217 (2007).

[2] T. Herr, et al., Temporal solitons in optical microresonators, *Nat. Photonics*, vol. 8, pp. 145-152 (2014).

[3] V.E. Lobanov, et al., Harmonization of chaos into a soliton in Kerr frequency combs, *Opt. Express*, vol. 24, pp. 27382-27394 (2016).

[4] J. K. Jang, et al., Temporal tweezing of light through the trapping and manipulation of temporal cavity solitons, *Nat. Commun.*, vol. 6, 7370 (2015).

[5] V.E. Lobanov, et al., Generation of platicons and frequency combs in optical microresonators with normal GVD by modulated pump, *EPL*, vol. 112, 54008 (2015).

# Sum-frequency generation in isotropic chiral material in case of high conversion efficiency.

I.A. Perezhgin<sup>1</sup>, K.S. Grigoriev<sup>2</sup>, N.N. Potravkin<sup>1</sup>, V.A. Makarov<sup>2</sup>

1 - International Laser Center of M.V. Lomonosov Moscow State University, Russia

2 - Physics Faculty of M.V. Lomonosov Moscow State University, Russia

*i.a.perez@gmail.com*

In previous studies [1,2] the problem of sum-frequency generation (SFG) in isotropic chiral medium was considered mostly for the spectroscopy of chiral solutions, when the conversion efficiency of the energy of incident radiation into the energy of radiation at sum-frequency (SF) was low [1]. Nevertheless, it was shown, that two elliptically polarized Gaussian beams propagating coaxially in such a medium generate an inhomogeneously polarized sum-frequency beam [2]. At present time there are artificially created materials (metamaterials) possessing the same symmetry as the isotropic chiral media, and having the efficient values of nonlinear second-order optical susceptibility  $\chi^{(2)}$  ( $\omega_3=\omega_1+\omega_2$ ) several orders higher compared to the ‘classical’ media of this kind (e.g., solutions of chiral molecules). In such materials, SFG can be used for the formation of light beams with inhomogeneous transversal polarization distributions controlled by incident beams, and for the design of optical logic elements. However, the undepleted pump approximation (UPA) widely used in theoretical works for the description of the evolution of SF beam now may have limited validity due to high conversion efficiency of SFG in such highly nonlinear materials.

We have carried out numerical modeling of three-wave mixing in isotropic chiral medium taking into account the evolution of intensity and polarization of all three propagating waves at fundamental and sum frequencies. The impact of the phase mismatch  $v_{SF}$  on the energy conversion efficiency (from fundamental waves to sum-frequency wave) observed in our study is the same, as predicted earlier analytically within the framework of UPA [1]. It is shown that for energy conversion efficiency (proportional to  $\chi^{(2)}$ ) less than 0.001, the UPA describes the evolution of intensity and polarization of SF beam with good precision (better, than 1%), and the polarization effects predicted earlier [2] are also observed in our numerical modeling. If the conversion efficiency increases up to 0.1, the SF beam cannot be correctly described by the UPA, while the fundamental beams remain almost unchanged. For higher values of conversion efficiency, strong changes of the intensity and polarization of fundamental beams occur, along with complex behavior of SF beam, which was not predicted earlier within the UPA theory framework.

Authors acknowledge the support of Russian Foundation for Basic Research, grants No 16-02-00154 and 18-32-00217.

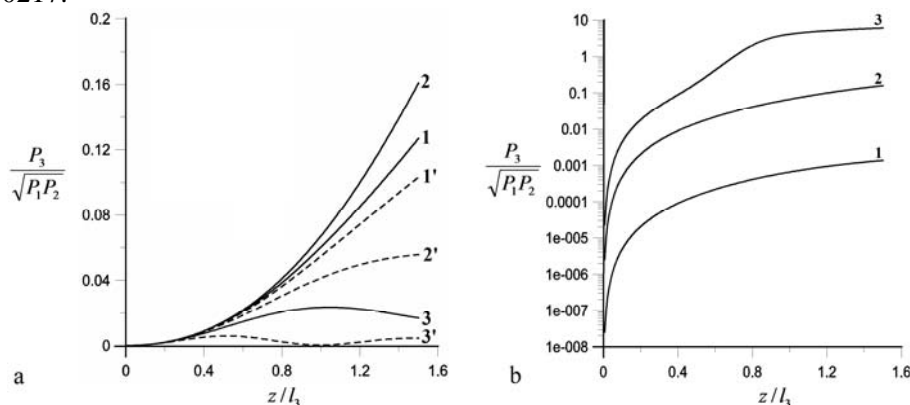


Fig. 1. a) The dependence of the normalized radiation power on the propagation coordinate for different values of the dimensionless phase mismatch  $v_{SF}=\Delta k l_3$ . Curves 1, 2 and 3 (solid lines) correspond to  $v_{SF} = 0.2; 2; 5$ , curves 1', 2' and 3' correspond to  $v_{SF} = -0.2; -1; -5$ . b) The dependence of the normalized radiation power on the propagation coordinate (log-scale) for different values of the energy conversion efficiency  $\sim 10^{-4}$  (curve 1);  $\sim 10^{-2}$  (curve 2);  $\sim 1$  (curve 3).

[1] N.I. Koroteev, V.A. Makarov, S.N. Volkov, Laser Phys., **9**, 655 (1999).

[2] S.N. Volkov, V.A. Makarov, I.A. Perezhgin, QuantumElectron., **36**, 860 (2006).

# Nonlinear optical waveguides: its performance and applications

S. KURIMURA<sup>1,2</sup>

1- National Institute for Materials Science, 1-1, Namiki, Tsukuba 305-0044, JAPAN  
kurimura.sunao@nims.go.jp

Polarity control in  $\chi^{(2)}$  materials has been appealing dramatic progress last two decades, which enables us to design intensity, spectral, and even phase profiles by polarity patterning. Electric-field poling first demonstrated by us in 1992, plays a key role in polarization reversal in ferroelectric materials such as lithium niobate. The technology opened a new horizon in applications of nonlinear optical / electro-optic devices.

## Mg:LN waveguide on LN platform [1]

Because of the high nonlinear coefficient  $d_{33}$  of 25 pm/V, polarization-reversed Mg:LN produces extremely high normalized efficiency of 4600%/W by combining with a ridge waveguide structure. The waveguide called adhered ridge waveguide (ARW), extends interaction length with tightly confined beam size, achieving an enhancement factor of  $>100$  [2]. The 4600%/W device yields 46% efficiency at 10 mW input power, especially being suitable for optical fiber communication operated in the power range of  $<0.1$ W. Such a waveguide works as a parametric amplifier, producing 14.2 dB gain at 1570 nm in difference frequency generation (DFG). The high gain performance helps to build a phase-sensitive amplifier for coherent optical communication.

The  $\chi^{(2)}$ -based device also exhibits ultrafast response in optical sampling due to its virtual transition nature in Mg:LN ARW. Sum frequency mixing between the 640 Gbps data stream and a local clock pulse, produces the error signal for phase locking at 780 nm (Fig.1 (a)). Combination of QPM ARW with a high-speed electronic circuit realizes clock frequency extraction at 640 Gbps from ultra high-speed data signals [3].

The excellent performance also achieved parametric down conversion at low pump power for entangled photon generation. Specially designed ARW produces orthogonally-polarized photon pairs by type II interaction with  $d_{24}$  component (Fig.1 (b)), generating bright narrowband polarization-entangled photons [4].

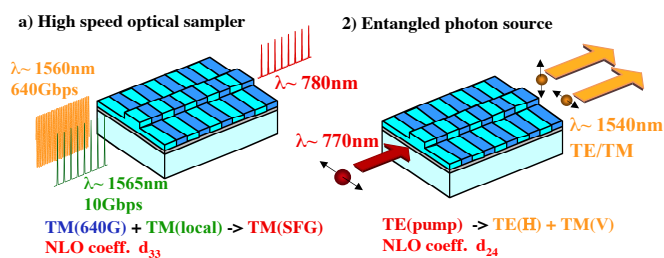


Fig.1 QPM ARW: (a) High speed optical sampler  
(b) Polarization-entangled photon source

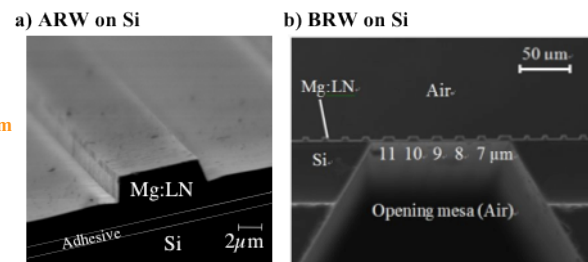


Fig.2 Mg:LN ridge waveguide on Si platform:  
(a) ARW: adhered on Si (b) BRW: bonded on Si

## Mg:LN waveguide on Si platform

Fabrication of a ridge waveguide onto the Si platform is a fascinating approach to hybrid silicon photonics for multi-function integration. Light emission and wavelength conversion are still challenges in Si due to the intrinsic material properties. Because of the centrosymmetric crystal structure of Si, it is difficult to fabricate an efficient nonlinear optical device on the Si platform. The solution we proposed is a hybrid integration with QPM ARW by building a Mg:LN block onto the Si.

We first demonstrated a Mg:LN ridge waveguide on Si with the conventional adhesion technology, as shown in Fig. 2(a). The device exhibits normalized SHG efficiency of 220%/Wcm<sup>2</sup> for 11mm-long interaction length, which encourages ourselves to try more sophisticated work. Nonlinear wavelength conversion between telecom bands was proved by DFG for wavelength-division multiplexing in Si-photonic optical bus system. Our recent device is based on surface-activated bonding technology, which is adhesive-free bonded ridge waveguide (BRW). Mg:LN bonded at room temperature on Si was fabricated into a ridge waveguide in a cladless membrane structure (Fig.2 (b)). The normalized SHG efficiency of  $\sim 120\%/Wcm^2$  was observed at telecom wavelength.

Waveguide nonlinear optical devices become more energy-efficient and have potential applications in various fields such as optical processing/bus and quantum optics. It is grateful to Mitsubishi Heavy Industries, Ltd. for their help for surface-activated bonding.

## References

- [1] S. Kurimura et al., Appl. Phys. Lett. 89, 191123(2006).  
[2] R. Koh et al., Opt. Exp. 19, p.11867 (2011).  
[3] L. K. Oxenlowe et al., J. Light. Tech. 27, p.205 (2009).  
[4] G. Fujii et al., Opt. Exp. 15, p.12769 (2007).

# Structure of polarization singularity lines in the near-field of golden spheroidal nanoparticle irradiated by a monochromatic plane wave

N. Yu. Kuznetsov<sup>1</sup>, I.A. Perezhogin<sup>2</sup>, K. S. Grigoriev<sup>1,2</sup>, V. A. Makarov<sup>1,2</sup>

*1 - Faculty of Physics, M. V. Lomonosov Moscow State University, Russia*

*1 - International Laser Center, M. V. Lomonosov Moscow State University, Russia*

*kir3740@yandex.ru*

The singularities of polarized light, such as the points of purely circular or purely linear polarization, appear naturally in many processes of light-matter interaction. The vast majority of research on polarization singularities is performed within paraxial approximation, which implies that the planes of polarization ellipses in propagating light beams and pulses are perpendicular to their axes. However, in more general kind of non-paraxial electromagnetic fields, which consist of plane waves travelling in different directions, all three Cartesian components of the electric field vector are present and the polarization ellipse can have any possible orientation of its plane. The main properties of polarization singularities in such fields were described in [1], but there are few papers that deal with these objects in real experiments or physical models.

A perfect example of non-paraxial light is the near-field of the metal nanoscale objects in plasmon resonance. In our work we consider the interaction of the golden spheroidal particle with the plane incident monochromatic wave. The distribution of the near-field was earlier found analytically in [2]. By means of linear interpolation over three-dimensional net we obtained the structure of lines of circular and linear polarization (C-lines and L-lines) and visualized it in wide range of the incident radiation parameters. The near-field of a nanoparticle contains two closed C-lines and two closed L-lines that are linked. The topological structure of the lines was shown to be remarkably stable: the number of the lines and their mutual entanglement remained unchanged for different angles of incidence of the plane wave and its different polarization states.

Authors acknowledge the support of Russian Foundation for Basic Research, grant 18-32-00217

[1] M. V. Berry, *J. Opt.*, 6, 657-678 (2004)

[2] E. Chubchev, Yu. Vladimirova, V. Zadkov, *Opt. Express.*, 22, 20432-20445 (2014)

# Validation of the Angular Quasi-Phase-Matching theory for the biaxial optical class using PPRKTP

**Dazhi Lu,<sup>1,4</sup> Alexandra Peña,<sup>1</sup> Patricia Segonds,<sup>1</sup> Jérôme Debray,<sup>1</sup> Simon Joly,<sup>2</sup> Andrius Zukauskas,<sup>3</sup> Fredrik Laurell,<sup>3</sup> Valdas Pasiskevicius,<sup>3</sup> Haohai Yu,<sup>4</sup> Huaijin Zhang,<sup>4</sup> Jiyang Wang,<sup>4</sup> Carlota Canalias,<sup>3</sup> Benoît Boulanger<sup>1</sup>**

<sup>1</sup> Univ. Grenoble Alpes, CNRS, Grenoble INP, Institut Néel, 38000 Grenoble, France

<sup>2</sup> IMS Laboratory, University of Bordeaux, UMR CNRS 5218, 33405 Talence, France

<sup>3</sup> Laser Physics, Applied Physics Department, Royal Institute of Technology, AlbaNova University Center, Roslagstullsbacken 21, 10691 Stockholm, Sweden

<sup>4</sup> State Key Lab. Crystal Materials, Inst. Crystal Materials, Shandong Univ., Jinan, China

dazhi.lu@neel.cnrs.fr

Nonlinear optics deals with a strong coupling between light and matter. Its ability to convert and tune the frequency range of existing laser sources is of prime importance in optical devices. Quasi-phase-matching (QPM) is one main approach in nonlinear optics by a periodic modulation of the sign of the crystal's second-order nonlinear coefficient. It gives the possibility to access to the highest coefficient of the second-order electric susceptibility tensor or to shape the spatial and spectral properties of light. The theory of angular quasi-phase matching (AQPM) has been proposed in 2007 [1]. It corresponds to a generalization of quasi-phase-matching since it is achieved at any angle with respect to the grating vector of the periodically poled medium.

Recently, significant improvement of the electric field poling or bonding techniques have led to larger aperture QPM crystals. Such large-size artificial materials not only allow laser beams with large apertures and high energies to be used, but they also give the possibility to implement AQPM scheme. This scheme was validated for the first time in 2009 in the case of the uniaxial optical class by studying a 5% MgO:PPLN crystal shaped as a sphere [2]. By studying second-harmonic generation (SHG) and difference-frequency generation (DFG), it had been shown in particular that AQPM brings giant spectral acceptances compared with BPM.

In this work, we report the first validation of the AQPM proposal in the case of the biaxial optical class by performing SHG at a fundamental wavelength of  $2.15 \mu\text{m}$  in a large-aperture periodically poled Rb-doped  $\text{KTiOPO}_4$  (PPRKTP) crystal [3] shaped as a sphere as shown in Fig. 1.

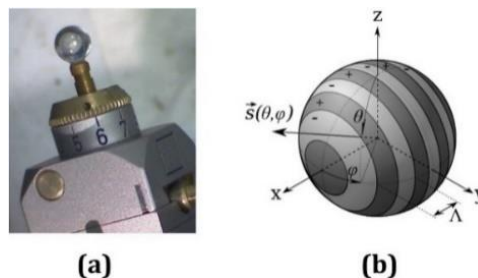


Fig. 1. (a) PPRKTP sphere used for the experiments. (b) Scheme of AQPM in the sphere where  $\Lambda$  is the grating periodicity along the  $x$ -axis and  $\vec{s}(\theta, \varphi)$  is the unit vector of the wave vectors of the interacting waves where  $(\theta, \varphi)$  are the angle of spherical coordinates in the dielectric frame  $(x, y, z)$ .

This validation includes two steps: one is the measurement of the phase-matching angles of the possible AQPM types, the other one is the comparison between the measured generated second-harmonic intensities and the corresponding calculations. The whole set of measurements and discussions will be presented at the conference.

[1] Y. Petit, B. Boulanger, P. Segonds, T. Taira, "Angular quasi-phase-matching," *Phys. Rev. A* 76, 1-7 (2007)

[2] P. Brand, B. Boulanger, P. Segonds, Y. Petit, C. Félix, B. Ménaert, T. Taira, and H. Ishizuki, "Angular quasi-phase-matching experiments and determination of accurate Sellmeier equations for 5%MgO:PPLN," *Opt. Lett.* 34(17), 2578-2580 (2009).

[3] A. Zukauskas, N. Thilmann, V. Pasiskevicius, F. Laurell, C. Canalias, "5 mm thick periodically poled Rb-doped KTP for high energy optical parametric frequency conversion;" *Opt. Mater. Express* 1, 201-206 (2011).

# Numerical modelling of WGM microresonator Kerr frequency combs in self-injection locking regime

**N.M. Kondratiev<sup>1</sup>, V.E. Lobanov<sup>1</sup>, R.R. Galiev<sup>1,3</sup>, N.G. Pavlov<sup>1,2</sup>, M.L. Gorodetsky<sup>1,3</sup>**

*1- Russian Quantum Center, 143025, Skolkovo, Russia*

*2- Moscow Institute of Physics and Technology, 141700, Dolgoprudny, Russia*

*3- Faculty of Physics, Lomonosov Moscow State University, 119991, Moscow, Russia*

*noxobar@mail.ru*

Frequency combs are of great importance for many modern applications in science and technology. Even more interest was attracted to this field, when they were shown to exist in whispering gallery mode (WGM) microresonators [1]. One of the most important objects associated with microresonator-based frequency combs is dissipative Kerr soliton (DKS) [2] representing coherent, broadband optical frequency combs with smooth spectral profile. The DKS may only exist if the pump is red detuned from a WGM resonance to compensate Kerr frequency shift. Usually, this can be achieved by tuning the pump laser frequency from the blue to the red slope of the resonance curve.

The obstacle lies in the temperature drop the resonator experiences when the pump laser transits from the effectively blue detuned (high intracavity power) to the red detuned (lower intracavity power) state. This sudden temperature drop leads to a blue-shift of the resonance frequency and a loss of the soliton state. On the other hand, when the tuning into the soliton state is too quick, the resonator is still cold and its subsequent heating will again lead to a loss of the soliton state. This problem was solved by tuning into the soliton state with an ideal, intermediate speed of frequency scan, such that the resonator reaches the soliton state in a thermal equilibrium, that is, neither too hot nor too cold.

We propose that this problem can be efficiently solved by the self-injection locking of the pump laser [3]. This method is widely used for effective stabilization of different lasers and for their linewidths narrowing [4]. Note, that in the locking regime, the generated frequency is rather close to the WGM resonance and detuning may be close but not equal to zero. The laser-microresonator frequency detuning and their phase distance define this detuning. In this way, by varying the laser diode frequency or laser-microresonator detuning inside the locking band one can control the generated light detuning and reach detuning value sufficient for soliton generation. When switching to the soliton state occurs, the circulating power in the resonator drops down, and the WGM resonance frequency may shift abruptly. However, in the self-locking regime, the pump frequency will follow the thermally-induced shift of the resonance frequency, and solitons survive. Furthermore, in the locking regime the scanning speed is significantly reduced (proportionally to the stabilization coefficient). We study the statistics of soliton generation in the absence of the self-injection locking and show that while the number of generated solitons is probabilistic the single-soliton state is more probable for smaller scanning speed. Thus, self-injection locking regime may provide favorable conditions for single-soliton generation.

Finally, we developed original model describing the process of the frequency comb generation in the self-injection locking regime and performed numerical modelling of this process. We confirmed our predictions and showed that nonlinear frequency shift helps to reach the desired detuning and reach the soliton comb state inside the locking band. We numerically demonstrated both soliton (anomalous dispersion) and platicon (normal dispersion) generation in self-injection locking regime. The platicon generation may be explained by the dispersion defect arising from self-injection locked mode shift [5].

This work was supported by the Russian Science Foundation (Project No. 17-12-01413).

[1] P. Del'Haye, et al., Optical frequency comb generation from a monolithic microresonator, *Nature*, vol. 450, pp. 1214–1217 (2007).

[2] T. Herr, et al., Temporal solitons in optical microresonators, *Nat. Photonics*, vol. 8, pp. 145-152 (2014).

[3] N. M. Kondratiev, et. al., Self-injection locking of a laser diode to a high-Q WGM microresonator, *Opt. Expr.*, vol. 25, pp. 28167-28178 (2017).

[4] W. Liang, et al., Ultralow noise miniature external cavity semiconductor laser, *Nature Comm.*, vol. 6, 7371 (2015).

[5] V.E. Lobanov, et. al., Frequency combs and platicons in optical microresonators with normal GVD, *Opt. Express* 23, 7713-7721 (2015).

# The third harmonic medium power W-band gyrotron for various applications

A.A. Bogdashov<sup>1</sup>, A.P.Fokin<sup>1</sup>, A.S. Sedov<sup>1</sup>, A.S. Zuev<sup>1</sup>

*1- Federal Research Center Institute of Applied Physics of the Russian Academy of Sciences (IAP RAS) 46 Ul'yanov Street, 603950, Nizhny Novgorod, Russia*

One of the most popular microwave frequency bands now is the W-band [1,2]. It is attractive by the atmospheric transparency window, which makes it promising for a number of scientific and technical applications including radiolocation, communication, detection of hidden objects and the creation of medical devices [3-6]. The output power level in both continuous and pulsed regimes for the aforementioned applications should be in the order of several kilowatts and above. This makes the gyrotron one of the most high-potential sources of electromagnetic radiation in this range [7].

One of the main subsystems of the gyrotron setup is a magnet that creates the necessary level of the guiding and cavity magnetic field in a given volume. Cryomagnets operating with low-temperature fluids are expensive and require special operating conditions. However, now there are cheaper projects of "warm" (with water or oil cooling) magnets with a bore hole diameter sufficient for a gyrotron and a field level of more than 1 T. The simplest estimates show that for the creation of a low-cost W-band gyrotron setup with a warm magnet it is required to operate at the third harmonic of the cyclotron frequency.

The improved design of an electrodynamic system based on the use of a diaphragm in the output waveguide is proposed. This system has been theoretically and numerically analyzed for a W-band gyrotron at the third harmonic of the cyclotron frequency. The optimal parameters of the diaphragm and its position have been selected. With that parameters, the highest value of the starting current of the competing mode is reached while maintaining the starting current of the operating mode. It allows to increase the output radiation power by more than 7 times. An estimate of the accuracy of the manufacturing of the diaphragm has been made. It holds out a hope of scaling this selection method into higher frequency ranges. Further development of this system is primarily tied with a more complex optimization of the system particularly the variation of the length of the cylindrical part of the cavity, which will allow reducing the share of ohmic losses while maintaining high efficiency. Besides the pending issue is the problem of transforming the working mode into modes with other azimuthal variations. However, it seems possible to minimize these losses by choosing the correct diaphragm profile.

The paper is based on the research results, which was conducted in the framework of projects of the Russian Science Foundation №17-79-10422.

[1] V. L. Bratman, A. G. Litvak, and E. V. Suvorov, Mastering the terahertz domain: sources and applications, *Physics-Uspekhi*, vol. 54, no. 8, pp. 837–844, Aug. 2011.

[2] N. Kumar, U. Singh, T. P. Singh, and A. K. Sinha, A Review on the Applications of High Power, High Frequency Microwave Source: Gyrotron, *Journal of Fusion Energy*, vol. 30, no. 4, pp. 257–276, Aug. 2011.

[3] W. M. Manheimer, On the possibility of high power gyrotrons for super range resolution radar and atmospheric sensing, *International Journal of Electronics*, vol. 72, no. 5–6, pp. 1165–1189, May 1992.

[4] B. Kapilevich and M. Einat, Detecting Hidden Objects on Human Body Using Active Millimeter Wave Sensor, *IEEE Sensors Journal*, vol. 10, no. 11, pp. 1746–1752, Nov. 2010.

[5] B. G. Danly et al., Development and Testing of a High-Average Power, 94-GHz Gyroklystron, *IEEE TRANSACTIONS ON PLASMA SCIENCE*, vol. 28, no. 3, p. 14, 2000.

[6] M. Pilosof and M. Einat, A 95 GHz mid-power gyrotron for medical applications measurements January 2015 *Review of Scientific Instruments* 86(016113) DOI10.1063/1.4906507

[7] Sung Gug Kim et al System Development and Performance Testing of a W-Band Gyrotron *J Infrared Milli Terahz Waves* DOI 10.1007/s10762-015-0221-1

# Generation of Platicons on Demand

**A.E. Shitikov<sup>1,2</sup>, V.E. Lobanov<sup>1</sup>, A.V. Cherenkov<sup>1,2</sup>, I.A. Bilenko<sup>1,2</sup>, M.L. Gorodetsky<sup>1,2</sup>**

*1- Russian Quantum Center, 143025, Skolkovo, Russia*

*2- Faculty of Physics, Moscow State University, 119991, Moscow, Russia*

*ShArtEv@gmail.com*

Crystalline microresonators with whispering gallery modes (WGM) are very promising for investigation of nonlinear effects due to uniquely high-quality factors in a wide spectral range. The power threshold of nonlinear effects is proportional to the inverse square of quality factor thus optical nonlinearity can be observed in ultrahigh-Q optical microresonators at a low power level. Kerr frequency combs are subject of the special interest and it can be generated in crystalline microresonators in a result of a cascade four-wave mixing process from a continuous wave laser [1].

Coherent low-noise frequency combs are of particular interest. These combs may be generated in the form of dissipative Kerr solitons in the spectral range with an anomalous group velocity dispersion (GVD) [2] and to date they have been already demonstrated on different platforms. However, most of the dielectric materials used for microresonators have normal GVD in the visible and mid-IR spectral ranges, prohibiting four-wave mixing gain and hence coherent and broadband soliton combs. It was shown recently that in the normal GVD regime coherent frequency combs can be achieved in the form of soliton-like pulses, so-called platicons [3]. It was also demonstrated that the efficiency of transformation of the pump power into the power of the frequency comb lines for platicons is far beyond bright solitons. This may be especially important for many practical implementations. Nowadays properties of platicons are investigated mostly theoretically and numerically [4,5].

In recent years, several methods for the generation of platicons were proposed: the use of a local dispersion perturbations caused by mode interactions [3,6], pump modulation at a frequency equal to the free spectral range (FSR) of a microresonator, bichromatic pump [4], and self-injection locking of a laser source to a mode of the WGM microresonator [7].

We observed experimentally different regimes of frequency combs generation in MgF<sub>2</sub> at 1064 nm with the bichromatic pump. We observed two different generation regimes. The first one was observed if and only if the frequency difference between pumps is equal to the FSR of the microresonator. It resulted in triangular form single-FSR spaced frequency comb. Another one was observed under the same condition but since the generation had started the frequency comb becomes stable with the single pump. The second approach provides rather indented envelope but can be a result of mode-crossings.

We also studied the possibility of frequency combs and platicons generation with self-injection locked laser diode at 780 nm. Different types of frequency combs were obtained and the spectra with platicon-like envelope were observed, narrow beatnote less than 10 Hz was detected respectively.

Pump modulation on a frequency equal to FSR of microresonator provides proper control on detuning and it should help to categorize results obtained previously with self-injection locking and bichromatic pump.

This work was supported by the Russian Foundation for Basic Research (project 17-02-00522).

- [1] P. Del'Haye, et al., Optical frequency comb generation from a monolithic microresonator, *Nature*, vol. 450, pp. 1214–1217 (2007).
- [2] V.E. Lobanov et al., Harmonization of chaos into a soliton in Kerr frequency combs, *Opt. Exp.*, vol. 24, pp. 27382-27394 (2016)
- [3] V.E. Lobanov et al., Frequency combs and platicons in optical microresonators with normal GVD, *Opt. Exp.*, vol. 23, pp. 7713-7721 (2015)
- [4] V.E. Lobanov, et al., Generation of platicons and frequency combs in optical microresonators with normal GVD by modulated pump, *EPL*, vol. 112, 54008 (2015).
- [5] A. V. Cherenkov et al, Raman-Kerr frequency combs in microresonators with normal dispersion, *Opt. Exp.*, vol. 25, pp. 31148-31158 (2017)
- [6] X.X. Xue, et al., Mode-locked dark pulse Kerr combs in normal-dispersion microresonators, *Nat. Photonics*, vol. 9, pp. 594-600, (2015)
- [7] W. Liang et al., Generation of a coherent near-infrared Kerr frequency comb in a monolithic microresonator with normal GVD, *Opt. Lett.*, vol. 39, pp. 2920-2923 (2014).

# Yb Doped Scheelite-Like Double Molybdate Single Crystals as UV to IR Light Down-Converters

**K.A.Subbotin<sup>1,2</sup>, A.I.Titov<sup>1,2</sup>, D.A.Lis<sup>1</sup>, V.A.Smirnov<sup>1</sup>, O.K.Alimov<sup>1</sup>, E.V.Zharikov<sup>1</sup>, I.A.Shcherbakov<sup>1</sup>**

*1- Prokhorov General Physics Institute of Russian Academy of Sciences, Vavilova str. 38, Moscow, Russia*

*2- Mendeleev University of Chemical Technology of Russia, Miusskaya sq. 9, Moscow, Russia*

[soubbot@lsk.gpi.ru](mailto:soubbot@lsk.gpi.ru), [soubbot1970@gmail.com](mailto:soubbot1970@gmail.com)

Nowadays more and more electric energy is generated by semiconductor photovoltaic (PV) cells over the world. However, the efficiency of such PV cells is limited by some fundamental regularities. One of them is: each photon absorbed by a PV-cell produces there just one electron-hole pair. The energy of this pair corresponds to bandgap of the cell material ( $E_g$ ), even if the energy of absorbed photon exceeds this bandgap by factor of 2-3. And all the excess energy transforms to heat. This limitation can be overcome by so called quantum cutting. In this case the special down-converting layer is introduced between Sun and PV-cell. This layer absorbs the high-energy (blue and UV) quanta and emits the doubled number of secondary quanta with two times lower energy, just slightly exceeding the semiconductor bandgap. Then, each of these secondary quanta produces its own electron-hole pair in the semiconductor photovoltaic cell, and, thus, the total energy of the preliminary high-energy quantum transforms into the energy of two electron-hole pairs.

The doubling of the excitations occurs due to the cooperative down-conversion: each donor centre after the UV excitation non-radiatively transfers its excited energy onto two acceptors simultaneously or consequently, and the acceptor relaxes with emission of light quantum. Our research is aimed to test the possibility of usage Yb-doped Scheelite-like molybdate and tungstate crystals as the efficient down-converters, enhancing the efficiency of crystalline silicon photovoltaic cells ( $E_g = 1,14$  eV).

We have grown and studied two big series of Yb doped Scheelite-like molybdate single crystals  $\text{NaGd}(\text{MoO}_4)_2$  and  $\text{NaLa}(\text{MoO}_4)_2$ . Yb concentrations in the melts were from 0 up to 30 at. %. The actual Yb concentrations in the crystals were determined from the optical absorption spectra near 1  $\mu\text{m}$  and the absorption cross-sections known from literature. Besides that, we have also grown and studied a number of Yb doped Scheelite-like crystals of other compositions:  $\text{Yb:CaMoO}_4$ ,  $\text{Yb,Li:CaMoO}_4$ ,  $\text{Yb:CaWO}_4$ ,  $\text{Yb:NaGd}(\text{WO}_4)_2$ ,  $\text{Yb:NaY}(\text{WO}_4)_2$ ,  $\text{Yb:NaGdMoWO}_8$ . In all the crystals (except the undoped ones) we have observed the efficient excitation of 1  $\mu\text{m}$   $\text{Yb}^{3+}$  emission by ‘soft’ UV light (260-360 nm). In molybdate crystals the UV excitation spectrum of  $\text{Yb}^{3+}$  luminescence extends to longer wavelengths, than for tungstates. Hence, molybdates can absorb and transform to Yb luminescence larger fraction of sunlight, than tungstates, and, therefore, they look more promising from the practical point of view.

Based on measurements the dependence of  $\text{Yb}^{3+}$  luminescence intensity at UV excitation upon its content in the samples (in comparison with the same dependence at a resonant IR-excitation directly into  $^2F_{5/2}$  excited state) we have made the conclusion that in heavily Yb doped crystals the mechanism of cooperative down-conversion from donors into the  $^2F_{5/2}$   $\text{Yb}^{3+}$  excited state switches on. In this case the UV quanta, absorbed by donors are transformed for doubled number of IR-quanta, emitted by  $\text{Yb}^{3+}$ . Thus, the studied crystals are promising down-converters for crystalline silicon PV cells.

The nature of donor centres in these crystals is still under the question. Initially, based on the literature data, we assumed that molybdate  $[\text{MoO}_4]^{2-}$  and tungstate  $[\text{WO}_4]^{2-}$  complexes are playing this role in the studied crystals. In fact, these complexes provide broadband luminescence of the crystals in visible region under UV-excitation. However, comparison of the luminescence intensities and decay kinetics for the undoped crystals, and crystals with different Yb concentrations contradict to this version. Charge transfer transitions in  $\text{Yb}^{3+}$ , or  $4f \leftrightarrow 5d$  transitions in  $\text{Yb}^{2+}$  could also, in principle, participate in the revealed down-conversion. However, study and comparison of the absorption spectra of all the studied molybdate and tungstate crystals with each other forced us to exclude this version as well. This work was supported by RFBR (Grant 17-02-01245)

# A possible mechanical realization of a femtosecond SRS optical system with spectral slicing

**Tamás Váczi, László Himics, Péter Schlosser, Barnabás Schlosser**

*Wigner Research Center for Physics, Institute of Solid State Physics and Optics,  
29-33 Konkoly-Thege str., H -1121.Budapest, Hungary*

*vaczi.tamas@wigner.mta.hu*

Stimulated Raman scattering (SRS) microscopy is a new way of biochemical imaging based on vibrational modes of Raman-active molecules. Recent developments are aimed at hyperspectral imaging with high spectral resolution. The spectrally intrinsically broad femtosecond lasers allow to cover a  $100 \text{ cm}^{-1}$  Raman wavenumber region however, detection requires advanced techniques. The spectral slicing approach uses a narrow Stokes beam and the modulation of the different spectral components of the pulse beam with different frequencies, with subsequent demodulation of the contribution of these components to the detected SRS signal. In this work an optical grid based light pulse shaping [1] was used to reach simultaneous multicolor SRS imaging.

The SRS system consists of a Coherent Chameleon dual output laser system generating phase-locked Stokes and pump pulse trains, enabling CARS and SRS microscopy. The Stokes output has fixed wavelength (1040 nm), the other is tunable. An optical grating is used to diffract the tunable beam onto a rotating mirror that scans it long an intensity modulation mask allowing to modulate the spectral components of the pulses at 20 different frequencies between 2 and 3 MHz.

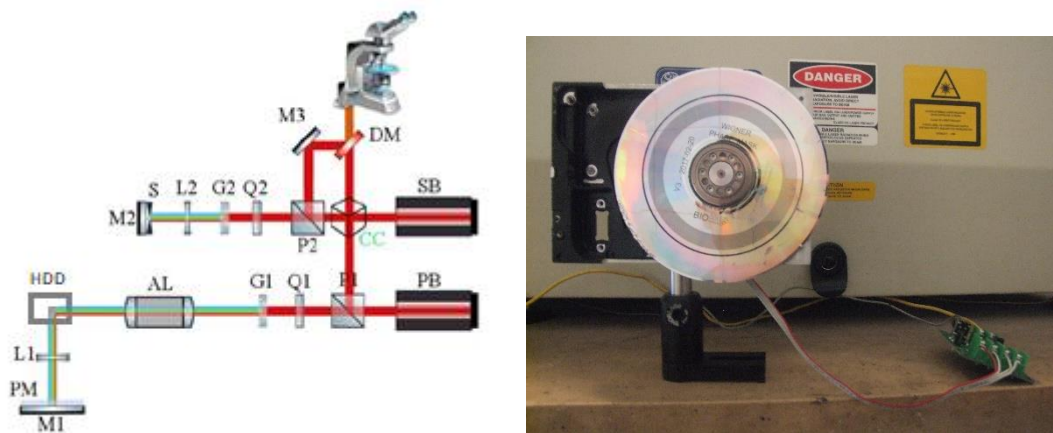


Figure 1. Optical design of the SRS system and its realization. P1 – polarizing beamsplitter, Q1 – quarter-wave plate, G1 – optical grating, AL – achromatic lens, HDD – with regulated motor and modulation mask, L1 – lens, PM – intensity mask, M1 – mirror, P2 – polarizing beamsplitter, Q2 – quarter-wave plate, G2 – optical grating, L2 – lens, S – slit, M2 – mirror, DM – dichroic mirror, M3 – mirror.

## Acknowledgment:

This work is co-funded by the NEURAM programme of the European Union under grant agreement No 712821 and by the VISGEN programme of the European Union under grant agreement No 734862. This work was supported also by the NVKP 16-1-2016-0043 project, implemented with the support provided from the National Research, Development and Innovation Fund of Hungary.

[1] M. Veres, L. Himics, I. Rigó, A. Nagy, S. Tóth, Sz. Kugler, P. Baranyai, A. Czitrovszky, T. Váczi, Proceedings of 18th International Conference on Laser Optics, Sankt Petersburg, Russia, 2018.06.04.-2018.06.08.

# **THz SOURCES AND APPLICATIONS**

# Beams with non-zero projection of the orbital angular momentum in the terahertz range: a review

**B. Knyazev**<sup>1,2</sup>

1- Budker Institute of Nuclear Physics SB RAS, 11, Lavrentieva Ave, Novosibirsk 630090, Russian Federation

2- Novosibirsk State University, 2, Pirogova St., Novosibirsk 630090, Russian Federation

*ba\_knyazev@phys.nsu.ru*

Solving Maxwell's equations in cylindrical coordinates yields states in quantum theory with definite values of energy  $\hbar\omega$ , longitudinal momentum  $\hbar k_z$  and total angular momentum projection  $\ell\hbar$  on the axis  $z$ , where  $\hbar$  is the Planck constant and a quantum number  $\ell = 0, \pm 1, \pm 2, \dots$ . The last quantity in optics is called the “topological charge.” The wave front of such a state is a helicoid, with the lines of force of the Poynting vector representing a screw line. From plane waves, such states differ by the nonzero orbital momentum projection on the direction of motion, and from spherical waves, by the definite direction of motion. For brevity, these states are referred to as “twisted photons” and the beams of such photons as “vortex beams” [1]. Such beams became possible only after the appearance of lasers. Experimentally, the beams with up to  $\ell \approx 10^4$  have been recently obtained [2]. Orbital angular momentum provides an additional degree of freedom with respect to the spin moment with an unlimited number of states, which opens, for example, the possibilities for creating multiplex communication channels. The high rotation energy of such beams can be used to control micromechanical systems. With the help of such beams it is possible to create optical traps for microobjects. To date, almost all studies of vortex beams in optics have been performed in the visible spectral range [3], while the region of long-wave radiation has been practically unexplored. The use of photon beams with large wavelengths, however, can be very useful in some applications. For example, in vortex beams, the ratio of the flux of angular momentum to the momentum flux increases linearly with increasing wavelength. This paper reviews the work in which beams of twisted photons of the terahertz range were formed. Vortex beams were created either using broadband terahertz radiation sources based on femtosecond lasers [4–7], or using monochromatic sources of radiation [8–10]. When creating terahertz vortex beams, various methods of their formation were used, more diverse than in the visible range. We note, however, that there are still few examples of the application of terahertz vortex beams. One interesting demonstration is the diffraction of vortex Bessel beam on a periodic grating of circular holes. A lattice of annular vortex beamlets was formed behind the grating at the Talbot distances.

Funding: Russian Science Foundation (14-50-00080); The Ministry of Education and Science of the Russian Federation (Minobrnauka) (RFMEFI62117X0012, 16.7894.2017/6/7).

- [1] B. Knyazev, V. Serbo, Beams of photons with a nonzero projection of the orbital angular momentum - new results, *Physics Uspekhi*, vol. 61(5) (2018) – in print.
- [2] R. Fickler, G. Campbell, B. Buchler, P. K. Lam, A. Zeilinger, Quantum entanglement of angular momentum states with quantum numbers up to 10,010. *Proceedings of the National Academy of Sciences*, vol. 113(48), pp. 13642-13647 (2016).
- [3] D. L. Andrews, M. Babiker (Eds), *The Angular Momentum of Light* (Cambridge Univ. Press) (2013).
- [4] J. He, X. Wang, D. Hu, J. Ye, S. Feng, Q. Kan, Y. Zhang, Generation and evolution of the terahertz vortex beam. *Optics Express*, vol. 21(17), pp. 20230-20239 (2013).
- [5] Z. Xie, X. Wang, J. Ye, S. Feng, W. Sun, T. Akalin, Y. Zhang, Spatial terahertz modulator. *Scientific Reports*, vol. 3, 3347 (2013).
- [6] K. Miyamoto, K. Suizu, T. Akiba, T. Omatsu, Direct observation of the topological charge of a terahertz vortex beam generated by a Tsurupica spiral phase plate. *Applied Physics Letters*, vol. 104(26), 261104 (2014).
- [7] R. Imai, N. Kanda, T. Higuchi, K. Konishi, M. Kuwata-Gonokami, Generation of broadband terahertz vortex beams. *Optics Letters*, v. 39(13), pp. 3714-3717 (2014).
- [8] X. Wei, C. Liu, L. Niu, Z. Zhang, K. Wang, Z. Yang, J. Liu, Generation of arbitrary order Bessel beams via 3D printed axicons at the terahertz frequency range. *Applied Optics*, vol. 54(36), pp. 10641-10649 (2015).
- [9] B. A. Knyazev, Y. Y. Choporova, M. S. Mitkov, V. S. Pavelyev, B. O. Volodkin, Generation of terahertz surface plasmon polaritons using nondiffractive Bessel beams with orbital angular momentum. *Physical Review Letters*, v. 115(16), 163901 (2015).
- [10] Y. Y. Choporova, B. A. Knyazev, G. N. Kulipanov, et al., High-power Bessel beams with orbital angular momentum in the terahertz range. *Physical Review A*, vol. 96(2), 023846 (2017).
- [11] Z. Wu, X. Wang, W. Sun, et al., Vectorial diffraction properties of THz vortex Bessel beams. *Optics Express*, vol. 26(2), pp. 1506-1520 (2018).
- [12] B. Knyazev, O. Kameshkov, N. Vinokurov, V. Cherkassky, Y. Choporova, V. Pavelyev, Quasi-Talbot effect with vortex beams and formation of vortex beamlet arrays. *Optics Express*, vol. 26(11), pp. 14174-14185(2018).

# Recent progress in continuous-wave-based terahertz technologies for industrial applications

**I.-M. Lee<sup>1</sup>, E. S. Lee<sup>1</sup>, K. Moon<sup>1</sup>, H.-S. Kim<sup>1</sup>, D. W. Park<sup>1</sup>, J. -W. Park<sup>1</sup>, J.-H. Shin<sup>1</sup>,  
H. C. Ryu<sup>2</sup>, and K. H. Park<sup>1</sup>**

*1-THz Creative Basic Research Section, Electronics and Telecommunications Research Institute, Daejeon  
34129, South Korea*

*2- Department of Convergence Science, Sahmyook University, Seoul 01795, South Korea*

*ilminlee@etri.re.kr*

Industrial applications of terahertz (THz) technologies have long been the pursuits of the field. For the use in a wide variety of industrial applications such as the non-destructive evaluations (NDEs), security, telecommunications, and medical imaging, THz technologies that can make a system of small and compact, not much expensive, and easy to be handled should be developed. For such requirements, THz technologies based on continuous-waves (CWs) have been regarded as the promising one, provided if we can improve the performance of CW systems by enhancing some important characteristics such as their emission powers or the detection sensitivities, for example. Under such convention, we have developed the key components for the photonics-based CW THz systems [1-4] of which performance are still on their improvements.

Recently, we are about to see some outcomes as the industrial applications of our photonics-based CW THz systems, especially in the NDEs in some manufacturing companies. Our CW-based THz system, as a proto-type for the actual implementation in the mass-production process of a manufacturing company, is a kind of real-time THz imaging system which can be used as a stand-off NDE instrument to find human errors that may occur in the manufacturing process and hard to be found with other technologies.

In the presentation, we will report our recent progress of our CW THz systems with some illustrative examples for their applications in various industrial field [5]. In addition, our recent efforts to enhance the performances of key components of CW THz systems will be briefly presented [6, 7]. We hope that our recent works in THz field would illustrate a promising potential of the CW THz technologies in the practical aspects.

- [1] N. Kim, J. Shin, E. Sim, C. W. Lee, D.-S. Yee, M. Y. Jeon, Y. Jang, and K. H. Park, "Monolithic dual-mode distributed feedback semiconductor laser for tunable continuous-wave terahertz generation," *Opt. Express*, vol. 17, no. 16, pp. 13851–13859 (2009).
- [2] K. Moon, D. W. Park, I. -M. Lee, N. Kim, H. Ko, S. -P. Han, D. Lee, J. -W. Park, S. K. Noh, and K. H. Park, "Low-temperature-grown InGaAs terahertz photomixer embedded in InP thermal spreading layer regrown by metalorganic chemical vapor deposition," *Opt. Lett.*, vol. 38, no. 24, pp. 5466–5469 (2013).
- [3] I.-M. Lee, N. Kim, E. S. Lee, S.-P. Han, K. Moon, and K. H. Park, "Frequency modulation based continuous-wave terahertz homodyne system", *Optics Express*, 23(2), pp. 846-858 (2015).
- [4] S.-P. Han, H. Ko, N. Kim, W.-H. Lee, K. Moon, I.-M. Lee, E. S. Lee, D. H. Lee, W. Lee, S.-T. Han, S.-W. Choi, and K. H. Park, "Real-time continuous-wave terahertz line scanner based on a compact  $1 \times 240$  InGaAs Schottky barrier diode array detector ", *Optics Express*, 22(23), pp. 28977-28983 (2014).
- [5] E. S. Lee, K. Moon, I.-M. Lee, H.-S. Kim, D. W. Park, J.-W. Park, D. H. Lee, S.-P. Han, N. Kim, and K. H. Park, "Semiconductor-based terahertz photonics for industrial applications," *J. Lightwave Tech.* 36(2), pp. 274-283 (2018).
- [6] J.-H. Shin, K. H. Park, and H.-C. Ryu, "Electrically controllable terahertz square-loop metamaterial based on VO<sub>2</sub> thin film," *Nanotechnology*, 27(19), 195202 (2018).
- [7] K. Moon, E. S. Lee, I.-M. Lee, D.-W. Park, and K. H. Park, "Photo-conductive detection of continuous THz waves via manipulated ultrafast process in nanostructures," *Appl. Phys. Lett.*, 112(3), 031102 (2018).

# Remote gas sensing using long distance THz pulses propagation in the atmosphere

**Tae-In Jeon**

*Korea Maritime and Ocean University, Busan, 49112, South Korea*

*jeon@kmou.ac.kr*

There have been many studies of gas scans using THz-TDS [1,2], and more recent studies have been carried out to detect gases remotely [3]. In recent times, there have been studies of broadband coherent THz pulse propagation in a 186-m and 910-m open path under atmospheric weather conditions [4,5], which provides information for important applications in the atmosphere. We successfully detected CO and N<sub>2</sub>O gases located 93m away from a THz transmitter and receiver chips using the long-path THz time-domain spectroscopy system. The round trip distances that THz pulse travels indoor and outdoor are 27.4m and 158.6m, respectively. Since the absorption of moisture into the outdoor environment can't be controlled, there are water resonances at 0.18, 0.32, 0.38, 0.45, and 0.47 THz in measured spectrum [4,5].

Figure 1 shows the measured THz pulses and spectra transmitter through a 1 m-long gas chamber composed 3 of 33.33 cm length small cells. Each cell is filled with CO gas. The time-domain THz pulses have many oscillations after the main THz pulse. These oscillations indicate resonance in spectrum. Figure 1(b) clearly shows the water resonances of reference and CO resonances of the gas at 0.35 and 0.47 THz. Unfortunately since the resonance at 0.47 THz is too close to the strong 0.45 THz water resonance, the CO resonance is not clear in the spectrum. However, the resonance at 0.35 THz is located between 0.32 and 0.38 THz water resonances. Therefore, the resonance at 0.35 THz can be used to remote gas sensing window for CO and N<sub>2</sub>O gases.

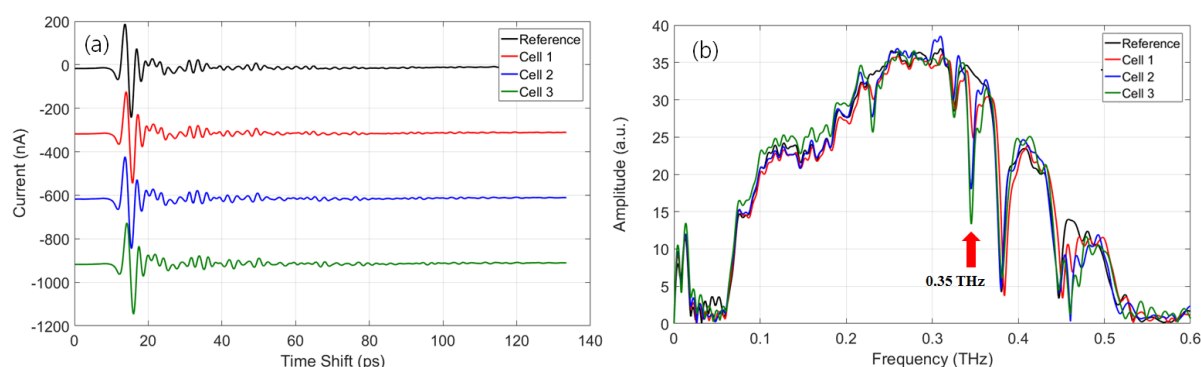


Fig. 1. Measured THz pulses and corresponding amplitude spectra with difference number of CO gas cell. (a) Time-domain THz pulses. (b) Frequency-domain spectra. The red arrow indicates CO resonance at 0.35 THz.

- [1] H. Harde, S. Keiding, and D. Grischkowsky, "THz commensurate echoes: Periodic rephrasing of molecular transitions in free-induction decay," *Phys. Rev. Lett.*, vol. 66, pp. 1834-1837, (1991).
- [2] H. Harde and D. Grischkowsky, "Coherent transients excited by subpicosecond pulses of THz radiation," *J. Opt. Soc. B*, vol. 8, pp. 1642-1651, (1991).
- [3] N. Shimizu, H.-J. Song, T. Furuta, R. Fukasawa, K. Suizu, T. Nagatsuma and Y. Kado, "Active gas sensing with sub-terahertz waves reflected from a wall," *Conference Digest of IRMMW-THz*, R5D7 1293, (2008).
- [4] E.-B. Moon, T.-I. Jeon, and D. Grischkowsky, "Long-Path THz-TDS Atmospheric Measurements between Buildings," *IEEE Trans. Terahertz Sci. Technol.* vol. 5, pp. 742-750 (2015).
- [5] G.-R. Kim, T.-I. Jeon, and D. Grischkowsky, "910-m propagation of THz ps pulses through the Atmosphere," *Opt. Express*, vol. 25, pp. 25422-25434, (2017).

# High resolution THz spectroscopy based on semiconductor superlattices and quantum cascade lasers

V.Vaks<sup>1,2</sup>, V.A.Anfertev<sup>1,2</sup>, E.G.Domracheva<sup>1,2</sup>, S.I.Pripolzin<sup>1</sup>, M.B.Chernyaeva<sup>1,2</sup>,  
A.Baranov<sup>3</sup>, R. Teissier<sup>3</sup>

1- IPM RAS, 7, Akademicheskaya str., Afonino village, Nizhny Novgorod region, 603087 Russia

2- Lobachevsky State University, 23, Gagarina av., Nizhny Novgorod, 603950 Russia

3- Institute of Electronics and Systems (IES), UMR 5214 CNRS - University of Montpellier, France

[vax@ipmras.ru](mailto:vax@ipmras.ru), [masha@ipmras.ru](mailto:masha@ipmras.ru)

Now the actual problems in the gas analysis field have been associated with development of novel methods of analytical research of multicomponent gas mixtures and its application in medical diagnostics (for example, exhaled breath analysis), safety (detection of explosives and poisonous substances) etc. Most of these applications call for precision quantifying of substance in a multicomponent gas mixture, which requires high sensitivity at a 30-100 ppt level. Today, there are a lot of papers which report detection of such gases as CO, NO, ammonia, methane in the infrared (IR) range with detection limit of about 1 ppm - 500ppb. Although, most of these results are obtained for two gas mixtures (usually gas-marker in mixture with N<sub>2</sub>), thus avoiding vibrational bands overlapping, which worsens selectivity and hinders gas identification in multicomponent mixtures. Among the spectroscopic methods, the only approach to date that ensures a near-theoretical-limit sensitivity along with a good spectral resolution limited just by the Doppler effect is the nonstationary spectroscopy based on free dumping polarization effect. Other advantages of the spectrometers include easy-to-use configuration and measurement time of several microseconds that provide registration of unstable gases. Application of this method will also benefit in registration of gas-markers absorption lines at one shot without overlapping effect and performing minimal measuring time of few microseconds. The promising approach is using the multichannel spectroscopic method of two ranges (subterahertz (subTHz) and terahertz (THz)).

The THz radiation sources of the spectrometer based on solid state harmonics generator and QCL are developed. The THz radiation source can be realized on the solid state generator or backward-wave oscillator with frequency multiplying. The multipliers on the base of Schottky diode or quantum semiconductor superlattice (SL) were used. It has a number of advantages comparing with other well-known microwave generators. Also for THz frequency range the QCLs can be used. IES is one of the few scientific centers in the world producing quantum cascade lasers operating in the THz domain. THz frequency range up to 4 THz is the optimal frequency range corresponding to the best QCL performances demonstrated to-date, for spectroscopy tests. QCLs have a high output power and can generate radiation in pulse and continuous modes together with fast tuning of frequency. The cornerstone of the QCL-based radiation source design is a phase-lock loop (PLL) and modulation system. The PLL systems for THz DFB QCL were elaborated. Detection of the radiation in THz frequency ranges are realized by the receiver block based on SL.

The preliminary investigations of gas-markers in THz frequency range have demonstrated the advantages of the high resolution THz spectrometer for noninvasive medical diagnostics based on exhaled breath research (diabetes, lung or gastrointestinal tract cancer), remote detection of explosives (e.g. RDX, PETN) for security systems and investigations of content of grain and food odors for agricultural applications.

The authors acknowledge for partial support from of the Russian Foundation for Basic Research (grant N 18-42-520050 r\_a\_povoljie, N 17-00-00184 KOMFI, N18-52-16017 NCNIL-a).

# Generation of terahertz and X-ray radiation from gas clusters and dynamics of the cluster formation process in Ar super-sonic jet

**A. Balakin<sup>1,2</sup>, M. Dzhidzhoev<sup>1</sup>, V. Gordienko<sup>1</sup>, I. Zhvanya<sup>1</sup>, I. Kotelnikov<sup>3,4</sup>, I. Ivanov<sup>1</sup>,  
N. Kuzechkin<sup>2,1</sup>, P. Solyankin<sup>2,1</sup>, A. Shkurinov<sup>1,2,5</sup>**

1- Faculty of Physics & International Laser Center, Lomonosov Moscow State University, Moscow 119991, Russia

2- Institute on Laser and Information Technologies of RAS, Branch of the FSRC "Crystallography and Photonics", RAS, Shatura, Moscow Region 140700, Russia

3- Novosibirsk State University, Novosibirsk, 630090, Russia

4- Budker Institute of Nuclear Physics of SB RAS, Novosibirsk 630090, Russia

5- The National University of Science and Technology MISiS, Moscow 119049, Russia

*a.v.balakin@physics.msu.ru*

We present results of our research on generation of terahertz (THz) and X-ray radiation in gas clusters under irradiation of Ar gas-cluster jet with high-intense femtosecond laser pulses.

We carried out a numerical simulation of cluster formation process in a super-sonic jet produced under adiabatic extension of gaseous Ar into vacuum (Fig.1), and found that the ratio between non-clusterized monomers, large and small size's clusters significantly varies along the jet propagation. It is shown that the spatial distribution of the cluster concentration represents the clustering dynamics in the jet expansion and that the distance from the nozzle output edge along the symmetry axis of the nozzle is an important parameter describing the properties of the cluster target.

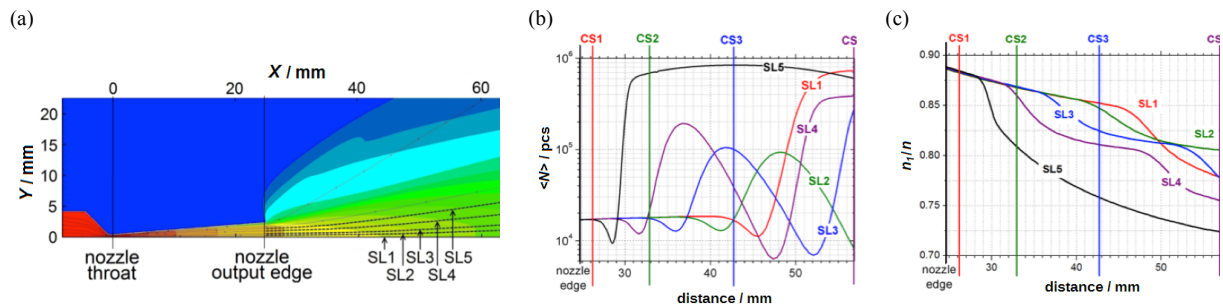


Fig.1 (a) Distribution of Ar atom density inside and outside of the conical nozzle ( $Y = 0$  corresponds to the axis of symmetry of the nozzle, SL1-SL5 represent five stream lines). The magnitude of the density is represented by a color scale:  $\sim 5 \text{ kg/m}^3$  (red),  $\sim 0.3 \text{ kg/m}^3$  (yellow),  $\sim 10^{-2} \text{ kg/m}^3$  (green),  $\sim 3 \times 10^{-4} \text{ kg/m}^3$  (blue), and  $\sim 10^{-5} \text{ kg/m}^3$  (dark blue). (b) The distributions of (a) mean cluster size  $\langle N \rangle$  and (c) ratio of monomer concentration  $n_1$  to the total atomic concentration  $n$  along five stream lines (SL1-SL5) as a function of the distance from the nozzle throat. The units of "pcs" represents the number of Ar atoms in a cluster.

Experimental results on studies of properties of THz and X-ray radiations jointly generated under the laser acting on the jet at various distances below the nozzle output edge are presented and discussed. We shown that the difference in the optimal laser pulse duration for the efficient generation of X-ray and that for the efficient generation of THz radiation can be explained by the different time periods required for the formation of electron subsystems in an Ar cluster.

It is shown that the THz and X-ray emission from the jet could be a useful tool for the study of clustering dynamics in the course of free expansion of gas through a conical nozzle into vacuum.

This work was supported in parts by the Ministry of Science and Higher Education within the State assignment FSRC «Crystallography and Photonics» RAS, by the RFBR under Grants 18-52-16016 and 17-02-01217, by the Ministry of Education and Science of the Russian Federation in the framework of the Increase Competitiveness Program of NUST "MISiS" (no. K2-2017-003).

# Gyrotrons as advanced instrumentation for modern THz applications

G. Denisov, A. Fokin, A. Fedotov, M. Glyavin, G. Golubiatnikov, M. Koshelev,  
M. Morozkin, R. Rozental, A. Sedov, A. Tsvetkov, I. Zotova

*Institute of Applied Physics RAS, 46 Ul'yanov str., 603950, Nizhny Novgorod, Russia*

*ap.fokin@mail.ru*

Development of modern THz applications needs controllable, stable and rather powerful sources of radiation [1]. Such applications as spectroscopy, security, materials processing are interested in the power level up to 1 kW, which nowadays is easily produced by a type of cyclotron resonance maser – gyrotrons. Recently, considerable progress has been achieved in the development of radiation control and stabilization systems, opening new prospects of application of gyrotrons in cutting-edge technology. The features of the advanced sub-THz gyrotrons can be divided into three groups: broadband frequency tuning, fast power and frequency modulation and precise frequency stabilization.

Broadband frequency tuning is achieved by the combination of cavity temperature frequency shift, which is controlled by chiller module in the cooling system and the concept of broadband tuning in the low-Q cavity. The consecutive excitation of longitudinal modes in the short cavity with high current allows tuning the output frequency in range of 5 % of the carrier.

The fast control of output power and frequency with modulation frequencies up to 1 MHz is achieved by the variation of the voltage at the isolated anode of the triode-type magnetron injection gun. The specially designed fast anode voltage control unit allows varying the voltage in range of 1 kV with speed better than 1kV/ $\mu$ s. Demonstrated parameters of the control system provide the possibility of formation of pulses with very short trailing edge, which can be used for the studies of plasma decay. Big modulation bandwidth opens up the possibility of data transmission, with speed more than 1 Mbit/s. The transmission of pseudo-random bit sequence using the sub-THz gyrotron with frequency of 263 GHz [2] as the source is presented in the fig.1.

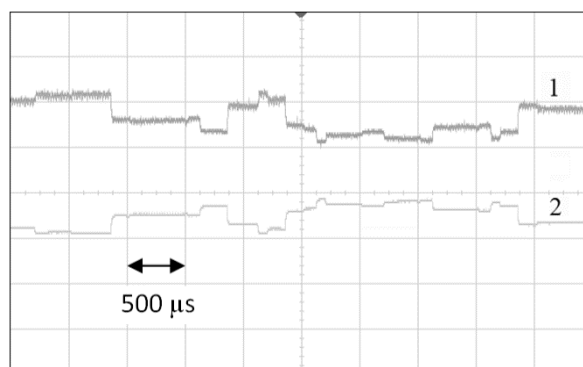


Fig. 1. Fast power modulation - pseudo-random bit sequence: control (modulating) signal (1), terahertz detector signal (2)

Development of the fast control system opened up the possibility of precise frequency stabilization using the phase-lock loop in the anode voltage control. Achieved spectrum width of 1 Hz (relative width  $\Delta f / f = 4 \cdot 10^{-12}$ ) and long-term stability defined by the reference clock opens new prospects of application of gyrotrons in spectroscopy [3].

The abovementioned achievements open up new prospects for the successful use of medium power THz band gyrotrons for the modern applications.

The work was supported by the Russian Science Foundation (RSF) project 14–12–00887.

- [1] S. S. Dhillon *et al.*, “The 2017 terahertz science and technology roadmap,” *J. Phys. D: Appl. Phys.*, vol. 50, no. 4, p. 43001, Feb. 2017.
- [2] M. Y. Glyavin *et al.*, “Experimental tests of a 263 GHz gyrotron for spectroscopic applications and diagnostics of various media,” *Rev. Sci. Instrum.*, 2015.
- [3] M. A. Koshelev, A. I. Tsvetkov, M. V. Morozkin, M. Y. Glyavin, and M. Y. Tretyakov, “Molecular gas spectroscopy using radioacoustic detection and high-power coherent subterahertz radiation sources,” *J. Mol. Spectrosc.*, vol. 331, pp. 9–16, 2017.

# NEW NONLINEAR CRYSTALS FOR THE GENERATION OF THZ LIGHT FROM OPTICAL RECTIFICATION

Cyril Bernerd<sup>1</sup>, Federico Sanjuan<sup>2</sup>, Emilie Hérault<sup>2</sup>, Jean-François Roux<sup>2</sup>, Jean-Louis Coutaz<sup>2</sup>, Takashi Notake<sup>3</sup>, Mio Koyama<sup>3</sup>, Hiroaki Minamide<sup>3</sup>, Hiromasa Ito<sup>3</sup>, Jiyang Wang<sup>4</sup>, Patricia Segonds<sup>1</sup>, David Jegouso<sup>1</sup>, Véronique Boutou<sup>1</sup> and Benoit Boulanger<sup>1,4</sup>

<sup>1</sup> Université Grenoble Alpes / CNRS, Institut Néel, 38402 Grenoble Cedex 09, France

<sup>2</sup> Université Savoie Mont-Blanc, IMEP-LAHC, UMR CNRS 5130, 73376 Le Bourget du Lac Cedex, France

<sup>3</sup>Tera-photonics laboratory, RIKEN Sendai, Miyagi 980-0845, Japan

<sup>4</sup>Institute of Functional Crystals, Tianjin University of Technology, Tianjin, 300384, China

[patricia.segonds@neel.cnrs.fr](mailto:patricia.segonds@neel.cnrs.fr)

We report a detailed study of 21 nonlinear crystals for the generation of coherent THz polychromatic light from Optical Rectification (OR) between two incoming wavelengths with close values generated by two independent nanosecond lasers, or between two Fourier components of the same femtosecond (fs) laser pulse.

In the THz range corresponding to the generated wavelength, we characterized the 21 nonlinear crystals using classical Fourier Transform InFraRed spectroscopy (FTIR) and Time-Domain spectroscopy (TDS) [1]. We recorded their transmission spectra in polarized light in the 0.1-2 THz and 2-20 THz ranges respectively. From TDS we determined the principal values of their refractive indices and absorption coefficients with an accuracy of  $10^{-2}$  and  $0.1 \text{ cm}^{-1}$  respectively. In the visible and near infrared range, corresponding to the pumping wavelengths, we considered transmission spectra, damage threshold and the Sellmeier equations describing the dispersion equations of the principal refractive indices, from literature [2]. We also used the Sellmeier equations that we refined for many nonlinear crystals over this range, by fitting direct measurements of phase-matching conditions recorded in our group [3].

Using the previous data, we calculated the coherence length associated with the generation of a monochromatic THz light from OR between two independent incoming wavelengths. We report such a generation well covering the THz transmission range with a coherence length larger than 1mm for the eight following crystals *i.e.* YCOB, BNA, LBO, CSP, AGS and GaP. We determined the phase-matching conditions associated to an infinite value of the coherence length for all 21 nonlinear studied crystals. Our calculations also yield the corresponding values of the independent incident wavelengths from the visible and near infrared transmission ranges of the crystals. We are currently implementing a new setup able to record the previous OR calculations for comparison.

We also calculated and measured the spectrum of the broadband THz light generated by OR of a fs laser pulse (0.8- $\mu\text{m}$  wavelength). The most intense energy from the 21 crystals was generated in a y-cut and 2.09 mm thick-BNA slab for OR type V with a peak value recorded around 0.8 THz. Since a maximal value of THz energy is expected above 1 THz according to our calculation, new experiments are in progress using a fs pulse tunable between 0.73 and 2.6  $\mu\text{m}$  in order to determine precisely at which pump wavelength it occurs.

[1] Coutaz J.-L., Garet F. and Wallace V. P., "Principles of THz time-domain spectroscopy", Pan Publishing, Singapore (2018), ISBN 9789814774567 (to appear).

[2] for example: Boursier E., Segonds P., Ménaert B. J., Inácio P. L., Panyutin V., Badikov V., Badikov D., Petrov V., Boulanger B. "Phase matching directions & refined Sellmeier equations of the monoclinic acentric crystal BaGa<sub>4</sub>Se<sub>7</sub>", Opt. Lett. 41(12), 2731-2734 (2016).

[3] Bernerd C., Segonds P., Debray J., Notake T., Koyama M., Minamide H., Ito H., Boulanger B., "Quadratic nonlinear optical properties of the organic N-benzyl-2-methyl-4-nitroaniline (BNA) biaxial crystal", Opt. Lett. 43(8), 1818-1821 (2018).

## Authors' list.

### Laser-matter interaction

Beránek LM-P-2  
Bulgakova LM-I-7  
Charipar LM-I-2  
De la Fuente LM-I-18  
Duchateau LM-I-3  
Gnilitskyi LM-O-2  
Gnilitskyi LM-O-7  
Golovan LM-P-3  
Guizard LM-I-5  
Ionel LM-P-1  
Ionin LM-I-12  
Kabashin LM-I-10  
Klimentov LM-I-4  
Kononenko LM-I-16  
Koroleva LM-P-10  
Krapivnitskaia LM-P-9  
Krasovskii LM-P-11  
Krasovskii LM-P-12  
Lizunov LM-O-5  
Lopez LM-I-14  
Matei LM-O-3  
Mazhukin LM-P-6  
Mulenko LM-I-15  
Novodvorsky LM-P-5  
Odintsova LM-O-1  
Pavlichenko LM-O-6  
Polyakov LM-P-4  
Samokhin LM-P-8  
Sentis LM-I-1  
Sentis LM-O-4  
Stoian LM-I-8  
Sugioka LM-I-11  
Timoshenko LM-I-17  
Veiko LM-I-9  
Zavestovskaya LM-I-6  
Zimnyakov LM-I-13  
Zubko LM-P-7

### Laser Systems and Materials

Adell LS-P-3  
Atta Khedr LS-P-6  
Camy LS-I-18  
Chen LS-I-9  
Cornago LS-O-14  
Cuerda LS-I-10  
Gomez-Fernandez LS-P-1  
Griebner LS-I-6

Ionin LS-O-1  
Ivleva LS-P-10  
Jambunathan LS-I-5  
Jambunathan LS-P-7  
Kharakhordin LS-O-5  
Kifle LS-O-8  
Kim LS-P-15  
Kozlova LS-P-9  
Krasovskii LS-P-17  
Lan LS-P-8  
Lazarev LS-I-15  
Lifante LS-I-11  
Loiko LS-I-3  
Loiko LS-O-12  
Medina LS-P-12  
Mena LS-P-4  
Mero LS-O-7  
Mikhailov LS-P-11  
Miyata LS-I-4  
Morozov LS-O-4  
Pasiskevicius LS-I-8  
Pedrol LS-P-13  
Posonova LS-P-5  
Pustovoy LS-P-14  
Pustovoy LS-P-16  
Rodenas LS-I-1  
Rotermund LS-I-17  
Sanina LS-O-6  
Schmid LS-O-9  
Schunemann LS-I-7  
Segonds LS-I-16  
Serres LS-O-13  
Tarabrin LS-O-15  
Tsvetkov LS-I-14  
Vojna LS-O-11  
Voloshin LS-O-10  
Yu LS-I-2  
Z. Pan LS-P-2  
Zhmurenkov LS-O-2

### Biophotonics

Achim (Popa) B-P-5  
Aksenova B-P-9  
Bhiri B-O-11  
Borisova B-I-14  
Esenaliev B-I-3  
Dubrovskiy B-P-8  
Gelikonov B-I-4  
Genina B-I-16

Genova B-P-4  
Glückstad B-I-6  
Glyavina B-P-2  
H. Pan LS-O-3  
Ham LS-I-12  
Heiner LS-I-13  
Hristu B-O-4  
Kirillin B-I-5  
Kistenev B-I-8  
Khilov B-O-10  
Klimova B-P-7  
Loginova B-O-6  
Nexha B-O-8  
Oliveira B-I-13  
Orlova B-O-9  
Perekatova B-O-1  
Perelman B-I-10  
Pini B-I-11  
Pochechuev B-O-3  
Priezzhev B-I-12  
Proskurin B-P-1  
Schneckenburger B-I-2  
Semyachkina-glushkovskaya B-I-1  
Sergeeva B-O-5  
Shaked B-I-9  
Solovieva B-O-2  
Terskov B-P-6  
Yanina B-P-3  
Yushkov B-O-7  
Zagaynova B-I-15  
Zaytsev B-I-7

### **Laser Diagnostics and Spectroscopy**

Kinyaevskiy LD-O-3  
Bratu LD-P-11  
Czitrovsky LD-I-2  
Golovan LD-I-5  
Golovan LD-P-6  
Golovan LD-P-7  
Himics LD-P-4  
Holomb LD-P-5  
Isaeva A.A LD-P-1  
Isaeva E.A LD-O-2  
Kugler LD-P-12  
Milekhin LD-I-6  
Mishina LD-I-4  
Nagy LD-I-3  
Pustovoy LD-P-10

Pustovoy LD-P-3  
Pustovoy LD-P-8  
Pustovoy LD-P-9  
Rigó LD-P-2  
Sedrine LD-I-7  
Timchenko LD-P-13  
Timchenko LD-P-14  
Timchenko LD-P-15  
Ushakova LD-O-1  
Veres LD-I-1

### **Nonlinear Optics and Photonics**

Dazhi Lu NL-O-1  
Grigoriev NL-I-5  
Kondratiev NL-O-2  
Kurimura NL-I-4  
Lobanov NL-I-2  
Perezhogin NL-I-3  
Sedov NL-P-1  
Shitikov NL-P-2  
Subbotin NL-P-3  
Ushakov NL-I-1  
Váczí NL-P-4

### **THz Sources and Applications**

Balakin THz-I-5  
Fokin THz-O-1  
Jeon THz-I-3  
Knyazev THz-I-1  
Lee THz-I-2  
Segonds THz-O-2  
Vaks THz-I-4

**ALT**  **INTERNATIONAL CONFERENCE**  
**Advanced Laser Technologies**